CENTRO INTERNACIONAL DE ESTUDOS
DE DOUTORAMENTO E AVANZADOS
DA USC (CIEDUS)

TESE DE DOUTORAMENTO

NEW THERAPEUTIC TARGETS IN THE DEVELOPMENT OF GASTRIC CANCER: FROM CHRONIC GASTRITIS TO GASTRIC CANCER

Saúl Leal López

ESCOLA DE DOUTORAMENTO INTERNACIONAL

PROGRAMA DE DOUTORAMENTO EN ENDOCRINOLOXÍA

SANTIAGO DE COMPOSTELA

2018

USC
UNIVERSIDADE
DE SANTIAGO
DE COMPOSTELA

DECLARACIÓN DO AUTOR DA TESE

New therapeutic targets in the development of gastric cancer: from chronic gastritis to gastric cancer

D. Saúl Leal López

Presento a miña tese, seguindo o procedemento axeitado ao Regulamento, e declaro que:

1) A tese abarca os resultados da elaboración do meu traballo.
2) De selo caso, na tese faise referencia ás colaboracións que tivo este traballo.
3) A tese é a versión definitiva presentada para a súa defensa e coincide coa versión enviada en formato electrónico.
4) Confirmo que a tese non incorre en ningún tipo de plaxio doutros autores nin de traballos presentados por min para a obtención doutros títulos.

En Santiago de Compostela, 18 de outubro de 2018

Asdo: Saúl Leal López

USC
UNIVERSIDADE
DE SANTIAGO
DE COMPOSTELA

AUTORIZACIÓN DOS DIRECTORES DA TESE

NEW THERAPEUTIC TARGETS IN THE DEVELOPMENT OF GASTRIC CANCER: FROM CHRONIC GASTRITIS TO GASTRIC CANCER

Dna. Yolanda Pazos Randulfe

D. Juan Enrique Domínguez Muñoz

D. Tomás García-Caballero Parada

INFORMAN:

Que a presente tese, correspóndese co traballo realizado por D. ***Saúl Leal López*** *baixo a miña dirección, e autorizo a súa presentación, considerando que reúne os requisitos esixidos no Regulamento de Estudos de Doutoramento da USC, e que como director desta non incorre nas causas de abstención establecidas na Lei 40/2015.*

En Santiago de Compostela, a 18 de outubro de 2018

Asdo. Y. Pazos Randulfe Asdo. J. E. Domínguez Muñoz Asdo. T. García-Caballero Parada

USC
UNIVERSIDADE
DE SANTIAGO
DE COMPOSTELA

O doutorando Saúl Leal López con DNI 33552644Z declara non ter ningún conflito de interese en relación coa tese de doutoramento.

En Santiago de Compostela, a 18 de Outubro de 2018

Asdo. Saúl Leal López

USC
UNIVERSIDADE
DE SANTIAGO
DE COMPOSTELA

INDEX

USC
UNIVERSIDADE
DE SANTIAGO
DE COMPOSTELA

INDEX 9
ABSTRACT 15
ABBREVIATIONS 19
INTRODUCTION 25
GASTRIC CANCER 27
Stomach anatomy 27
Signs and symptoms 29
Risk factors and aetiology 30
Gastric carcinogenesis 31
Epidemiology 38
Classification 39
Early diagnosis 41
THE OBESTATIN/GPR39 SYSTEM 45
Obestatin signalling 47
The obestatin/GPR39 system in stomach 49
OBJECTIVES 51
MATERIALS AND METHODS 55
MATERIALS 57
CELLS 57
HUMAN SAMPLES 57
METHODS 65
Immunoblot analysis 65
Cell proliferation assays 66
Immunocytochemistry 68
Immunohistochemistry 70
Immunofluorescence analysis 70
Array protein assays 71

Migration and invasion assays 73
RNA extraction, cDNA synthesis and real-time PCR 74
NMR Analisis 75
Data analysis 78
Ethical guidelines 79
RESULTS 81
CHAPTER 1: ROLE OF THE OBESTATIN/GPR39 SYSTEM IN THE PHYSIOLOGY OF GASTRIC ENZYMES 83
GPR39 is expressed in the chief cells of the fundic glands in the healthy human stomach 83
Obestatin stimulates pepsinogen and lipase secretion in human stomach explant cultures 89
Obestatin effect on RTKs activation in healthy human stomach 94
..... 95
Obestatin stimulates proteases secretion in healthy human stomach 96
Molecular mechanisms involved in the obestatin-induced secretion of pepsinogen 98
CHAPTER 2. ROLE OF THE OBESTATIN/GPR39 SYSTEM IN HUMAN GASTRIC CANCER CELL LINES 101
The obestatin/GPR39 system is expressed in human gastric cancer cell lines 101
Obestatin stimulates proliferation in gastric cancer cells 102
Obestatin inhibits migration and invasion of NCI-N87 cell line 105
Obestatin modifies the expression of *nm23-H1* and nm23-H1 in gastric cancer cells 108
Obestatin effect on epithelial-mesenchymal transition and angiogenesis in NCI-N87 cell line 110
Obestatin activates Akt and ERK 1/2 in NCI-N87 cells 115

Basal expression of GPR39 and EGFR in AGS, KATO-III and NCI-N87 cells 116
Obestatin effect on EGFR phosphorylation in AGS, KATO-III and NCI-N87 cells 118
Obestatin effect on PAR expression in AGS, KATO-III and NCI-N87 cells 119
CHAPTER 3: OBESTATIN/GPR39 SYSTEM IN PRECANCEROUS LESIONS OF HUMAN STOMACH 123
GPR39 is expressed exclusively in the chief cells of the oxyntic mucosa 123
Obestatin/GPR39 system expression in precancerous lesions 124
Basal expression of GPR39, EGFR and IGF-IR in healthy stomach, gastritis or atrophy 128
Obestatin/GPR39 system effect on protease regulation in healthy stomach, gastritis or atrophy 129
CHAPTER 4. STUDY OF HUMAN BIOFLUIDS FROM PATIENTS GROUPED ACCORDING TO CORREA'S CASCADE TO GASTRIC CANCER BY NMR METABOLOMICS 133
Plasma 133
Urine 135
DISCUSSION 163
CONCLUSIONS 183
RESUMO 187
ACKNOWLEDGMENTS 199
BIBLIOGRAPHY 203
SUPPLEMENTARY MATERIAL 217

USC
UNIVERSIDADE
DE SANTIAGO
DE COMPOSTELA

ABSTRACT

USC
UNIVERSIDADE
DE SANTIAGO
DE COMPOSTELA

ABSTRACT

The fact that gastric cancer presents a poor prognosis underlines the importance of having tools for early diagnosis. In that sense, the objective of this doctoral thesis is the study of the obestatin/GPR39 system in development, maintenance and malignancy of gastric cancer. Our results confirm that this system is involved in the secretion of gastric enzymes; and the development of gastric cancer by being able to intervene in epithelial-mesenchymal transition, proliferation, migration and invasion of gastric cancer cells. The expression of GPR39 in the chief cells shows the possible importance of the system in SPEM that is key to the evolution to intestinal metaplasia, dysplasia and finally cancer. Obestatin-stimulable RTKs and MMPs are expressed in a differential way in the Correa sequence, evidencing the role of this system in gastric cancer. The metabolomic study of biofluids reveals their informative capacity for biomarkers identification and the establishment of reliable non-invasive protocols.

Keywords: obestatin, GPR39, gastric cancer, pepsinogen, lipase, metabolomics.

RESUMO

O feito de que o cancro gástrico presente unha mala prognose subliña a importancia de dispoñer de ferramentas para unha diagnose temperá. Neste senso, o obxectivo desta tese doutoral é o estudo do sistema obestatina/GPR39 no desenvolvemento, mantemento e malignidade do cancro gástrico. Os nosos resultados confirman que este sistema está involucrado na secreción de encimas gástricos e no desenvolvemento do cancro gástrico ao intervir na transición epitelio-mesénquima, proliferación, migración e invasión de células cancerígenas gástricas. A expresión do GPR39 nas células principais mostra a posíbel importancia do sistema na SPEM que é clave para a evolución cara a metaplasia intestinal, displasia e finalmente o cancro. Os RTKs e MMPs estimulables con obestatina exprésanse dun xeito diferencial na secuencia de Correa, evidenciando o papel deste sistema no cancro gástrico. O estudo metabolómico dos biofluídos revela a súa

capacidade informativa para a identificación de biomarcadores que permiten o establecemento de protocolos fiables e non invasivos.

Termos chave: obestatina, GPR39, cancro gástrico, pepsinóxeno, lipase, metabolómica.

RESUMEN

El hecho de que el cáncer gástrico presente un mal pronóstico subraya la importancia de disponer de herramientas para su diagnóstico precoz. En ese sentido, el objetivo de esta tesis doctoral es el estudio del sistema obestatina/GPR39 en el desarrollo, mantenimiento y malignidad del cáncer gástrico. Nuestros resultados confirman que este sistema está involucrado en la secreción de enzimas gástricas y en el desarrollo de cáncer gástrico al intervenir en la transición epitelio-mesénquima, proliferación, migración e invasión de células cancerígenas gástricas. La expresión del GPR39 en las células principales muestra la posible importancia del sistema en la SPEM que es clave para la evolución hacia la metaplasia intestinal, la displasia y finalmente el cáncer. Los RTKs y MMPs estimulables con obestatina se expresan de manera diferencial en la cascada de Correa, evidenciando el papel de este sistema en el cáncer gástrico. El estudio metabolómico de los biofluidos revela su capacidad informativa para la identificación de biomarcadores y el establecimiento de protocolos fiables y no invasivos.

Palabras clave: obestatina, GPR39, cáncer gástrico, pepsinógeno, lipasa, metabolómica.

ABBREVIATIONS

USC
UNIVERSIDADE
DE SANTIAGO
DE COMPOSTELA

1D: One-dimensional
2D: Two-dimensional
3D: Three-dimensional
AC: Adenylate cyclase
ADAM: A desintegrin and metalloproteinase
ADAMTS: A desintegrin and metalloproteinase with thrombospondin motifs
Akt: Serine/threonine kinase (protein kinase B)
ANOVA: Analysis of variance
ATP: Adenosine triphosphate
BrdU: Bromodeoxiuridine
BSA: Bovine serum albumin
CaMKII: Calmodulin-dependent protein kinase II
cAMP: Cyclic adenosine monophosphate
CC2: Cell conditioning solution 2
cDNA: Complementary DNA
CTS: Cathepsin
D_2O: Deuterated water
DAB: 3-3'-Diaminobenzidine
DAG: Diacylglycerol
DDR: Discoidin domain receptor
DNA: Deoxyribonucleic acid
ECL: Enterochromaffin-like
EDTA: Ethylenediaminetetraacetic acid
EGF: Epidermal growth factor
EGFR: Epidermal growth factor receptor
EMT: Epithelial-mesenchymal transition
EphR: Ephrin receptor
ER: Endoplasmic reticulum
ERK1/2: Extracellular signal-regulated kinase-1/2
EUS: Endoscopic ultrasound
FBS: Foetal bovine serum
GAPDH: Glyceraldehyde 3-phosphate dehydrogenase
GIST: Gastrointestinal stromal tumour

GPCR: G-protein-coupled receptor
GPR39: G-protein 39-coupled receptor
HDGC: Hereditary diffuse gastric cancer
HHS: Harry´s haematoxylin solution
HRP: Horseradish peroxidase
hRPEs: Human retinal pigmented epithelial cells
IC: Immunocytochemistry
IF: Immunofluorescence
IGF1R: Insulin-like growth factor-1 receptor
IgG: Immunoglobulin G
IH: Immunohistochemistry
IM: Intestinal metaplasia
IP3: Inositol trisphosphate
kDa: kiloDalton
KLK: Kallikrein
MALT: Mucosa-associated lymphoid tissue
MD: Moderately differentiated
MMP: Metalloproteinase
mRNA: Messenger RNA
mTOR: Mammalian target of rapamycin
mTORC1: mTOR complex 1
mTORC2: mTOR complex 2
NMR: Nuclear magnetic resonance
OB: Obestatin
O/N: Overnight
OPLS-DA: Orthogonal projections to latent structures discriminant analysis
PAR-2: Proteinase-activated receptor 2
PBS: Phosphate buffer saline
PBST: Phosphate buffer saline containing Tween-20
PC: Proprotein convertase
PCA: Principal component analysis
PC1: Principal component 1
PC2: Principal component 2

PD: Poorly differentiated
PEDF: Pigment epithelium derived factor
PFA: Paraformaldehyde
PGI: Pepsinogen I
PI3K: Phosphatidylinositol 3-kinase
PKA: Protein kinase A
PKC: Protein kinase C
PLC: Phospholipase C
PLS-DA: Partial least squares-discriminant analysis
POS: Position
ppm: Part per million
qPCR: Quantitative polymerase chain reaction
RNA: Ribonucleic acid
RT: Room temperature
RTK: Receptor tyrosine kinase
SDS: Sodium dodecyl sulphate
SEM: Standard error of the mean
siRNA: Small interfering RNA
SPEM: Spasmolytic polypeptide expressing metaplasia
Src: Proto-oncogene tyrosine-protein kinase
TBS: Tris buffer solution
TBST: Tris buffer solution containing Tween-20
TNM: Tumour, node and metastasis cancer classification
TOCSY: Total correlation spectroscopy
TSP: Trimethylsilylpropionic acid
VEGF: Vascular endothelial growth factor
VEGFR: Vascular endothelial growth factor receptor
WB: Western blot
WD: Well differentiated
WHO: World Health Organization

USC
UNIVERSIDADE
DE SANTIAGO
DE COMPOSTELA

INTRODUCTION

USC
UNIVERSIDADE
DE SANTIAGO
DE COMPOSTELA

GASTRIC CANCER

Gastric cancer is a disease caused by the uncontrolled growth of the stomach epithelium cells with the capacity to invade and destroy other tissues. In case of metastasis, it infiltrates the lymphatic vessels or accesses the bloodstream, and can spread to any part of the body, particularly liver, lining of the abdomen, lung and bone. The patterns of metastasis differ notably depending on the histological type[1]. Cardia cancer exhibits a completely different metastatic behavior than non-cardia cancer.

STOMACH ANATOMY

Anatomically, the stomach is divided into four large sections: cardia, the part that joins the esophagus; fundus, located in the upper curved part; body, central part formed by the lesser curvature and the greater curvature; and pylorus, which connects with the duodenum and contains the pyloric antrum (**Scheme 1**).

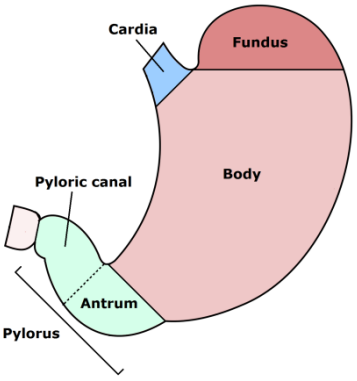

Scheme 1. Anatomical division of the human stomach. Cardia, fundus, body or corpus and pylorus are the four parts into which stomach is divided.

[1] Riihimäki M, Hemminki A, Sundquist K, *et al.* Metastatic spread in patients with gastric cancer. Oncotarget. 2016;7(32):52307-16.

Histologically, the stomach wall is divided into five layers: mucosa, the innermost layer where glands meet and most tumors develop; submucosa, a support layer; muscularis propria, consisting of three layers of muscle responsible for the movement to mix the stomach contents; subserosa and serosa, the two outermost layers that surround stomach.

In the clinical classification of tumours, the layers are important in determining the extent of the cancer and its prognosis. As cancer progresses to the outermost layers, its stage becomes more advanced and prognosis is worse.

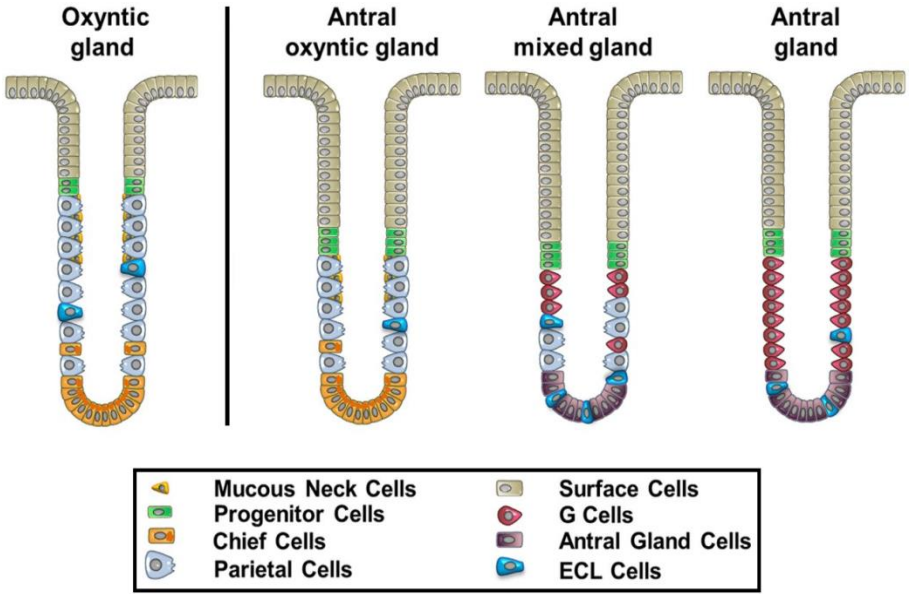

Scheme 2. Antral and fundic gland representation. Oxyntic gland represents the typical type of gland present in the body and the bottom of the human stomach. In human antrum, three types of glands were shown to exist: antral oxyntic gland, antral mixed gland and gastrin cell containing the antral gland. ECL cells, enterochromaffin-like cells. Modified from: Choi E, *et al.* Gut 2014;63:1711-20, with permission of BMJ Publishing Group Ltd.

Three types of glands are distinguished according to their location.

- Fundic or oxyntic glands, which are found in the corpus and fundus of stomach and are the most abundant type. They are characterized by straight tubules perpendicular to the surface. At the isthmus of these glands, foveolar cells, also called mucous neck cells, which secrete mucus are located. Underneath, the parietal cells that secrete hydrochloric acid (HCl) and intrinsic factor, and the enteroendocrine cells, responsible for hormones and peptides production. can be found. At the base of gland, the chief cells that secrete gastric lipase and pepsinogen I are presented.
- Cardiac glands, are found in the cardias and secrete mucus by foveolar cells. Simple tubular with short ducts or composed racemose types are present in cardias.
- Pyloric glands, branched and contoured tubules located in the antrum, secrete gastrin by G cells. Underneath, the enteroendocrine cells and at the base, the antral gland cells are located. Heterogeneous types of antral glands have been observed in the transition zones with the body of the stomach, as shown in **Scheme 2**.

SIGNS AND SYMPTOMS

In early stages, this type of cancer is often either asymptomatic or it may cause nonspecific symptoms. Among the most common symptoms of the early stages are indigestion, heartburn, and bloated sensation after eating. As the tumor progresses, weakness, fatigue, bloating of the stomach after meals, abdominal pain in the upper abdomen, nausea and occasional vomiting, diarrhea or constipation may develop. Later, tumor enlargement can cause weight loss or bleeding with vomiting blood or blood in the stool and sometimes leading to anemia.

Once symptoms appear, the tumour stage is usually advanced and metastasis may occur. Screening for gastric cancer is not routinely performed in Europe and the United States, so detection depends only on the symptoms caused by the tumour. Because of this, 90% of diagnosed adenocarcinomas are in an

advanced stage[2], which contributes to the typical poor prognosis of this tumour.

RISK FACTORS AND AETIOLOGY

A multi-factorial model of gastric cancer (CG) is now accepted, in which the combination of environmental and genetic factors are involved in the carcinogenic process[3]. However, the main cause of this type of tumor is chronic infection with *Helicobacter pylori (H. pylori)*, which is responsible for 6.2% of all cancer cases worldwide[4]. This bacterium is only related to non-cardia tumours[5], causing 89% of these cases[4]. However, only 1-3% among infected individuals will develop stomach cancer[6].

While the incidence of cardia tumours remains stable, the observed reduction in the incidence of non-cardia gastric cancer may be due to increased control of *H. pylori* through improved sanitation or antibiotic treatments leading to a reduction in the prevalence of infection in developed countries[7]. The carcinogenic mechanism of *H. pylori* is associated with interactions between bacterial virulence factor, such as CagA and VacA and host inflammatory responses[8] cooperating to initiate the gastric cancer development[9]. The exact transmission route of *H. pylori* infection has not yet been established. It can spread directly from one person to another, mainly faecal-oral or oral-oral, or

[2] Everett SM, Axon ATR. Early gastric cancer in Europe. Gut. 1997;41:142-150.
[3] González CA, Sala N, Rokkas T. Gastric cancer: epidemiologic aspects. *Helicobacter*. 2013;18:34-8.
[4] Plummer M, Franceschi S, Vignat J, *et al.* Global burden of gastric cancer attributable to *Helicobacter pylori*. Int J Cancer. 2015;136(2):487-90.
[5] *Helicobacter* and Cancer Collaborative Group. Gastric cancer and *Helicobacter pylori*: a combined analysis of 12 case control studies nested within prospective cohorts. Gut. 2001;49:347–53.
[6] Noto JM, Peek RM, *Helicobacter pylori*: an overview. Methods Mol. Biol. 2012;921:7–10.
[7]Hooi JKY, Lai WY, Ng WK, *et al.* Global Prevalence of *Helicobacter pylori* Infection: Systematic Review and Meta-Analysis. Gastroenterology. 2017;153(2):420-429.
[8]Wang F, Meng W, Wang B, *et al. Helicobacter pylori*-induced gastric inflammation and gastric cancer. Cancer Lett. 2014;345(2):196-202.
[9]Chiba T, Marusawa H, Seno H, *et al.* Mechanism for gastric cancer development by *Helicobacter pylori* infection. J Gastroenterol Hepatol. 2008;23:1175–81.

indirectly from by environmental sources, through the consumption of contaminated food or water[10].

Dietary factors involved in the development of gastric cancer include salt, salted or smoked foods, red meat, and pickled vegetables. The consumption of fresh fruits and vegetables shows a protective effect. Smoking tobacco increases the risk of cancer gastric by 60% in men and 20% in women[11]. Alcohol consumption was also reported as a risk factor[12], as well as age and sex. The average age of diagnosis is 68 years, with a male-to-female ratio of 2:1.

Although the majority appears sporadically, between 5 and 10% of gastric cancer cases familial clustering is observed[13], Hereditary diffuse gastric cancer (HDGC) represents 1-3% of all cases and is characterized by a mutation in the CDH1 gene that encodes E-cadherin[14].

GASTRIC CARCINOGENESIS

Gastric adenocarcinoma is preceded by a cascade of premalignant lesions triggered by *H. pylori* infection. Chronic inflammation is followed by changes in the stomach mucosa resulting in atrophy and metaplasia. In 1975, Correa proposed a model of gastric carcinogenesis[15] in which an association is established between intestinal metaplasia and intestinal-type gastric carcinoma. It was revised in 1988[16] and 1992[17] and consists of the following

[10] Mladenova I, Durazzo M. Transmission of *Helicobacter pylori*. Minerva Gastroenterol Dietol. 2018;64(3):251-254.
[11] Ladeiras-Lopes R, Pereira AK, Nogueira A, *et al.* Smoking and gastric cancer: systematic review and meta-analysis of cohort studies. Cancer Causes Control. 2008;19(7):689–701.
[12] Jedrychowski W, Wahrendorf J, Popiela T, *et al.* A case-control study of dietary factors and stomach cancer risk in Poland. *Int J Cancer*. 1986;37(6):837–842.
[13] La Vecchia C, Negri E, Franceschi S, *et al.* Family history and the risk of stomach and colorectal cancer. *Cancer*. 1992;70(1):50–55.
[14] Skierucha M, Milne AN, Offerhaus GJ, *et al.* Molecular alterations in gastric cancer with special reference to the early-onset subtype. World J Gastroenterol. 2016;22(8):2460–2474.
[15] Correa P, Haenszel W, Cuello C, *et al.* A model for gastric cancer epidemiology. Lancet. 1975;2:58–60.
[16] Correa P. A human model of gastric carcinogenesis. Cancer Res. 1988;48:3554–60.
[17] Correa P. Human gastric carcinogenesis: a multistep and multifactorial process – First American Cancer Society Award lecture on cancer epidemiology and prevention. Cancer Res. 1992;52:6735–40.

steps: the normal gastric mucosa is infected by *H. pylori* and non-atrophic gastritis occurs, leading to atrophic gastritis, intestinal metaplasia, dysplasia and finally cancer (**Scheme 3**).

Expressing data in percentages, half of cases of *H. pylori* infection will develop atrophic gastritis to some degree during their lifetime, and in about 10% of the infected subjects, atrophic gastritis will finally be moderate or severe[18,19,20]. In the latter category, between 2.5 and 5% may acquire cancer[21].

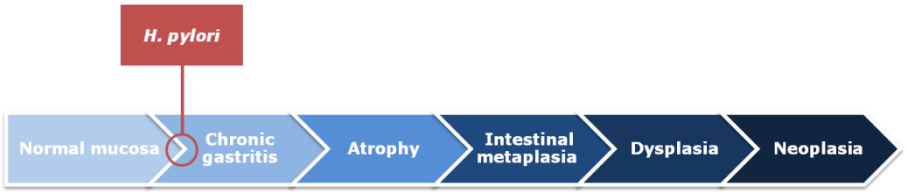

Scheme 3. Graphic representation of the model on gastric carcinogenesis proposed by Correa.

Chronic *H. pylori* infection initiates both prominent inflammation and loss of parietal cells, known as oxyntic atrophy. These acid-secreting cells act as a coordinated source of a number of growth factors involved in the proper differentiation from other lineages, particularly the zymogen-secreting chief cells[22,23]. The combination of prominent inflammation with oxyntic atrophy is a prerequisite for the development of metaplasia to gastric

[18] Kuipers EJ, Uyterlinde AM, Peña AS, *et al.* Long-term sequelae of *Helicobacter pylori* gastritis. Lancet. 1995;345:1525–8.
[19] Sipponen P, Helske T, Järvinen P, *et al.* Fall in the prevalence of chronic gastritis over 15 years: analysis of outpatient series in Finland from 1977, 1985, and 1992. Gut. 1994;35:1167–71.
[20] Maaroos HI, Vorobjova T, Sipponen P, *et al.* An 18-year follow-up study of chronic gastritis and *Helicobacter pylori* association of CagA positivity with development of atrophy and activity of gastritis. Scand J Gastroenterol. 1999;34:864–9.
[21] Ebule IA, Djune Fokou AK, Sitedjeya Moko IL *et al.* Prevalence of *H. pylori* Infection and Atrophic Gastritis among dyspeptic subjects in Cameroon using a Panel of Serum Biomarkers (PGI, PGII, G-17, HpIgG). Sch. J. App. Med. Sci. 2017;5(4A):1230-1239.
[22] Li Q, Karam SM, Gordon JI. Diphtheria toxin-mediated ablation of parietal cells in the stomach of transgenic mice. J Biol Chem. 1996;271:3671–3676.
[23] Bredemeyer AJ, Geahlen JH, Weis VG, *et al.* The gastric epithelial progenitor cell niche and differentiation of the zymogenic (chief) cell lineage. Dev Biol. 2009;325:211–224.

adenocarcinoma[24]. In humans, two types of metaplasia emerge: intestinal metaplasia and spasmolytic polypeptide expressing metaplasia (SPEM) (**Scheme 4**). Both have been associated with progression to intestinal gastric cancer[25,26,27,28].

Intestinal metaplasia is characterized by the presence of goblet cells[29], exclusive to the intestine and not to the healthy stomach. These cells express intestinal markers such as Muc2 and Trefoil factor 3 (TFF3), among others[30,31].

In SPEM, the metaplastic mucosal cells exhibit morphological characteristics of deep antral gland cells or Brunner's glands and express Muc6 and Trefoil factor 2 (TFF2)[32], but gastrin cells in the SPEM glands have not been observed. The strong association between SPEM with chronic *H. pylori* infection and gastric adenocarcinoma has been demonstrated in several studies[28].

---

[24] El-Zimaity HMT, Ota H, Graham DY, *et al.* Patterns of gastric atrophy in intestinal type gastric carcinoma. Cancer. 2002;94:1428–1436.
[25] Hattori T. Development of adenocarcinomas in the stomach. Cancer. 1986;57:1528–1534.
[26] Xia HH, Kalantar JS, Talley NJ, *et al.* Antral-type mucosa in the gastric incisura, body and fundus (antralization): A link between *Helicobacter pylori* infection and intestinal metaplasia. Am. J. Gastroenterol. 2000;95:114–121.
[27] Schmidt PH, Lee JR, Joshi V, *et al.* Identification of a metaplastic cell lineage associated with human gastric adenocarcinoma. Lab. Invest. 1999;79:639–646.
[28] Halldorsdottir AM, Sigurdardottir M, Jonasson JG, *et al.* Spasmolytic polypeptide expressing metaplasia (SPEM) associated with gastric cancer in Iceland. Dig. Dis. Sci. 2003;48:431–441.
[29] Morson BC. Intestinal metaplasia of the gastric mucosa. Br J Cancer. 1955;9:365–376.
[30] Ectors N, Dixon MF. The prognostic value of sulphomucin positive intestinal metaplasia in the development of gastric cancer. Histopathology. 1986;10:1271–1277.
[31] Lee HJ, Nam KT, Park HS, *et al.* Gene expression profiling of metaplastic lineages identifies CDH17 as a prognostic marker in early-stage gastric cancer. Gastroenterology. 2010;139(1):213-25.
[32] Schmidt PH, Lee JR, Joshi V, *et al.* Identification of a metaplastic cell lineage associated with human gastric adenocarcinoma. Lab. Invest. 1999;79:639–646.

Chronic *Helicobacter* infection in mice leads to loss of parietal cells and inflammation throughout the mucosa[33,34,35], developing SPEM after 4 to 6 months of infection and dysplasia at 12 months[33]. However, these mice never develop intestinal metaplasia, suggesting that SPEM is the primary pre-neoplastic metaplasia in mice.

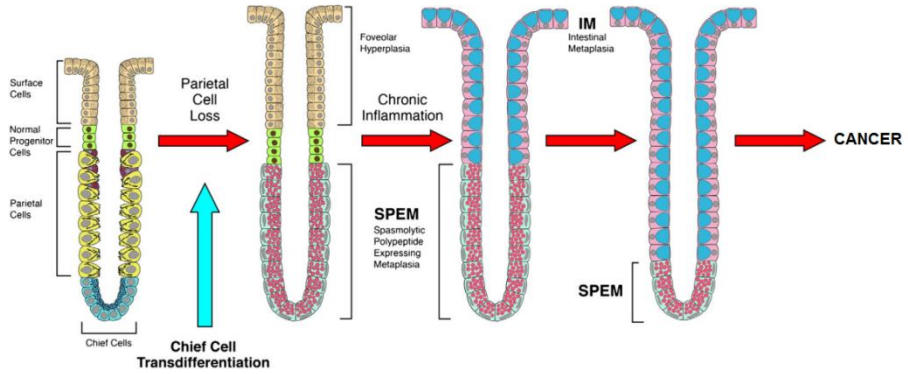

Scheme 4. Proposed model for the origin and progression of gastric metaplasias. Oxyntic atrophy originated by loss of parietal cells triggers chief cell transdifferentiation into SPEM. In the presence of chronic inflammation by *H. pylori* infection, intestinal metaplasia evolves in the context of pre-existing SPEM, and subsequent dysplasia and gastric cancer. Taken from: Goldenring JR et al. Exp Cell Res. 2011;317(19):2759-64, with permission of Elsevier.

Studies were performed to distinguish the role of oxyntic atrophy and inflammation in the development of SPEM, using DMP-777 administration to induce acute oxyntic atrophy without inflammation. DMP-777 is a Leukocyte elastase (HLE) inhibitor that acts as a protonophore with specificity for parietal cell membranes leading its loss in high doses. Mice develop oxyntic atrophy after 3 days of administration of DMP-777 in the absence of inflammation, resulting in SPEM after 10 to 14 days of

[33] Wang TC, Goldenring JR, Dangler C, *et al.* Mice lacking secretory phospholipase A2 show altered apoptosis and differentiation with *Helicobacter felis* infection. Gastroenterology. 1998;114:675–689.
[34] Fox JG, Li X, Cahill RJ, Andrutis K, *et al.* Hypertrophic gastropathy in *Helicobacter felis*-Infected wild type C57BL/6 mice and p53 hemizygous transgenic mice. Gastroenterology. 1996;110:155–166.
[35] Fox JG, Wang TC, Rogers AB, *et al.* Host and microbial constituents influence *Helicobacter pylori*-induced cancer in a murine model of hypergastrinemia. Gastroenterology. 2003;124:1879–1890.

treatment[36]. Following it for more than a year, dysplasia is not observed[37]. These data confirm that the loss of parietal cells causes SPEM, but an inflammatory context is needed for the pre-carcinogenic process may continue.

Furthermore, *Helicobacter* infection in immunocompromised mice does not develop oxyntic atrophy and therefore does not develop SPEM or progress to dysplasia[38].

Because *H. pylori* infection does not cause intestinal metaplasia in mice, Mongolian gerbils have been used to elucidate the relationship of SPEM to intestinal metaplasia[39]. The development of SPEM was observed in only 3 weeks after *Helicobacter* infection while intestinal metaplasia emerged later at 24 and 39 weeks of infection. The sites of intestinal metaplasia were surrounded by the mucosa with pre-existing SPEM. In addition, single gland units were present containing both types of metaplasia, seen in humans as well[40]. These data support that SPEM is the first metaplasia to develop after oxyntic atrophy, and then in the presence of an inflammatory environment, the intestinal metaplasia emerges as a second metaplastic transition.

H. pylori and EGFR transactivation

Epidermal growth factor receptor (EGFR) is a therapeutic target for several types of neoplasms in addition to gastric cancer. Phosphorylation and activation of EGFR increases the transcriptional activity of proto-oncogene β-catenin by inactivating GSK3β.

---

[36] Nomura S, Yamaguchi H, Wang TC, *et al.* Alterations in gastric mucosal lineages induced by acute oxyntic atrophy in wild type and gastrin deficient mice. Amer. J. Physiol. 2004;288:G362–G375.

[37] Goldenring JR, Ray GS, Coffey RJ, *et al.* Reversible drug-induced oxyntic atrophy in rats. Gastroenterology. 2000;118:1080–1093.

[38] Fox JG, Blanco M, Murphy JC, *et al.* Local and systemic immue responses in murine *Helicobacter felis* active chronic gastritis. Infect. Immun. 1993;61:2309–2315.

[39] Yoshizawa N, Takenaka Y, Yamaguchi H, *et al.* Emergence of spasmolytic polypeptide-expressing metaplasia in Mongolian gerbils infected with *Helicobacter pylori*. Lab Invest. 2007;87:1265–1276.

[40] El-Zimaity HMT, Ramchatesingh J, Saeed MA, *et al.* Gastric intestinal metaplasia: subtypes and natural history. J. Clin. Pathol. 2001;54:679–683.

H. pylori infection and gastric atrophy are closely related to EGFR deregulation[41,42,43,44]. This receptor can be activated in two ways. On the one hand, directly through interaction with ligands, which initiate dimerization and increased kinase activity. On the other hand, cytokines, such as tumor necrosis factor-α (TNFα), G-protein coupled receptors (GPCRs), and cell adhesion molecules transactivate EGFR in gastric epithelial cells[45,46]. This crosstalk is mediated by metalloproteinase-dependent cleavage of EGFR ligands, in a similar manner to *H. pylori*-induced transactivation of EGFR[41,47]. In this case, required metalloproteinases could be members of the family of disintegrins and metalloproteinases, such as ADAM, namely ADAM-17.

H. pylori amplifies EGFR signalling both by activation and decreasing receptor degradation via endocytosis blocking[48]. Cellular responses are

---

41 Wallasch C, Crabtree JE, Bevec D, *et al.* *Helicobacter pylori*-stimulated EGF receptor transactivation requires metalloprotease cleavage of HB-EGF. Biochem. Biophys. Res. Commun. 2002;295:695–701.

42 Romano M, Ricci V, Di Popolo A, *et al. Helicobacter pylori* upregulates expression of epidermal growth factor-related peptides, but inhibits their proliferative effect in MKN 28 gastric mucosal cells. J. Clin. Invest. 1998;101:1604–1613.

43 Schiemann U, Konturek J, Assert R, *et al.* mRNA expression of EGF receptor ligands in atrophic gastritis before and after *Helicobacter pylori* eradication. Med. Sci. Monit. 2002;8:CR53–CR58.

44 Wong BC, Wang WP, So WH, *et al.* Epidermal growth factor and its receptor in chronic active gastritis and gastroduodenal ulcer before and after *Helicobacter pylori* eradication. Aliment Pharmacol. Ther. 2001;15:1459–1465.

45 Prenzel N, Zwick E, Daub H, *et al.* EGF receptor transactivation by G.-protein-coupled receptors requires metalloproteinase cleavage of proHB-EGF. Nature. 1999;402:884–888.

46 Pece S, Gutkind JS. Signaling from E-cadherins to the MAPK pathway by the recruitment and activation of epidermal growth factor receptors upon cell-cell contact formation. J. Biol. Chem. 2000;275:41227–41233.

47 Keates S, Sougioultzis S, Keates AC, *et al.* cag+ *Helicobacter pylori* induce transactivation of the epidermal growth factor receptor in AGS gastric epithelial cells. J. Biol. Chem. 2001;276:48127–48134.

48 Bauer B, Bartfeld S, Meyer TF. *H. pylori* selectively blocks EGFR endocytosis via the non-receptor kinase c-Abl and CagA. Cell. Microbiol. 2009;11:156–169.

affected by this transactivation, such as apoptosis[49,50], cell polarity[51], migration[52] or proliferation[53,54] (**Scheme 5**).

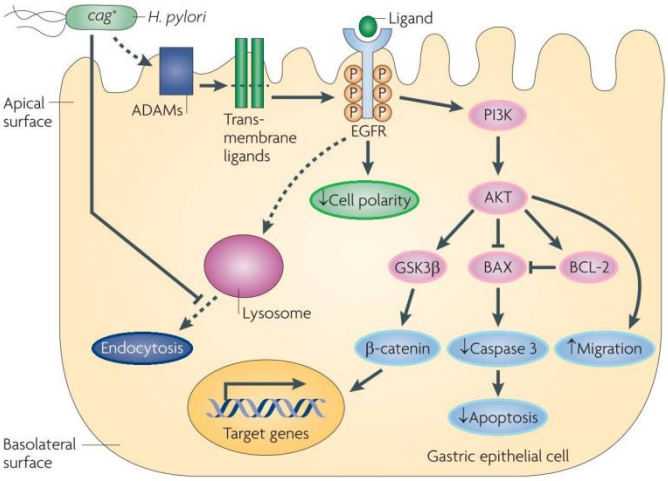

Scheme 5. Transactivation of EGFR by *H. pylori* and induced cellular consequences with carcinogenic potential. *Helicobacter pylori* transactivates epidermal growth factor receptor (EGFR) through cleavage, which is dependent on the disintegrin and metalloproteinase (ADAM) family proteinases, of EGFR ligands. One downstream target of EGFR transactivation is PI3K–AKT, which leads to AKT-dependent cell migration, inhibition of apoptosis and β-catenin activation. BAX, BCL-2-associated X protein; GSK3β, glycogen synthase kinase-3β; P, phosphorylation. Taken from: Polk DB *et al.* Nat Rev Cancer. 2010; 10(6): 403–414, with permission of Springer Nature.

[49] Cover TL, Krishna US, Israel DA,*et al.* Induction of gastric epithelial cell apoptosis by *Helicobacter pylori* vacuolating cytotoxin. Cancer Res. 2003;63:951–957.
[50] Maeda S, Yoshida H, Mitsuno Y, *et al.* Analysis of apoptotic and antiapoptotic signalling pathways induced by *Helicobacter pylori*. Gut. 2002;50:771–778.
[51] Saadat I, Higashi H, Obuse C, *et al. Helicobacter pylori* CagA targets PAR1/MARK kinase to disrupt epithelial cell polarity. Nature. 2007;447:330–333.
[52] Nagy TA, Frey MR, Yan F, *et al. Helicobacter pylori* regulates cellular migration and apoptosis by activation of phosphatidylinositol 3-kinase signaling. J. Infect. Dis. 2009;199:641–651.
[53] Peek RM Jr, Moss SF, Tham KT, *et al. Helicobacter pylori cagA*+ strains and dissociation of gastric epithelial cell proliferation from apoptosis. J. Natl Cancer Inst. 1997;89:863–868.
[54] Peek RM Jr, Wirth HP, Moss SF, *et al. Helicobacter pylori* alters gastric epithelial cell cycle events and gastrin secretion in Mongolian gerbils. Gastroenterology. 2000;118:48–59.

EPIDEMIOLOGY

According to the latest WHO study, 951,594 new stomach cancer cases occurred in 2012 making it the fifth most common cause of cancer in the world[55]. Generally, incidence rates are about two or three times as high in men as in women and vary according to geographical locations. Eastern Asia (notably in Korea, Mongolia, Japan, and China), Central and Eastern Europe, and South America have the highest rates while Northern America and Africa have the lowest. Thus, environmental conditions and lifestyle are of great importance in the development of gastric cancer.

Among the diagnosed cases, only a small part of them are detected in the early stages. Therefore, this type of cancer has a poor prognosis and usually has a survival rate of less than 20%[56]. With an estimated 723,073 deaths worldwide, gastric cancer becomes the third most common cause of cancer death.

However, during the past decades, both incidence and mortality rates have been fallen throughout most developed countries[57]. In addition, the same reduction has been seen in the typically most affected areas[58] involving factors such as improved living conditions, healthier diets, screening programmes for early detection of disease and reduction of chronic *H. pylori* infection due to improvements in drinking water sanitation or antibiotics[59,60].

Despite the overall decline in gastric cancer, an increase in the incidence of gastric cardia adenocarcinoma is seen in Europe and Northern America due

---

[55] Globocan 2012.International Agency for Research on Cancer. World Health Organization. http://gco.iarc.fr/today/home.
[56] Orditura M, Galizia G, Sforza V, *et al.* Treatment of gastric cancer. World J Gastroenterol. 2014;20:1635-49.
[57] Kelley JR, Duggan JM. Gastric cancer epidemiology and risk factors. J Clin Epidemiol. 2003;56(1):1–9.
[58] Bertuccio P, Chatenoud L, Levi F, *et al.* Recent patterns in gastric cancer: a global overview. Int J Cancer. 2009;125:666-73.
[59] Goh KL, Chan WK, Shiota S, *et al.* Epidemiology of Helicobacter pylori infection and public health implications. Helicobacter. 2011;Suppl 1:1-9.
[60] Parkin DM. The global health burden of infection-associated cancers in the year 2002. Int J Cancer. 2006;118:3030-44.

to obesity more evident[61,62,63], but reflux[64], mechanical forces of elevated intra-abdominal pressure[65], diet[66], or endocrinological mechanisms[67] are postulated as possible risk factors. Particularly in Spain, 7,810 new cases of gastric cancer are diagnosed and 5,389 people die per year. Despite the decline in mortality risk observed, the areas with the highest incidence are Castilla y León and the Atlantic coast of Galicia.

CLASSIFICATION

More than 90% of gastric tumors are adenocarcinomas originating from mucosal cells. MALToma is a type of non-Hodgkin's lymphoma that originates from B cells of the mucosa-associated lymphoid tissue (MALT). It accounts for 5% of cases. To a lesser extent, gastrointestinal stromal tumours (GIST), originating in the interstitial Cajal cells, and carcinoid tumours in which neuroendocrine cells are responsible are also detected.

Grades of gastric cancer

System of gradation based on the degree of differentiation of tumor cells and their level of proliferation. G1 indicates well differentiated (WD) and low growth; G2, moderately differentiated (MD); G3, poorly differentiated (PD); and G4 undifferentiated and fast growth.

---

61 Chow WH, Blot WJ, Vaughan TL, *et al.* Body mass index and risk of adenocarcinomas of the esophagus and gastric cardia. J Natl Cancer Inst. 1998;90:150–5.

62 Lagergren J, Bergström R, Olof N. Association between body mass and adenocarcinoma of the esophagus and gastric cardia. Ann Intern Med. 1999;130:883–90.

63 Wu AH, Wan P, Bernstein L. A multiethnic population-based study of smoking, alcohol and body size and risk of adenocarcinomas of the stomach and esophagus (United States). Cancer Causes Control. 2001;12:721–32.

64 Derakhshan MH, Malekzadeh R, Watabe H, *et al.* Combination of gastric atrophy, reflux symptoms and histological subtype indicates two distinct aetiologies of gastric cardia cancer. Gut. 2008;57:298–305.

65 Robertson EV, Derakhshan MH, Wirz AA, *et al.* Central obesity in asymptomatic volunteers is associated with increased intrasphincteric acid reflux and lengthening of the cardiac mucosa. Gastroenterology. 2013;145:730–9.

66 Bertuccio P, Rosato V, Andreano A, *et al.* Dietary patterns and gastric cancer risk: a systematic review and meta-analysis. Ann Oncol. 2013;24:1450–8

67 Olefson S, Moss SF. Obesity and related risk factors in gastric cardia adenocarcinoma. Gastric Cancer. 2015;18(1):23-32.

Histopathological classifications

- **Laurén classification**

It was established in 1965 and is the most widely used classification. It divides tumours into two groups, intestinal or diffuse type adenocarcinoma.[68] A third rare group was later included[69].

Intestinal type adenocarcinoma is characterized by irregular tubular structures described by tumour cells, and associated with intestinal metaplasia and *H. pylori* infection. This type of tumour may be presented as well, moderate or poorly differentiated.

Diffuse type adenocarcinoma is characterized by the presence of tumour cells that secrete mucus. If the mucus is not expelled, it remains within the cell in large amount and moves the nucleus to the periphery, making the cells resemble signet rings, establishing signet-ring cell type. It metastasizes faster than the intestinal type and is poorly differentiated.

Approximately 54% are intestinal type, 32% diffuse type, and 15% indeterminate type.

- **WHO classification**

The World Health Organization (WHO) published in 2010 one of the most comprehensive pathohistological classification as it includes low frequency tumor types. It comprises three large groups, epithelial, non-epithelial and secondary tumours. Epithelial tumours include intraepithelial neoplasias, carcinomas (comprising adenocarcinomas) and carcinoids. Lymphomas and sarcomas are included in the second group, as well as other uncommon variants.

---

[68] Laurén P. The two histological main types of gastric carcinoma: Diffuse and so-called intestinal-type carcinoma an attempt at a histo-clinical classification. Acta Pathol Microbiol Scand. 1965;64:31-49.

[69] Leocata P, Ventura L, Giunta M, *et al.* Gastric carcinoma: a histopathological study of 705 cases. Ann Ital Chir. 1998;69:331-7.

Clinical classifications

The most relevant clinical classifications include staging, TMN or Borrmann classifications. Classification by stages is based on extent of cancer in the layers of stomach, as well as lymph nodes. From stage 0 which is *in situ* tumor to stage 4 in which tumour has already metastasized[70]. Similarly, a more complex classification, TNM involves size and spread of tumour (T), whether it has invaded lymph nodes (N) or has spread to other parts of the body (M). However, Borrmann classification was developed for advanced tumors, in which type I is polyposis, type II ulcerated, type III ulcerated-inflammatory and type IV diffuse infiltrant.

EARLY DIAGNOSIS

Gastric cancer presents a poor prognosis because it is usually diagnosed in advanced stages due to the absence of a clear symptomatology. This fact underlines the importance of having tools for early diagnosis of the disease or even for detecting precarcinogenic states.

It is known that infection by *H. pylori* causes chronic gastritis, the first link in the sequence to stomach cancer, according to the Correa model. Gastritis can progress in half of the cases to some degree of atrophy. Atrophic gastritis is considered as a predictor of the appearance of gastric adenocarcinoma[71,72,73], so its diagnosis is crucial to know the risk of developing this type of tumour. Currently, histology is the gold standard for diagnosing these pathologies although it is an invasive and expensive procedure. Patients undergo an

[70] Edge SB, Byrd DR, Compton CC, *et al.* AJCC cancer staging manual. 7th ed. New York: Springer-Verlag. 2009.
[71] Tanaka A, Kamada T, Inoue K, *et al.* Histological evaluation of patients with gastritis at high risk of developing gastric cancer using a conventional index. Pathol Res Pract 2011; 207:354–8.
[72] Toyoshima O, Yamaji Y, Yoshida S, *et al.* Endoscopic gastric atrophy is strongly associated with gastric cancer development after Helicobacter pylori eradication. Surg Endosc. 2017; 31(5): 2140–2148.
[73] Shichijo S, Hirata Y, Niikura R, *et al.* Histologic intestinal metaplasia and endoscopic atrophy are predictors of gastric cancer development after Helicobacter pylori eradication. Gastrointest Endosc. 2016;84(4):618-24.

endoscopic ultrasound (EUS) of the upper gastrointestinal tract in which stomach biopsies are collected for further pathological analysis.

Atrophic gastritis has traditionally been classified using the Sydney system, a classification and grading system based on the integration of histological and endoscopic parameters. They are graduated in normal or mild, moderate or severe altered. It was updated in 1994 by improving the terminology[74], but despite this, the system presented problems to diagnose and graduate atrophy, as well as in knowing its nature in a robust way[75]. To overcome these limitations, a new system was created called OLGA (Operative Link on Gastritis Assessment) in which it is postulated that there are two types of atrophy, one caused by the loss of glandular units with fibrosis of the own lamina and the other by replacement of the native by metaplastic glands[76].

The examination of gastric biomarkers from blood have been used for decades to diagnose corpus atrophic gastritis in a non-invasive way[77,78], particularly in Japan[79,80,81,82,83]. Subjects with a high risk of gastric cancer were

[74] Dixon MF, Genta RM, Yardley JH, *et al.* Classification and grading of gastritis. The updated Sydney system. International Workshop on the Histopathology of Gastritis, Houston, 1994. Am J Surg Pathol 1996;20:1161-81.
[75] Aydin O, Egilmez R, Karabacak T, *et al.* Interobserver variation in histopathological assessment of *Helicobacter pylori* gastritis World J Gastroenterol. 2003 Oct;9(10):2232-5.
[76] Rugge M, Correa P, Di Mario F, *et al.* OLGA staging for gastritis: A tutorial. Dig Liv Dis 2008;40(8):650-8.
[77] Karnes WE Jr, Samloff IM, Siurala M, *et al.* Positive serum antibody and negative tissue staining for *Helicobacter pylori* in subjects with atrophic body gastritis. Gastroenterology. 1991;101:167–174.
[78] Broutet N, Plebani M, Sakarovitch C, *et al.* Pepsinogen A, pepsinogen C, and gastrin as markers of atrophic chronic gastritis in European dyspeptics. Br J Cancer. 2003;88:1239–1247.
[79] Miki K, Morita M, Sasajima M, *et al.* Usefulness of gastric cancer screening using the serum pepsinogen test method. Am J Gastroenterol. 2003;98:735–739.
[80] Kitahara F, Kobayashi K, Sato T, *et al.* Accuracy of screening for gastric cancer using serum pepsinogen concentrations. Gut. 1999;44:693–697.
[81] Kiyohira K, Yoshihara M, Ito M, *et al.* Serum pepsinogen concentration as a marker of *Helicobacter pylori* infection and the histologic grade of gastritis; evaluation of gastric mucosa by serum pepsinogen levels. J Gastroenterol. 2003;38:332–338.
[82] Shiotani A, Iishi H, Uedo N, *et al.* Histologic and serum risk markers for noncardia early gastric cancer. Int J Cancer. 2005;115:463–469.
[83] Urita Y, Hike K, Torii N, *et al.* Serum pepsinogens as a predicator of the topography of intestinal metaplasia in patients with atrophic gastritis. Dig Dis Sci. 2004;49:795–801.

detected by determining the serum pepsinogen I and pepsinogen I/II ratio[84,85].

In recent years, more complete serological tests have been developed that do not only measure pepsinogen to diagnose the disease in a much less invasive manner[86]. Pepsinogen I, pepsinogen II and gastrin-17 by ELISA and anti-*H. pylori* antibodies are evaluated. Atrophy of the gastric mucosa reduces gastrin synthesis by affecting the G cells of the antrum and reduces the production of intrinsic factor, HCl and pepsinogen by affecting the parietal and chief cells of the body, respectively. Thus, from a blood sample it is possible to determine the type of atrophy that a patient presents.

Metabolomics

The identification of new biomarkers can be performed effectively by metabolomics, consisting of metabolites analysis in a biological sample[87]. Among the most common analytical techniques used in metabolomics are NMR spectroscopy[88], GC/MS[89] and LC/MS[90.91]. NMR is an optimal technique for analyzing biofluids and complex solutions.

Although not as sensitive as the other techniques, it is reproducible, quantifiable, non-destructive and non-selective. In this sense, NMR based metabolic profiling of biofluids has been widely employed to search for

---

84 Ohata H, Kitauchi S, Yoshimura N, *et al.* Progression of chronic atrophic gastritis associated with *Helicobacter pylori* infection increases risk of gastric cancer. Int J Cancer. 2004;109:138–43.

85 Watabe H, Mitsushima T, Yamaji Y, *et al.* Predicting the development of gastric cancer from combining *Helicobacter pylori* antibodies and serum pepsinogen status: a prospective endoscopic cohort study. Gut. 2005;54:764–68.

86 Agréus L, Kuipers EJ, Kupcinskas L, *et al.* Rationale in diagnosis and screening of atrophic gastritis with stomach-specific plasma biomarkers. Scand J Gastroenterol 2012;47(12):1525.

87 Nicholson JK, Lindon JC. Systems biology: Metabonomics. Nature. 2008;455(7216):1054–6.

88 Nicholson JK, Lindon JC, Holmes E. Metabonomics: understanding the metabolic responses of living systems to pathophysiological stimuli via multivariate statistical analysis of biological NMR spectroscopic data. Xenobiotica. 1999;29(11):1181–9.

89 Dunn WB, Bailey NJ, Johnson HE. Measuring the metabolome: current analytical technologies. Analyst. 2005;130(5):606–25.

90 Zhang X, Wei D, Yap Y, *et al.* Mass spectrometry-based "omics" technologies in cancer diagnostics. Mass Spectrom Rev. 2007;26(3):403–31.

91 Yin P, Zhao X, Li Q, *et al.* Metabonomics study of intestinal fistulas based on ultraperformance liquid chromatography coupled with Q-TOF mass spectrometry (UPLC/Q-TOF MS). J Proteome Res. 2006;5(9):2135–43.

potential biomarkers for an early diagnosis in numerous pathologies[92], such as cancer[93,94], cardiovascular[95,96,97], endocrine[98], infectious[99,100,101], kidney injury/ urinary infections[102], neurological[103], and respiratory diseases[104].

Among the new methodology in the field of clinical diagnosis, metabolomics using nuclear magnetic resonance (NMR) spectroscopy has, as one of the main expectations, the identification of biomarkers in biofluid samples for an early diagnosis in a specific disease.

This approach is direct since when comparing biofluids of healthy and sick individuals, metabolites can be identified that only correlate with the diseased state. In addition, it has the advantage of being a quick and non-invasive method, requiring the simple collection of samples of urine, blood or saliva

---

92 Duarte IF, Diaz SO, Gil AM. NMR metabolomics of human blood and urine in disease research. J Pharm Biomed Anal. 2014;93:17–26. Epub 2014/05/24.

93 Bujak R, Daghir E, Rybka J, *et al.* Metabolomics inurogenital cancer. Bioanalysis. 2011; 3:913–923.

94 DeFeo EM, Wu CL, McDougal WS *et al.* A decade in prostate cancer:from NMR to metabolomics. Nat. Rev. Urol. 2011;8:301–311.

95 Ruperez FJ, Ramos-Mozo P, Teul J *et al.* Metabolomic study of plasma ofpatients with abdominal aortic aneurysm. Anal. Bioanal. Chem. 2012; 403:1651–1660.

96 Kang SM, Park JC, Shin MC, *et al.* ^{1}H nuclear magnetic resonance based metabolic urinary profiling of patientswith ischemic heart failure. Clin Biochem. 2011 Mar;44(4):293-9.

97 Bernini P, Bertini I, Luchinat C, *et al.* The cardiovascular risk of healthy individuals studied by NMR metabonomics of plasma samples, J. Proteome Res. 2011;10:4983–4992.

98 Pathmasiri W, Pratt KJ, Collier DN, *et al.* Integrating metabolomic signatures and psychosocial parameters in responsivity to an immersion treatment model for adolescent obesity. Metabolomics. 2012;8:1037–1051.

99 Munshi SU, Taneja S, Bhavesh NS, *et al.* Metabonomic analysis of hepatitis E patients shows deregulated metabolic cycles and abnormalities in amino acid metabolism. J. Viral Hepat. 2011;18:E591–E602.

100 Maher AD, Cysique LA, Brew BJ, *et al.* Statistical integration of ^{1}H NMR and MRS data from different biofluids and tissues enhances recovery of biological information from individuals with HIV-1 infection. J. Proteome Res. 2011;10:1737–1745.

101 Sengupta A, Ghosh S, Basant A, *et al.* Global host metabolic response to Plasmodium vivax infection: a H-1 NMR based urinary metabonomic study. Malar. J. 2011;10:384.

102 Weiss RH, Kim K. Metabolomics in the study of kidney diseases. Nat. Rev. Nephrol. 2012; 8:22–33.

103 Xu XH, Huang Y, Wang G, *et al.* Metabolomics: a novel approach to identify potential diagnostic biomarkers and pathogenesis in Alzheimer's disease. Neurosci. Bull. 2012; 28:641–648.

104 Adamko DJ, Sykes BD, Rowe BH, *et al.* The metabolomics of asthma novel diagnostic potential. Chest . 2012;141:1295–1302.

from patients. NMR is useful in the development of reliable and non-invasive protocols for the diagnosis of diseases in early stages, so it could be relevant in the context of atrophic gastritis, as precursor pathology of stomach cancer.

Numerous studies of metabolomics in gastric cancer have been published, mostly using different types of liquid or gas chromatography combined with mass spectroscopy. Differential metabolites are found when comparing patients with cancer and healthy controls. Carbohydrates, amino acids, lipids and nucleic acids are the groups of metabolites affected. As for metabolomics based on NMR, studies also observe metabolic differences between the two groups. However, different pathological types in the Correa model has not been widely studied yet. Yu *et al.* using gas chromatography time-of-flight mass spectrometry (GC/TOF-MS) in plasma samples, demonstrated that metabolic profiles were different in gastric cancer in relation to the precancerous stages but intestinal metaplasia was similar to cancer[105]. Another study based on ^{1}H-NMR urinary metabolomics, despite achieving an area under the curve (AUC) of 0.95 comparing gastric cancer and healthy controls based on three-metabolite model, did not show clear differences between patients with precarcinogenic lesions with cancer or healthy control groups[106].

THE OBESTATIN/GPR39 SYSTEM

Although several molecules have been identified as key in gastric cancer, they are not clinically applied as biomarkers because of their questioned predictive value, being an obstacle for the development of more effective treatments.

A approximation way for the identification of therapeutic targets is the study of systems related to the proliferation of gastric cancer cells. In this sense, obestatin, a 23 amino acid hormone that is derived from the proteolytic

[105] Yu L, Aa J, Xu J, *et al.* Metabolomic phenotype of gastric cancer and precancerous stages based on gas chromatography time-of-flight mass spectrometry. J Gastroenterol Hepatol 26: 1290-1297, 2011.
[106] Chan AW, Mercier P, Schiller D, *et al.* ^{1}H-NMR urinary metabolomic profiling for diagnosis of gastric cancer. Br J Cancer. 2016;114(1):59-62.

Scheme 6. Superimposition of the 20 best representative structures of human obestatin, as calculated from the NMR data for the peptide in SDS micelles. Modified from Alén BO *et al.* PLoS One. 2012;7(10):e45434. (Open access).

cleavage of preproghrelin, originally isolated in the stomach[107] (**Scheme 6**) and its receptor, GPR39, which is involved in both physiological functions and pathologies such as cancer. GPR39 was first characterized in 1997[108], it contains 435 amino acids with seven transmembrane domains. Two different transcripts, GPR39-1a and GPR39-1b, derived from an alternative splicing process, were identified[109].

At the time of its discovery, obestatin was described as an antagonist of ghrelin establishing its anorexogenic role. Although this effect was discarded, over the years many functions have been described for this peptide. Obestatin promotes cell survival and proliferation[110,111,112], participates in glucose

[107] Zhang JV, Ren PG, Avsian-Kretchmer O, *et al.* Obestatin, a peptide encoded by the ghrelin gene, opposes ghrelin's effects on food intake. Science. 2005;310:996-9.

[108] McKee KK , Tan CP, Palyha OC, *et al.* Cloning and characterization of two human G protein-coupled receptor genes (GPR38 and GPR39) related to the growth hormone secretagogue and neurotensin receptors. Genomics. 1997;46:426-34.

[109] Zhang Y, Zhao H, Peng H, *et al.* Two alternatively spliced GPR39 transcripts in seabream: molecular cloning, genomic organization, and regulation of gene expression by metabolic signals. J Endocrinol. 2008;199:457-70.

[110] Camina JP, Campos JF, Caminos JE, *et al.* Obestatin-mediated proliferation of human retinal pigment epithelial cells: regulatory mechanisms. J Cell Phsiol. 2007;211:1-9.

[111] Granata R, Settanni F, Gallo D, *et al.* Obestatin promotes survival of pancreatic β-cells and human islets and induces expression of genes involved in the regulation of β-cell mass and function. Diabetes. 2008;57:967-79.

[112] Zhang JV, Jahr H, Luo CW, *et al.* Obestatin induction of early-response gene expression in gastrointestinal and adipose tissues and the mediatory role of G protein-coupled receptor, GPR39. Mol endocrinol. 2008;22:1464-75.

metabolism, favours adipogenesis[113] and exerts myogenic[114,115], cardiovascular[116,117] and central effects[118,119,120], among others. Obestatin is produced mostly in the stomach and circulating levels have been found. On average, an adult person would have around 50-100 pg/mL in fasting blood. Obestatin levels, like ghrelin, have been decreased in both overweight and obese patients[121]. In addition, patients with anorexia nervosa have seen higher fasting concentrations than healthy controls, showing a reduction with the glucose tolerance test in both groups[122]. These findings postulate obestatin as a possible novel gastrointestinal hormone.

OBESTATIN SIGNALLING

The mitogenic effect of obestatin, described in pancreatic β cells and preadipocytes, is due to binding to GPR39 which stimulates ERK1/2 phosphorylation and potentially Akt[123]. In primary cultures of human retinal pigmented epithelial cells (hRPEs), obestatin induced dose-dependent cell

---

113 Gurriarán-Rodríguez U, Al-Massaddi O, Roca-Rivada A, *et al.* Obestatin as a regulator of adipocyte metabolism and adipogenesis. J Cell Mol Med. 2011;15:1927-40.

114 Gurriarán-Rodríguez U, Santos-Zas I, Al-Massadi O, *et al.* The obestatin/GPR39 system is up-regulated by muscle injury and functions as an autocrine regenerative system. J Biol Chem. 2012;287:38379-89.

115 Gurriarán-Rodríguez U, Santos-Zas I, González-Sánchez J, *et al.* Action of obestatin in skeletal muscle repair: stem cell expansion, muscle growth, and microenvironment remodeling. Mol Ther. 2015;23:1003-21.

116 Xin X, Ren AJ, Zheng X, *et al.* Disturbance of circulating ghrelin and obestatin in chronic heart failure patients especially in those with cachexia. Peptides. 2009;30:2281-5.

117 Ozbay Y, Aydin S, Dagli AF, *et al.* Obestatin is present in saliva: alterations in obestatin and ghrelin levels of saliva and serum in ischemic heart disease. BMB Rep. 2008;41:55-61.

118 Carlini VP, Schioth HB, de Barioglio SR. Obestatin improves memory performance and causes anxiolytic effects in rats. Biochem Biophys Res Commun. 2007;352:907-12.

119 Szakacs J, Csabafi K, Liptak N, *et al.* The effect of obestatin on anxietylike behaviour in mice. Behav Brain Res. 2015;293:41-5.

120 Samson WK, White MM, Price C, *et al.* Obestatin acts in brain to inhibit thirst. Am J Physiol-Regul Integr Comp Physiol. 2007;292:R637-43.

121 Nakahara T, Harada T, Yasuhara D, *et al.* Plasma obestatin concentrations are negatively correlated with body mass index, insulin resistance index, and plasma leptin concentrations in obesity and anorexia nervosa. Biol Psychiatry. 2008;64(3):252-5.

122 Harada T, Nakahara T, Yasuhara D, *et al.* Obestatin, acyl ghrelin, and des-acyl ghrelin responses to an oral glucose tolerance test in the restricting type of anorexia nervosa. Biol Psychiatry. 2008;63(2):245-7.

123 Gargantini E, Grande C, Trovato L, *et al.* The role of obestatin in glucose and lipid metabolism. Horm Metab Res. 2013;45:1002-8.

proliferation with MEK/ERK 1/2 phosphorylation, involving consecutive activation of Gi, PI3K, novel PKC (probably PKCε), and Src for ERK 1/2 activation[110]. The same results in ERK signaling have been observed in human gastric carcinoma cells KATO-III[124]. This group dilucidated a transmembrane signalling pathway responsible for obestatin induced-Akt activation in human gastric carcinoma cells, KATO-III and AGS (**Scheme 7**). Results showed that Akt activation requires the phosphorylation at T308 in the A-loop by the phosphoinositide-dependent kinase 1 (PDK1) and S473 within the HM by the mammalian target of rapamycin (mTOR) kinase complex 2 (mTORC2: RICTOR, mLST8, mSin1, mTOR kinase) with participation neither of $G_{i/o}$-protein nor G_{β} dimers. Obestatin induces the association of GPR39/beta-arrestin 1/Src signalling complex triggering the transactivation of the epidermal growth factor receptor (EGFR) and the consequent Akt activation[125]. Upon administration of obestatin, phosphorylation of both mTOR (S2448) and p70S6K1 (T389) is elevated with a time course in parallel to Akt activation. In this sense, Src performs as a switch that activates proteases to begin EGF-like ligands release on the cell surface, which bind to and activate EGFR posteriorly.

[124] Pazos Y, Álvarez CJ, Camina JP, *et al.* Stimulation of extracellular signal-regulated kinases and proliferation in the human gastric cancer cells KATO-III by obestatin. Growth Factors. 2007;25:373-81.

[125] Alvarez CJ, Lodeiro M, Theodoropoulou M, *et al.* Obestatin stimulates Akt signalling in gastric cancer cells through β-arrestin- mediated epidermal growth factor receptor transactivation. Endocr-Relat Cancer. 2009;16:599-611.

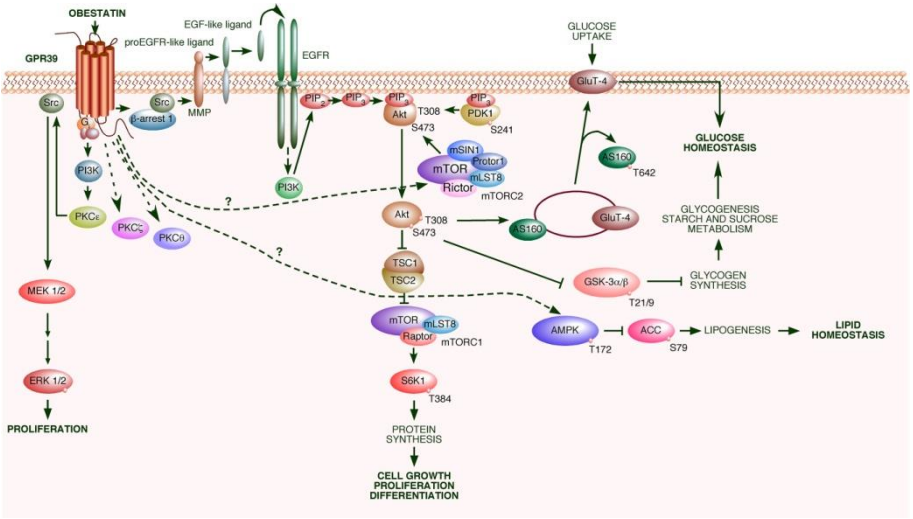

Scheme 7. Proposed model of signalling pathway for Akt and ERK1/2 activation in response to obestatin. Traslocation of β-arrestins 1 to obestatin receptor (GPR39) allows its association with Src. β-arrestin 1 activates Src (phosphorylation at Y416) triggering the transactivation of EGFR and the subsequent downstream Akt signalling. Modified from: Álvarez C *et al.* Endocr-Relat Cancer. 2009;16:599-611, with permission of Bioscientifica Limited.

THE OBESTATIN/GPR39 SYSTEM IN STOMACH

In a healthy human stomach, obestatin expression was observed in the neuroendocrine cells and GPR39 expression was observed in the chief cells of the fundic glands. After the retrospective study of 28 patients with gastric adenocarcinomas, no expression of obestatin was found; however, a GPR39 expression positively correlated with the dedifferentiation degree of the tumour was observed. These findings postulate GPR39 as a good prognostic marker in this pathology[126].

The implication of the obestatin/GPR39 system has been studied in vitro using gastric cancer cell lines. In AGS, a line derived from a gastric adenocarcinoma, obestatin administration favours epithelial-mesenchymal

[126] Alen BO, Leal-Lopez S, Alen MO, *et al.* The role of the obestatin/GPR39 system in human gastric adenocarcinomas. Oncotarget. 2016;7:5957-71.

transition (EMT) and angiogenesis. In addition, changes in cell morphology and an increase in proliferation, migration and invasion of these cells have been observed[126].

According to the obestatin signaling model, Src functions as a switch in the activation of MMPs that release EGF-like ligands that subsequently bind and activate to EGFR. Alterations in expression or mutations in the EGFR family have been implicated in tumor progression[127,128,129]. The studies in gastric cancer cells showed that treatment with obestatin not only regulates MMPs and EGFR, but several families of proteases and RTKs are over-regulated too, establishing the obestatin/GPR39 system as the key to the process of activating cancer-related pathways[130].

[127] Bhola NE, Grandis JR . Crosstalk between G-protein-coupled receptors and epidermal growth factor receptor in cancer. Front Biosci. 2008;13:1857-65

[128] Normanno N, De Luca A, Bianco C, *et al.* Epidermal growth factor receptor (EGFR) signalling in cancer. Gene. 2006;366:2-16.

[129] Ohtsu H, Dempsey PJ, Eguchi S. ADAMs as mediators of EGF receptor transactivation by G-protein-coupled receptors. Am J Phys Cell Physiol. 2006;291:C1-10.

[130] Alén BO. Fundamental structural and biochemical features for the obestatin/GPR39 system mitogenic action. Thesis dissertation. Univesidade de Santiago de Compostela, Santiago de Compostela, Spain. 2016. http://hdl.handle.net/10347/14993

OBJECTIVES

USC
UNIVERSIDADE
DE SANTIAGO
DE COMPOSTELA

The obestatin/GPR39 system regulates the expression of distinctive proteins of the epithelial mesenquimal transition, angiogenesis, cell morphology, proliferation, and invasion of gastric cancer cells, suggesting its applicability to counteract the fundamental mechanisms associated to the development of gastric cancer. If we also consider its relationship with the pathogenesis of gastric human adenocarcinomas and/or clinical result, undoubtedly new ways are opened for the detection and treatment of this type of cancer. Therefore, it is fundamental to explore the way of action of the obestatin/GPR39 system in the pathogenesis of gastric cancer, from the molecular and cellular interactions to the physiological mechanisms and the associated pathological alterations.

The main objective of this doctoral thesis is the study of the GPR39/obestatin system in the development, maintenance and malignancy of the gastric cancer.

This objective is divided into the following subobjectives:

1. To study of the functionality of the obestatin/GPR39 system in healthy stomach.

2. To study of the role of the obestatin/GPR39 system in gastric cancer cell lines.

3. To study of the obestatin/GPR39 system expression in the progression to gastric cancer.

4. To study human biofluids from patients grouped according to Correa's cascade to gastric cancer by NMR metabolomics.

USC
UNIVERSIDADE
DE SANTIAGO
DE COMPOSTELA

MATERIALS AND METHODS

MATERIALS

The peptides, the primary antibodies, the secondary antibodies, the other chemicals, the proteome profiler human protease array and the human RTK phosphorylation antibody array are listed in **Table 2**, **3**, **4**, **5**, **6** and **7**, respectively. Manufacters of all other materials utilized are stated along the text.

CELLS

Cell culture

The following human gastric cancer cells lines were used in this work. AGS and KATO-III cells were purchased from Sigma/ATCC. NCI-N87 cell line was kindly provided by Dr. A. Cervantes (Cancer Area at the Institute of Health Research INCLIVA, Valencia, ES).

All of the cell lines used in this work were cultured as described by the supplier (ATCC, Manassas, VA, US) with 100 U/mL penicillin G, 100 mg/mL streptomycin sulphate and 2.5 mM L-glutamine with 5% CO_2 at 37 °C. Cells were passaged at 85-90% confluence using Accutase® (Sigma-Aldrich, St. Louis, MO, US).

Table 1. Cells. Relation of human cell lines and its growth medium used in this work. FBS: fetal bovine serum.

Cell line	Growth medium (v/v)
AGS. Gastric adenocarcinoma	HAM´s F12 + 10% FBS
KATO III. Gastric carcinoma	RPMI 1640 + 10% FBS
NCI-N87. Gastric carcinoma	DMEM F12 + 10% FBS

HUMAN SAMPLES

Stomach endoscopies

The study protocol of stomach endoscopies was approved by the local ethical committee (CAEI Galicia, 2014/050) and carried according to the Declaration of Helsinki and its latter amendments. All 110 patients signed the informed consent prior to the inclusion in the study.

Samples from the collection of a recent study by our research group, carried out by F. Macías, on the diagnostic efficacy of a panel of serological biomarkers were used to determine the existence of chronic atrophic gastritis compared to histology in patients with uninvestigated dyspepsia. A mapping was performed by taking biopsies from four parts of the stomach (antrum, body, fundus and incisura angularis) for a correct classification of the patients. Histological classification was performed according to the updated Sidney visual system scale[74].and the OLGA[131] and OLGIM[132] systems: 39 were health, 42 non atrophic gastritis, 13 corpus atrophy, 11 antrum atrophy and 5 multifocal atrophy. An external group of dysplasia was formed to perform the immunohistochemical study of the complete carcinogenic sequence. *Helicobacter pylori* infection was diagnosed by three different methods: culture, urease test and histological visualization.

Two stomach biopsies from fundus were transferred to the laboratory, at the time of the endoscopy, one in a saline buffer and the other in formaldehyde 4% solution at room temperature. The biopsy collected in formalin was fixed in the same solution overnight for immunohistochemistry analysis. The other biopsy was divided in two comparable sections. The pieces were placed in 96-multiwell dishes and warmed up in DMEM medium without phenol red supplemented with 100 U/mL penicillin G, 100 U/mL streptomycin sulfate and 2.5 mM L-glutamine with 5% CO_2 at 37 °C. Briefly, the pieces placed in 200 µL medium were treated with human obestatin 200 nM for 2 h. After this time, secretomes were collected and tissues were placed at 4 °C and disposed for immunoblot analysis.

Secretome. Every secretome was collected, centrifuged (1800 rpm, 5 min). Protease inhibitor cocktail (PIC; Sigma Chemical Co, St. Louis, MO, US) and phosphatase inhibitor cocktail (PHI; Sigma Chemical Co, St. Louis, MO, US) were added to the samples and stored at -80 °C until use.

---

131 Rugge M, Genta RM. OLGA Group. Staging gastritis: an international proposal. Gastroenterology 2005;129:1807-8.

132 Capelle LG, de Vries AC, Haringsma J, Ter Borg F, de Vries RA, Bruno MJ et al. The staging of gastritis with the OLGA system by using intestinal metaplasia as an accurate alternative for atrophic gastritis. Gastrointest Endosc 2010;71(7):1150-8.

Lysate. After the explant culture, all of tissues were weighted and processed for immunoblot.

Biofluids

The study was carried out with the protocol approved by the local ethical committee (CAEI Galicia, 2014/050). Blood and urine samples were collected from the same patients explained in the previous point.

Urine samples: The urine was collected in a 100 mL sterile container. Information on how to do this was explained to the patient and the necessary material was provided. The samples were kept on ice (4 ºC) and sodium azide (NaN_3) 0.05% w/v was added to avoid bacterial growth. Urine was stored in aliquots at -80 ºC until analysis.

Plasma samples: A 4 mL tube with lithium heparin was used for the blood sample to reduce interferences in the subsequent analysis and turned 180° about 8-10 times. Blood was centrifuged at 1600 xg at 4 ºC for 15 min to obtain plasma. It was stored in aliquots at -80 ºC until analysis.

Stomach from bariactric surgery

The study protocol was approved by the local ethical committee (CAEI Galicia, 2009/118 and 2014/050) and was therefore performed in accordance with the ethical standards laid down in the 1964 Declaration of Helsinki and its latter amendments. All persons gave their informed consent prior to their inclusion in the study.

The stomach samples were obtained from patients who underwent bariatric surgery thanks to the collaboration of Dr. J Baltar, doctor of the General and Digestive Surgery Service at the Complexo Hospitalario Universitario de Santiago de Compostela. These patients were free of *Helicobacter pylori*. The samples were obtained from the fundic region of the stomach, and originated from macro- and microscopically normal gastric mucosa.

Tissues were transferred to the laboratory, at the time of the surgery, in a saline solution at room temperature. The tissue was divided in comparable sections (13-14), approximately 1.5 cm^2 each. One of the portions was fixed using formaldehyde overnight for immunohistochemistry analysis. The rest

of the pieces were placed in 6-multiwell dishes and warmed up in DMEM medium without phenol red supplemented with 100 U/mL penicillin G, 100 U/mL streptomycin sulfate and 2.5 mM L-glutamine with 5% CO_2 at 37 °C. After this process, a kinetic and a dose-response study was performed. Briefly, the pieces placed in 5 mL medium were treated with human obestatin (50, 100 and 200 nM) for different times (5, 20, 40 and 60 min). After the corresponding treatments, secretomes were collected and tissues were placed at 4 °C and disposed for immunoblot, immunohistochemical or protein array analysis.

Secretome. Every secretome was collected, centrifuged (1800 rpm, 5 min), and the supernatant was then filtered with a 3 KDa Amicon filter (Merck Millipore, Billerica, MA, US) and concentrated by centrifugation (3,200 rpm, 4 °C) to a final volume of approximately 750 μL. Protease inhibitor cocktail (PIC; Sigma Chemical Co, St. Louis, MO, US) and phosphatase inhibitor cocktail (PHI; Sigma Chemical Co, St. Louis, MO, US) were added to the samples and stored at -80 °C until use.

Lysate. After the explant culture, all of the tissues were weighted. Then, each explant was divided in two pieces. The first piece was fixed in formaldehyde overnight for IH. From the second one, the mucosa was separated from the muscularis and weighted. This mucosa was then processed for immunoblot or protein array.

Tables

Table 2. Peptides. Relation of the peptides used in the different analyses performed in this work.

Materials	Code	Manufacturer
Human obestatin	471-97	California Peptide Research Inc (Napa, CA, US)
Human obestatin	SE-4764	Biomedal (Sevilla, ES)

Table 3. Primary antibodies. Relation of the antibodies used in the different analyses performed in this work. Abbreviations: IC: immunocytochemistry; IF: immunofluorescence; IH: immunohistochemistry; WB: western blot.

Antibodies	Use	Dilution	Code	Manufacturer
Anti-Human GPR39 (C-terminal region) Antibody	IC, IH IF WB	1:500 1:500 1:1000	SAB4200185	Sigma Chemical
Anti-GPR39 Antibody	WB	1:1000	NLS139	Novus Biologicals
Anti-GPCR GPR39 Antibody	WB	1:1000	ab39227	Abcam
Anti-Mouse/Rat/Human Obestatin Peptide Antibody	IC, IH	1:500	OBSN11-A	Alpha Diagnostic International
Phospho-p44/42 MAPK (Erk1/2) (Thr202/Tyr204) Antibody	WB	1:2500	9101S	Cell Signaling Technology
Phospho-Akt (Ser473) Antibody	WB	1:1000	9271	Cell Signaling Technology
Phospho-PKCα/β II (Thr638/641) Antibody	WB	1:1000	9375	Cell Signaling Technology
Anti-phospho PKC γ (T674)	WB	1:1000	KAP-PK012	Stressgen
Phospho-PKA C (Thr197) (D45D3)	WB	1:1000	5661	Cell Signaling Technology
Anti- Gastric Lipase Antibody	IC, IF, IH WB	1:50 1:1000 1:1000	sc-390749	Santa Cruz BioTech.
Anti-Pepsinogen I antibody [7G3]	IC IF, IH	1:50 1:1000	ab50123	Abcam
Anti-Pepsinogen I antibody	WB	1:2500	ab135403	Abcam
Anti-Cathepsin D Antibody (C-5)	WB	1:200	sc-377124	Santa Cruz BioTech.
Anti-Cathepsin L Antibody	WB	1:1000	ab133641	Abcam
Anti-Cathepsin Z Antibody (F-6)	WB	1:500	sc-376976	Santa Cruz BioTech.
Anti-GAPDH Antibody	WB	1:2000	ab9485	Abcam
Anti-Active beta-Catenin Antibody	WB	1:1000	05-665	Millipore
Anti-E-Cadherin (M168) Antibody	IF WB	1:500- 1:1000 1:1000	ab76055	Abcam
Anti-N-Cadherin (EPR1791-4) Antibody	WB	1:1000	ab76011	Abcam
Anti-Vimentin Antibody	WB	1:1000	ab92547	Abcam
Anti-Flk1 (C-1158) Antibody	WB	1:500	sc-504	Santa Cruz BioTech.
Anti-VEGF (A-20) Antibody	WB	1:500	sc-152	Santa Cruz BioTech.
Anti-PEDF (H-125) Antibody	WB	1:500	sc-25594	Santa Cruz BioTech.
Anti-EGFR Antibody	WB	1:1000	2232	Cell Signaling Technology

Table 3 (continued). Primary antibodies. Relation of the antibodies used in the different analyses performed in this work. Abbreviations: WB: western blot.

Antibodies	Use	Dilution	Code	Manufacturer
Anti phospho-EGFR (Tyr845)-R Antibody	WB	1:200	Sc-23420	Santa Cruz BioTech.
Anti phospho-EGF Receptor (Tyr992) Antibody	WB	1:1000	2235	Cell Signalling Tech.
Anti Phospho-EGF Receptor (Tyr1045) Antibody	WB	1:1000	2237	Cell Signalling Tech.
Anti EGFR Phosphorylated (Tyr1068) Antibody	WB	1:500	656302	Biolegend
Anti EGFR vIII Antibody	WB	1:250	Orb 191506	BioOrbyt
Anti PAR1-Thrombin receptor Antibody	WB	1:1000	NBP2-61770	Novus
Anti-PAR2 Antibody	WB	1:1000	Ab180953	Abcam
Anti-PAR4 Antibody	WB	1:1000	NBP1-71365	Novus
Anti Human NM23-H1 Antibody	WB	1:1000	MAB6256	R&D Systems

Table 4. Secondary antibodies. Relation of the secondary antibodies used in the different analyses performed in this work. Abbreviations: IC: immunocytochemistry; IF: immunofluorescence; IH: immunohistochemistry; WB: western blot.

Antibodies	Use	Dilution	Code	Manufacturer
EnVision™ FLEX, High pH, (Link)	IC IH	Ready to Use	K8000	Dako Agilent
Peroxidase-AffiniPure Goat Anti-Rabbit IgG (H+L)	WB	1:10000	111-035-003	Jackson ImmunoResearch Europe
Peroxidase-AffiniPure Goat Anti-Mouse IgG (H+L)	WB	1:10000	115-035-003	Jackson ImmunoResearch Europe
Alexa Fluor 594 Antibody	IF	1:1000	A-11012	ThermoFisher Scientific
Alexa Fluor 488 Goat Anti-mouse	IF	1:1000	A11029	ThermoFisher Scientific
Goat Anti-Rabbit IgG Fc (Alexa Fluor® 488)	IF	1:1000	ab150089	Abcam

Table 5. Other chemicals. Relation of the other chemicals used in the different analyses performed in this work. Abbreviations: IA: invasion assay; IC: immunocytochemistry; IF: immunofluorescence.

Other chemicals	Use	Dilution	Code	Manufacturer
ProLong™ Gold Antifade Mountant with DAPI	IF	Ready to use	P36931	Invitrogen
Phalloidin CruzFluor™-594	IF	1:1000	sc-363795	Santa Cruz Biotechnology, Inc.
Calcein acetoxymethyl ester	IA	4 µmol/L		Invitrogen

Table 6. Proteome profiler human protease array. Human proteases included in the array and the corresponding coordinates. R&D Systems (Minneapolis, MN, US).

Coordinate	Analyte/Control	Isoform Specificity	Alternate nomenclature
A1,A2	**Reference spots**		**RS**
A3,A4	**ADAM8**	**Ectodomain**	**MS2, CD156a**
A5,A6	**ADAM9**	**Ectodomain**	**MDC9, meltrin g**
A7, A8	**ADAMTS1**	**Proform**	**METH1**
A9, A10	**ADAMTS13**	**Active**	**von Willebrand factor-cleaving protease**
A11, A12	**Cathepsin A**	**Proform & Active**	**CTSA, Lysosomal Carboxypeptidase A**
A13, A14	**Cathepsin B**	**Proform**	**CTSB, APPS, CPSB**
A15, A16	**Cathepsin C**	**Proform & Active**	**CTSC**
A17, A18	**Cathepsin D**	**Proform & Active**	**CTSD, CPSD**
A19, A20	**Reference Spots**		**RS**
B3, B4	**Cathepsin E**	**Proform & Active**	**CTSE, CATE**
B5, B6	**Cathepsin L**	**Proform & Active**	**CTSL, CATL, MEP, Cathepsin L1**
B7, B8	**Cathepsin S**	**Proform & Active**	**CTSS**
B9, B10	**Cathepsin V**	**Proform & Active**	**CTSV, CTSL2, CTSU, Cathepsin L2**
B11, B12	**Cathepsin X/Z/P**	**Proform & Active**	**CTSX, CTSZ**
B13, B14	**DPPIV/CD26**	**Ectodomain**	**ADABP, ADCP2**
B15, B16	**Kallikrein 3/PSA**	**Proform & Active**	**KLK3, hK3, KLK2A1**
B17, B18	**Kallikrein 5**	**Proform & Active**	**KLK4, SCTE, KLKL2**
C3, C4	**Kallikrein 6**	**Proform & Active**	**KLK6**
C5, C6	**Kallikrein 7**	**Proform & Active**	**KLK7, SCCE, PRSS6, hK7**
C7, C8	**Kallikrein 10**	**Proform & Active**	**KLK10, NES1, PRSSL1**
C9,C10	**Kallikrein 11**	**Proform & Active**	**KLK11, TLSP, PRSS20**
C11,C12	**Kallikrein 13**	**Proform & Active**	**KLK13, KLKL4**
C13,C14	**MMP1**	**Proform & Active**	**Collagenase 1, Interstitial Collagenase**
C15,C16	**MMP2**	**Proform & Active**	**Gelatinase A**
C17,C18	**MMP3**	**Proform & Active**	**Stromelysin-1**
D3,D4	**MMP7**	**Proform & Active**	**Matrilysin, PUMP1**

Table 6 (continued). Proteome profiler human protease array. Human proteases included in the array and the corresponding coordinates. R&D Systems (Minneapolis, MN, US).

Coordinate	Analyte/Control	Isoform Specificity	Alternate nomenclature
D5,D6	**MMP8**	Proform & Active	Collagenase 2, Neutrophil Collagenase
D7, D8	**MMP9**	Proform & Active	Gelatinase B, CLG4B, GELB
D9, D10	**MMP12**	Proform & Active	Macrophague Elastase
D11, D12	**MMP13**	Proform	Collagenase 3
D13, D14	**Neprilysin/CD10**	Ectodomain	MME, NEP, CALLA
D15,D16	**Presenilin-1**	N-terminal fragment	PSEN1, AD3, PS-1
D17,D18	**Proprotein Convertase 9**	Active	PC9, NARC1
E1, E2	**Reference spots**		RS
E3, E4	**Proteinase 3**	Active	PRTN3, Myeloblastin
E5, E6	**uPA/Urokinase**	Proform & Active	Urokinase-type Plasminogen Activator, PLAU
E7,E8	Negative Control		Control (-)

Table 7. Human RTK phosphorylation antibody array. Human RTKs included in the array and the corresponding coordinates. Abcam (Cambridge, UK).

Coordinate	Analyte/Control	Coordinate	Analyte/Control	Coordinate	Analyte/Control
A1, B1	**POS 1**	C1, D1	**POS 2**	E3, F3	**POS 3**
G1, H1	**ABL1**	I1, J1	**ACK1**	K1,L1	**ALK**
A2, B2	**NEG**	C2, D2	**NEG**	E2, F2	**Axl**
G2, H2	**Blk**	I2, J2	**BMX**	K2, L2	**Btk**
A3, B3	**Csk**	C3,D3	**Dtk**	E3, F3	**EGF R**
G3, H3	**Eph A1**	I3, J3	**Eph A2**	K3, L3	**Eph A3**
A4, B4	**Eph A4**	C4, D4	**Eph A5**	E4, F4	**Eph A6**
G4, H4	**Eph A7**	I4, J4	**Eph A8**	K4, L4	**Eph B1**
A5, B5	**Eph B2**	C5,D5	**Eph B3**	E5, F5	**Eph B4**
G5, H5	**EphB6**	I5, J5	**EerB2**	K5, L5	**EerB3**
A6, B6	**EerB4**	C6, D6	**FAK**	E6, F6	**FER**
G6, H6	**FGF R1**	I6, J6	**FGF R2**	K6, L6	**FGF R2 (α isoform)**
A7, B7	**Fgr**	C7, D7	**FRK**	E7, F7	**Fyn**
G7, H7	**Hck**	I7, J7	**HGF R**	K7, L7	**IGF IR**
A8, B8	**Insulin R**	C8,D8	**Itk**	E8, F8	**JAK1**
G8, H8	**JAK2**	I8, J8	**JAK2**	K8, L8	**LCK**

Table 7 (continued). Human RTK phosphorylation antibody array. Human RTKs included in the array and the corresponding coordinates. Abcam (Cambridge, UK).

Coordinate	Analyte/Control	Coordinate	Analyte/Control	Coordinate	Analyte/Control
A9, B9	**LTK**	C9, D9	**Lyn**	E9, F9	**MAT K**
G9, H9	**M-CSFR**	I9, J9	**MUSK**	K9, L9	**NGFR**
A10, B10	**PDGFR-α**	C10, D10	**PDGFR-β**	E10, F10	**PYK2**
G10, H10	**RET**	I10, J10	**ROR 1**	K10, L10	**ROR 2**
A11, B11	**ROS**	C11, D11	**RYK**	E11, F11	**SCFR**
G11, H11	**SRMS**	I11, J11	**SYK**	K11, L11	**Tec**
A12, B12	**Tie-1**	C12, D12	**Tei-2**	E12, F12	**TNK-1**
G12, H12	**TRK B**	I12, J12	**TXK**	K12, L12	**NEG**
A13, B13	**Tyk 2**	C13, D13	**TYRO10**	E13, F13	**VEGFR 2**
G13, H13	**VEGFR 3**	I13, J13	**ZAP70**	K13, L13	**POS 4**

METHODS

IMMUNOBLOT ANALYSIS

Immunoblot analysis in cells

Serum-starved cells were stimulated with obestatin and for the indicated time period and doses at 37 °C. The medium was then aspirated, and cells were lysed in ice-cold lysis buffer [50 mM Tris-HCl pH 7.2, 150 mM NaCl, 1 mM EDTA, 1% (v/v) NP-40, 0.25% (w/v) Na-deoxycholate, protease inhibitor cocktail (PIC) (1:100, Sigma Chemical Co., St. Luis, MO, US), phosphatase inhibitor cocktail (PHIC) (1:100, Sigma Chemical Co., St. Luis, MO, US)]. The soluble cell lysates were pre-cleared by centrifuging at 14,000 rpm for 15 min. The protein concentration was evaluated with the QuantiPro™ BCA Assay kit (Sigma Chemical Co., St. Luis, MO, US). The same amount of protein for each sample was separated on 7 or 10% SDS/polyacrylamide gels and transferred to nitrocellulose membranes (Bio-Rad, Hercules, CA, US). The blots were incubated with 5% bovine serum albumin (BSA) in a Tris buffer solution (TBS) containing Tween-20 (TBST) [20 mM Tris-HCl (pH 8.0), 150 mM NaCl, 0.1% (v/v) Tween-20, solution used for all incubation

and washing steps] for 1 h. The blots were then incubated with the corresponding primary antibodies, according to the above indications, and were subsequently incubated with the corresponding peroxidase-conjugated IgG antibody. After washing, the signals were visualized using an ECL plus Western Blotting Detection System (Pierce ECL Western Blotting Substrate; Thermo Fisher Scientific, Pierce, Rockford, IL). Blots shown are representative of three or more experiments. The image processing was performed using the NIH Image Sofware ImageJ 1.50b (National Institutes of Health, Bethesda, MD, US).

Inmunoblot analysis in human tissue samples

Tissues were disrupted and homogenized in ice-cold lysis buffer [50 mM Tris-HCl pH 7.2, 150 mM NaCl, 1 mM EDTA, 1% (v/v) NP-40, 0.25% (w/v) Na-deoxycholate, protease inhibitor cocktail (PIC) (1:100, Sigma Chemical Co., St. Luis, MO, US), phosphatase inhibitor cocktail (PHIC) (1:100, Sigma Chemical Co., St. Luis, MO, US)] with 5 mm stainless steel beads using a Tissue lyser (Qiagen, Hilden, DE) at 30 Hz for 3 min. The soluble cell lysates were pre-cleared by centrifuging at 14,000 rpm for 15 min. After centrifugation at 14,000 xg for 5 min at RT, supernatants were recovered and the protein was quantified with the QuantiProTM BCA Assay kit (Sigma Chemical Co., St. Luis, MO, USA). The same amount of protein for each sample was separated on 7-10% SDS/polyacrylamide gels and transferred to nitrocellulose membranes (Bio-Rad, Hercules, CA, US). The blots were then incubated with the corresponding antibodies and processed as described above. The image processing was performed using the NIH Image Sofware ImageJ 1.50b (National Institutes of Health, Bethesda, MD, US).

CELL PROLIFERATION ASSAYS

For NCI-N87 cells, cell proliferation was measured using a bromodeoxiuridine (BrdU) cell proliferation enzyme-linked immunosorbent assay (ELISA) kit (Roche Diagnostics, Mannheim, DE). The BrdU assay was performed according to the manufacturer's protocol. Cells were cultured in a 96-well multiplate at a density of 2-5 x 10^3 cells per well in the culture medium

described above for 24 h. The procedure comprised the following steps: 1) 0% FBS for 24 h; 2) stimulation with obestatin and for the indicated time period and doses; 3) incubation with BrdU-labeling solution (10 µL, 3 h, 37 °C); 4) removal of labeling solution and fixing with FixDenat solution (200 µL, 30 min, 25 °C); 5) incubation with anti-BrdU-peroxidase (POD) antibody solution (100 µL, 90 min, 25 °C); and, 6) washing followed by the addition of substrate solution (100 µL, 30 min). The BrdU incorporation was quantified using the spectrophotometric absorbance (370 nm) measured with a VersaMaxPLUS Reader (Molecular Devices, Sunnyvale, CA, US). The mean absorbance of the control cells represented 100% cell proliferation, and the mean absorbance of the treated cells was related to the control values to determine sensitivity. In all cases, each experiment point was replicated eight times. For AGS and non-adherent cell line KATO III, a Trypan Blue protocol was used for viable cell counting. To ensure the reliability of the experimental procedure, the adherent HT-29 cell line was also subjected to the same protocol. In brief, the cells were cultured in a 96-well multiplate at a density of 5 x 10^3 cells per well in the serum-free medium described in Table 2 for 24 h. The cells were then treated with 100 nM human obestatin, 10% FBS (positive control), 40 µM $ZnCl_2$, and 100 nM obestatin plus 40 µM $ZnCl_2$ for 48 h. For cell counting, a cell suspension in PBS was prepared. Sequentially, 0.5 mL of 0.4% Trypan Blue solution (w/v), 0.3 mL PBS and 0.2 mL of the cell suspension were added to a test tube, mixed thoroughly, and allowed to stand for 5-15 min. A hemacytometer was used to count viable cells as non-viable cells stained blue. Total cells were calculated using the following equations: Cells per mL = the average count per square × dilution factor × 10^4 (count 10 squares). Total Cells = cells per ml × the original volume of fluid from which cell sample was removed. Cell Viability (%) = total viable cells (unstained) ÷ total cells (stained and unstained) × 100. In all cases, each experiment point was replicated eight times.

IMMUNOCYTOCHEMISTRY

Immunocytochemistry detection of GPR39 and obestatin in AGS, KATO-III and NCI-N87 cells

AGS and KATO-III. Cells were cultured at a density of 4-8 x 10^3 cells per well in the culture medium described above on 8-well Lab-Tek II chamber slides covered with cell conditioning solution 2 (CC2) glass slide coverslips. After 2 days, the medium was renewed, and the cells were cultured in a serum-free medium (300 µL) for 24 h. After this time, the intact cells were fixed in 96% ethanol for 1 h. The immunocytochemical technique was automatically performed using an AutostainerLink 48 instrument (Dako Agilent Technologies, Glostrup, DK). The corresponding primary antibodies was used. EnVision™ peroxidase FLEX/HRP (Dako Agilent Technologies, Glostrup, DK) was employed as a detection system. Briefly, the procedure comprised the following steps: 1) epitope retrieval in 10 mM citrate buffer (pH 6.0) using a microwave (750 W, 10 min); 2) incubation with peroxidase-blocking agent (5 min); 3) incubation without (negative control) or with primary antibody (30 min); 4) incubation with labeled polymer-horseradish peroxidase (HRP, dextran polymer conjugated with HRP and affinity-isolated immunoglobulins); 30 min); 5) incubation with 3,3'-diaminobenzidine (DAB)-tetrahydrochloride (Dako Liquid DAB + Substrate-chromogen system) (10 min); and 6) counterstaining with Harris hematoxylin solution (HHS) (9 min). In all cases, triplicate dishes were used for each experimental point. Digital images of cells were acquired with a Zeiss Axio Vert.A1 fluorescence microscope (Carl Zeiss AG, Oberkochen, Germany).

NCI-N87 cells. Cells were cultured at a density of 4-5 x 10^3 cells per well in the culture medium described above on 8-well Lab-Tek II chamber slides covered with cell conditioning solution 2 (CC2) glass slide coverslips. At the next day the intact cells were fixed in formol 4 ºC for 15 min, methanol -20 ºC for 4 min and acetone -20 °C for 2 min. Briefly, the procedure comprised the following steps: 1) epitope retrieval with Dako cytomation Target Retrieval Solution pH 6.0 1x for 20 min by microwave incubation at 750 W and cooling at RT for 20 min; 2) incubation without (negative control) or with the corresponding antibody overnight RT; 3) incubation with peroxidase-

blocking agent for 10 min; 4) incubation with labelled polymer-horseradish peroxidase (HRP, dextran polymer conjugated with HRP and affinity-isolated immunoglobulins) for 30 min; 5) incubation with 3,3'-diaminobenzidine (DAB)-tetra hydrochloride (Dako Liquid DAB + Substrate-chromogen system) for 10 min; and finally 6) counterstaining with Harris haematoxylin solution (HHS) (30 s). In all cases, triplicate dishes were used for each experimental point.

Immunocytochemistry detection of pepsinogen and gastric lipase in AGS and NCI-N87 cells

Cells were cultured directly on the glass slides in the culture medium described above. At the next day the intact cells were fixed in formol 4 ºC for 15 min, methanol -20 ºC for 4 min and acetone -20 °C for 2 min. Briefly, the procedure comprised the following steps: 1) epitope retrieval with Dako cytomation Target Retrieval Solution pH 6.0 1x for 20 min by microwave incubation at 750 W and cooling at RT for 20 min; 2) permeabilized with 0,25% Triton X-100 in PBS for 20 min; 3) incubation without (negative control) or with the corresponding antibody overnight RT; 3) incubation with peroxidase-blocking agent for 10 min; 4) incubation with labelled polymer-horseradish peroxidase (HRP, dextran polymer conjugated with HRP and affinity-isolated immunoglobulins) for 30 min; 5) incubation with 3,3'-diaminobenzidine (DAB)-tetra hydrochloride (Dako Liquid DAB + Substrate-chromogen system) for 10 min; and finally 6) counterstaining with Harris haematoxylin solution (HHS) (30 s). In all cases, triplicate dishes were used for each experimental point.

IMMUNOHISTOCHEMISTRY

Immunohistochemistry detection of GPR39, obestatin, pepsinogen I and gastric lipase in human gastric mucosa samples

Immunohistochemistry was performed according to the protocol used by Raghay *et al.*[133] In brief, the samples were immersion-fixed in 10% buffered formalin for 24 h, dehydrated and embedded in paraffin by a standard procedure. The 3 μm-thick sections were mounted on Histobond adhesion microslides (Marienfeld, Lauda-Königshofen, DE), dewaxed and rehydrated. Antigen retrieval was performed in PT-Link (Dako Agilent Technologies, Glostrup, DK) for 20 min at 97 °C in low pH buffered solution (Dako Agilent Technologies, Glostrup, DK). The immunohistochemical technique was automatically performed using an AutostainerLink 48 instrument (Dako Agilent Technologies, Glostrup, DK). For detection of obestatin, GPR39, pepsinogen I and gastric lipase, the corresponding antibodies were incubated for 20 min. EnVision™ peroxidase FLEX/HRP (Dako Agilent Technologies, Glostrup, DK) was employed as a detection system. All sections were counterstained with HHS for 15 min. Photographs were taken using Olympus BX51 microscope (Olympus Corporation, Japan).

IMMUNOFLUORESCENCE ANALYSIS

Immunofluorescence detection of F-actin and E-cadherin in AGS, KATO III and NCI-N87 cells

Cells were cultured at a density of 10 x 10^5 cells per well in the culture media described above on 12-well plates. After 2 days, medium was renewed, and cells were cultured in a serum-free medium for 24 h. Serum-starved cells were stimulated or not with obestatin (200 nM, 48 h) at 37 °C. After 48 h, intact cells were fixed with 4% buffered paraformaldehyde with PBS (PFA-PBS) for 30 min, washed, permeabilized with 0.25% Triton X-100 in PBS for 45 min, and blocked with 1% BSA in PBS containing 0.2% Tween-20 (PBST) for 30 min. Cells were incubated with anti-E-cadherin mouse monoclonal antibody

[133] Raghay K, Garcia-Caballero T, Bravo S, *et al.* Ghrelin localization in the medulla of rat and human adrenal gland and in pheochromocytomas. Histol Histopathol. 2008;23:57-65.

diluted in 1% BSA in PBST (1:500 in AGS and 1:1000 in KATO-III and NCI-N87 cells) for 1 h at RT. After three washes with PBS, cells were incubated with the secondary antibody (Alexa 488 anti-mouse antibody (1:1000)) and Phalloidin CruzFluor 594 in 1% BSA in PBST (1:1000) for 1 h at RT. DAPI was used to counterstain the cell nuclei. Digital images of cells were acquired with a Zeiss Axio Vert.A1 fluorescence microscope (Carl Zeiss AG, Oberkochen, Germany).

ARRAY PROTEIN ASSAYS

Human Phospho-RTK Array and analysis

To analyze the activation profiles of RTKs the human RTK Phosphorylation Antibody Array (Abcam, Cambridge, UK) was used according to the manufacturer's instructions. This method allows simultaneous detection of the relative tyrosine phosphorylation levels of 71 different phospho-RTKs. Each array contained duplicate validated control and capture antibodies for specific RTKs. Stomach samples were placed in 6-multiwell dishes and warmed up in DMEM medium without phenol red supplemented with 100 U/mL penicillin G, 100 U/mL streptomycin sulfate and 2.5 mM L-glutamine with 5% CO_2 at 37 °C. The pieces placed in 5 mL medium were treated with human obestatin (200 nM) for 5 min. After the corresponding treatment, tissues were directly lysed in ice-cold lysis buffer [50 mM Tris-HCl (pH 7.2), 150 mM NaCl, 1 mM EDTA, 1% (v/v) NP-40, 0.25% (w/v) Na-deoxycholate, PIC (1:100), PHIC (1:100)]. Tissue lysates were diluted in a ratio 1:10 for further steps. Lysates were pre-cleared by centrifugation (14,000 rpm, 15 min, 4°C), and the protein concentration was quantified using the QuantiProTM BCA assay kit (Sigma Chemical Co, St. Louis, MO, US). The membranes were incubated with 200 μg of protein. Briefly, phospho-RTK array membranes were blocked with Block Buffer (30 min) and incubated O/N with 1 mL of cell and tissue lysate after normalization for equal amounts of protein. After extensive washing with Wash Buffer the membranes were incubated with Biotinylated Anti-Phosphotyrosine Antibody (RT, 2 h). After extensive washing with Wash Buffer the membranes were incubated with HRP-Conjugated Streptavidin (RT, 2 h). Each array was then incubated with

equal volumes (1:1) of Detection Buffer C and Detection Buffer D, and exposed to X-ray film (1-10 min). Dot blot densitometric analysis of the immunoblots was performed in duplicate, using NIH ImageJ software 1.50b (National Institutes of Health, Bethesda, MD, US). The relative phosphorylation profiles in 2 groups were normalized by using mean of positive control spots that are located in all 4 corners of the array. Fold changes were calculated by dividing untreated phosphorylation profile to treated profile accordingly[134].

Human Protease Array and analysis

To analyze the expression profiles of protease proteins we used the Proteome Profiler™ Human Antibody Array Kit (R&D Systems, Minneapolis, MN, USA), according to the manufacturer's instructions. This method allows for simultaneous detection of the relative expression levels of 34 different proteases. Each array contained duplicate validated control and capture antibodies for specific proteases. Lysate and secretome of the stomach explants were used. Stomach samples were placed in 6-multiwell dishes and warmed up in DMEM medium without phenol red supplemented with 100 U/mL penicillin G, 100 U/mL streptomycin sulfate and 2.5 mM L-glutamine with 5% CO_2 at 37 °C. The pieces placed in 5 mL medium were treated with human obestatin (200 nM) for 20 min. After the corresponding treatment, secretomes were collected and tissues were placed at 4 °C.

Secretome. Every secretome was collected, centrifuged (1800 rpm, 5 min), and the supernatant was then filtered with a 3 KDa Amicon filter (Merck Millipore, Billerica, MA, US) and concentrated by centrifugation (3,200 rpm, 4 °C) to a final volume of approximately 750 μL. Protease inhibitor cocktail (PIC; Sigma Chemical Co, St. Louis, MO, US) and phosphatase inhibitor cocktail (PHIC; Sigma Chemical Co, St. Louis, MO, US) were added to the samples and stored at -80 °C until use.

[134] Kumar D, Moore R, Nash A, *et al.* Decidual GM-CSF is a critical common intermediate necessary for thrombin and TNF induced in-vitro fetal membrane weakening. Placenta. 2014;35:1049-56.

Lysate. After the explant culture, all of the tissues were weighted. Then, each explant was divided in two pieces. The first piece was fixed in formaldehyde overnight for IH. From the second one, the mucosa was separated from the muscularis and weighted. This mucosa was directly lysed in ice-cold lysis buffer [50 mM Tris-HCl (pH 7.2), 150 mM NaCl, 1 mM EDTA, 1% (v/v) NP-40, 0.25% (w/v) Na-deoxycholate, PIC (1:100), PHIC (1:100)]. Tissue lysates were diluted in a ratio 1:10 for further steps.

Lysates and secretomes were pre-cleared by centrifugation (14,000 rpm, 15 min, 4°C), and the protein concentration was quantified using the QuantiProTM BCA assay kit (Sigma Chemical Co, St. Louis, MO, US). The membranes were incubated with 200 μg of lisate or 200 μg of secretome protein. Briefly, protease array membranes were blocked with Block Buffer for 1 hour. Supernatants and lysates of treated and untreated cells were centrifuged and mixed with 15 μl of Detection Antibody Cocktail for 1 h at RT. Then, the membranes were incubated with the sample/antibody mixtures O/N at 4 °C on a rocking platform. Following a washing step to remove unbound material, membranes were incubated with Streptavidin-HRP reagent for 30 minutes. The unbound Streptavidin-HRP reagent was washed with Wash Buffer. Each array was then incubated with Chemi Reagent Mix, and exposed to X-ray film for 1-10 minutes. Dot blot densitometric analysis of the immunoblots was performed in duplicate, using NIH ImageJ software 1.49 (National Institutes of Health, Bethesda, MD, US). The relative expression profiles in 2 groups were normalized by using mean of positive control spots that are located in all 4 corners of the array. Fold changes were calculated by dividing untreated expression profile to treated profile accordingly[134].

MIGRATION AND INVASION ASSAYS

Wound healing assay (migration assay)

NCI-N87 cells were analysed in a wound healing assay using IBIDI culture inserts (IBIDI GmbH, Martinsried, Germany) according to the manufacturer's protocol. The cells were seeded, grown to 100% confluence and serum deprived for 24 h. IBIDI culture inserts were removed and the

two cell islands were washed with PBS to remove debris. Cells were maintained in culture medium or culture medium with obestatin 200 nM, FBS or both. The progress of migration was photographed immediately at the beginning (0 h), at 24 and 36 h. The wound was calculated by tracing along the border of the scratch using the ImageJ64 analysis software and using the following equation: %wound closure=[[wound area (0 h)-wound area (x h)]/ wound area (0 h)] x 100[114].

In vitro Invasion Assay

The migration and invasion assays were carried out using a Transwell chamber (Corning, NY, USA). The inserts contained an 8 μm pore size polycarbonate membrane Cells were seeding into the upper chambers at a density of 5-7x10^4 in starved medium and stimulated with obestatin 200 nM, FBS 10% or both at 37 °C and the cells were allowed to migrate and invade. After 24 h incubation at 37 °C, non-invasive cells were scrubbed off the upper surface of the membrane using a moist cotton-tipped swab. Invasive cells on the lower surface of the membrane, which had invaded the extracellular matrix and migrated through the polycarbonate membrane, were stained by 4 μmol/L calcein-acetoxymethyl ester (Invitrogen, Carlsbad, CA, USA). The number of invading cells was counted in 10 random high-powered fields per filter by Zeiss Axio Vert.A1 fluorescence microscope (Carl Zeiss AG, Oberkochen, Germany) using a x10 objective. The invasion was calculated using the ImageJ64 analysis software.[135]

RNA EXTRACTION, cDNA SYNTHESIS AND REAL-TIME PCR

Adherent cells were solubilized in 1 mL of TRI Reagent® (Molecular Research Center, Inc. Cincinnati, USA) and total cellular RNA was isolate according to manufacturer´s instructions.

After DNase I treatment (Thermo Fisher Scientific, Waltham, MA), 1 μg of total RNA was reverse transcribed using High-Capacity cDNA Reverse Transcription Kits (Applied Biosistems, Thermo Fisher Scientific, Waltham, MA). Real-time PCR was carried out in Applied Biosystems StepOnePlusTM Real-Time PCR System (Applied Biosystems/Ambion, TX, USA) using

[135] Gao Z, Wang X, Wu K, *et al.* Pancreatic stellate cells increase the invasion of human pancreatic cancer cells through the stromal cell-derived factor-1/CXCR4 axis. Pancreatology 2010;10:186–193.

Luminaris HiGreen qPCR Master Mix (Thermo Fisher Scientific). The $2-\Delta\Delta Ct$ method was used to analyse the relative changes in each gene's expression normalized against B2M or GAPDH mRNA expression. Sequences of the primers used in this study were as follows:

B2M
Fw 5'-ACTGAATTCACCCCCACTGA-3'
Rv 5'-CCTCCATGATGCTGCTTACA-3'

GAPDH
Fw 5'-GACAGTCAGCCGCATCTTCT-3'
Rv 5'-TTAAAAGCAGCCCTGGTGAC -3'

NM23H1
Fw 5'-CAGCCGGAGTTCAAACCTA-3'
Rv 5'-GTATAATGTTCCTGTCAACTTGT-3'

NMR ANALISIS

The NMR spectra of urine and plasm samples were measured at 300 K in an 14.1 T Bruker Avance III spectrometer (proton frequency 600 MHz) equipped with a cryoprobe for use with 5 mm standard tubes. The spectrometer was coupled to an automatic sample changer and the process of shimming and acquisition of spectra was fully automatized which provided high throughput and reproducibility. The spectrometer control software was TopSpin 3.5pl6.

Sample preparation

The preparation of a sample for NMR measurement follows previously published protocols for urine and plasm samples[136,137].

Urine samples: Careful thawing of samples at room temperature. Centrifugation for 5 to 10 minutes at 2000 xg. Into a new tube, add 900 µL of urine and 100 µL of buffer (1.5M KH_2PO_4 in D_2O, 0.1% TSP, 0.01 NaN_3,

[136] Dona AC, Jiménez B, Schäfer H, *et al.* Precision High-Throughput Proton NMR Spectroscopy of Human Urine, Serum, and Plasma for Large-Scale Metabolic Phenotyping. Anal. Chem. 2014;86(19):9887-94
[137] Beckonert O, Keun HC, Ebbels TM *et al.* Metabolic profiling, metabolomic and metabonomic procedures for NMR spectroscopy of urine, plasma, serum and tissue extracts. Nature Protocols. 2007;2(11):2692-703.

(pH7.4)). Mixing the buffered urine 30sec. Transfer 600 µL well mixed sample into 5mm NMR-tube.

Plasma samples: Careful thawing of samples at room temperature. . Into a new tube, add 400 µL of and 400µL of buffer (0.4 g TSP, 10.05 G Na_2PO_4 x $7H_2O$, 5 mL NaN_3 (4%), 100 mL D_2O, H_2O up to 500 mL (pH 7.4))

These protocols include the addition to the sample of a certain volume of buffer to adjust the pH to 7.4. The buffer was prepared in the solvent D_2O for deuterium lock and contains dissolved a small proportion of a chemical shift reference compound that is the sodium salt of (trimethyl) propionic-2,2,3,3 D acid (TSP) that is used for internal reference (dTSP= 0 ppm)[138,139].

One-dimensional 1D ^1H NMR spectrum of urine samples were measured using a 1D noesy-presaturation pulse sequence (sequence *noesygppr1d* of the Bruker library) for strong suppression of the water resonance (~4.7 ppm) [140]. The following acquisition conditions were used: 32 scans, 4 dummy-scans, fid acquired with 64 k, mixing time 10 ms, acquisition time 2.72 s and the inter-scan relaxation delay (d_1) is 4 s. The total acquisition time of the spectrum is ca. 4 min.

One-dimensional 1D ^1H CPMG presaturation spectrum of plasma samples were measured with the Carr-Purcell-Meiboom-Gill sequence for filtering out the peaks of large macromolecules or aggregates providing a spectrum that reflects exclusively the peaks of small metabolites[141] (sequence cpmggpr1d of the Bruker library). The presaturation was applied at the frequency of the water resonance (~4.7 ppm) during the inter-scan relaxation delay (d1) of 4 s. The following acquisition conditions were used: 32 scans, 4 dummy-scans, fid acquired with 74 k, acquisition time 3.0 s, and the duration of the CPMG block was 76.8 ms. The total acquisition time of the spectrum is ca. 4 min.

---

[138] Wishart DS. Quantitative metabolomics using NMR. TrAC Trends in Analytical Chemistry. 2008;27:228-37.

[139] Giraudeau P. Quantitative 2D liquid-state NMR. Magn Reson Chem. 2014;52(6):259-72.

[140] Zheng G, Torres AM, Price WS. WaterControl: self-diffusion based solvent signal suppression enhanced by selective inversion. Magn Reson Chem. 2017;55(5):447-451.

[141] Louis E, Bervoets L, Reekmans G. *et al.* Phenotyping human blood plasma by 1H-NMR: a robust protocol based on metabolite spiking and its evaluation in breast cancer. Metabolomics. 2015;11:225-36.

NMR spectra of the urine or plasma samples were processed with software MestreNova 12.0 (*Mestrelab Research*). Free induction decays (FIDs) were zero filled to 128 k, apodized with 0.3 Hz line-broadening exponential function and 0.01 Hz gaussian function and Fourier transformed. Each spectrum was manually phased and baseline corrected and referenced to the TSP signal (δ_{TSP}=0 ppm). The set of spectra were stacked and the full spectral width was integrated by data binning. A binning width step of 0.04 and 0.01 ppm was used for urine and plasma samples, respectively. Finally, binned integrals corresponding to empty regions of the spectrum were excluded from the subsequent analysis, as well as the binned data around the suppressed water solvent peak at ~4.7 ppm. In the case of the urine samples binned integrals in the proximity of the broad peak of urea at ~5.8 ppm were also excluded from the analysis.

Multivariate and univariate analysis

Multivariate statistical analysis

The T2 filtered 1H NMR spectra of patients were divided into spectral regions (bins) of 0.03 and 0.01 ppm width urine and plasma samples, respectively, for statistical analyses. Integrals (bin intensities) were obtained using the Average Sum method in both samples and creatinine normalizatión in urine too. This binning process was performed automatically using the MestReNova software (version 10.0.1, MestreLab Research), and covered the entire spectrum from 0 to 10 ppm. The region 4.5 to 5.15 ppm could not be analysed due to the applied water suppression, while the spectrum was divided into segments ranging from 9.5 to 0.5 ppm. Bin intensities were obtained and analyzed using the metabolomic data processing server MetaboAnalyst 4.0 (http://www.metaboanalyst.ca) (Xia Lab, McGill University, Sainte-Anne-de-Bellevue, Quebec, CA). Specifically, data were pre-processed for normalization and scaling, to remove possible bias from sample variability and preparation. Data were normalized to the total spectral area and subsequently scaled by Pareto scaling (mean-centered and divided by the square root of the standard deviation of each variable).

The normalized features were subsequently analyzed by PCA to detect intrinsic clusters and outliers within the data set. PCA transforms a set of correlated variables into a smaller set of uncorrelated variables called principal components (PC). To maximize separation between samples, partial least-squares discriminant analysis (PLS-DA) and ortho PLS-DA (OPLS-DA) were performed.

Univariate analysis

Univariate statistics were performed on the selected variables as an alternative measure of variable importance. To determine if changes in bin intensities were statistically significant fold changes (threshold 1.3), non-parametric Wilcoxon rank-sum scores and Volcano plot were calculated using MetaboAnalyst 4.0. Significant differences were considered when pertaining p values were less than 0.05.

Quantification of metabolites in urine samples

Quantification of 50 metabolites was performed using the Bruker IVDr Quantification in URine B.I.Quant-UR b™ module. The metabolites analyzed are listed in **Table 8.**

Table 8. Metabolites analized by Quantification in URine B.I.Quant-UR b™ module in urine samples.

Creatinine	Glycine	Acetic acid	2-Methylsuccinic acid	Allantoin
Dimethylamine	Guanidinoacetic acid	Citric acid	2-Oxoglutaric acid	Allopurinol
Trimethylamine	Methionine	Formic acid	3-Hydroxybutyric acid	Caffeine
1-Methylhistidine	N,N-Dimethylglycine	Fumaric acid	Acetoacetic acid	Inosine
2-Furoylglycine	Sarcosine	Imidazole	Acetone	D-Galactose
4-Aminobutyric acid	Taurine	Lactic acid	Oxaloacetic acid	D-Glucose
Alanine	Valine	Proline betaine	Pyruvic acid	D-Lactose
Arginine	Benzoic acid	Succinic acid	1-Methyladenosine	D-Mannitol
Betaine	D-Mandelic acid	Tartaric acid	1-Methylnicotinamide	D-Mannose
Creatine	Hippuric acid	Trigonelline	Adenosine	Myo-Inositol

DATA ANALYSIS

All of the data are reported as the mean ± SEM. A Shapiro-Wilk normality test was performed for each data set. T-tests were carried out for comparisons between two samples. Unpaired t-test was used to assess the statistical significance of one-way or two-way analysis when the test statistic followed a normal distribution. Mann-Whitney test was employed to assess the statistical significance of one-way or two-way analysis when the test statistic did not follow a normal distribution. For multiple comparisons, a statistical ANOVA

analysis was performed using an analysis of variance with the Bonferroni post hoc test. Values of $P<0.05$ were considered to be statistically significant and are marked with an asterisk (*) or a hash (#). Double and triple asterisk (** and ***) or double and triple hash (## and ###) denote $P<0.01$ and $P<0.001$, respectively.

ETHICAL GUIDELINES

The development of this doctoral thesis was carried out in compliance with the Declaration of Helsinki of the World Medical Association 1964 and successive ratifications on ethical principles for medical research on humans, the Convention for the Protection of Human Rights and Dignity of the Human Being with regard to the Applications of Biology and Medicine, done in Oviedo on 4 April 1997, ratified by Spain on 23 July 1999 (Official State Gazette of 2000) and successive updates. Likewise, the new instructions contained in Regulation (EU) 2016/679 of the European Parliament and of the Council of 27 April 2016 on the protection of natural persons with regard to the processing of personal data and on the free movement of such data, and repealing Directive 95/46/EC (General Data Protection Regulation, GDPR) were complied with.

The researchers were familiar with the protocol and data collection. Essential documents were maintained to demonstrate the validity of the study and the integrity of the data collected. The master files were constituted at the beginning of the study, maintained during its conduct and preserved in accordance with applicable regulations. The Research Ethics Committee (REC)

reviewed all relevant study documentation in order to safeguard the rights, safety and well-being of patients. The study was only conducted at the site where the REC authorisation was obtained.

Access to patient samples and clinical data was made from the diagnostic database encoded in the Digestive System Service at Complexo Hospitalario Universitario de Santiago de Compostela (CHUS).

The researchers participating in this study undertook that all clinical data collected from the study subjects will be separated from personal identification data to ensure patient anonymity; respecting the Personal Data Protection Law (Organic Law 15/1999, of 13 December), the RB 1720/2007 of 21 December, which approves the Regulations for the development of Organic Law 15/1999, to Law 41/2002, of 14 November (basic regulator of patient autonomy and rights and obligations in matters of information and clinical documentation) as well as Law 3/2001, of 28 May, (regulator of the informed consent and of the clinical history of the patients), the law 3/2005, of the 7 of March, of modification of the law 3/2001 and the Decree 29/2009 of the 5 of February, by which the access to the electronic clinical history is regulated and the Order SSI/81/2017 by which the right to the privacy of the patient is regulated and the access to the clinical history by the students and residents in Sciences of the Health.

The clinical data of the patients were collected in a dissociated manner by the researcher linked to Servizo Galego de Saúde (SERGAS) in the study-specific Data Collection Notebook (DCN). Each DCN was coded, protecting the patient's identity. Only the research team and the health authorities, with a duty of confidentiality, had access to all the data collected for the study. Only information that cannot be identified could be transmitted to third parties.

Sample handling followed the provisions of Law 14/2007 of July 3 on Biomedical Research and RD 1716/2011, of November 18, which establishes the basic requirements for the authorization and operation of biobanks for biomedical research purposes and the treatment of biological samples of human origin, and regulates the operation and organization of the National Registry of Biobanks for biomedical research. The samples of this study (paraffin blocks) were obtained in an assistance context and were stored in the Pathological Anatomy Service at CHUS. Once the study was finished, the immunohistochemical preparations were preserved anonymized.

In the case of human cell lines, the AGS, KATO-III and NCI-N87 lines are commercial human cell lines (Sigma-Aldrich - ECACC).

RESULTS

CHAPTER 1: ROLE OF THE OBESTATIN/GPR39 SYSTEM IN THE PHYSIOLOGY OF GASTRIC ENZYMES

Pepsinogens, aspartic proteinases that hydrolyse peptides in acid environments, are mainly synthesized in the chief cells of the stomach mucosa but also in the mucous neck cells. Pepsinogen I (PGI or PGA) is produced in the fundus and body of the stomach (oxyntic mucosa), whereas pepsinogen II (PGII or PGC) is produced in the antrum (pyloric mucosa) and duodenum[142].

Gastric lipase is a type of acid lipase that acts at low pH and is also produced by chief cells. It is not as effective as alkaline lipases, such as pancreatic lipase, as it is only able to break down one fatty acid from the triacylglycerides. The resulting diglyceride cannot be absorbed by the epithelium of the gastrointestinal tract. However, in pancreatic pathologies where the activity of the pancreatic lipase is compromised, the gastric lipase is able to partially compensate it[143].

Our recent findings regarding the expression of GPR39 in the chief cells of the stomach[126] and, especially, the determination of the specific interaction between obestatin and GPR39[115], prompted us to investigate the function of the obestatin/GPR39 system in these exocrine cells.

GPR39 IS EXPRESSED IN THE CHIEF CELLS OF THE FUNDIC GLANDS IN THE HEALTHY HUMAN STOMACH

Our group recently reported the expression of the obestatin/GPR39 system in the healthy mucosa of the human stomach. Obestatin positive expression was found exclusively in the neuroendocrine cells localized from the neck to the base of the gastric glands in the oxyntic mucosa[126]. The serial sections (3 μm) utilized for the immunohistochemistry technique allowed us to determine the expression of the same cells for GPR39, pepsinogen I and lipase. Regarding GPR39 expression, intense staining was found in chief cells

[142] Chu S, Schubert ML. Gastric secretion. Curr. Opin. Gastroenterol. 2012;28:587-593.

[143] Carrière F, Grandval P, Renou C, *et al.* Quantitative study of digestive enzyme secretion and gastrointestinal lipolysis in chronic pancreatitis. Clin Gastroenterol Hepatol. 2005;3(1):28-38.

of the fundic glands **(Figure 1.1a to 1.1c)**. Parietal cells were negative **(Figure 1.1c)**. Concerning pepsinogen I, strong positivity was observed in the same cells, being negative for the parietal cells too. The chief cells possessed many pepsinogen I secretion granules **(Figure 1.1d to 1.1f)**. Lipase expression was also concentrated in the chief cells **(Figure 1.1g to 1.1i)**.

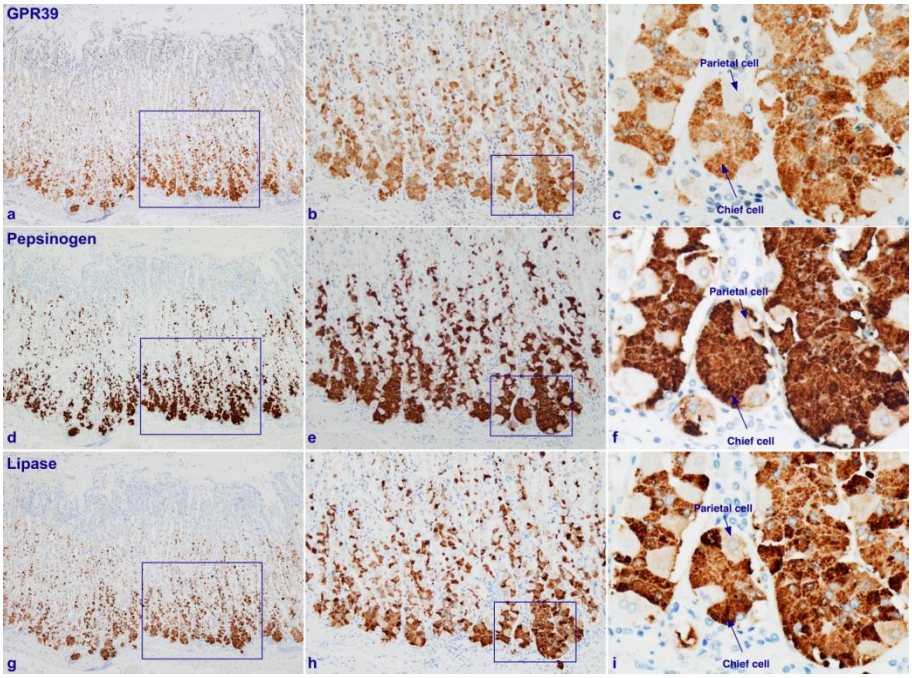

Figure 1.1. Immmunohistochemical expression of GPR39, pepsinogen I, and gastric lipase in human healthy stomach. Expression at the base of the oxyntic gland. a There was no GPR39 expression in the mucosal cells or parietal cells of the oxyntic glands. An intense immunostaining was present in the chief cells situated at the base of the oxyntic glands (x4). **b** Magnification view (x10) of the GPR39 intense immunostaining in the chief cells of the oxyntic glands. **c** At higher magnification, GPR39 producing cells were clearly recognized with brownish staining in the cytoplasm. Parietal cells were negative for GPR39 (x40). **d** Serial section (3 μm) of the same sample labeled for pepsinogen I. The intense pepsinogen I expression was observed mainly in the chief cells at the base of the oxyntic glands (x4), although some cells were positive in the neck zone. **e** Magnification view of the pepsinogen I positivity at the base of the oxyntic gland (x10). **f** A higher magnification view shows that pepsinogen I expressing cells were filled with numerous secretion granules showing a specific labeling for pepsinogen I. Parietal cells were negative for pepsinogen I (x40). **g** Serial section (3 μm) of the same sample labeled for lipase. The intense lipase expression was observed in the chief cells at the base of the oxyntic glands (x4). **h** Magnification view of the lipase positivity at the base of the oxyntic gland (x10). **f** A higher magnification view shows that lipase expressing cells were filled with numerous secretion granules showing a specific labeling for this enzyme. Parietal cells were negative for lipase (x40).

Figure 1.2 shows magnified areas in the neck region of the fundic glands. GPR39 positivity was also detected in a few cells located between the neck and the base of the glands (**Figure 1.2a** to **1.2c**). These cells might be immature chief cells migrating towards the base of the oxyntic gland, namely, pre-chief cells or transitional cells. Indeed, it has been described that chief cells derive from an intermediate cell type, characterized by abundant mucinous vesicles in the neck of the gland, the mucous neck cells, through a process of transdifferentiation[144]. For pepsinogen I expression, the positivity was also found in the mucous neck cells and in the cells located at the boundaries between the neck and the base also positive for GPR39, the pre-chief cells (**Figure 1.2d** to **1.2f**). However, lipase immunoreactivity was only observed in the same cells than GPR39 (**Figure 1.2g** to **1.2i**).

To confirm GPR39 expression, we studied GPR39 expressing cells by immunofluoresecence. In this case, no serial sections were used. As shown in **figure 1.3a** to **1.3c**, the GPR39 immunoreactive cells (green) were also positive for pepsinogen I (red). GPR39 positivity was limited to the chief cells at the base and to pre-chief cells, which are located in the intermediate zone and also expressed pepsinogen I[145]. In addition, some cells located at the neck section were found to be strongly immunolabeled for pepsinogen but negative for GPR39, the mucous neck cells (**Figure 1.3c**). **Figure 1.3e** shows a magnification at the lower region of the glands showing the colocalization of both proteins in the chief cells (pink arrow). Regarding lipase expression, this protein (red) and GPR39 (green) colocalized in the chief and pre-chief cells of the oxyntic glands (**Figure 1.3e** to **1.3g**). **Figure 1.3i** shows a magnification at the lower region of the glands displaying the colocalization of these two proteins also in the chief cells (pink arrow).

---

[144] Goldenring JR, Nam KT, Mills JC. The origin of pre-neoplastic metaplasia in the stomach: chief cells emerge from the Mist. Exp. Cell Res. 2011;317:2759-64.

[145] Cornaggia M, Capella C, Riva C, *et al.* Electron immunocytochemical localization of pepsinogen I (PgI) in chief cells, mucous-neck cells and transitional mucous-neck/chief cells of the human fundic mucosa. *Histochemistry*. 1986;85, 5-11.

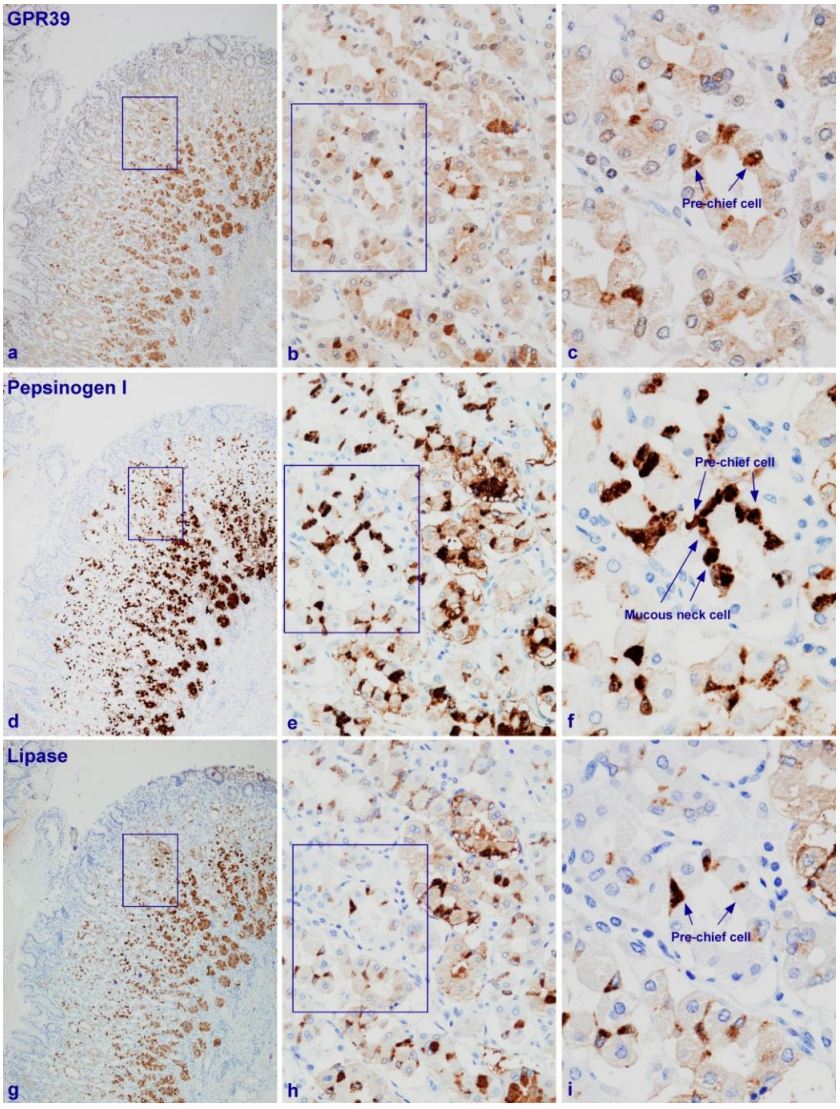

Figure 1.2. Immmunohistochemical expression of GPR39, pepsinogen I, and gastric lipase in human healthy stomach. Expression at the neck of the oxyntic gland. a General view of GPR39 expression in the oxyntic mucosa (x4). **b** Magnification view (x10) of the GPR39 intense immunostaining in a few cells of the neck section. **c** At higher magnification, GPR39 producing cells were clearly recognized with brownish staining in the cytoplasm. These cells might be immature chief cells emerging to the base of the oxyntic gland (pre-chief cells; x40). **d** Serial sections (3 μm) of the same sample labeled for pepsinogen I (x4). **e** Magnification view of the pepsinogen I positivity at the neck zone (x10). **f** A higher magnification view shows two cell types showing a specific labeling for pepsinogen I. The pre-chief cells immune-reactive to GPR39 were also positive for pepsinogen I. In addition, the mucous neck cells were found to be strongly immunolabeled for pepsinogen I but negative for GPR39 (x40).

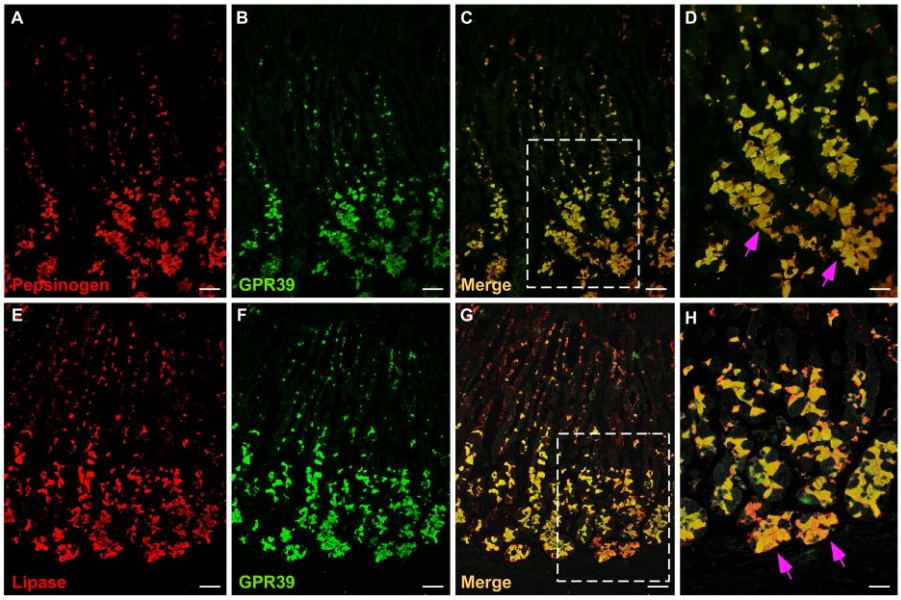

Figure 1.3. Immunofluorescence detection of GPR39, pepsinogen I, and gastric lipase in human healthy stomach. The figure shows immunofluorescence detection of pepsinogen (red, **a**) GPR39 (green, **b**) in the same section of the human gastric mucosa (10x). Micrograph **c** (merged) shows the colocalization of both proteins in the same cells primarily at the base of the fundic glands. **d** At the lower region of the glands, pepsinogen I and GPR39 expression was found in the chief cells (pink arrow). Immunofluorescence detection of lipase (red, **e**) and GPR39 (green, **f**), in the same section of the human gastric mucosa (10x). Micrograph **g** (merged) shows the colocalization of both proteins in the same cells mostly at the base of the fundic glands. **h** At the lower region of the glands, lipase and GPR39 expression was found in the chief cells (pink arrow). **d-h** Micrographs magnification at x20.

Taking into account the GPR39 location found in the chief cells of the oxyntic glands, the obestatin/GPR39 system could regulate secretion of digestive enzymes such as pepsinogen and lipase in these cells, an important role for gastric physiology. Previous studies have demonstrated that treatment with obestatin 200 nM stimulated pepsinogen I secretion in AGS cells at 40 min. In addition, GPR39 deficiency by siRNA knockdown revealed a significant decrease in obestatin-stimulated pepsinogen secretion respect to control siRNA measured in secretome. Therefore, obestatin exerts its stimulatory effect through the GPR39 receptor in AGS cells[130]. However, no detectable expression was found for gastric lipase in this cell line by immunohistochemistry, as shown in the **figure 1.4**.

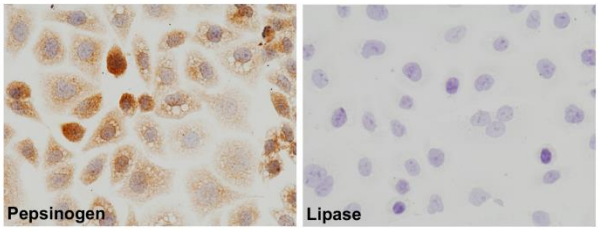

Figure 1.4. Immunocytochemical expression of pepsinogen I and gastric lipase in AGS cells. Images were taken under 20x objective magnification. A negative control without primary antibody showed no positivity (data not shown).

NCI-N87 cells were selected for the analysis of the enzymatic gastric secretion. These cells are the best *in vitro* model to study the cellular and molecular regulatory mechanisms of human gastric mucosa functions, as they express both pepsinogen I and gastric lipase[146].

Expression of the obestatin/GPR39 system was analyzed by immunoblot in NCI-N87 cells (**Figure 1.5**). Both obestatin and GPR39 were expressed intensely in these cells. In addition, positivity of pepsinogen I and gastric lipase has also been shown, confirming the model for the synthesis and secretion of chief cell zymogens[146].

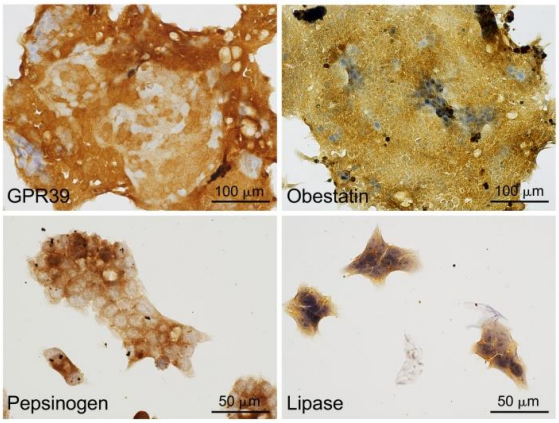

Figure 1.5. Immunocytochemical expression of GPR39, obestatin, pepsinogen and lipase in NCI-N87 cells. Objective magnification x20 in upper images and x40 in bottom images.

[146] Basque JR, Chénard M, Chailler P, *et al.* Gastric cancer cell lines as models to study human digestive functions. J Cell Biochem. 2001;81(2):241-51.

NCI-N87 were treated with exogenous obestatin to analyze the variations in the secretion of pepsinogen I and gastric lipase. A time course was performed and cell secretomes were analyzed by immunoblot. These samples need to be concentrated for analysis since they were very diluted and gastric enzymes were present in low quantity. Several methods of sample concentration were tested but the results were variable and none of them was a reproducible procedure (data not shown).

OBESTATIN STIMULATES PEPSINOGEN AND LIPASE SECRETION IN HUMAN STOMACH EXPLANT CULTURES

Due to the fact that we could not either observe any lipase expression on AGS cells, and nor observe any reproducible data of lipase secretion in NCI-N87 cells, we decided to test obestatin effect directly on an *ex vivo* system of human stomach explant cultures (**Figure 1.6**). This system had already been described and used to study pepsinogen secretion in the late 1970s by Kondo[147]. Human stomachs from patients who underwent bariatric surgery were used. With these samples, a kinetic and a dose-response study was performed. The stomach specimens were treated with human obestatin (50, 100 and 200 nM) for the indicated times (20, 40 and 60 min). The upper part of **figure 1.6** shows representative blots out of four different samples (four patients), for the presence of GPR39, pepsinogen I and gastric lipase in the lysate and the secretion of pepsinogen and lipase in the secretome. Only the mucosa was utilized after the secretome was collected to avoid conflicting results, as the smooth muscle also expressed GPR39 (unpublished results). The below part of **figure 1.6** shows the secretion pattern of pepsinogen after obestatin treatment. Obestatin stimulates pepsinogen secretion in a dose dependent manner, being significant for the doses of 100 and 200 nM compared to the control sample at 20 min (≈39% and ≈66% over control, respectively), for 200 nM at 40 min (≈51% over control) and 100 nM at 60 min (≈64% over control) (**Table S1**).

[147] Kondo T, Yamada S. Studies on synthesis and secretion of pepsinogen in human gastric corpus mucosa by use of organ culture method. Nihon Shokakibyo Gakkai Zasshi. 1979;**76**:1067-1079.

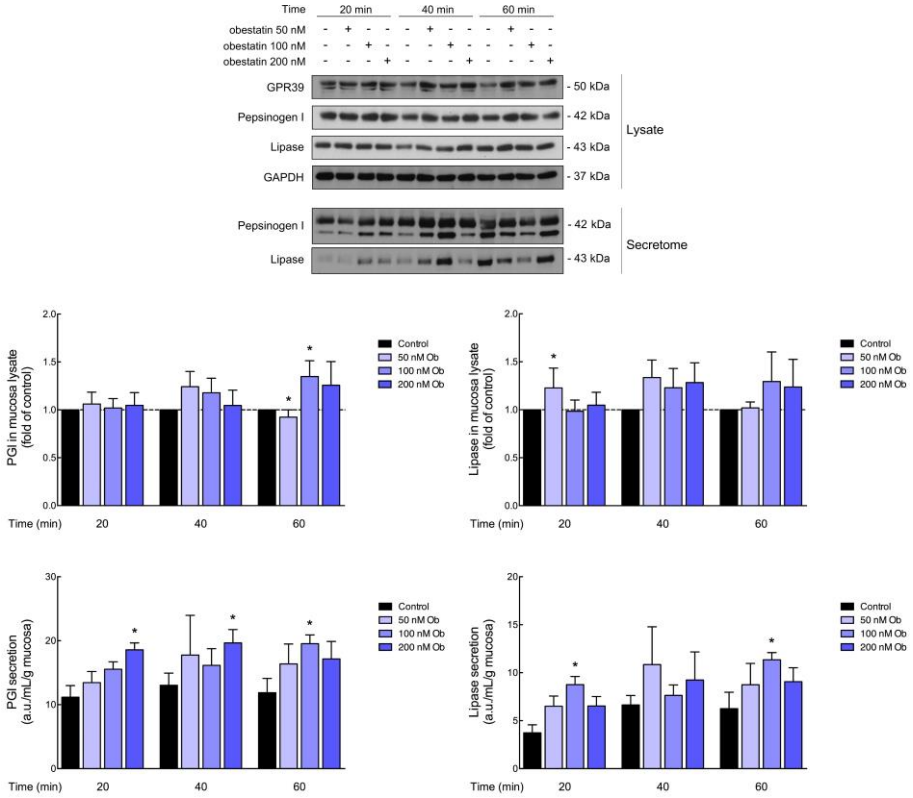

Figure 1.6. Obestatin stimulated secretion of pepsinogen I and gastric lipase in explants of healthy human stomach. Kinetic and dose response study of PGI and lipase secretion after obestatin treatment (50, 100 and 200 nM) at 20, 40 and 60 minutes after stimulation. Analysis of the expression in the mucosa lysate of GPR39, pepsinogen and lipase. Protein expression was normalized by GAPDH. Data were expressed as mean±SEM obtained from intensity scans of 4 different patients. The asterisk (*) indicates $P<0.05$ when comparing each obestatin group with the control. Analysis of pepsinogen and lipase in secretome, equal volume of secretome was loaded into the gel and protein expression was normalized by mucosal weight. The protein level was expressed as fold change in relation to the untreated control explant. Data were expressed as mean±SEM obtained from 4 different patients. The asterisk (*) indicates $P<0.05$ when comparing each obestatin group with the control.

Regarding lipase secretion, obestatin stimulates its secretion from the stomach explants significantly for the dose of 100 nM at 20 and 60 min(≈111% and ≈75% over control, respectively) (**Table S2**).

Analysis of the mucosa lysate revealed that pepsinogen showed no variation at 20 or 40 min with obestatin treatment. It only manifested a decrease with dose 50 nM and an increase to 100 nM significantly at 60 min. As for gastric lipase, expression was significantly greater at 20 min with obestatin 50 nM treatment. In general, both pepsinogen and lipase showed a tendency to increase after obestatin treatment relative to untreated sample.

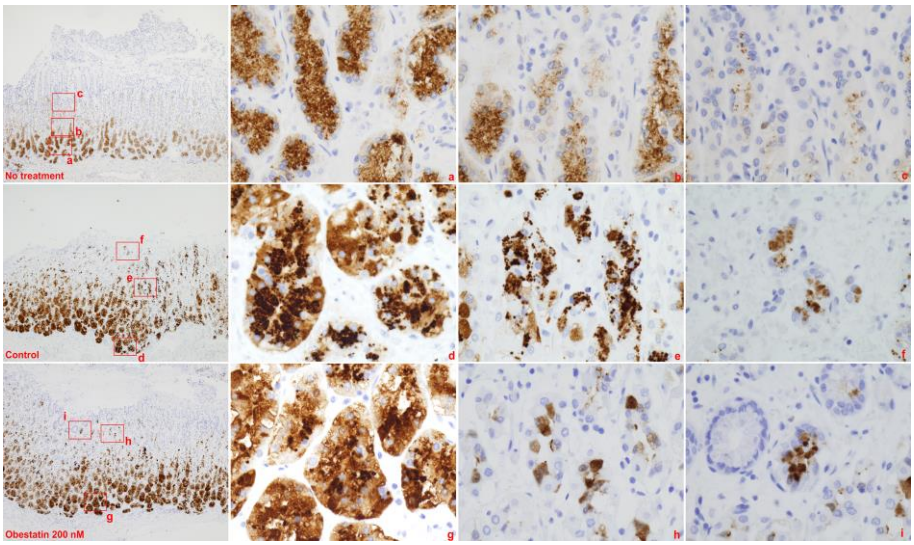

Figure 1.7. Immunohistochemical expression of pepsinogen in a tissue sample of a patient compared to the explant in culture (control and 200 nM obestatin treated tissue at 20 min; same patient). The upper row shows the expression of pepsinogen in a healthy human stomach. On the left, general view. **a,** detailed areas of the base, **b** on the neck and **c** upper oxyntic gland. The middle row shows the expression of pepsinogen in control explant in culture for 20 min. On the left, general view. **d,** detailed areas of the base, **e** on the neck and **f** upper oxyntic gland. The bottom row shows the expression of pepsinogen in explant in culture treated with obestatin 200 nM for 20 min. On the left, general view. **g,** detailed areas of the base, **h** on the neck and **i** upper oxyntic gland. General views were taken under x4 magnification and detailed areas under x20.

Figure 1.7 shows the immunohistochemical expression of pepsinogen in a tissue sample of a patient compared to the explant in culture (control and 200 nM obestatin treated tissue at 20 min; same patient). This time and dose corresponded to the obestatin maximum stimulatory effect on pepsinogen secretion. Pepsinogen expression was observed with the same pattern as described above in the untreated sample. However, in both explants in culture

(control and obestatin treated) pepsinogen expression was observed along the oxyntic glands, even at the top of the gland, together with a less intense expression in the chief cells at the base of the glands for the obestatin treated explant. The pictures at the right (**Figure 1.7a** to **1.7f**) show magnification sections (x20) of the original pepsinogen-staining picture (x4). **Figure 1.8** shows the result for the lipase staining in these samples. In this case, the time and the dose corresponded to 20 min and 100 nM obestatin. Similar pattern of staining was observed for this enzyme compared to **figure 1.7**, with a lesser intense positivity in the chief cells at the base of the oxyntic gland for the obestatin treated explant. **Figure 1.8a** to **1.8f** show magnification sections (x20) of the original lipase-staining stomach (x4). The immunohistochemical analysis of both gastric enzymes was carried out in the same way at 60 min post-obestatin stimulation and the same results were observed (data not shown).

Obestatin stimulates Akt and ERK 1/2 in healthy human stomach

Obestatin action is exerted through the signaling model described in human gastric cancer lines, AGS and KATO-III[125]. Akt and ERK1/2 are early targets of each of the two pathways that obestatin activates in parallel.

To dilucidated wether obestatin triggered the same signalling pathway in a healthy environment, a dose-response assay was performed on the ex vivo explant culture of healthy human stomach described above. In that way, human stomach pieces were treated with human obestatin (50, 100 and 200 nM) for 5 min. Activation of these targets was studied by analysis of the phosphorylated forms pAkt (S473) and pERK1/2 (T202/Y204), as shown in **figure 1.9.**

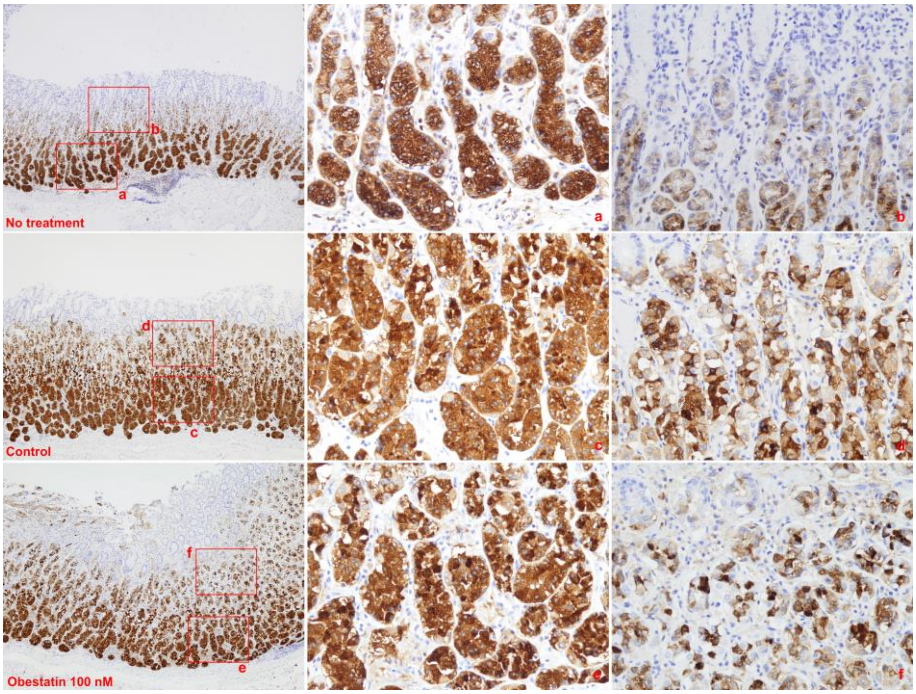

Figure 1.8. Immunohistochemical expression of lipase in a tissue sample of a patient compared to the explant in culture (control and 200 nM obestatin treated tissue at 20 min; same patient). The upper row shows the expression of lipase in a healthy human stomach. On the left, general view. **a,** detailed areas of the base and **b** on the neck of the oxyntic gland. The middle row shows the expression of lipase in control explant in culture for 20 min. On the left, general view. **c**, detailed areas of the base and **d** on the neck of the oxyntic gland. The bottom row shows the expression of lipase in explant in culture treated with obestatin 200 nM for 20 min. On the left, general view. **e**, detailed areas of the base and **f** in the neck of the oxyntic gland. General views were taken under x4 magnification and detailed areas under x20.

Treatment with obestatin significantly increased the activation of Akt (Ob 50 nM, 1.43±0.16; Ob 100 nM, 1.59±0.12; Ob 200 nM, 1.58±0.01) and ERK1/2 (Ob 50 nM, 1.27±0.09; Ob 100 nM, 2.09±0.52; Ob 200 nM, 2.61±0.44) in a dose-dependent manner in the three concentrations respect to the untreated control.

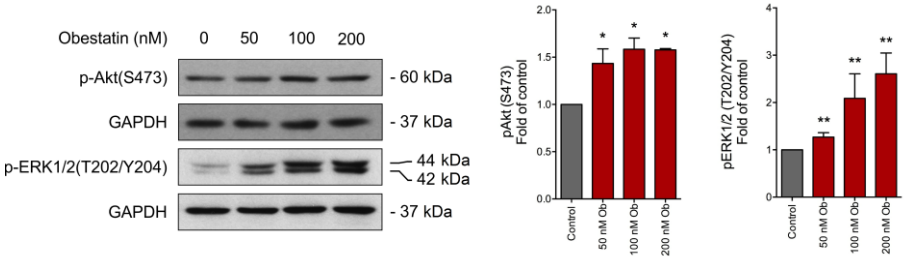

Figure 1.9. Obestatin effect on Akt and ERK1/2 activation in healthy human stomach. Stomach explants were treated with obestatin (50, 100 and 200 nM) for 5 minutes. ERK1/2 and Akt phosphorylation were quantified using densitometry and expressed as the fold change relative to the phosphorylation obtained for unstimulated explant (mean±SEM) of three independent experiments). Protein expression was normalized relative to GAPDH. Single and double asterisk (*,**) expresses P<0.05 and P<0.01, respectively, when comparing treated with untreated group.

OBESTATIN EFFECT ON RTKS ACTIVATION IN HEALTHY HUMAN STOMACH

Akt pathway is activated by the obestatin-induced EGFR transactivation through GPR39. Knowing that obestatin is capable of activating many others RTKs in gastric cancer cells[130], this effect was tested on a healthy stomach. Stomach explants were treated with 200 nM obestatin for 5 min, dose at which there is increased activation of the molecular targets involved in the obestatin signalling pathway. Equal amount of protein from gastric mucosal lysate has been incubated in each array (200 μg).

Among the 71 RTKs and Src family of protein tyrosine kinases (SFKs) studied, 36 showed a reduction and 35 an increase in their phosphorylation levels with obestatin treatment. Blk, EGFR and ROR2 were downregulated while EphA4, EphB1, EphB3 and HGFR were significantly over-activated (**Figure 1.10**).

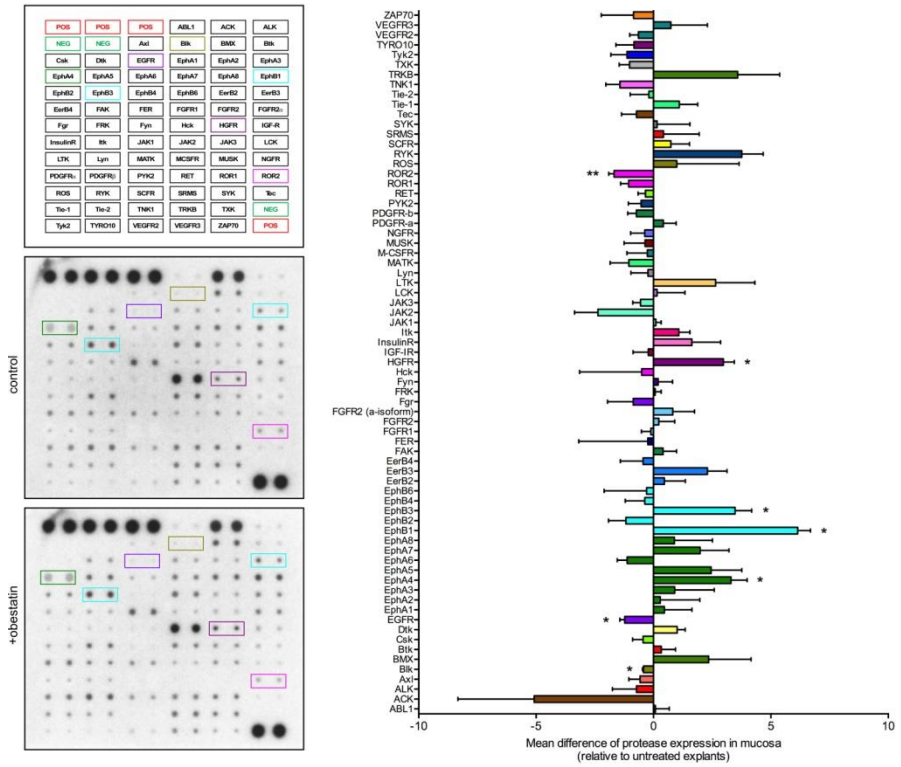

Figure 1.10. Differential expression of phosphorylated RTKs and SFKs in obestatin treated compared to untreated healthy stomach. Out of the 71 RTKs analysed in the Human RTK Phosphorylation Antibody Array, two showed less phosphorylation and another 5 were activated by the obestatin treatment significatively. 200 µg of mucosa lysate protein were run on each array. Asterisk (*) indicates $P<0.05$.

OBESTATIN STIMULATES PROTEASES SECRETION IN HEALTHY HUMAN STOMACH

Obestatin functions as a switch of metalloproteases (MMPs) involved in the transactivation process of EGFR and other RTKs, following the signaling route described. Previous studies show that obestatin stimulates protease secretion in gastric cancer cells[130].

The secretion of proteases induced by obestatin was analyzed in healthy human stomach using a proteases array. Stomach explants were treated with obestatin 200 nM for 20 min, which is the time and concentration in which the obestatin- stimulated secretion of pepsinogen was significantly higher. Secretomes and lysates were used for analysis. The same volume (200 μL) of secretome was incubated on each array. Data were normalized by their corresponding mucose weight. The treated explants present the muscular layer of the stomach. This smooth muscle expresses GPR39 and can secrete proteases by obestatin treatment. The mucosa lysate has been used as a control to avoid conflictive data. Protease analysis was performed incubating the same amount of lysate protein (200 ug) in each array.

Treatment with obestatin led to an increase in the secretion of the 35 proteases studied, 29 significantly (**Figure 1.11**). Among them, neprilysin, presenilin-1, proprotein convertase 3, proteinase 3 and members of the ADAMs, Cathepsins, Kallikreins and MMPs families

Taking the mucosal lysate data, it was observed that with the exception of DPPIV, the expression of the remaining 34 proteases was over-regulated in obestatin treatment (**Figure 1.12**). ADAM 9, cathepsin S and V, KLK-11, MMP-9, and proteinase 3 showed a stronger obestatin-dependent reduction.

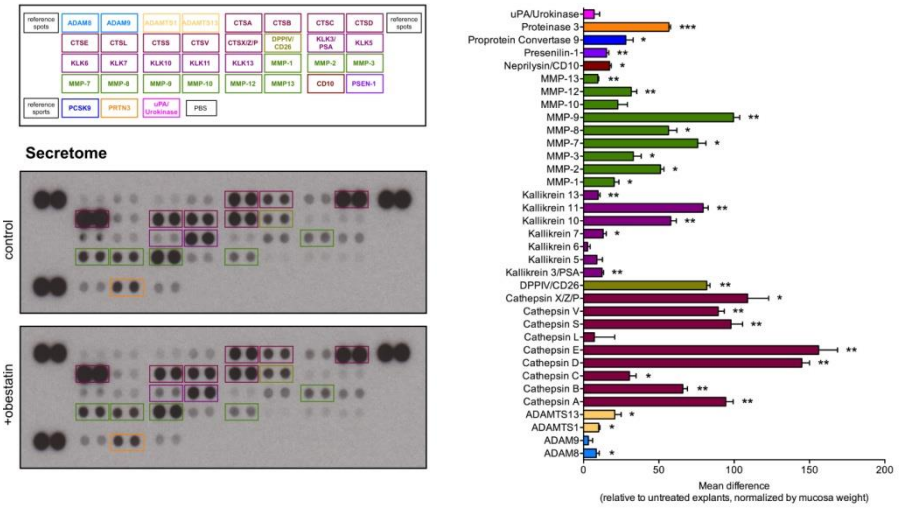

Figure 1.11. Differential expression of proteases in obestatin treated compared to untreated secretomes of human stomach explant. All 35 proteases analysed were over-regulated, 29 of them significantly (P<0.05) in obestatin-treated (200 nM, 20 min) compared to untreated human stomach explant. The same volume (200 µL) of secretome was incubated on each array. Data were normalized by their corresponding explant weight.

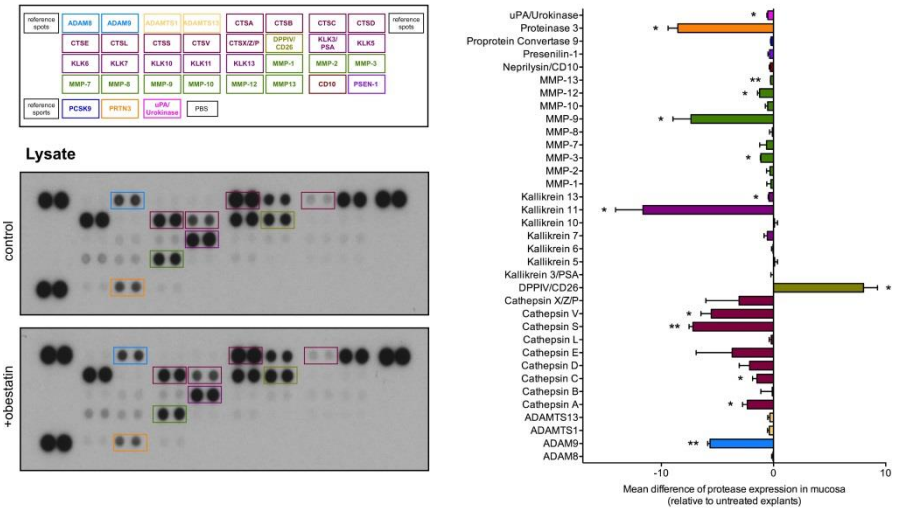

Figure 1.12. Differential expression of proteases in obestatin treated compared to untreated mucosa lysates of human stomach explant. Out of the 35 proteases analysed, 32 were down-regulated and 13 of them significantly, while 3 proteases are over-regulated and only one of them significantly (P<0.05) in obestatin-treated (200 nM, 20 min) compared to untreated human stomach explant. The same amount of protein (200 µg) of mucosa lysate protein were incubated on each array.

MOLECULAR MECHANISMS INVOLVED IN THE OBESTATIN-INDUCED SECRETION OF PEPSINOGEN

Two main intracellular signaling pathways are involved in pepsinogen secretion in chief cells: a) cAMP-dependent protein kinase A (PKA) signalling; and, b) phosphatidyl inositol-phospholipase C (PI-PLC)/ inositol triphosphate (IP_3)/ Ca^{2+}/calmodulin-dependent protein kinase II (CaMKII) signaling[148]. However, to our knowledge, no intracellular signalling pathways have been described for gastric lipase secretion.

To dilucidate whether obestatin stimulated enzymatic secretion in the human stomach explants involved any of these signalling pathways, several key targets were analyzed. In that sense, phosphorylation of PKA (T197) involved in the cAMP pathway and phosphorylation of PKCα/β (T638/641) and PKC γ (T674) involved in the Ca^{2+} dependent pathway have been analyzed (**Figure 1.13**).

Obestatin activated PKA significantly in a dose-dependent manner in all concentrations (Ob 50 nM, 1,50±0,19; Ob 100 nM, 1,94±0,59; Ob 200 nM, 3,80±0,80). PKCα/β was activated by obestatin in all treatments significantly (Ob 50 nM, 1,53±0,09; Ob 100 nM, 1,71±0,44; Ob 200 nM, 1,48±0,22). Finally, PKCγ also showed a significantly dose-dependent activation by obestatin (Ob 50 nM, 1,38±0,13; Ob 100 nM, 1,52±0,16; Ob 200 nM, 1,76±0,18).

[148] Raufman JP. Gastric chief cells: Receptors and signal transduction mechanisms. Gastroenterology. 1992;102:699-710.

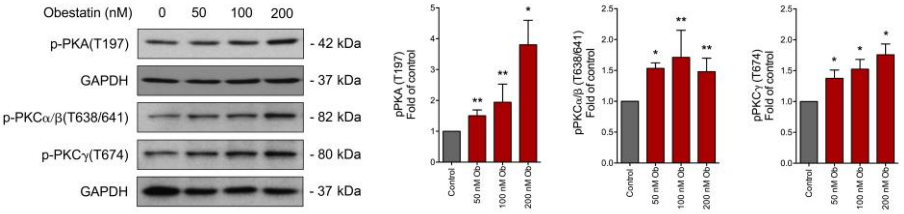

Figure 1.13. Obestatin induces activation of PKA, PKCα/β and PKCγ.in healthy human stomach. Stomach explants were treated with obestatin (50, 100 and 200 nM) for 5 minutes. PKA, PKCα/β and PKCγ phosphorylation were quantified using densitometry and expressed as the fold change relative to the phosphorylation obtained for unstimulated explant (mean±SEM) of three independent experiments. Protein expression was normalized relative to GAPDH. Single and double asterisk (*,**) expresses $P<0.05$ and $P<0.01$, respectively, when comparing treated with untreated group.

USC
UNIVERSIDADE
DE SANTIAGO
DE COMPOSTELA

CHAPTER 2. ROLE OF THE OBESTATIN/GPR39 SYSTEM IN HUMAN GASTRIC CANCER CELL LINES

The obestatin/GPR39 system regulated proliferation, the epithelial-mesenchymal transition, facilitating the capacity of migration, invasion and metastasis in AGS, a cell line derived from a moderately differentiated adenocarcinoma. This, together with the relationship between the expression of GPR39 and the pathogenesis of human gastric adenocarcinomas provides the basis for including GPR39 as a prognostic marker of these tumors[126]. Obestatin/GPR39 system could be a key in the development of new pathways for the detection and treatment of gastric cancer. These findings lead us to corroborate the implication of the obestatin/GPR39 system in other cell lines, such as the KATO-III that comes from a poorly differentiated carcinoma and the NCI-N87 that derives from a liver metastasis of a well differentiated carcinoma, to deepen in the mode of action of the obestatin/GPR39 system in gastric cancer.

THE OBESTATIN/GPR39 SYSTEM IS EXPRESSED IN HUMAN GASTRIC CANCER CELL LINES

GPR39 and obestatin expression was determined in the three human gastric cancer lines: AGS, KATO-III and NCI-N87. As shown in **Figure 2.1**, expression of the obestatin/GPR39 system was detected by immunocytochemistry in the studied cell lines. All three lines expressed the obestatin/GPR39 system with different levels of intensity. No immunostaining was found in negative controls incubated without primary antibody (data not shown). AGS cells showed an intense and diffuse immunostaining for obestatin in the cytoplasm while the expression of GPR39 was located in the perinuclear zone. KATO-III cell line had an intense obestatin immunostaining in the cytoplasm and a perinuclear GPR39 immunostaining. NCI-N87 presented intense and diffuse cytoplasmic positivity for both obestatin and GPR39.

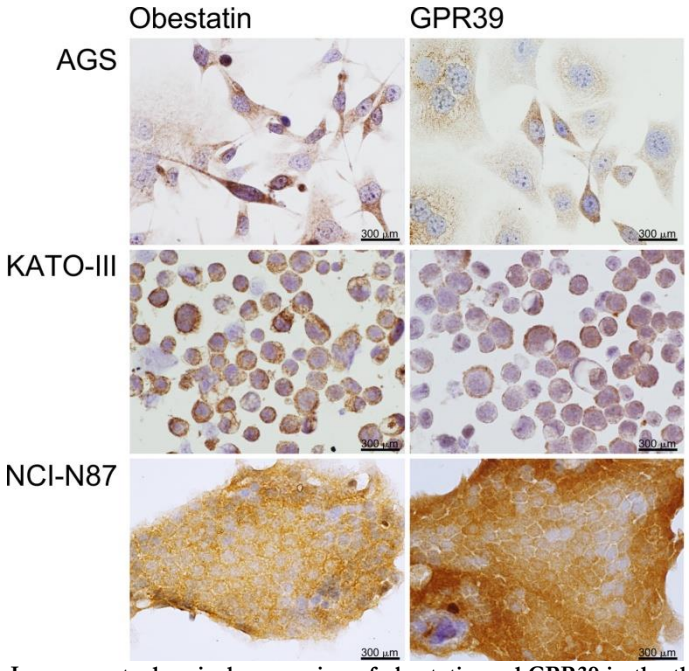

Figure 2.1. Immunocytochemical expression of obestatin and GPR39 in the three human gastric cancer cell lines. (See text below). Objective magnification x20.

OBESTATIN STIMULATES PROLIFERATION IN GASTRIC CANCER CELLS

Previous research by our group has shown that the obestatin/GPR39 system causes cell proliferation and migration of various human carcinogenic lines. After checking the expression of the obestatin/GPR39 system in the three cell lines of this study, the effect of exogenous administration of obestatin on cell proliferation and cell viability was analyzed by manual counting in AGS and KATO-III cells and cell proliferation by incorporation of BrdU in NCI-N87.

Figure 2.2 shows the mitogenic effect of obestatin in AGS line cell (46.20±8.66% over control). Similarly, in KATO-III cells there was also an increase in proliferation with obestatin treatment (45.12±4.11% over control) as shown in **figure 2.3.**

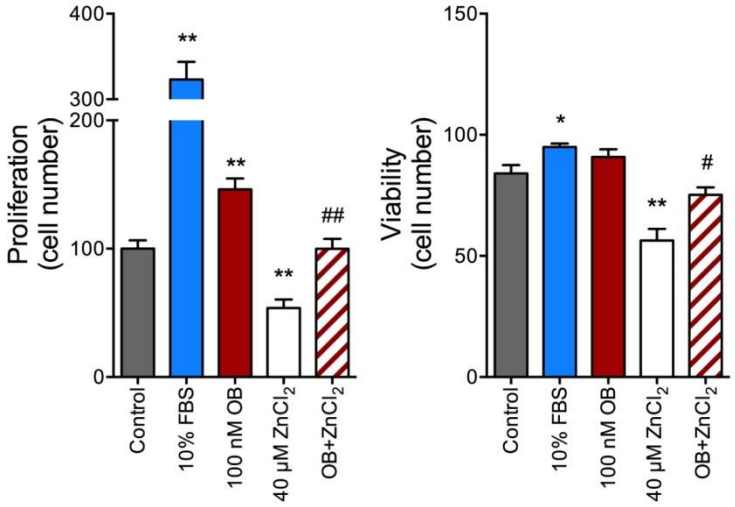

Figure 2.2. Mitogenic effect of obestatin in AGS cell line . Cells were treated with FBS (10% v/v) (positive control), obestatin (100 nM), $ZnCl_2$ (40 µM) and $ZnCl_2$ (40 µM) plus obestatin (100 nM). Proliferation was evaluated after 48 hours of stimulation through manual counting and viability with blue trypan staining. The data are expressed as a percentage of basal untreated cell proliferation (Mean± SEM). Single and double asterisk (*,**) expresses P< 0,05 and P< 0,01, respectively, when comparing the group treated with FBS or obestatin with the control. Single and double hash (#,##) expresses P<0.05 and P<0.01, respectively, when comparing the group treated with $ZnCl_2$ plus obestatin with the $ZnCl_2$ treated group.

Zn^{+2} has been described as a ligand for GPR39. The dose used to activate GPR39 was found in the literature. We have tested the effect of Zn^{+2} on gastric tumour cell proliferation, an effect described and regulated by the obestatin/GPR39 system. To do this, we treat the AGS and KATO-III cells with 40 µM Zn^{+2}, and perform a manual count taking into account the subpopulation characteristics of KATO-III cells (adherent and floating). The results were surprising: both AGS and KATO-III cells went into apoptosis after treatment with Zn^{+2} (53.85±6.59% and 30.59±3.27%, respectively). However, the viable cells present in the samples were able to proliferate significantly when co-treated with obestatin+Zn^{+2}, reaching control-like values for AGS cells (100.00±7.69% and 58.82±2.78%, respectively). These results are correlated with the numbers obtained for cell viability.

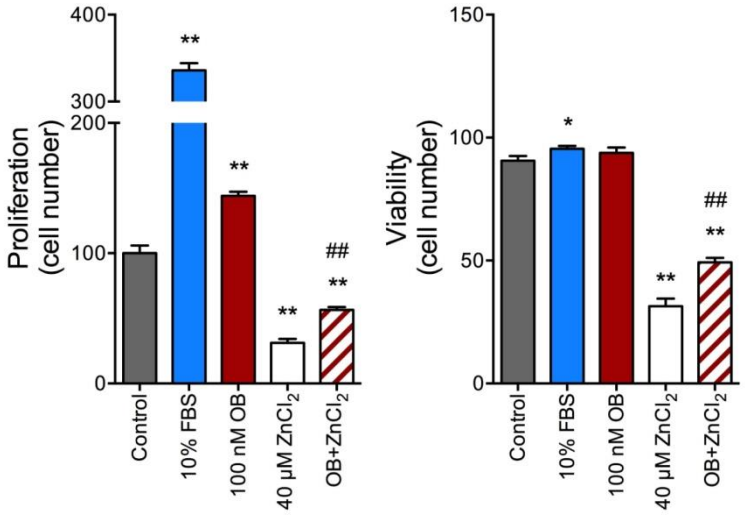

Figure 2.3. Mitogenic effect of obestatin in KATO-III cell line . Cells were treated with FBS (10% v/v) (positive control), obestatin (100 nM), ZnCl2 (40 µM) and ZnCl2 (40 µM) plus obestatin (100 nM). Proliferation was evaluated after 48 hours of stimulation through manual counting and viability with blue trypan staining. The data are expressed as a percentage of basal untreated cell proliferation (Mean± SEM). Single and double asterisk (*,**) expresses P< 0,05 and P< 0,01, respectively, when comparing the group treated with FBS or obestatin with the control. Single and double hash (#,##) expresses P<0.05 and P<0.01, respectively, when comparing the group treated with ZnCl2 plus obestatin with the ZnCl2 treated group

Regarding NCI-N87 cell line, treatment with exogenous obestatin caused a significant increase in proliferation measured by the incorporation of BrdU (60.82±2.83% over the control; **figure 2.4**).

Proliferation and viability assay using manual counting could not be performed on this cell line. The nature of their growth in colonies formed from closely bonded cells means that when they are detached, dispersion into single cells cannot be assured, hindering a proper cell count.

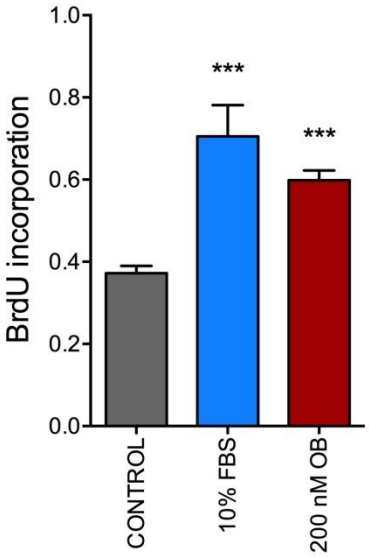

Figure 2.4. Mitogenic effect of obestatin in NCI-N87 cell line. Cells were treated with obestatin (200 nM) and FBS (10% v/v) as a positive control. Cell proliferation was evaluated after 48 hours of treatment with the addition of BrdU. The data are expressed as a percentage of basal untreated cell proliferation (Mean± SEM). Triple asterisk (***) expresses P<0.001 when comparing the treated group with control.

OBESTATIN INHIBITS MIGRATION AND INVASION OF NCI-N87 CELL LINE

Previous results from our research group determined that the obestatin/GPR39 system was involved in activating both migration and invasion of AGS cell line[126].

To validate the observed effect on AGS cell line, the impact of obestatin (200 nM) treatment on NCI-N87 cell migration was evaluated using FBS 10% as a positive control, as well as a co-treatment with obestatin and FBS, for 24 and 36 hours (**Figure 2.5**).

It was observed that the stimulation with obestatin decreased migration at both times (10.40±0.48% and 8.25±0.61%, respectively) compared to controls (15.31±0.91% and 14.75±0.66%, respectively).

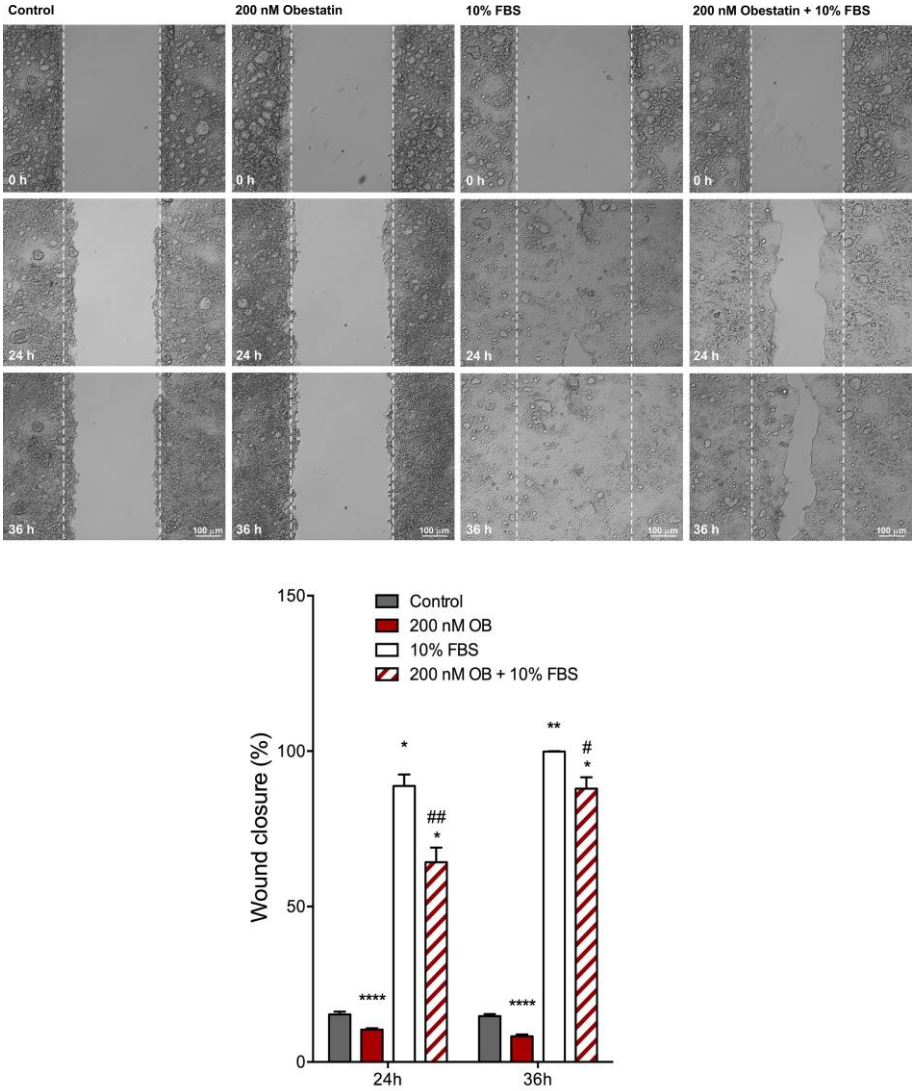

Figure 2.5. Inhibition of NCI-N87 cell migration promoted by obestatin. Cells were treated or not with obestatin (200 nM), FBS (10% v/v) or both. The wound area was calculated using the ImageJ64 analysis software and following the equation: % wound closure =[[wound area (0h)-wound area (xh)]/wound area (0h)] x 100. Single, double or quadruple asterisk (*, **, ****) expresses P< 0.05, P< 0.01 and P< 0.001, respectively, when comparing the treated group with the untreated group. Single and double hash (#, ##) expresses P< 0.05 and P< 0.01, respectively, when comparing the obestatin 200 nM + FBS 10% group with the FBS 10% group.

As expected, positive control with FBS 10% significantly stimulated cell migration at 24 and 36 h (88.79±3.66% and 99.88±0.08%, respectively). However, co-treatment of FBS with obestatin 200 nM inhibited FBS-mediated migration, reducing wound closure by 27.63±4.71% at 24 h and 11.99±3.71% at 36 h.

Taking into account these data on cell migration, the role of obestatin in the invasion process in this cell line was analyzed. Permeable cell culture inserts with a polycarbonate membrane were used. Pores of 8 μm allow cells to cross the membrane. The invasive capacity of NCI-N87 cells has been studied by putting them in contact with the medium with or without obestatin (200 nM). As shown in **figure 2.6**, obestatin significantly reduced cell invasion by 51.83±15.68% over the control.

In KATO-III the migration test was performed by wound healing using the adherent subpopulation (data not shown). The results were not satisfactory since it is not a cell line properly adherent and they are easily detached, in addition to the fact that both populations are in equilibrium and the two phenotypes are established again with time.

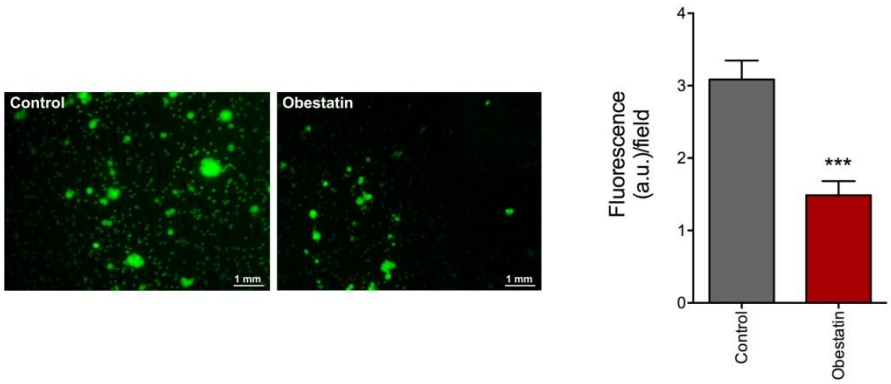

Figure 2.6. Inhibition of NCI-N87 cell invasion triggered by obestatin. Cells were treated or not with obestatin (200 nM). Migratory cells pass through the membrane to the lower side while non-migratory cells were removed from the upper side. The data are expressed as mean±SEM from three independent experiments. Triple asterisk (***) expresses P<0.001 when comparing the treated with the untreated group.

OBESTATIN MODIFIES THE EXPRESSION OF *NM23-H1* AND NM23-H1 IN GASTRIC CANCER CELLS

The first metastasis suppressor gene, *nm23-H1*, was identified by differential colony hybridization in 1988[149]. *nm23* was the cDNA chosen after different studies because its expression was negatively regulated in five metastatic cell lines, compared to two lines with a lower degree of metastasis. Ectopic expression of nm23 suppressed metastasis without altering the growth of the primary tumour.

Due to the data found in NCI-N87 cell line regarding migration and invasion, contrary to what was observed in AGS, both expression of nm23-H1 protein and *nm23-H1* gene were studied after treatment with obestatin in the studied cell lines.

AGS cells showed no significant difference in expression of the nm23-H1 gene when treated with obestatin (200 nM) for 24 h (**Figure 2.7A**). In addition, no effect was seen on the expression of protein analyzed by immunoblot with the same stimulus (**Figure 2.7E**).

In KATO-III cell line, the expression of the nm23-H1 gene was analyzed separately in the adherent, in the floating and in the total population (**Figure 2.7B**). Obestatin was found to cause an increase in expression of the nm23-H1 gene in the adherent population (41.18%±11.76) while reducing it in the floating population (42.35%±3.53).

In the total population, the significant increase in both gene and protein expression was maintained with 24 h obestatin treatment (29.41±7.06 and ≈69.44%, respectively) (**Figure 2.7E**).

[149] Steeg PS, Bevilacqua G, Pozzatti R, *et al.* Altered expression of NM23, a gene associated with low tumor metastatic potential, during Adenovirus 2 Ela inhibition of experimental metastasis. Cancer Research. 1988;48(22):6550–54.

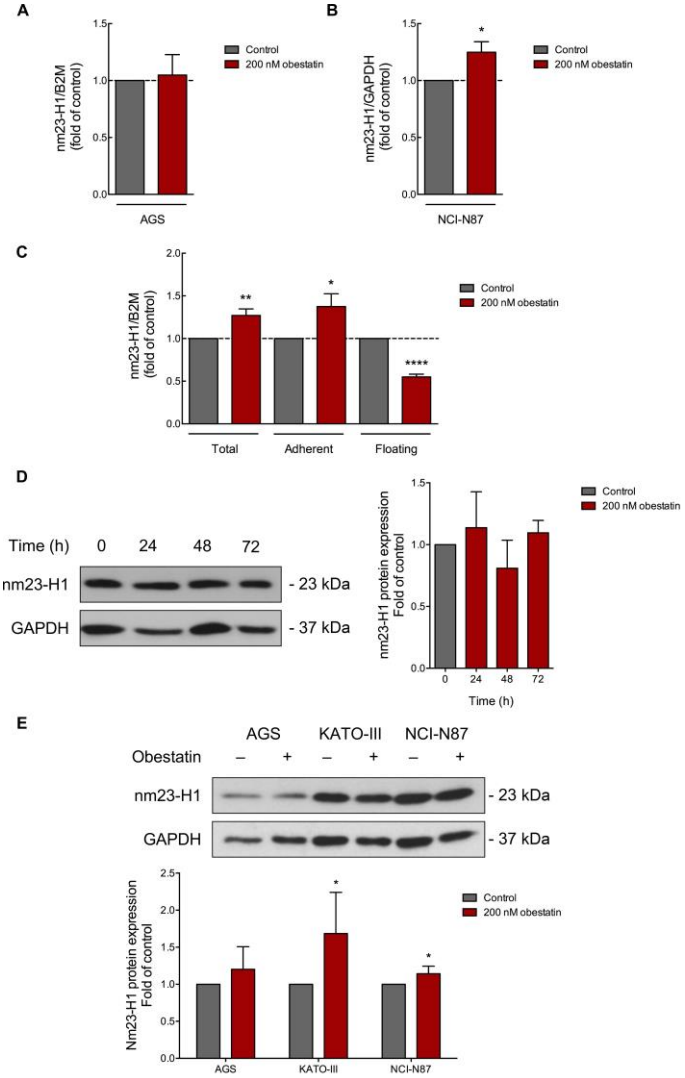

Figure 2.7. Level of expression of mRNA and protein of the tumour suppressor nm23-H1 in AGS, KATO-III and NCI-N87 cells stimulated with obestatin 200 nM. *nm23-H1* mRNA levels (qPCR) at 24 h in AGS (A), KATO-III (B) and NCI-N87 (C). The values of qPCR were normalized with the B2M levels in AGS and KATO-III or GAPDH in NCI-N87 and the mean of two independent readings. Data are expressed as mean±SEM. Single, double and triple asterisk (*, **, ***) denotes P< 0.05, P< 0.01 and P< 0.001, respectively, when comparing the treated with the untreated group. D) nm23-H1 protein levels at 24, 48 and 72 h in NCI-N87. E) nm23-H1 protein levels at 24 h in AGS, KATO-III and NCI-N87. Protein expression was normalized for GAPDH. Data were expressed as mean±SEM of three independent experiments. Single asterisk (*) denotes P<0.05 when comparing the treated with the untreated group.

Figures 2.7C and **E** show the data obtained for the expression of messenger RNA and protein nm23-H1 in NCI-N87 cells, respectively. Obestatin triggered an increase in the expression of both gene and protein nm23-H1 after 24 h treatment (26.09%±8.69 and 18.05%±6.53, respectively). A correlation was observed between both data and a significantly relevant increase. However, the kinetics performed for protein expression study at 24, 48 and 72 h showed non-statistically significant variable results (**Figure 2.7D**) that require additional assays. These results could be due to the diversity of subpopulations described in this cell line[150].

OBESTATIN EFFECT ON EPITHELIAL-MESENCHYMAL TRANSITION AND ANGIOGENESIS IN NCI-N87 CELL LINE

During the epithelial-mesenchymal transition (EMT), epithelial cells undergo changes in the cytoskeleton, in the signalling that defines cell form and in gene expression to achieve an increase in migration and the acquisition of an invasive phenotype, essential in metastatic progression.[151] It is characterized by the loss of E-cadherin and the increase of mesenchymal targets such as N-cadherin, vimentin or β-catenin. It is a transitory and reversible process, called in the second case, mesenchymal-epithelial transition (MET), a process that is involved in the establishment of metastatic cells in their new location.

In the case of AGS cells, our group has demonstrated that obestatin treatment causes an increase in mesenchymal markers, thus favouring the EMT[126]. For KATO-III cell line this experiment has not been carried out. The characteristics of this cell line, with a floating and adherent phenotype interchangeable with one another makes the experiment much more difficult to analyse.

[150] Chailler P, Ménard D. Establishment of human gastric epithelial (HGE) cell lines exhibiting barrier function, progenitor, and prezymogenic characteristics. J Cell Physiol. 2005;202:263–274.
[151] Wu WK, Cho CH, Lee CW, *et al.* Dysregulation of cellular signaling in gastric cancer. Cancer Lett. 2010;295:144-53.

As obestatin treatment decreased migration and invasion but increased proliferation in NCI-N87 cells, the role of obestatin in the EMT was determined by studying the expression of E-cadherin, β-catenin, N-cadherin and vimentin (**Figure 2.8**).

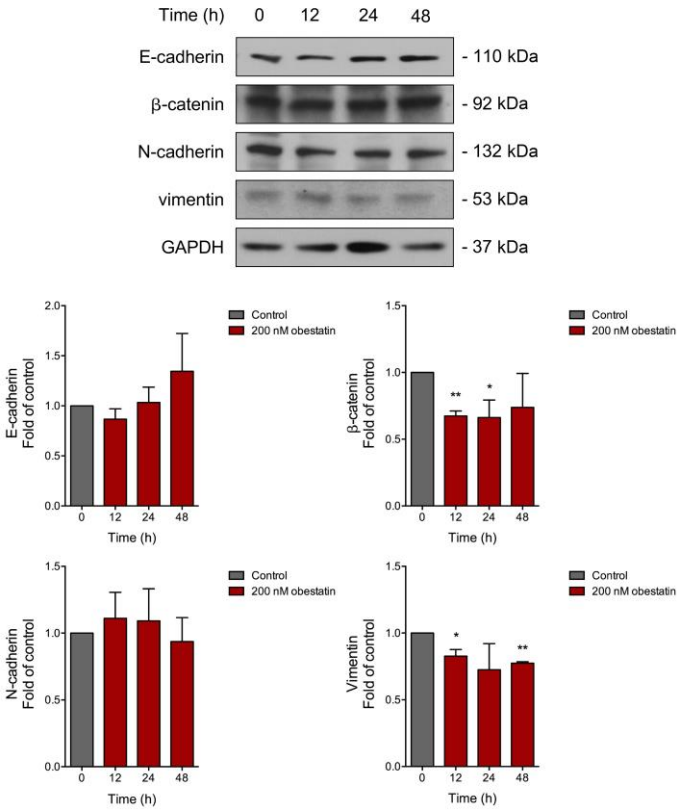

Figure 2.8. Immunoblot analysis of the EMT in NCI-N87 cell line. Cells were stimulated with obestatin (200 nM) during 12, 24, 48 h and the blots were incubated with the corresponding antibodies to E-cadherin, β-catenin, N-cadherin and vimentin. Protein expression was normalized relative to GAPDH. Data were expressed as mean±SEM after being obtained from intensity scans of independent experiments. Single and double asterisk (*,**) denotes P<0,05, P<0,01, respectively, when treated and untreated groups are compared.

With obestatin treatment (200 nM), levels of β-catenin (active form) and vimentin decreased, although after 48 h of stimulation only the decrease in vimentin (22.62±1.13%) was significant. N-cadherin did not show any change with obestatin stimulus nor epithelial marker E-cadherin, although a tendency to increase with respect to control was observed.

Angiogenesis is essential for the spread and establishment of tumour metastases[152]. We tested whether obestatin could affect the VEGF/VEGFR2 pro-angiogenic system. As **figure 2.9** shows, NCI-N87 cells stimulated with obestatin trended to reduce VEGFR2 levels, but not significantly. However, VEGF showed a significant decrease at 12 and 24 h (24.81±8.26 and 24.50±9.80 with respect to control, respectively). In addition, the anti-angiogenic factor PEDF exhibited a slight tendency to increase with obestatin treatment, but did not become statistically significant. Immunofluorescence was used to test the effect of obestatin on the distribution of the epithelial marker E-cadherin and the reorganization of cytoskeleton with phalloidine staining of the actin filaments (F-actin) in the three cell lines of the study (**Figure 2.10**).

It has been described that AGS cells possess an E-cadherin mutation, leading to a truncated form of the protein that is not expressed[153]. This is consistent with the fact that it was barely detected in control. However, obestatin treatment led to the formation of visible E-cadherin granules. This could indicate the formation of vesicles that send the protein to degrade, explaining the migratory capacity of obestatin observed in these cells[130].

With respect to KATO-III, a clear increase in E-cadherin expression was observed when treated with obestatin. In addition, the number of cells was also higher evidencing the proliferative role of obestatin in this cell line.

---

[152] Bielenberg DR, Zetter BR. The Contribution of Angiogenesis to the Process of Metastasis. Cancer J. 2015; 21(4): 267–273.

[153] Oliveira MJ, Costa AM, Costa AC, *et al.* CagA associates with c-Met, E-cadherin, and p120-catenin in a multiproteic complex that suppresses *Helicobacter pylori*-induced cell-invasive phenotype. J Infect Dis. 2009;200:745-55.

NCI-N87 cells are characterized by having E-cadherin in zonula adherens at cell-cell junctions[154]. Obestatin treatment provoked a reorganization of E-cadherin, going from being expressed in a generalized way in control to only in certain areas. In addition, it was observed that F-actin labelling seems to be disposed in the opposite way to E-cadherin, showing zones of a clear differential expression of both proteins.

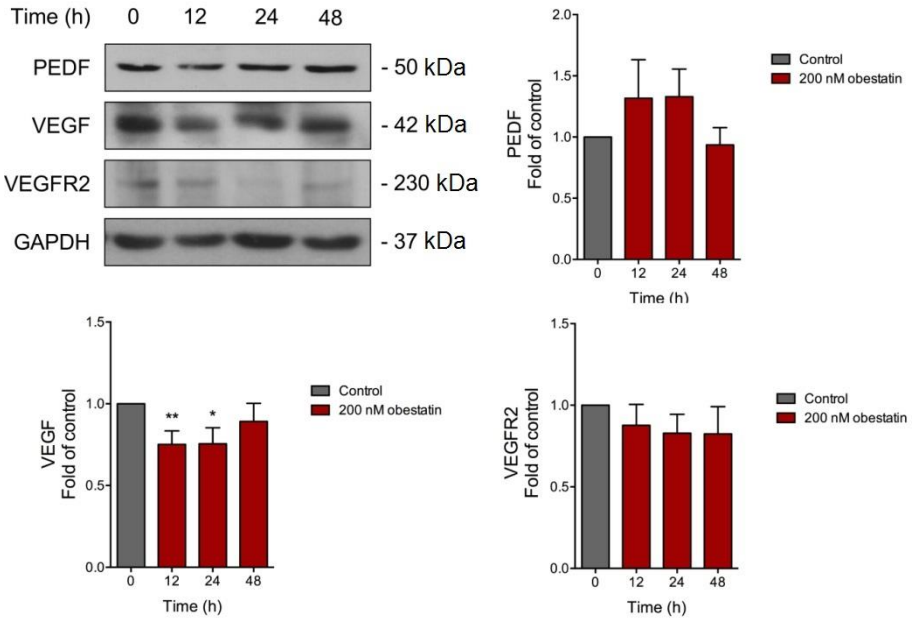

Figure 2.9. Immunoblot analysis of angiogenesis in NCI-N87 cell line. Cells were stimulated with obestatin (200 nM) for 12, 24, 48 h and the blots were incubated with the corresponding antibodies to PEDF, VEGF and VEGFR2. Protein expression was normalized relative to GAPDH. Data were expressed as mean±SEM after being obtained from intensity scans of independent experiments. Single and double asterisk (*,**) denotes $P < 0,05$, $P < 0,01$, respectively, when comparing treated and untreated groups.

[154] Basque JR, Chénard M, Chailler P. Gastric cancer cell lines as models to study human digestive functions. Journal of Cellular Biochemistry. 2001, 81:241-251.

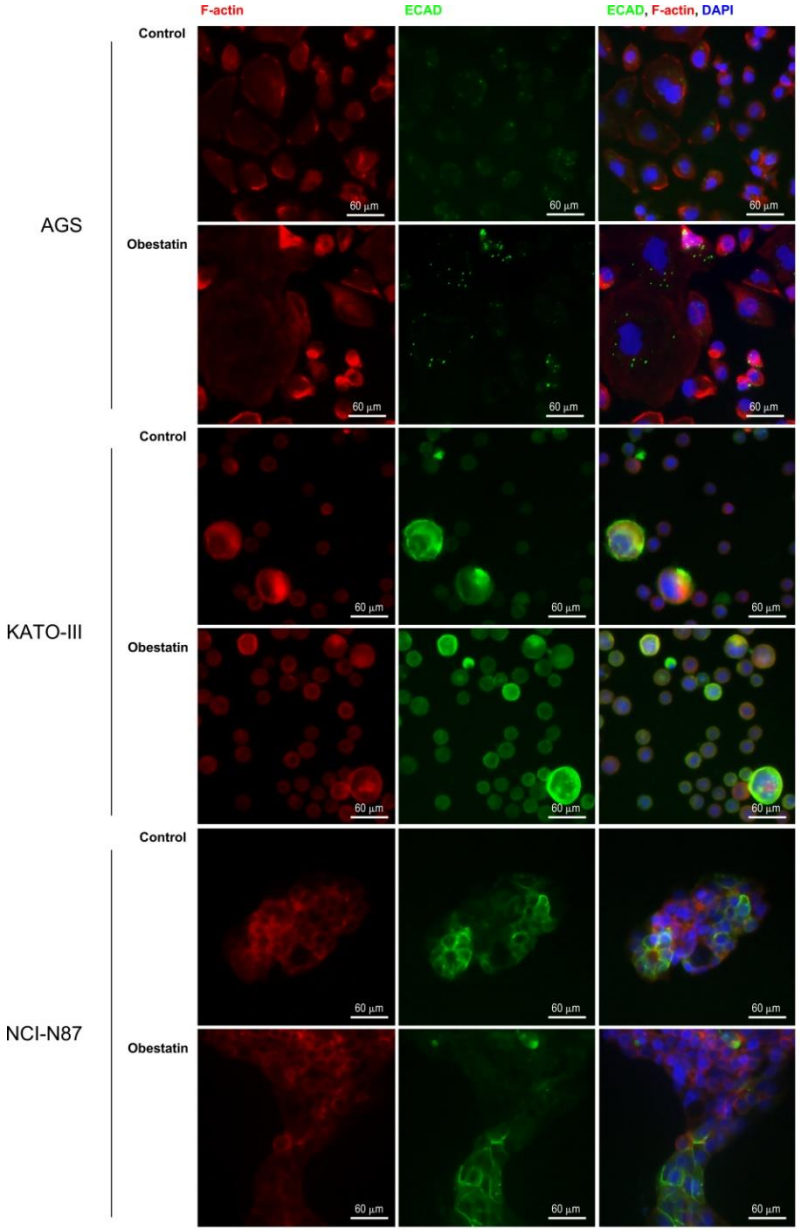

Figure 2.10. Obestatin effect on E-cadherin and cytoskeleton reorganization in AGS, KATO-III and NCI-N87 cells. Cells were stimulated with obestatin (200 nM) for 48h. E-cadherin (green) was then evaluated as well as Phalloidin CruzFluor™ 594 Conjugate (red) to visualize F-actin and DAPI (blue) to visualize nuclei by immunoflorescence. Objective magnification 20x.

This could be reflecting that obestatin favours some of subpopulations presented by NCI-N87, because it is a heterogeneous cell line composed of diverse phenotypic variants, including non-epithelial cells.[155] Future studies will be necessary to clarify this hypothesis. At the same time, it is evidenced that obestatin treatment induced a change in cell morphology, favouring NCI-N87 cell elongation. Its colony-forming growth pattern with dense clusters of cells does not allow a clear visualization of this effect.

OBESTATIN ACTIVATES AKT AND ERK 1/2 IN NCI-N87 CELLS

Obestatin performs its function through signalling pathway described by our research group. According to this, obestatin activates two parallel routes in which both ERK 1/2 and Akt are key targets in each of them.

The obestatin signalling pathway was reported from AGS and KATO-III cell experiments. We tested the effect of obestatin on the activation of these proteins in NCI-N87 cells. Akt phosphorylation in S473 residue and ERK1/2 phosphorylation in T202/Y204 were studied. For this, NCI-N87 cells were stimulated with obestatin (200 nM) performing a kinetic study at 5, 10, 20, 30 and 60 min.

Figure 2.11 shows a maximum activation at 5 min for ERK1/2 (1.30±0.11 with respect to the control) and a maximum at 10 min for Akt (1.87±0.27 with respect to the control). As expected, Akt activation was delayed with respect to ERK1/2, because it does not occur directly, as it required EGFR transactivation.

[155] Saraiva-Pava K, Navabi N, Emma C Skoog EC. New NCI-N87-derived human gastric epithelial line after human telomerase catalytic subunit over-expression. World J Gastroenterol. 2015; 21(21): 6526–6542.

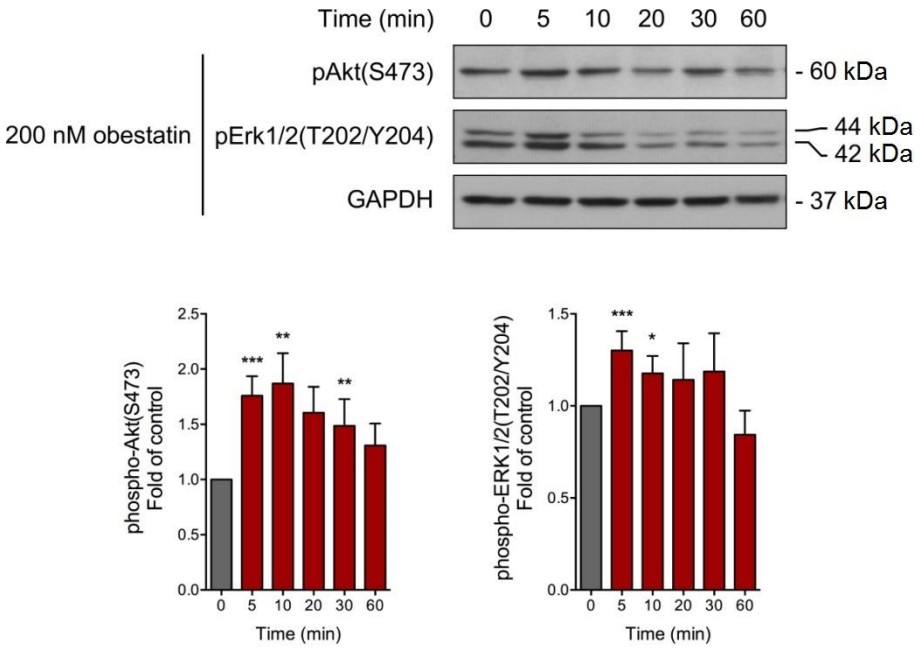

Figure 2.11. Obestatin effect on Akt and ERK1/2 activation in NCI-N87 cells. Cells were treated with obestatin (200 nM) for 5, 10, 20, 30 and 60 minutes. ERK1/2 and Akt phosphorylation were quantified using densitometry and expressed as the fold change relative to the phosphorylation obtained for unstimulated cells (mean±SEM) of five independent experiments).. Protein expression was normalized relative to GAPDH. Single, double and triple asterisk (*, **, ****) expresses $P < 0.05$, $P < 0.01$ and $P < 0.001$, respectively, when comparing treated with untreated group.

BASAL EXPRESSION OF GPR39 AND EGFR IN AGS, KATO-III AND NCI-N87 CELLS

The epidermal growth factor receptor (EGFR) belongs to the tyrosine kinase receptor family (RTKs). Activation of this receptor by its ligand initiates several downstream signalling pathways, such as RAS/RAF/MAP kinase and PI3K/Akt/mTOR, which play an important role in cellular processes such as proliferation, growth, survival, motility and tissue invasion[156].

[156] Kanat O, O'Neil B, Shahda S. Targeted therapy for advanced gastric cancer: A review of current status and future prospects. World J Gastrointest Oncol. 2015; 7(12): 401–410.

Overregulation of EGFR has been correlated with a more aggressive phenotype of tumour and worse clinical results in patients with gastric cancer[157,158], making it a good therapeutic target. Current strategies for targeting EGFR include the use of monoclonal antibodies directed against the extracellular part and tyrosine kinase inhibitors (TKIs) in the intracellular domain[156]. There are several mutant forms of EGFR, such as the isoform EGFRvIII which is unable to bind to any known ligand. Tumour progression and poor prognosis have been shown to correlate with this aberrant signalling.

The obestatin/GPR39 system signalling path describes the existence of a crosstalk between GPR39 and EGFR, in which the EGFR is transactivated by GPR39 with β-arrestins interaction and Src activation.

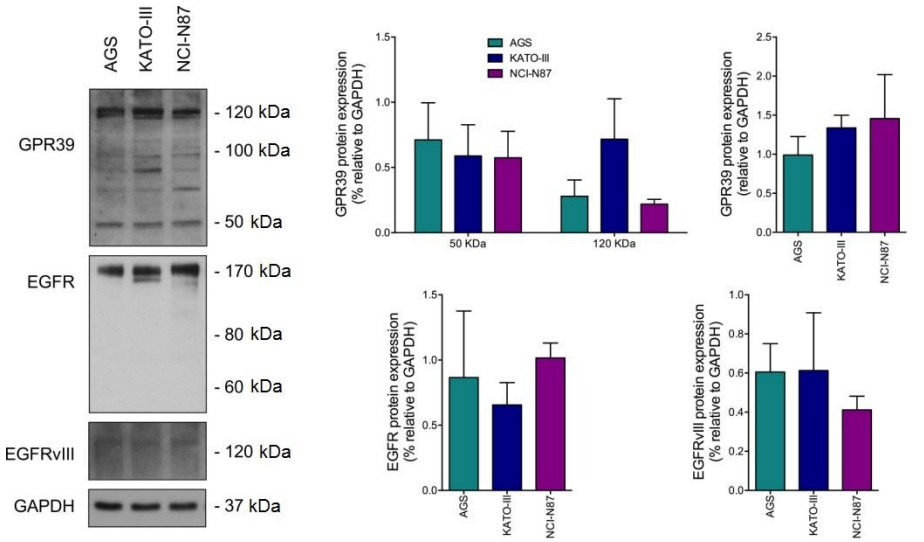

Figure 2.12. Expression of GPR39, EGFR and EGFRvIII. Expression of the levels of GRP39, EGFR isoforms and EGFRvIII in the three cell lines. Protein expression was normalized relative to GAPDH. Data were quantified and expressed as mean±SEM from four independent experiments.

[157] Martinelli E, De Palma R, Orditura M *et al.* Anti-epidermal growth factor receptor monoclonal antibodies in cancer therapy. Clin Exp Immunol. 2009; 158:1–9.
[158] Normanno N, De Luca A, Bianco C *et al.* Epidermal growth factor receptor (EGFR) signaling in cancer. Gene. 2006; 366:2–16.

In order to reveal the role of EGFR in obestatin/GPR39 signalling in the three cell lines, basal expression of GPR39 and EGFR/EGFRvIII was determined by immunoblot. All cell lines expressed GPR39 as reflected in **figure 2.12**. This expression was not limited only to the usual band of 50 kDa, but a very intense band at 120 kDa appeared, which could evidence the presence of dimers, already described for GPR39 and GHSR1a when samples were processed at different temperatures.[159]

EGFR was also expressed by the three cell lines, being NCI-N87 the one that presented a greater amount. However, the expression of EGFR vIII was very low in all of them, meaning that it should not play an important role in these systems.

OBESTATIN EFFECT ON EGFR PHOSPHORYLATION IN AGS, KATO-III AND NCI-N87 CELLS

Knowing that EGFR was expressed in the three cell lines, it was decided to assess the activation of this receptor by analyzing phosphorylation in different residues. Treating the cells with obestatin (200 nM) for 5 and 10 min, the phosphorylation of EGFR at 845, 992, 1045 and 1068 tyrosine residues was evaluated by immunoblot.

As shown in **figure 2.13**, in AGS cell line there was a non-significant tendency to increase EGFR phosphorylation when stimulated with obestatin. In KATO-III cells, when treated with obestatin, there was also a tendency to increase phosphorylation at 1045 and 992 residues. Surprisingly, 1068 and 845 tyrosines showed a significant reduction of their phosphorylation at 10 min. On the other hand, obestatin treatment in NCI-87 cells showed a tendency to decrease phosphorylation of the four EGFR residues.

[159] Cunningham, PS. The ghrelin receptor isoforms (GHS-R1a and GHS-R1b) and GPR39: an investigation into receptor dimerisation. Doctoral dissertation. Queensland University of Technology, Queensland, Australia. 2010.

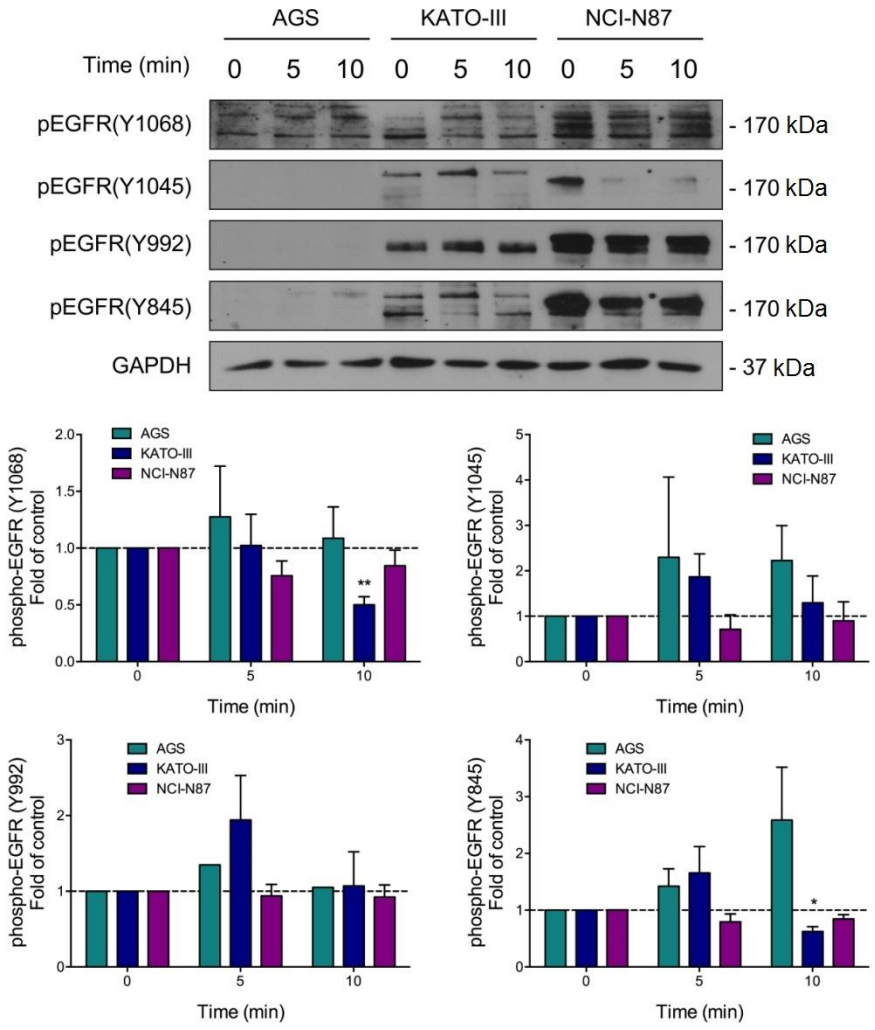

OBESTATIN EFFECT ON PAR EXPRESSION IN AGS, KATO-III AND NCI-N87 CELLS

The protease activated receptors (PARs) are receptors coupled to G proteins, which as their name suggests, their activation mechanism is based on proteolytic excision at a extracellular N-terminal segment to expose a new ligand domain bound to N-terminus, which binds and activates the split receptor[160].

Three of the family members, PAR1, PAR3 and PAR4, are thrombin activated receptors. However, PAR2 is activated by other proteases including trypsin, tryptase and Factor Xa[161]. They play an important role in physiological functions and haemostasis is one of the best known[161,162,163].

In addition, their implication was demonstrated in certain diseases such as cancer, involving in tumour progression[164] and metastasis[165]. The obestatin/GPR39 system is involved in RTKs transactivation and expression regulation of different proteases. Both families of proteins are overregulated in different pathologies including cancer. Bearing in mind that the role of PARs in the control of gastric cancer has been demonstrated[166], it has led us to consider the role of obestatin in the regulation of these receptors.

---

160 Han N, Jin K, He K. Protease-activated receptors in cancer: A systematic review. Oncology Letters. 2011; 2(4):599-608.

161 O'Brien P, Molino M, Kahn M *et al.* Protease activated receptors: theme and variations. Oncogene. 2001;20(13):1570-1581.

162 Zhao P, Metcalf M, Bunnett NW. Biased signaling of protease-activated receptors. Front Endocrinol (Lausanne).2014;5:67.

163 Griffin JH, Zlokovic BV, Mosnier LO. Activated protein C: biased for translation. Blood. 2015;125(19):2898-2907.

164 Jin E, Fujiwara M, Pan X *et al.* Protease-activated receptor (PAR)-1 and PAR-2 participate in the cell growth of alveolar capillary endothelium in primary lung adenocarcinomas. Cancer. 2003;97: 703-713.

165 D'Andrea MR, Derian CK, Santulli RJ *et al.* Differential expression of protease-activated receptors-1 and -2 in stromal fibroblasts of normal, benign, and malignant human tissues. Am J Pathol. 2001;158: 2031-2041.

166 Sedda S, Marafini I, Caruso R *et al.* Proteinase activated-receptors-associated signaling in the control of gastric cancer. World J Gastroenterol. 2014;20:11977-84.

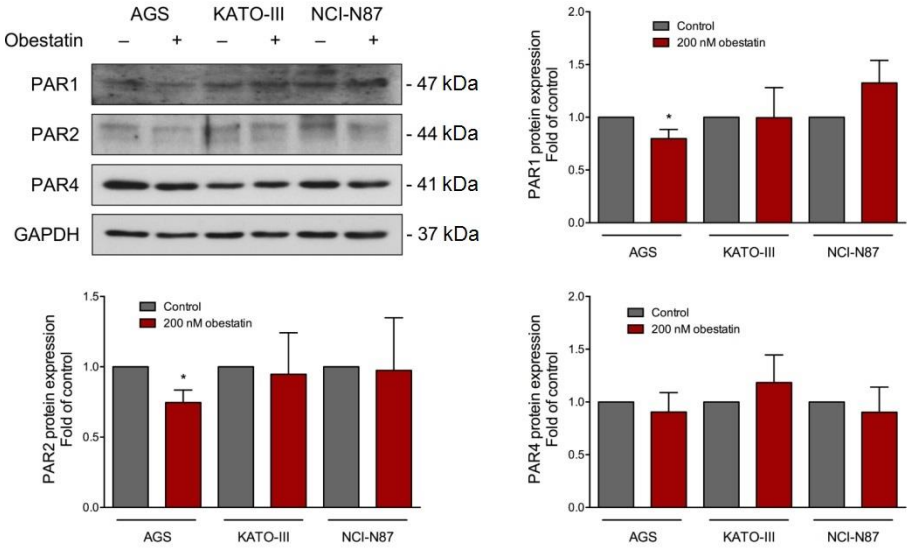

Figure 2.14. Obestatin effect on PAR expression in AGS, KATO-III and NCI-N87 cells. Cells were stimulated with obestatin (200 nM) for 24 h. Protein expression was normalized relative to GAPDH. Data were quantified and expressed as mean±SEM from three independent experiments. Single and double asterisk (*, **) denotes P< 0.05 and P< 0.01, respectively, when comparing treated and untreated groups.

Using the three cell lines, obestatin stimulation (200 nM) was performed for 24 h and PAR expression was analyzed by immunoblot. Observing **figure 2.14**, PAR-1 expression was only significantly modified in AGS cells, showing a decrease with obestatin treatment compared to control (0.80±0.09 compared to control). In the case of NCI-N87, a slight increase in expression was seen while in KATO-III no variations were observed. PAR-2 expression was significantly reduced again with the obestatin stimulus only in AGS cells (0,75±0,09 with respect to the control), not offering changes in the rest of cell lines. On the other hand, PAR-4 did not show differences in its expression in any of the three lines, only observing a slight tendency in KATO-III cells to increase its expression with obestatin treatment.

CHAPTER 3: OBESTATIN/GPR39 SYSTEM IN PRECANCEROUS LESIONS OF HUMAN STOMACH

The obestatin/GPR39 system has been implicated in the development of gastric cancer, evidencing a correlation between the GPR39 expression and the tumour differentiation degree. Poorly differentiated adenocarcinomas showed the strongest positivity. GPR39 could therefore be established as a prognostic marker for this type of pathology[126].

Correa in 1975 proposed a model of gastric carcinogenesis. It was updated several times over the years, but the fundamental idea is that the healthy mucosa is infected by *H. pylori*, developing a gastritis that evolves to atrophy. Subsequently, intestinal metaplasia and dysplasia follow one another, being the prelude to stomach cancer[15].

In order to deepen the role in the initiation, development and maintenance of gastric cancer, we decided to study this system in the premalignant stages of the Correa model.

GPR39 IS EXPRESSED EXCLUSIVELY IN THE CHIEF CELLS OF THE OXYNTIC MUCOSA

The expression of the obestatin/GPR39 system in a healthy human stomach has been evaluated in previous studies. Obestatin is expressed in the enteroendocrine cells and GPR39 in the chief cells of the oxyntic glands[126]. To verify that the expression of GPR39 is located exclusively in these glands, an immunohistochemical analysis was carried out using a stomach sample from a transition zone between the oxynthic and antral glands **(Figure 3.1)**. In hematoxylin-eosin (H+E) staining, the antral glands stained with a pink coloration being more eosinophilic, while the oxyntic glands were stained violet by zymogenic cells containing large amounts of rugged endoplasmic reticulum (RER). GPR39 immunostaining was observed at the base of the oxyntic glands. Almost all of the antral glands have been negative, with the exception of some cells compatible with chief cells. These cells are characteristically located in the oxyntic gland, but the Goldenring group has

shown that the antral oxyntic gland, a type of antral transition gland, presents them[167].

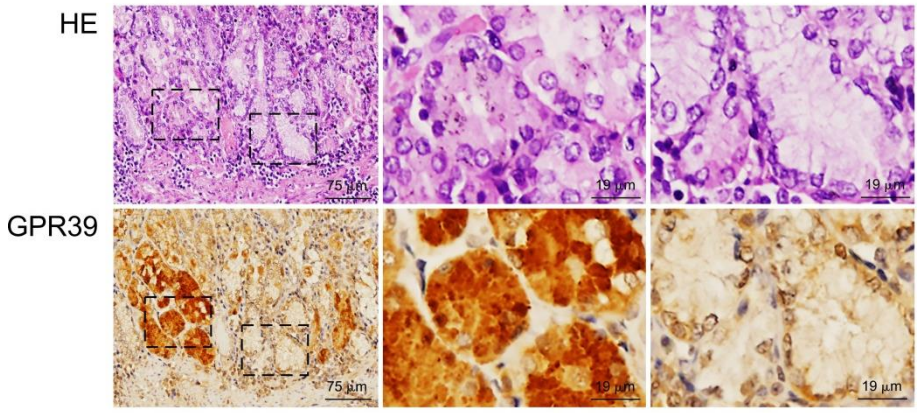

Figure 3.1. GPR39 expression in the transition zone of a healthy human stomach. Upper panel A) HE staining under 20x magnification. B) Detailed area of oxyntic gland. C) Detailed area of antral gland. Bottom panel D) Expression of GPR39 under 20x magnification. E) Detailed area of oxyntic gland and F) Detailed area of antral gland. Detailed zones under 63x magnification.

OBESTATIN/GPR39 SYSTEM EXPRESSION IN PRECANCEROUS LESIONS

Since the expression of the obestatin/GPR39 system is circumscribed to the oxyntic glands, an immunohistochemical analysis was performed on human stomach fundus biopsies of the 5 different stages of the Correa gastric carcinogenesis model: healthy stomach, gastritis, atrophy, intestinal metaplasia and dysplasia. The expression of obestatin, GPR39 and pepsinogen was studied in a series of 10 patients per group.

Obestatin was expressed in enteroendocrine cells in all groups (**Figure 3.2**). Despite the existence of variable data between patients in the same group, significant differences were not detected when comparing the different groups in the sequence.

[167] Choi E, Roland JT, Barlow BJ, *et al*. Cell lineage distribution atlas of the human stomach reveals heterogeneous gland populations in the gastric antrum. Gut. 2014;63(11):1711-20.

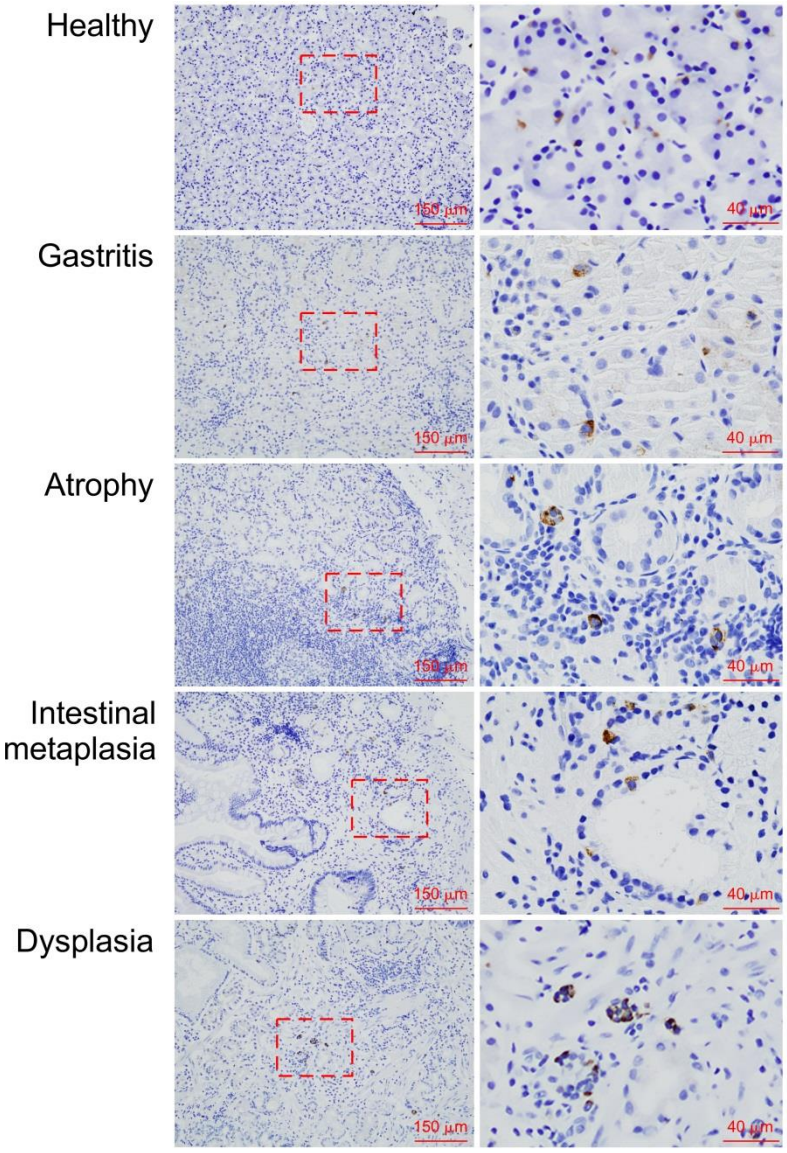

Figure 3.2. Obestatin expression in precancerous lesions of human gastric fundus. Representative images of obestatin expression from 10 patients per group. General view at x10 and detailed area at x40 magnification.

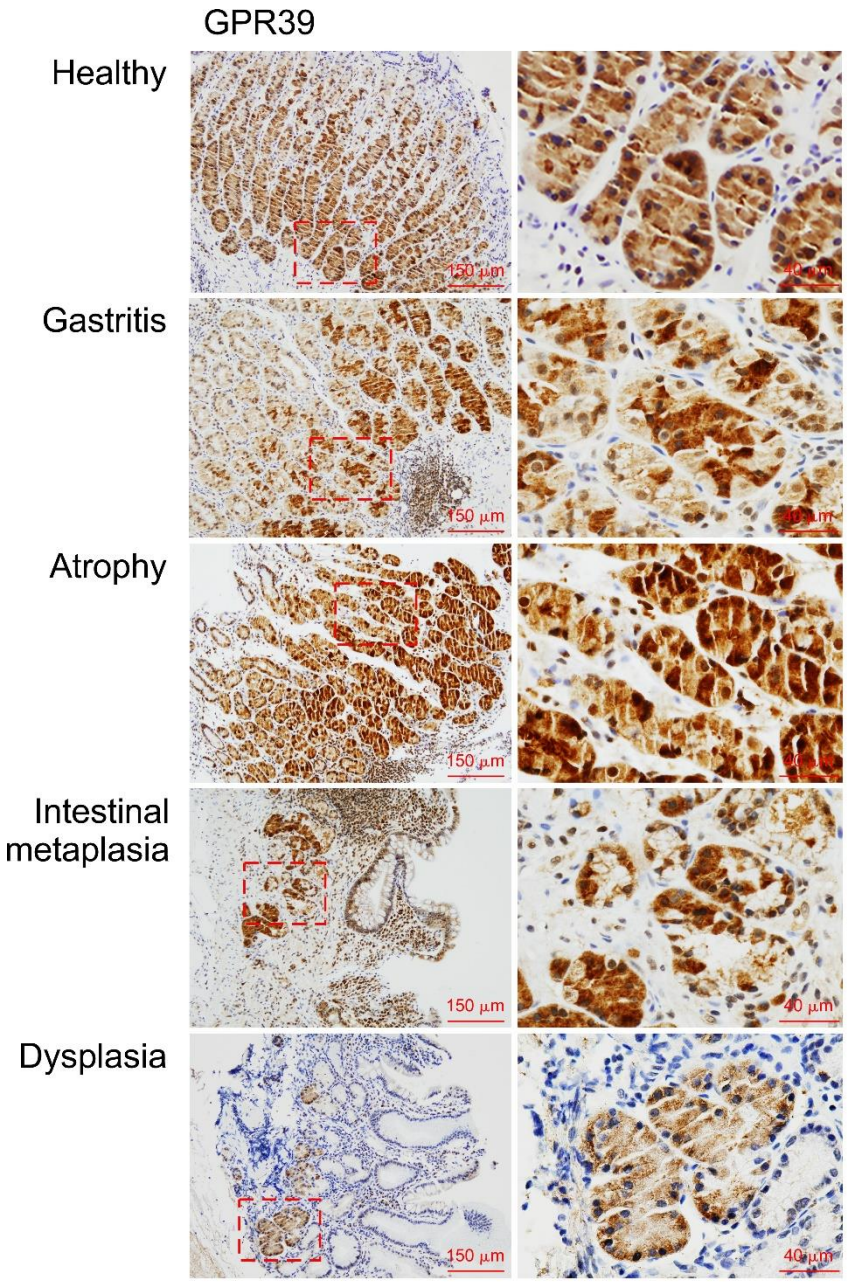

Figure 3.3. Expression of GPR39 in precancerous lesions of the human gastric fundus. Representative images of immunohistochemical expression from 10 patients per group. General view in x10 and detailed area with x40 magnification

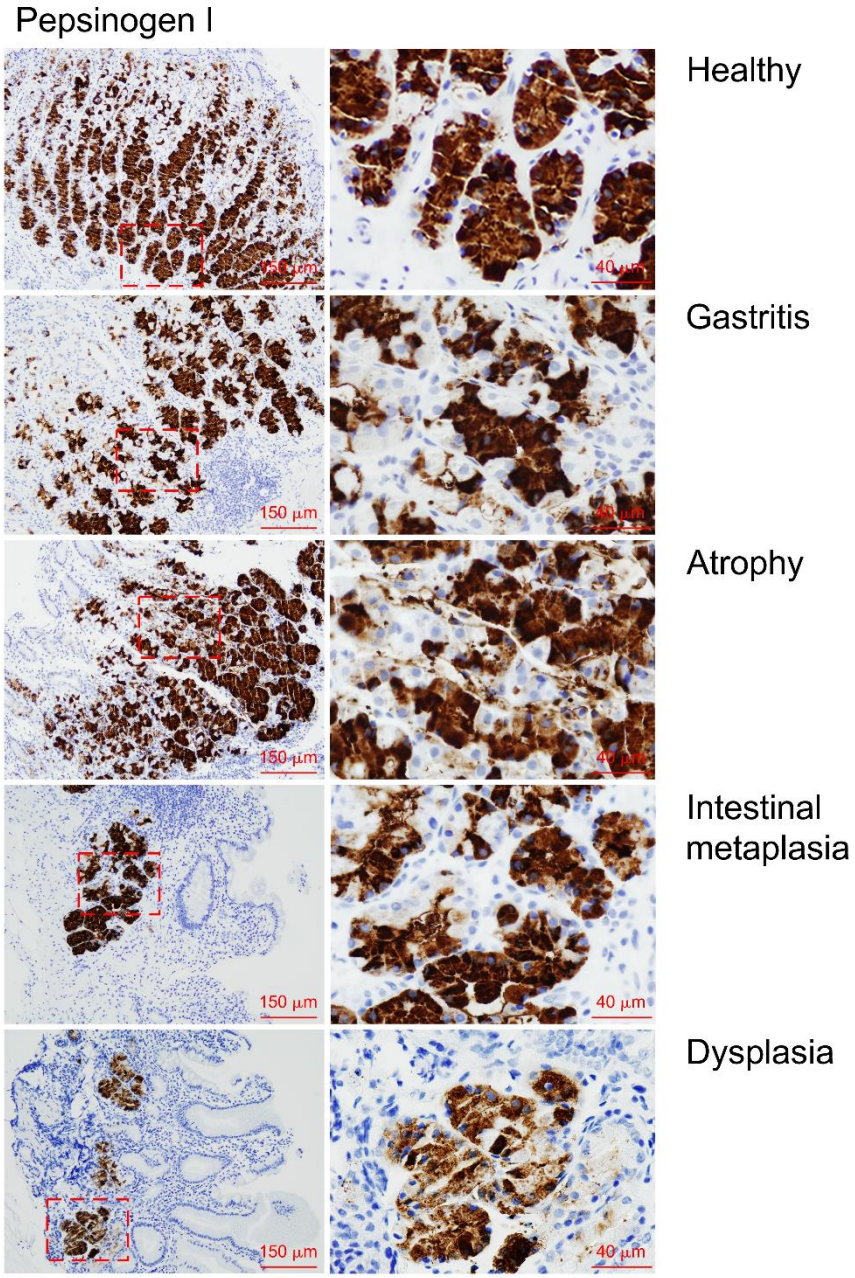

Figure 3.4. Expression of pepsinogen I in precancerous lesions of the human gastric fundus. Representative images of immunohistochemical expression from 10 patients per group. General view in x10 and detailed area with x40 magnification

The serial sections (3 μm) utilized for the analysis immunohistochemistry allowed us to identify the positive cells for GPR39 and pepsinogen I (**Figure 3.3** and **3.4**). GPR39 was expressed in the same cells as pepsinogen (PGI), the chief cells of the oxyntic glands. When comparing the expression of GPR39 and PGI, it is observed that there are no differences in the level of expression since the chief cells of the base of the gland are always positive.

BASAL EXPRESSION OF GPR39, EGFR AND IGF-IR IN HEALTHY STOMACH, GASTRITIS OR ATROPHY

Previous studies show that obestatin is capable of over-regulating a large number of RTKs in gastric cancer cells. Among them, EFGR and IGF-IR are significantly transactivated by the obestatin/GPR39 system. An immunoblot analysis has been carried out to deepen the role of this system in the precarcinogenic stage. To begin with, the basal levels of GPR39, EGFR, EGFR vIII and IGF-IR have been analyzed in gastric fundus of healthy, gastritis and atrophic patients (**Figure 3.5**).

GPR39 expression was significantly reduced in atrophy with respect to healthy and gastritis groups. As mentioned above, the quality of the samples is critical in these results. In an atrophic context obtaining a deep biopsy encompassing the entire gland is much more difficult. For that reason, as GPR39 is expressed in the chief cells of the base of the gland, GPR39 level of expression was not reliable in the atrophy group.

EGFR showed a similar expression pattern, with a significant decrease in atrophy with respect to the other groups. The tumour variant EGFR vIII has not been detected in any case (data not shown).

Conversely, the expression of IGF-IR showed a positive correlation with the degree of pathology, evidencing a significant increase in atrophy with respect to the other groups.

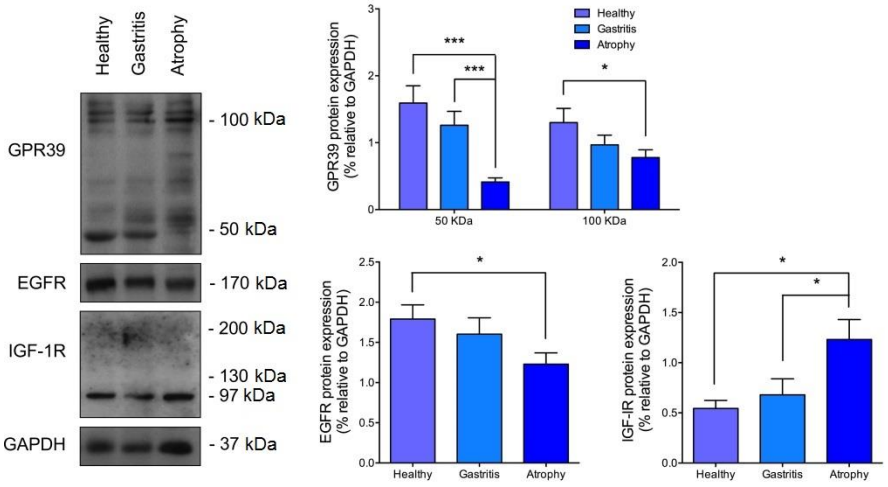

Figure 3.5. Basal expression of GPR39, EGFR and IGF-IR in healthy stomach, gastritis or atrophy. Protein expression was normalized relative to GAPDH. Data were quantified and expressed as mean±SEM from eight independent experiments. Single, double and triple asterisk (*, **, ****) expresses $P < 0.05$, $P < 0.01$ and $P < 0.001$, respectively, when comparing between groups.

OBESTATIN/GPR39 SYSTEM EFFECT ON PROTEASE REGULATION IN HEALTHY STOMACH, GASTRITIS OR ATROPHY

The obestatin/GPR39 system acts as a regulating factor for proteases, which are essential for the transactivaton of other GPCRs and the triggering of the signalling pathway described for this system.

The functionality of the obestatin/GPR39 system has been studied by exogenous obestatin administration to the fundus biosies of healthy, gastritis and atrophy patients. The biopsies were placed in medium with obestatin 200 nM for 2 h and the analysis of enzymes and different proteases in lysate was performed by immunoblot. (**Figure 3.6**).

Pepsinogen I shows a gradual reduction from healthy group to atrophy and obestatin treatment tends to increase its expression in all cases. Similar pattern

of expression is observed in gastric lipase and obestatin also tends to increase levels in all groups.

Despite variations, a slight increase in basal expression of cathepsin D has been observed in gastritis and atrophy with respect to control. Obestatin showed overexpression in the atrophy group, while healthy and gastritis remained unchanged.

Cathepsin L was also studied. In this case, three bands corresponding to the different isoforms were detected: precursor (52 kDa), intermediate (38 kDa) and mature form (25 kDa). Many proteases are synthesized as pro-enzymes that need to be processed until reaching the mature form that is functionally active. In this case, the immature form increases as the pathology progresses while the intermediate mature cone form shows the inverse trend. Obestatin treatment did not show major changes in the immature form of cathepsin L.

The intermediate form was increased in the healthy and atrophy with treatment. Finally, active cathespin L tended to decrease in healthy and gastritis with treatment with obestatin stimulus. In general, analyzing the expression of total cathepsin L, there is a tendency to reduce as the Correa sequence advances and the exogenous treatment of obestatin did not cause substantial changes.

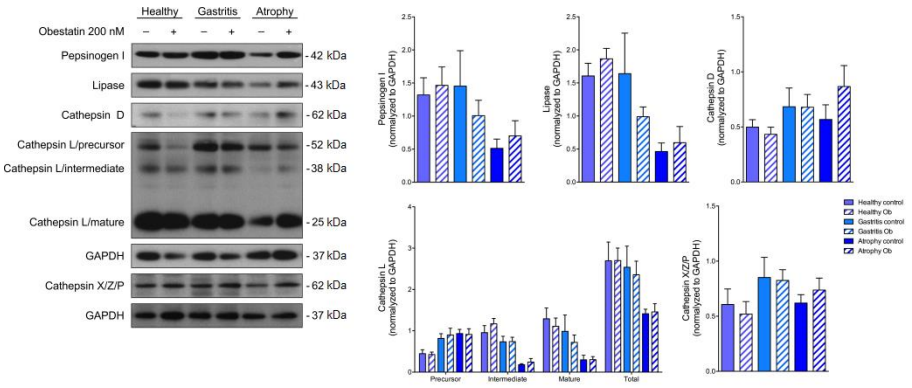

Figure 3.6. Obestatin/GPR39 system effect on protease regulation in healthy stomach, gastritis or atrophy. Gastric fundus biopsies were stimulated with obestatin 200 nM during 2 h.Protein expression was normalized relative to GAPDH. Data were quantified and expressed as mean±SEM from six independent experiments.

Finally, cathepsin Z remained stable in all three groups. While healthy stomach stimulation with obestatin reduced its levels, in gastritis and atrophy there was a tendency to increase with treatment.

CHAPTER 4. STUDY OF HUMAN BIOFLUIDS FROM PATIENTS GROUPED ACCORDING TO CORREA'S CASCADE TO GASTRIC CANCER BY NMR METABOLOMICS

Metabolomics is a very useful tool for the biomarker identification. The under-diagnosis of gastritis and atrophy pathologies make it necessary to create reliable protocols for their effective detection. Through the analysis of plasma and urine in 109 and 108 patients, respectively, ^{1}H-NMR experiments have been carried out to identify metabolites predictive of *H. pylori* infection, as well as gastritis and atrophy.

PLASMA

We have evaluated the applicability of ^{1}H NMR spectroscopy in the diagnosis of gastritis and atrophy and *H. pylori* infection by analyzing plasma samples of 109 patients, 39 healthy controls 42 gastritis and 28 atrophy. Spectral regions were binned in segments of 0.01 ppm width for statistical analysis. The intensities of the generated bins were analyzed statistically.

Multivariate analysis

The PCA analysis revealed a strong separation of patients into two groups with only one component (**Figure 4.1**). This separation is not related to any known variable in our study. Both groups contain a similar number of patients so we decided to perform the analysis of both groups separately.

A new PCA analysis reveals that new subgroups are formed. Given the limited number of patients, no new fragmentation can be carried out to avoid loss of robustness.

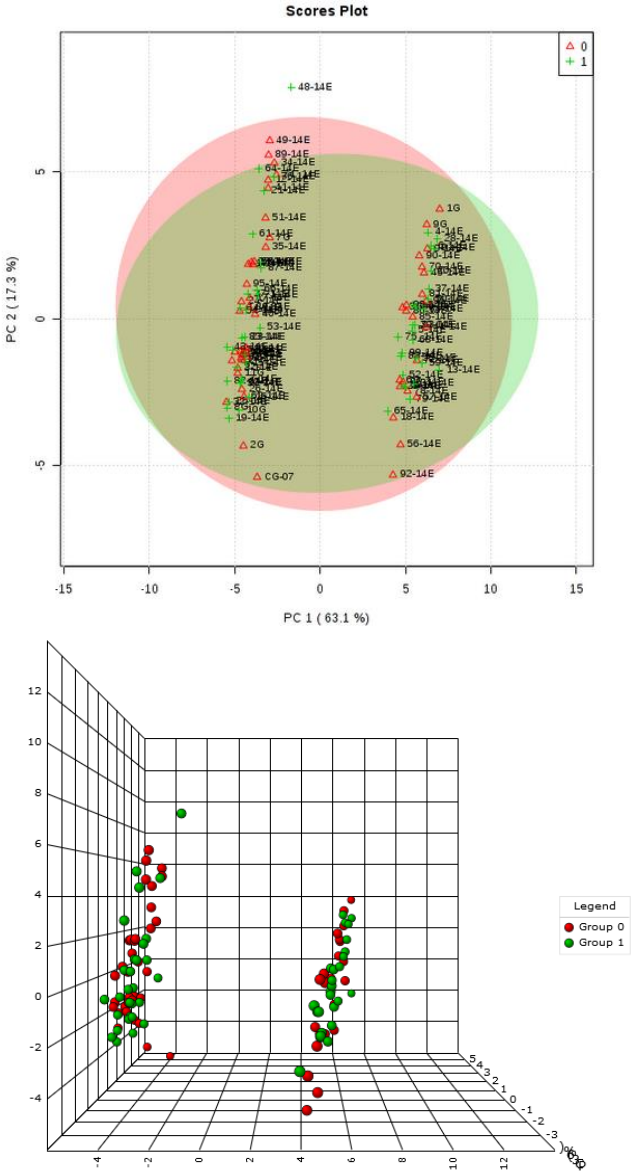

Figure 4.1. PCA analysis for *H. pylori* infection *versus* no infection in plasma samples. Upper image. Two-dimensional PCA score plot. Red triangles: no infection samples. Green crosses: *H. pylori* infection samples. **Bottom image.** Three-dimensional PCA score plot. Red circles: no infection samples. Green circles: *H. pylori* infection samples. Strong separation in two groups is observed with this analysis but does not correspond to that of the variables studied.

URINE

Similarly to plasma samples. we have used ^{1}H NMR spectroscopy to the diagnosis of gastritis and atrophy and *H. pylori* infection by analyzing urine samples of 108 patients, 38 healthy controls 42 gastritis and 28 atrophy. Spectral regions were binned in segments of 0.03 ppm width for later statistical analysis.

Multivariate analysis

The PCA analysis of the bins intensities showed a strong separation in two groups of patients. A two-dimensional scatter plot indicated a clear unsupervised separation with the first component PC1 (**Figure 4.2**). The smallest group contained 30 patients. This separation could not be explained with the available metadata, so we decided to eliminate them from the study. In addition, PCA revealed two outliers that were located out from the Hotelling T^2 distribution ellipses and were also excluded from further analysis.

Statistical analysis was performed again with the 76 remaining cases. No age-related groupings were observed in the PCA score plots but sex-related groupings were identified by supervised test. PLSDA discriminated well both groups by three principal components but some overlap persists when considering only PC1 and PC2 while OPLS-DA test discriminated perfectly with only two components (**Figure 4.3**). To avoid that this separation by sex could influence in our study, we analyzed men (graphs framed in yellow from now on) and women (graphs framed in purple from now on) separately.

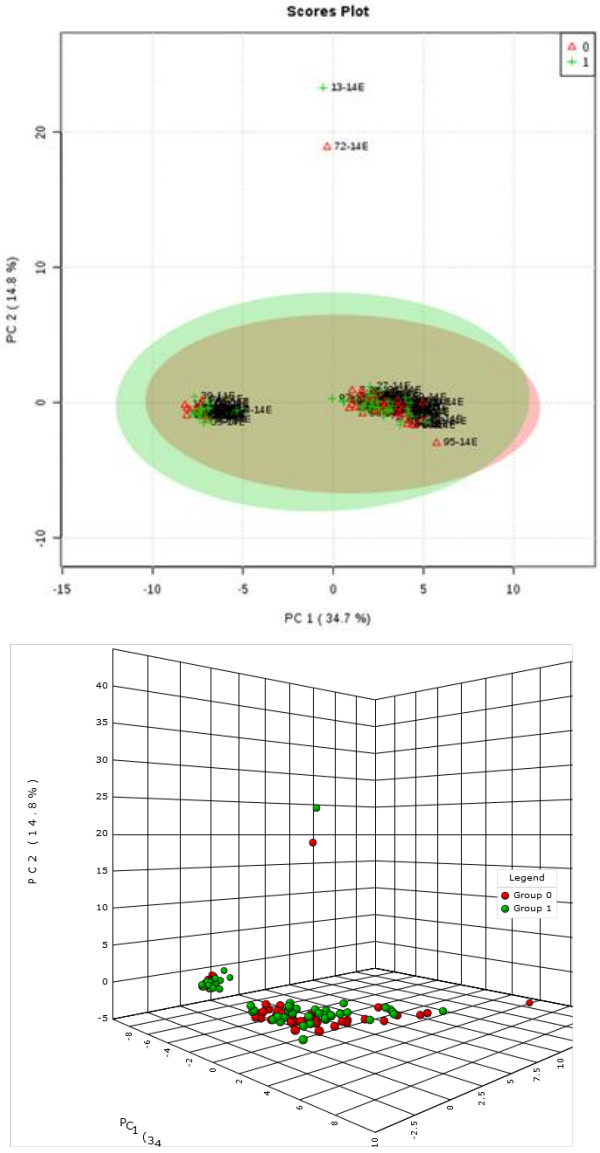

Figure 4.2. PCA analysis for *H. pylori* infection versus no infection in urine samples. Upper image: Two-dimensional PCA score plot. Red triangles: no infection samples. Green crosses: *H. pylori* infection samples. **Bottom image**: Three-dimensional PCA score plot. Red circles: no infection samples. Green circles: *H. pylori* infection samples. Strong separation in two groups is observed with this analysis but does not correspond to that of the variables studied.

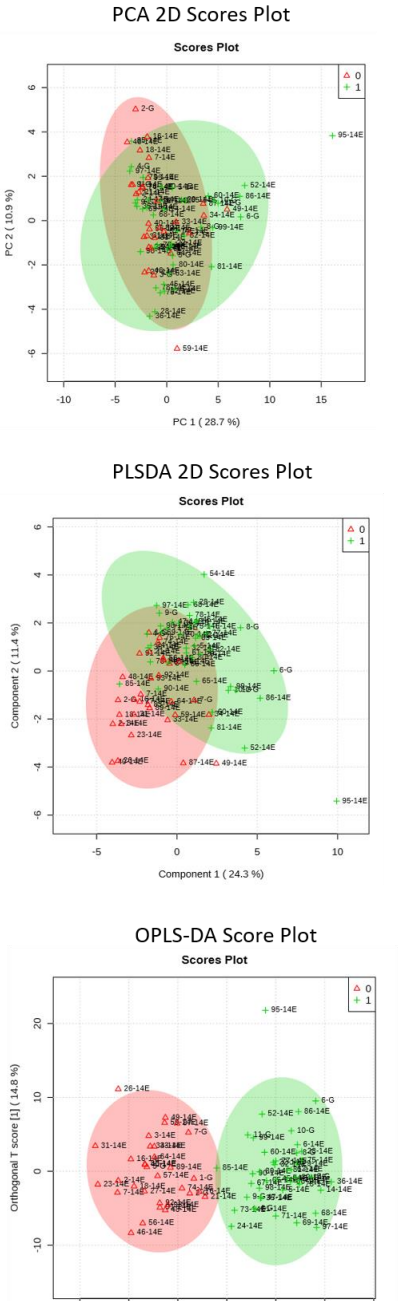

Figure 4.3. Multivariate analysis for men *versus* women in urine samples. Upper image: Two-dimensional PCA score plot. **Middle image:** Two-dimensional PLSDA score plot. **Bottom image:** Two-dimensional OPLS-DA score plot. Red triangles: men. Green crosses: women.

Helicobacter pylori

Multivariate analysis of ^{1}H-NMR spectra between controls without infection and patients with *H. pylori* infection was performed. In both cases men and women, PCA revealed no differences in the distribution of both groups. Among the supervised method, PLSDA showed a slight separation but not significant (**Figure 4.4**). The difference between groups was not so evident to be able to be observed in this type of analysis. Similarly, the same results were obtained in the multivariate analysis of women (**Figure 4.5**).

A univariate analysis was performed to find out if there was any region of the spectrum that was significantly different to predict *H. pylori* infection. In males, Fold Change (FC) analysis revealed 21 spectra bins in males and 11 in females as statistically significant. Most of them belong to the upper part of the spectrum. Volcano plot, which is a combination of the Fold Change (FC) and Student's *t*-test, distinguished 5 significant bins in men and 3 in women. A total of 8 spectral bins were found common in both sexes (**Figures 4.6** to **4.9**).

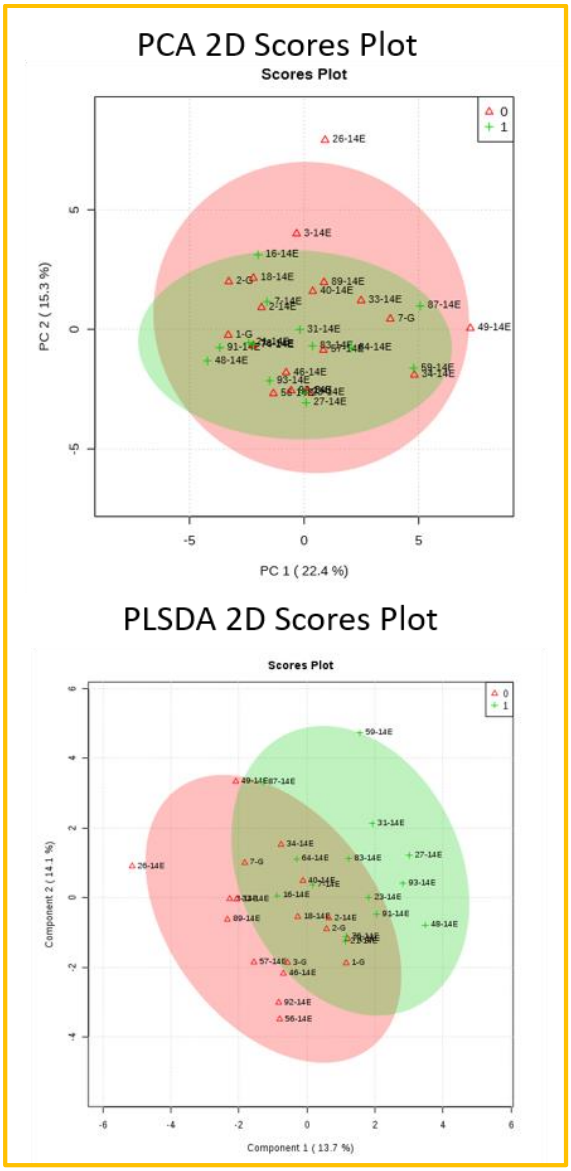

Figure 4.4. Multivariate analysis for *H. pylori* infection *versus* no infection in male urine samples. Upper image.Two-dimensional PCA score plot. **Bottom image.** Two-dimensional PLSDA score plot. Red triangles: no infection samples. Green crosses: *H. pylori* infection samples.

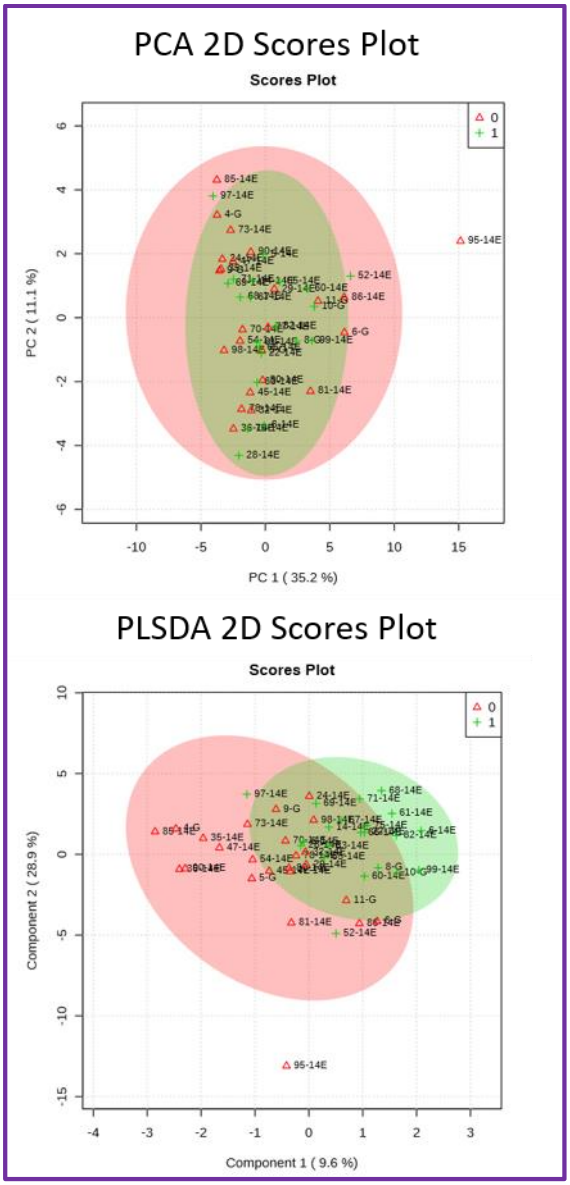

Figure 4.5. Multivariate analysis for *H. pylori* infection *versus* no infection in female urine samples. Upper image.Two-dimensional PCA score plot. **Bottom image.** Two-dimensional PLSDA score plot. Red triangles: no infection samples. Green crosses: *H. pylori* infection samples.

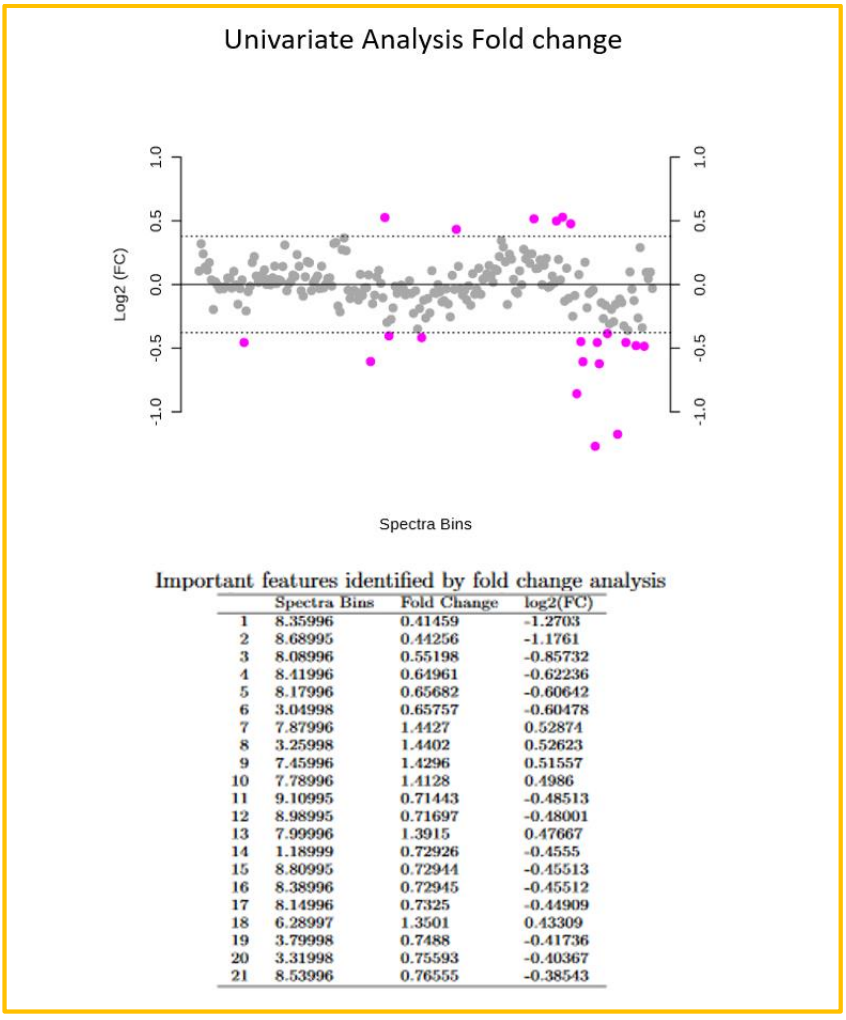

Important features identified by fold change analysis

	Spectra Bins	Fold Change	log2(FC)
1	8.35996	0.41459	-1.2703
2	8.68995	0.44256	-1.1761
3	8.08996	0.55198	-0.85732
4	8.41996	0.64961	-0.62236
5	8.17996	0.65682	-0.60642
6	3.04998	0.65757	-0.60478
7	7.87996	1.4427	0.52874
8	3.25998	1.4402	0.52623
9	7.45996	1.4296	0.51557
10	7.78996	1.4128	0.4986
11	9.10995	0.71443	-0.48513
12	8.98995	0.71697	-0.48001
13	7.99996	1.3915	0.47667
14	1.18999	0.72926	-0.4555
15	8.80995	0.72944	-0.45513
16	8.38996	0.72945	-0.45512
17	8.14996	0.7325	-0.44909
18	6.28997	1.3501	0.43309
19	3.79998	0.7488	-0.41736
20	3.31998	0.75593	-0.40367
21	8.53996	0.76555	-0.38543

Figure 4.6. Univariate analysis Fold change for *H. pylori* infection versus no infection in male urine samples. Upper image. Highlighted bins mean significantly different with P<0.05 with a threshold of 1.3. **Bottom table.** Significant bins are listed in the table.

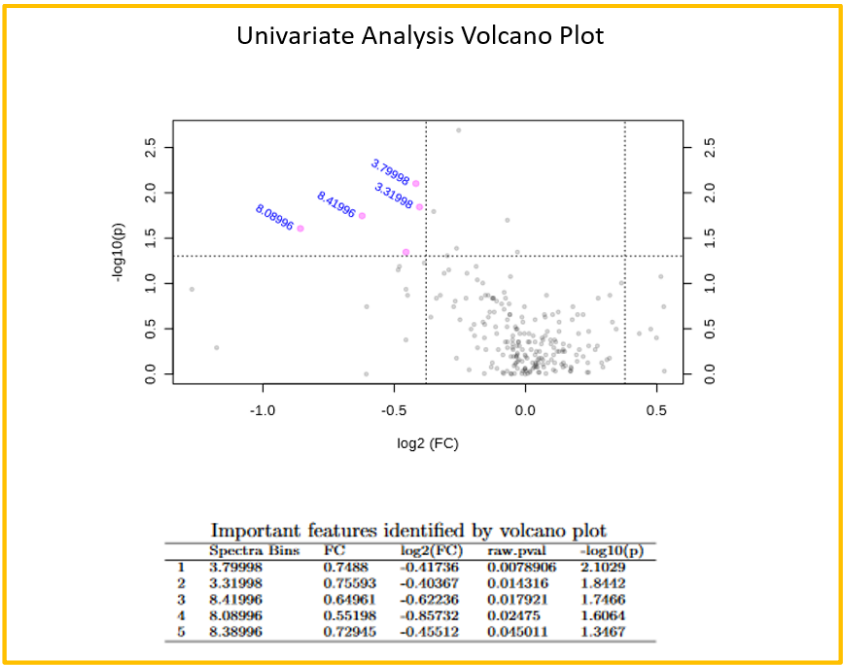

Important features identified by volcano plot

	Spectra Bins	FC	log2(FC)	raw.pval	-log10(p)
1	3.79998	0.7488	-0.41736	0.0078906	2.1029
2	3.31998	0.75593	-0.40367	0.014316	1.8442
3	8.41996	0.64961	-0.62236	0.017921	1.7466
4	8.08996	0.55198	-0.85732	0.02475	1.6064
5	8.38996	0.72945	-0.45512	0.045011	1.3467

Figure 4.7. Univariate analysis Volcano Plot for *H. pylori* infection versus no infection in male urine samples. Upper image. Highlighted bins mean significantly different with P<0.05. **Bottom table.** Significant bins are listed in the table.

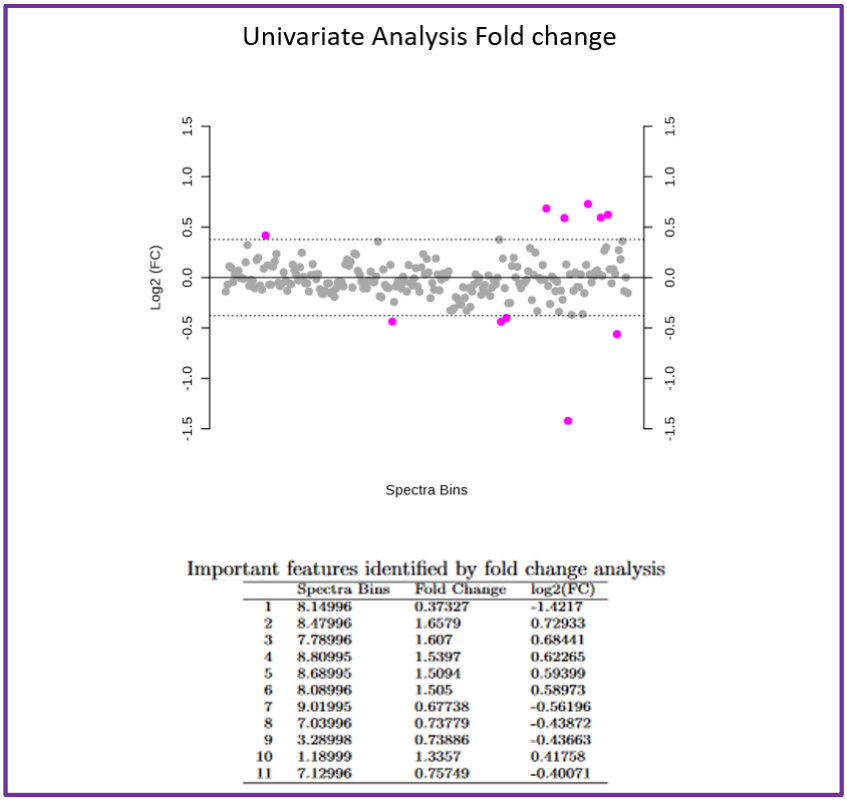

Important features identified by fold change analysis

	Spectra Bins	Fold Change	log2(FC)
1	8.14996	0.37327	-1.4217
2	8.47996	1.6579	0.72933
3	7.78996	1.607	0.68441
4	8.80995	1.5397	0.62265
5	8.68995	1.5094	0.59399
6	8.08996	1.505	0.58973
7	9.01995	0.67738	-0.56196
8	7.03996	0.73779	-0.43872
9	3.28998	0.73886	-0.43663
10	1.18999	1.3357	0.41758
11	7.12996	0.75749	-0.40071

Figure 4.8. Univariate analysis Fold change for *H. pylori* infection versus no infection in female urine samples. Upper image. Highlighted bins mean significantly different with P<0.05 with a threshold of 1.3. **Bottom table.** Significant bins are listed in the table.

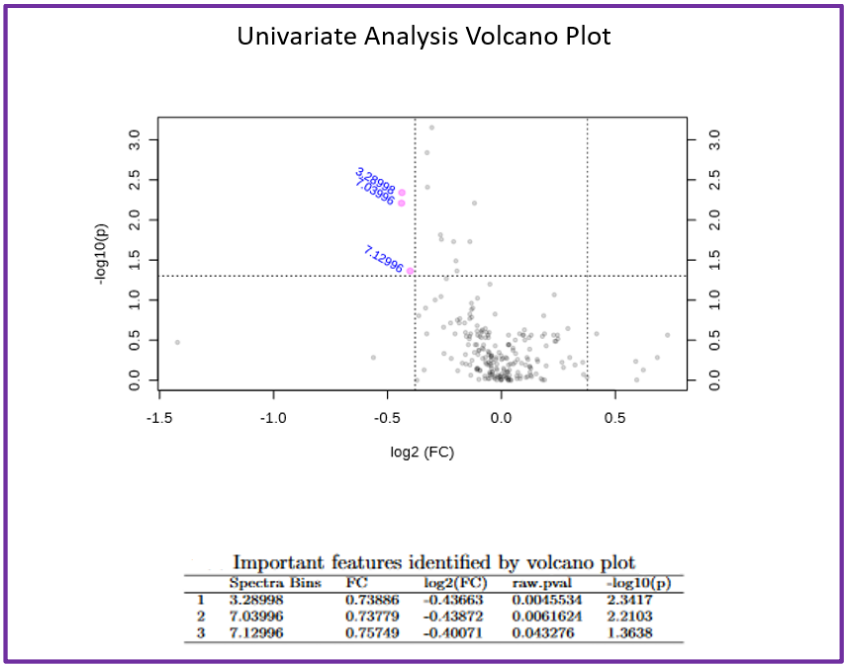

Important features identified by volcano plot

	Spectra Bins	FC	log2(FC)	raw.pval	-log10(p)
1	3.28998	0.73886	-0.43663	0.0045534	2.3417
2	7.03996	0.73779	-0.43872	0.0061624	2.2103
3	7.12996	0.75749	-0.40071	0.043276	1.3638

Figure 4.9. Univariate analysis Volcano Plot for *H. pylori* infection versus no infection in female urine samples. Upper image. Highlighted bins mean significantly different with P<0.05. **Bottom table.** Significant bins are listed in the table.

Gastritis and atrophy *vs* healthy

In the same way, the multivariate and univariate analysis was tested using the variable healthy *versus* gastritis and atrophy. PCA and PLSDA were performed and no differences have been found either in men or women. The supervised tests were only able to separate the groups slightly, but there was still a great overlap (**Figures 4.10** and **4.11**).

However, univariate analysis revealed better results. In men, 22 bins were significants using Fold Change and 3 with Volcano Plot (**Figures 4.12** and **4.13**), while in women, Fold Change determined 11 significants bins and 2 bins by Volcano Plot (**Figures 4.14** and **4.15**). At least, 5 bins were shared in both sexes.

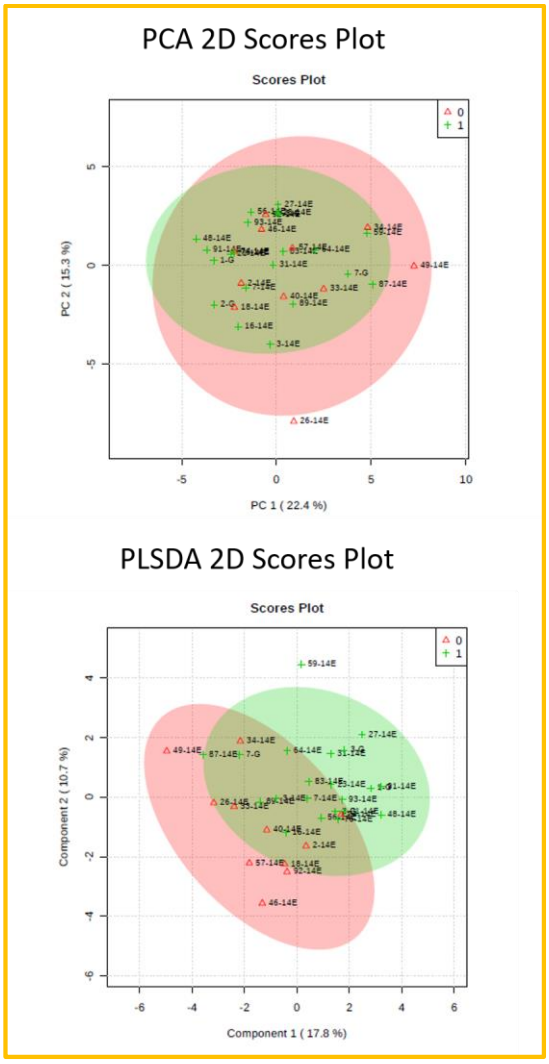

Figure 4.10. Multivariate analysis for healthy *versus* unhealthy (gastritis and atrophy) in male urine samples. Upper image. Two-dimensional PCA score plot. **Bottom image.** Two-dimensional PLSDA score plot. Red triangles: healthy patients. Green crosses: unhealthy patients.

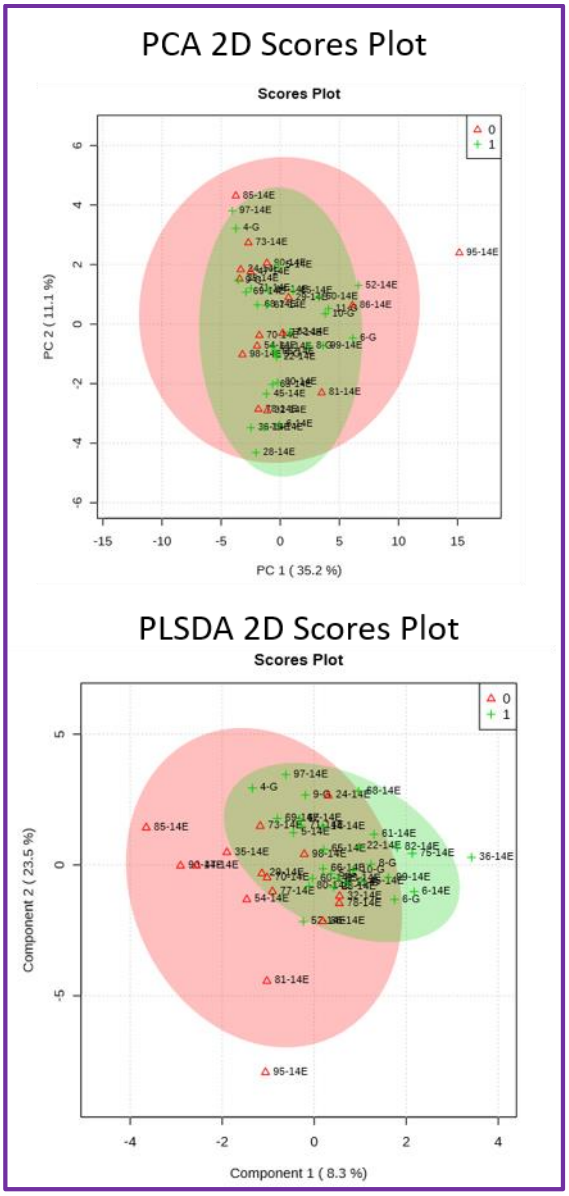

Figure 4.11. Multivariate analysis for healthy *versus* unhealthy (gastritis and atrophy) in female urine samples. Upper image. Two-dimensional PCA score plot. **Bottom image.** Two-dimensional PLSDA score plot. Red triangles: healthy patients. Green crosses: unhealthy patients.

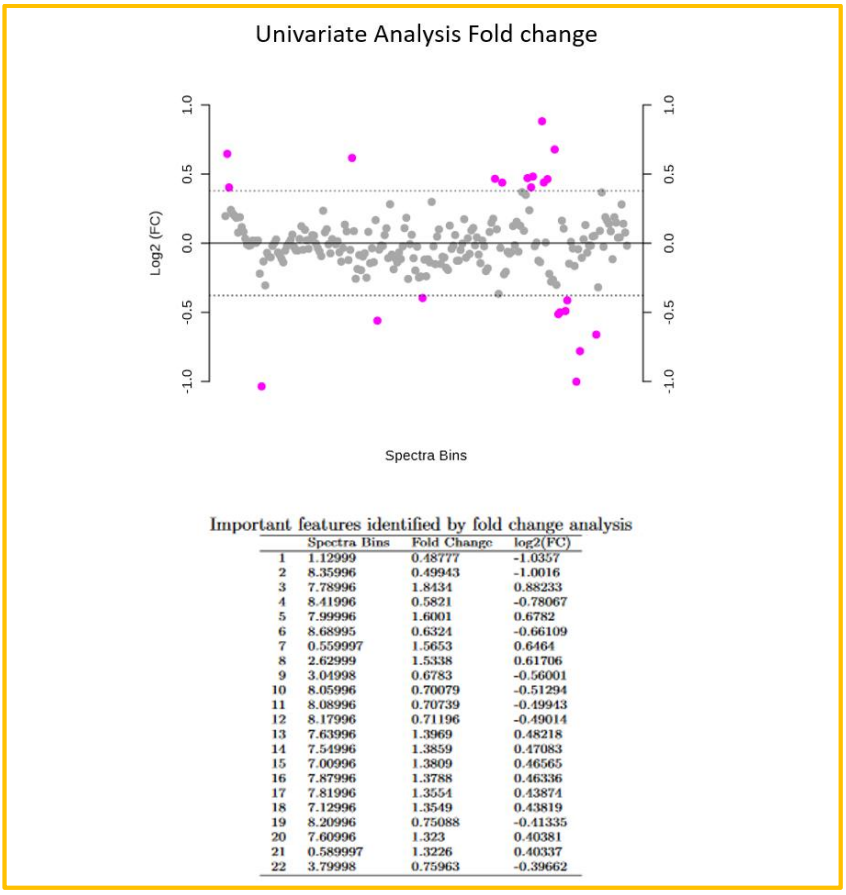

Important features identified by fold change analysis

	Spectra Bins	Fold Change	log2(FC)
1	1.12999	0.48777	-1.0357
2	8.35996	0.49943	-1.0016
3	7.78996	1.8434	0.88233
4	8.41996	0.5821	-0.78067
5	7.99996	1.6001	0.6782
6	8.68995	0.6324	-0.66109
7	0.559997	1.5653	0.6464
8	2.62999	1.5338	0.61706
9	3.04998	0.6783	-0.56001
10	8.05996	0.70079	-0.51294
11	8.08996	0.70739	-0.49943
12	8.17996	0.71196	-0.49014
13	7.63996	1.3969	0.48218
14	7.54996	1.3859	0.47083
15	7.00996	1.3809	0.46565
16	7.87996	1.3788	0.46336
17	7.81996	1.3554	0.43874
18	7.12996	1.3549	0.43819
19	8.20996	0.75088	-0.41335
20	7.60996	1.323	0.40381
21	0.589997	1.3226	0.40337
22	3.79998	0.75963	-0.39662

Figure 4.12. Univariate analysis Fold change for healthy *versus* unhealthy (gastritis and atrophy) in male urine samples. Upper image. Highlighted bins mean significantly different with P<0.05 with a threshold of 1.3. **Bottom table.** Significant bins are listed in the table.

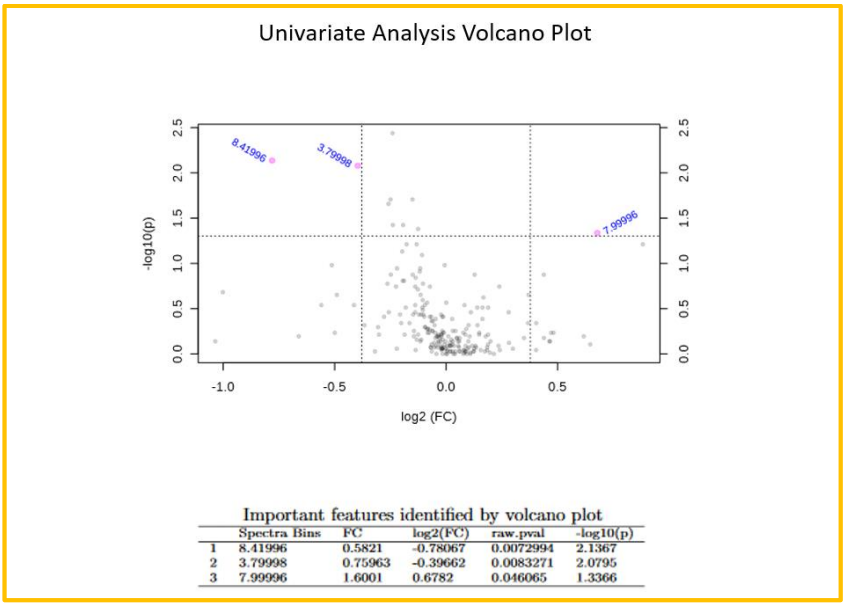

Important features identified by volcano plot

	Spectra Bins	FC	log2(FC)	raw.pval	-log10(p)
1	8.41996	0.5821	-0.78067	0.0072994	2.1367
2	3.79998	0.75963	-0.39662	0.0083271	2.0795
3	7.99996	1.6001	0.6782	0.046065	1.3366

Figure 4.13. Univariate analysis Volcano plot for healthy *versus* unhealthy (gastritis and atrophy) in male urine samples. Upper image. Highlighted bins mean significantly different with P<0.05. **Bottom table.** Significant bins are listed in the table.

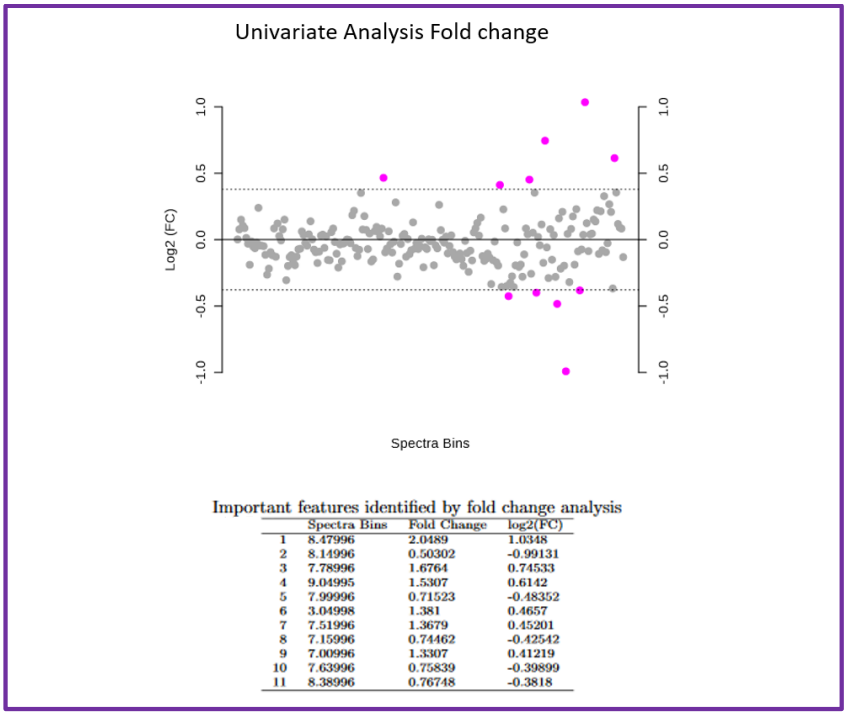

Important features identified by fold change analysis

	Spectra Bins	Fold Change	log2(FC)
1	8.47996	2.0489	1.0348
2	8.14996	0.50302	-0.99131
3	7.78996	1.6764	0.74533
4	9.04995	1.5307	0.6142
5	7.99996	0.71523	-0.48352
6	3.04998	1.381	0.4657
7	7.51996	1.3679	0.45201
8	7.15996	0.74462	-0.42542
9	7.00996	1.3307	0.41219
10	7.63996	0.75839	-0.39899
11	8.38996	0.76748	-0.3818

Figure 4.14. Univariate analysis Fold change for healthy *versus* unhealthy (gastritis and atrophy) in female urine samples. Upper image. Highlighted bins mean significantly different with P<0.05 with a threshold of 1.3. **Bottom table.** Significant bins are listed in the table.

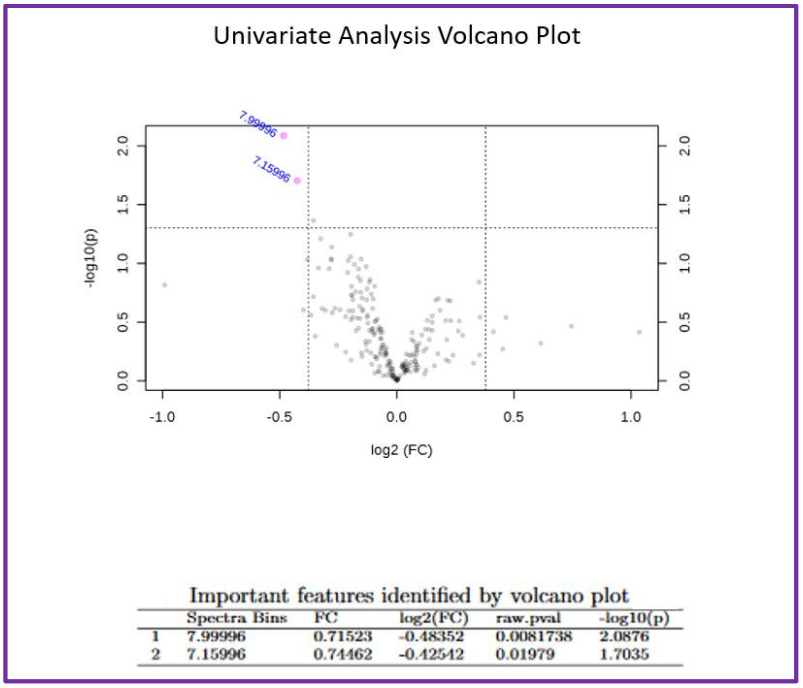

Important features identified by volcano plot

	Spectra Bins	FC	log2(FC)	raw.pval	-log10(p)
1	7.99996	0.71523	-0.48352	0.0081738	2.0876
2	7.15996	0.74462	-0.42542	0.01979	1.7035

Figure 4.15. Univariate analysis Volcano plot for healthy *versus* unhealthy (gastritis and atrophy) in female urine samples. Upper image. Highlighted bins mean significantly different with P<0.05. **Bottom table.** Significant bins are listed in the table.

Creatinine normalization

Normalization to a metabolite that is expressed in a constant way can be performed[168]. We utilized creatinine as a reference because it is the most common metabolite used. Multivariate PCA and PLS-DA analysis did not show a good separation pattern. Slight grouping by sexes has been observed so we decided to analyze both sexes separately as in the previous case.

H. pylori

The multivariate analysis performed was not valid for separating the groups formed. Univariate analysis in men revealed that 26 bins were significantly different (**Figure 4.16** and **4.17**), while in women 25, 9 and 17 bins were found in Fold Change, Wilcoxon Rank Test and Volcano Plot, respectively. (**Figure 4.18**, **4.19** and **4.20**).

Gastritis and atrophy *versus* healthy

The univariate analysis was used to find possible differences between the stablished groups. In men, FC and Volcano plot found 51 statistically significant bins between the studied variable (**Figures 4.21** and **4.22**). In the case of women, a total of 66 bins were found significant in Fold change, Wilcoxon and Volcano Plot (**Figures 4.23**, **4.24** and **4.25**).

[168] Craig A, Cloarec O, Holmes E, et al. Scaling and Normalization Effects in NMR Spectroscopic Metabonomic Data Sets. Anal. Chem. 2006;78 (7):2262–67.

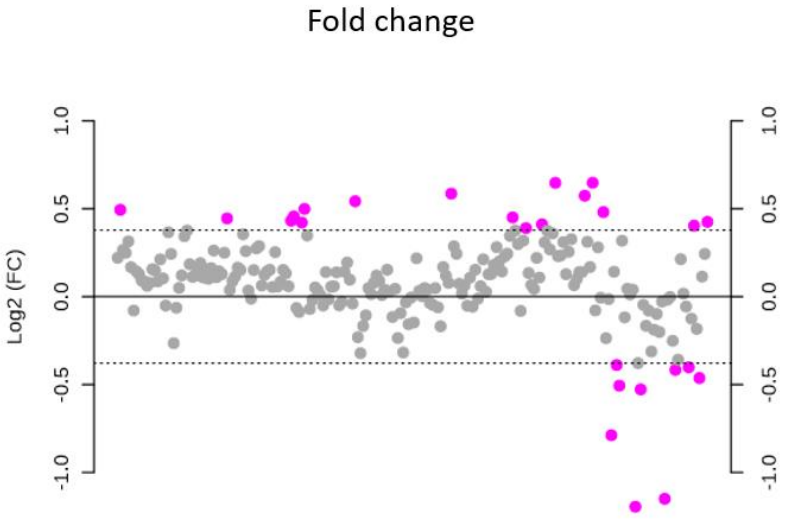

Important features identified by fold change analysis

	Spectra Bins	Fold Change	log2(FC)
1	8.36116	0.43683	-1.1948
2	8.69081	0.4507	-1.1498
3	8.09145	0.57913	-0.78804
4	7.88167	1.567	0.64804
5	7.46212	1.5663	0.64734
6	6.29336	1.5014	0.58633
7	7.79177	1.4891	0.57442
8	3.26659	1.4569	0.54292
9	8.4211	0.69387	-0.52726
10	8.18135	0.70396	-0.50644
11	2.66722	1.4133	0.49911
12	0.569458	1.4083	0.49396
13	8.00155	1.396	0.48129
14	9.11036	0.72563	-0.46269
15	2.54735	1.3718	0.45611
16	6.98263	1.367	0.45101
17	1.79815	1.3615	0.44515
18	2.51738	1.3496	0.4325
19	9.44001	1.3432	0.42568
20	2.63726	1.3395	0.42165
21	8.81068	0.74941	-0.41617
22	7.31228	1.3302	0.41159
23	9.05043	1.323	0.40379
24	8.99049	0.75679	-0.40204
25	7.13247	1.3104	0.39002
26	8.15139	0.76383	-0.38867

Figura 4.16. Univariate analysis Fold change for *H. pylori* infection *versus* no infection in male urine samples normalized by creatinine. Upper image. Highlighted bins mean significantly different with P<0.05 with a threshold of 1.3. **Bottom table.** Significant bins are listed in the table.

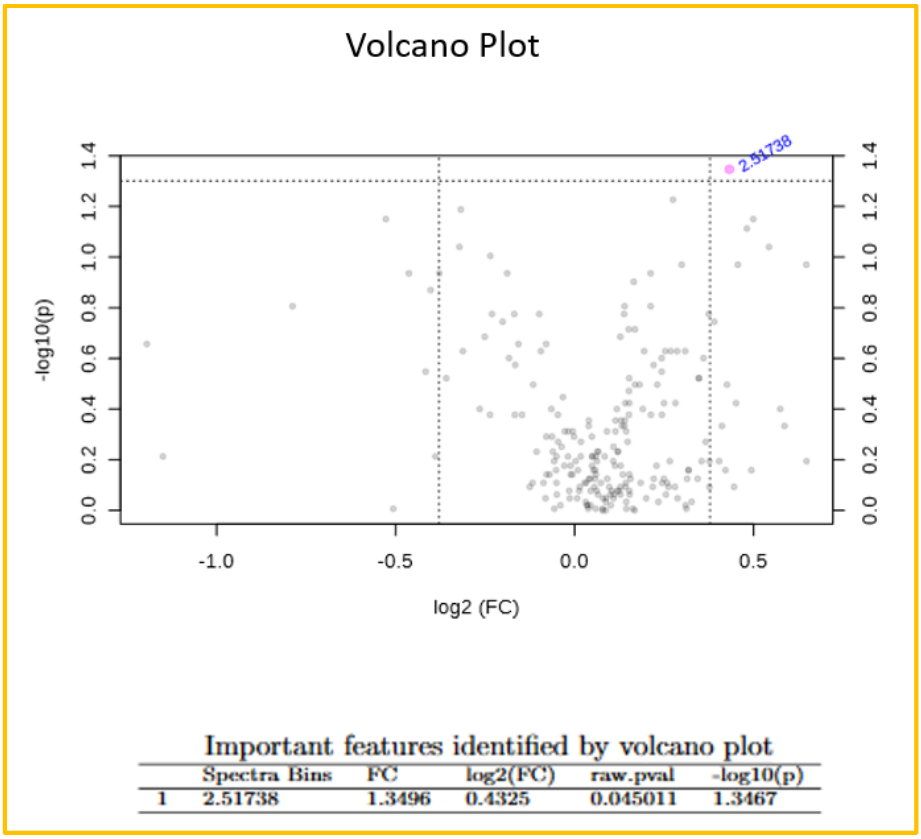

Important features identified by volcano plot

	Spectra Bins	FC	log2(FC)	raw.pval	-log10(p)
1	2.51738	1.3496	0.4325	0.045011	1.3467

Figure 4.17. Univariate analysis Volcano Plot for *H. pylori* infection *versus* no infection in male urine samples normalized by creatinine. Upper image. Highlighted bins mean significantly different with P<0.05. **Bottom table.** Significant bins are listed in the table.

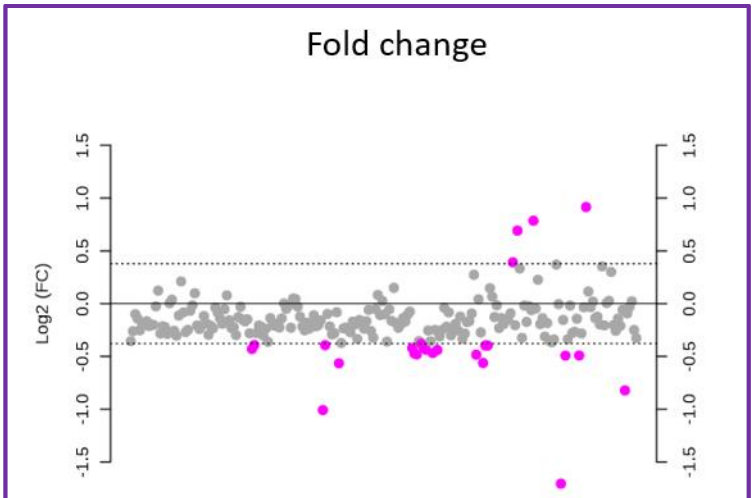

Important features identified by fold change analysis

	Spectra Bins	Fold Change	log2(FC)
1	8.15139	0.30684	-1.7044
2	3.08678	0.49718	-1.0082
3	8.48103	1.8862	0.91548
4	9.02046	0.56582	-0.82159
5	7.79177	1.7243	0.78604
6	7.58199	1.6162	0.69263
7	3.29655	0.67609	-0.56471
8	7.13247	0.6773	-0.56212
9	8.21132	0.71129	-0.49149
10	8.39113	0.71186	-0.49034
11	7.04257	0.71547	-0.48304
12	6.2634	0.71656	-0.48083
13	6.23343	0.72134	-0.47125
14	6.47317	0.72346	-0.46702
15	6.53311	0.73756	-0.43917
16	6.38327	0.73896	-0.43644
17	2.1278	0.74281	-0.42894
18	6.20346	0.74697	-0.42088
19	6.3533	0.75092	-0.41327
20	7.16244	0.75965	-0.39659
21	7.19241	0.75979	-0.39632
22	3.11675	0.7614	-0.39327
23	7.52206	1.3121	0.39193
24	2.15777	0.76235	-0.39148
25	6.32333	0.76872	-0.37947

Figura 4.18. Univariate analysis Fold change for *H. pylori* infection *versus* no infection in female urine samples normalized by creatinine. Upper image. Highlighted bins mean significantly different with P<0.05 with a threshold of 1.3. **Bottom table.** Significant bins are listed in the table.

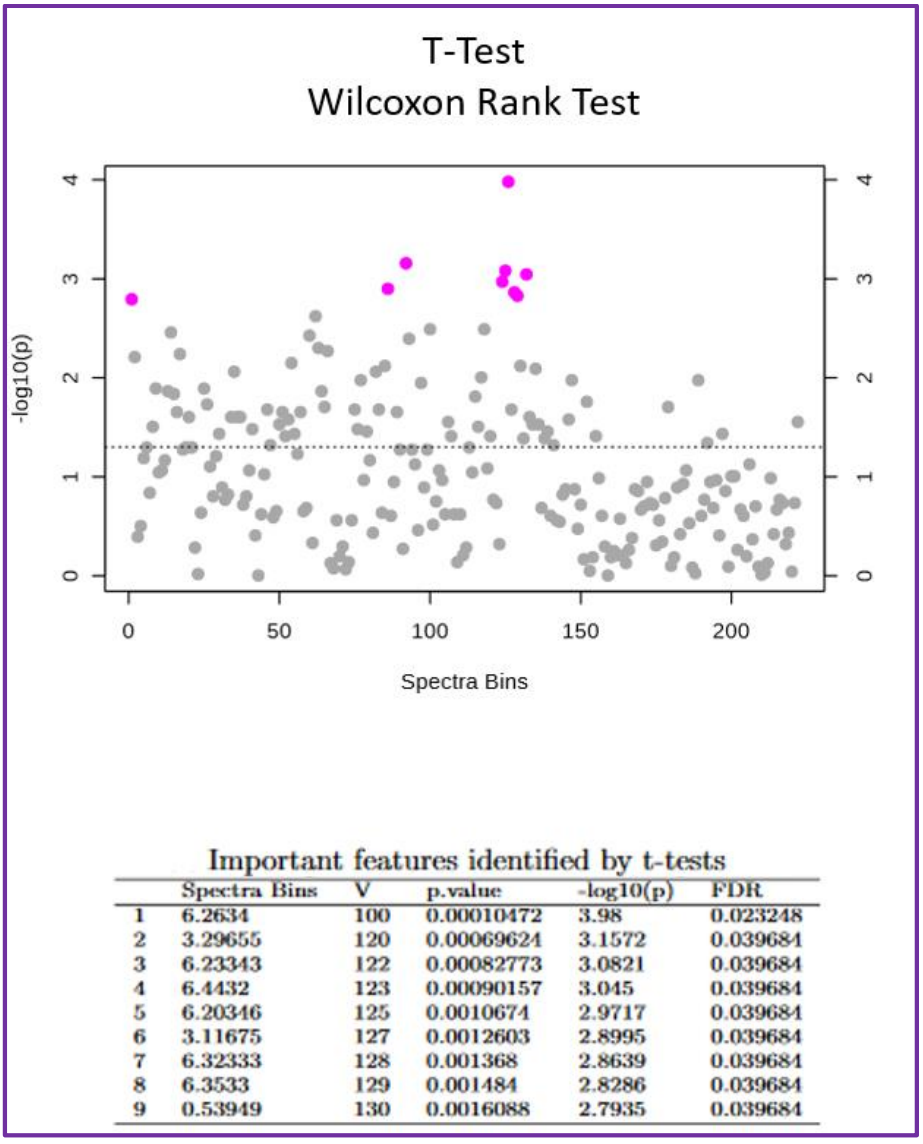

Important features identified by t-tests

	Spectra Bins	V	p.value	-log10(p)	FDR
1	6.2634	100	0.00010472	3.98	0.023248
2	3.29655	120	0.00069624	3.1572	0.039684
3	6.23343	122	0.00082773	3.0821	0.039684
4	6.4432	123	0.00090157	3.045	0.039684
5	6.20346	125	0.0010674	2.9717	0.039684
6	3.11675	127	0.0012603	2.8995	0.039684
7	6.32333	128	0.001368	2.8639	0.039684
8	6.3533	129	0.001484	2.8286	0.039684
9	0.53949	130	0.0016088	2.7935	0.039684

Figure 4.19. Univariate analysis Wilcoxon Rank Test for *H. pylori* infection *versus* no infection in female urine samples normalized by urine. Upper image. Highlighted bins mean significantly different with P<0.05. **Bottom table.** Significant bins are listed in the table.

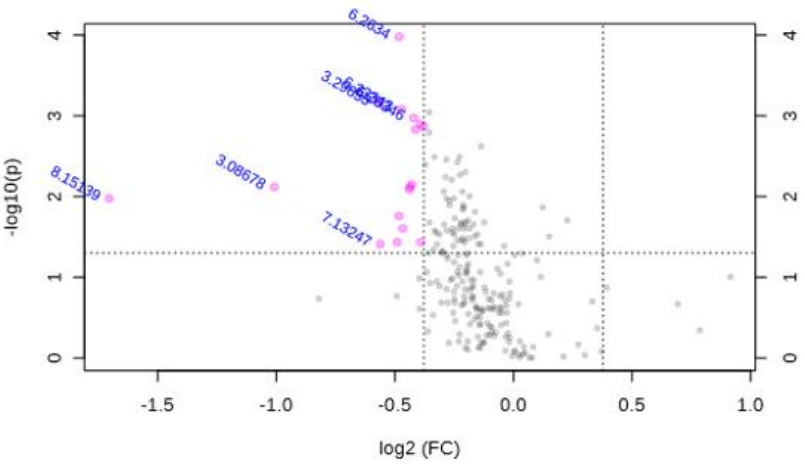

Important features identified by volcano plot

	Spectra Bins	FC	log2(FC)	raw.pval	-log10(p)
1	6.2634	0.71656	-0.48083	0.00010472	3.98
2	3.29655	0.67609	-0.56471	0.00069624	3.1572
3	6.23343	0.72134	-0.47125	0.00082773	3.0821
4	6.20346	0.74697	-0.42088	0.0010674	2.9717
5	3.11675	0.7614	-0.39327	0.0012603	2.8995
6	6.32333	0.76872	-0.37947	0.001368	2.8639
7	6.3533	0.75092	-0.41327	0.001484	2.8286
8	2.1278	0.74281	-0.42894	0.0070924	2.1492
9	3.08678	0.49718	-1.0082	0.0075911	2.1197
10	6.38327	0.73896	-0.43644	0.0075911	2.1197
11	6.53311	0.73756	-0.43917	0.0081202	2.0904
12	8.15139	0.30684	-1.7044	0.010573	1.9758
13	7.04257	0.71547	-0.48304	0.017465	1.7578
14	6.47317	0.72346	-0.46702	0.024894	1.6039
15	8.39113	0.71186	-0.49034	0.036788	1.4343
16	2.15777	0.76235	-0.39148	0.036788	1.4343
17	7.13247	0.6773	-0.56212	0.038823	1.4109

Figure 4.20. Univariate analysis Volcano Plot for *H. pylori* infection *versus* no infection in female urine samples normalized by creatinine. Upper image. Highlighted bins mean significantly different with P<0.05. **Bottom table.** Significant bins are listed in the table.

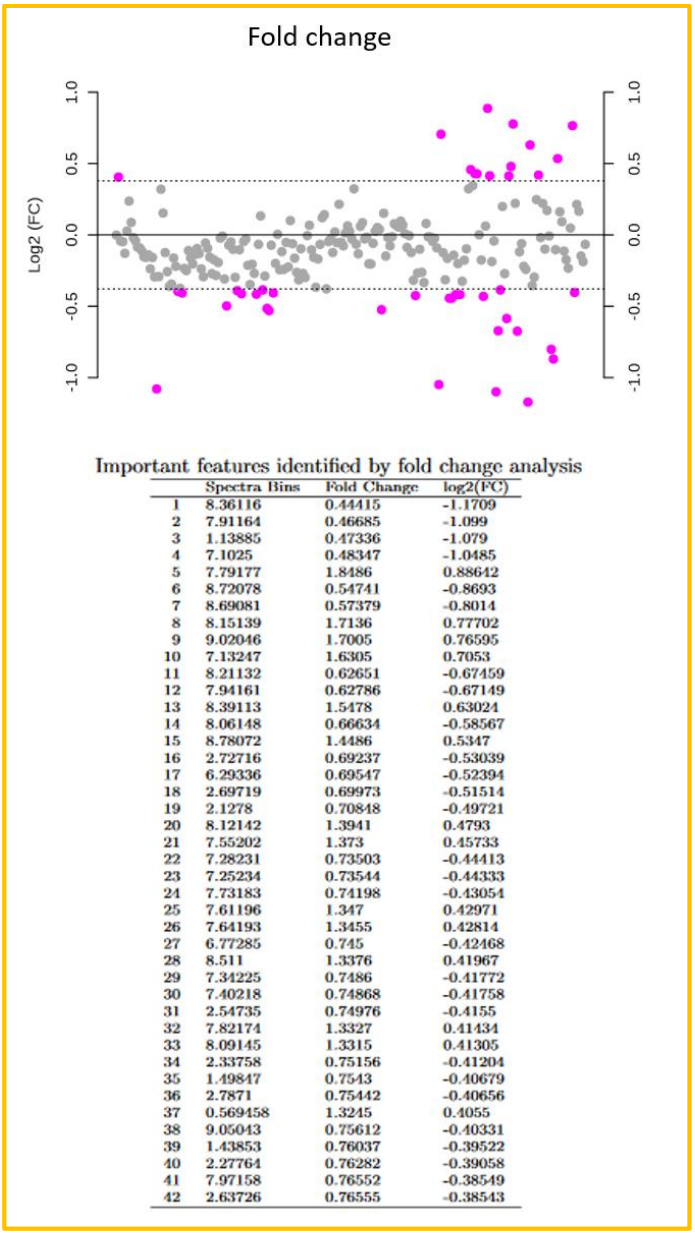

Important features identified by fold change analysis

	Spectra Bins	Fold Change	log2(FC)
1	8.36116	0.44415	-1.1709
2	7.91164	0.46685	-1.099
3	1.13885	0.47336	-1.079
4	7.1025	0.48347	-1.0485
5	7.79177	1.8486	0.88642
6	8.72078	0.54741	-0.8693
7	8.69081	0.57379	-0.8014
8	8.15139	1.7136	0.77702
9	9.02046	1.7005	0.76595
10	7.13247	1.6305	0.7053
11	8.21132	0.62651	-0.67459
12	7.94161	0.62786	-0.67149
13	8.39113	1.5478	0.63024
14	8.06148	0.66634	-0.58567
15	8.78072	1.4486	0.5347
16	2.72716	0.69237	-0.53039
17	6.29336	0.69547	-0.52394
18	2.69719	0.69973	-0.51514
19	2.1278	0.70848	-0.49721
20	8.12142	1.3941	0.4793
21	7.55202	1.373	0.45733
22	7.28231	0.73503	-0.44413
23	7.25234	0.73544	-0.44333
24	7.73183	0.74198	-0.43054
25	7.61196	1.347	0.42971
26	7.64193	1.3455	0.42814
27	6.77285	0.745	-0.42468
28	8.511	1.3376	0.41967
29	7.34225	0.7486	-0.41772
30	7.40218	0.74868	-0.41758
31	2.54735	0.74976	-0.4155
32	7.82174	1.3327	0.41434
33	8.09145	1.3315	0.41305
34	2.33758	0.75156	-0.41204
35	1.49847	0.7543	-0.40679
36	2.7871	0.75442	-0.40656
37	0.569458	1.3245	0.4055
38	9.05043	0.75612	-0.40331
39	1.43853	0.76037	-0.39522
40	2.27764	0.76282	-0.39058
41	7.97158	0.76552	-0.38549
42	2.63726	0.76555	-0.38543

Figura 4.21. Univariate analysis Fold change for healthy *versus* unhealthy (gastritis and atrophy) in male urine samples normalized by creatinine. Upper image. Highlighted bins mean significantly different with P<0.05 with a threshold of 1.3. **Bottom table.** Significant bins are listed in the table.

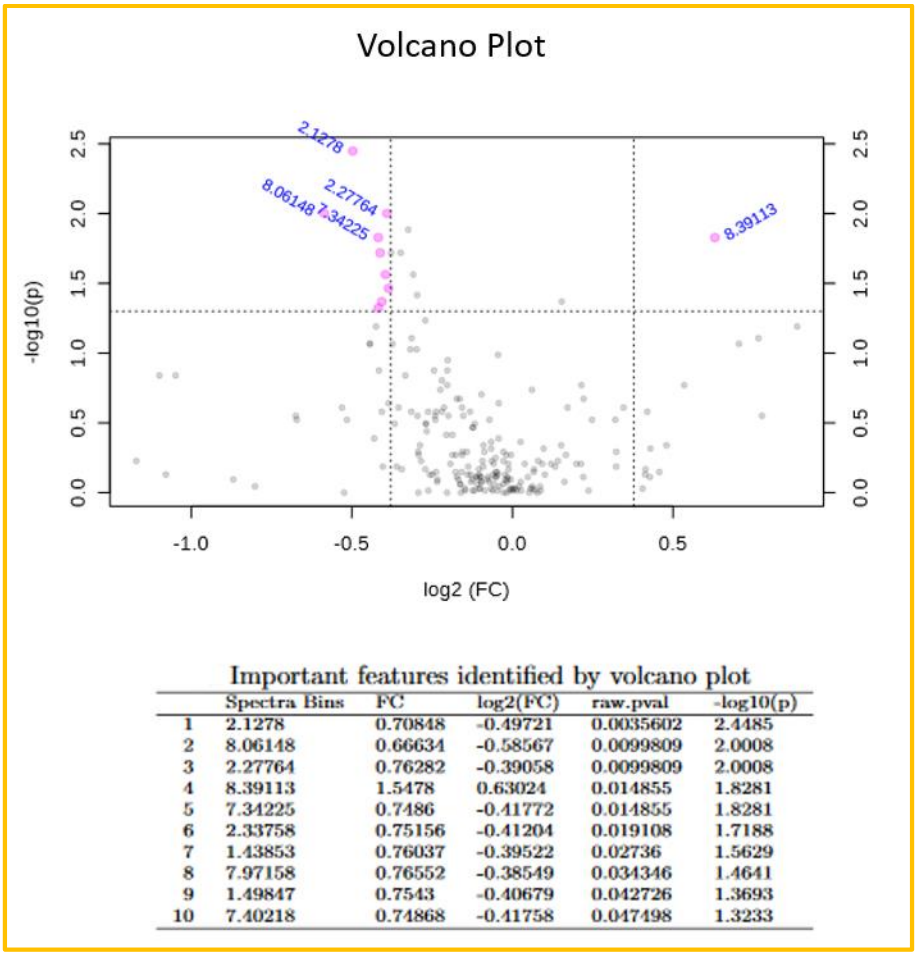

Important features identified by volcano plot

	Spectra Bins	FC	log2(FC)	raw.pval	-log10(p)
1	2.1278	0.70848	-0.49721	0.0035602	2.4485
2	8.06148	0.66634	-0.58567	0.0099809	2.0008
3	2.27764	0.76282	-0.39058	0.0099809	2.0008
4	8.39113	1.5478	0.63024	0.014855	1.8281
5	7.34225	0.7486	-0.41772	0.014855	1.8281
6	2.33758	0.75156	-0.41204	0.019108	1.7188
7	1.43853	0.76037	-0.39522	0.02736	1.5629
8	7.97158	0.76552	-0.38549	0.034346	1.4641
9	1.49847	0.7543	-0.40679	0.042726	1.3693
10	7.40218	0.74868	-0.41758	0.047498	1.3233

Figura 4.22. Univariate analysis Volcano plot for healthy *versus* unhealthy (gastritis and atrophy) in male urine samples normalized by creatinine. Upper image. Highlighted bins mean significantly different with P<0.05. **Bottom table.** Significant bins are listed in the table.

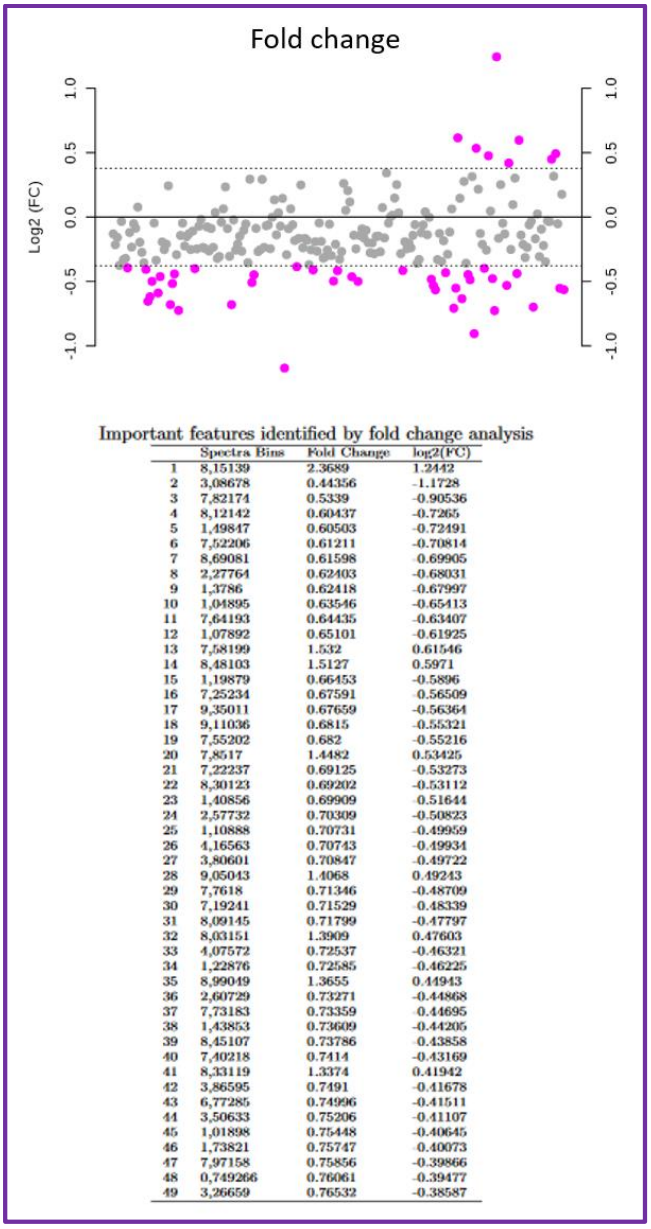

Important features identified by fold change analysis

	Spectra Bins	Fold Change	log2(FC)
1	8,15139	2.3689	1.2442
2	3,08678	0.44356	-1.1728
3	7,82174	0.5339	-0.90536
4	8,12142	0.60437	-0.7265
5	1,49847	0.60503	-0.72491
6	7,52206	0.61211	-0.70814
7	8,69081	0.61598	-0.69905
8	2,27764	0.62403	-0.68031
9	1,3786	0.62418	-0.67997
10	1,04895	0.63546	-0.65413
11	7,64193	0.64435	-0.63407
12	1,07892	0.65101	-0.61925
13	7,58199	1.532	0.61546
14	8,48103	1.5127	0.5971
15	1,19879	0.66453	-0.5896
16	7,25234	0.67591	-0.56509
17	9,35011	0.67659	-0.56364
18	9,11036	0.6815	-0.55321
19	7,55202	0.682	-0.55216
20	7,8517	1.4482	0.53425
21	7,22237	0.69125	-0.53273
22	8,30123	0.69202	-0.53112
23	1,40856	0.69909	-0.51644
24	2,57732	0.70309	-0.50823
25	1,10888	0.70731	-0.49959
26	4,16563	0.70743	-0.49934
27	3,80601	0.70847	-0.49722
28	9,05043	1.4068	0.49243
29	7,7618	0.71346	-0.48709
30	7,19241	0.71529	-0.48339
31	8,09145	0.71799	-0.47797
32	8,03151	1.3909	0.47603
33	4,07572	0.72537	-0.46321
34	1,22876	0.72585	-0.46225
35	8,99049	1.3655	0.44943
36	2,60729	0.73271	-0.44868
37	7,73183	0.73359	-0.44695
38	1,43853	0.73609	-0.44205
39	8,45107	0.73786	-0.43858
40	7,40218	0.7414	-0.43169
41	8,33119	1.3374	0.41942
42	3,86595	0.7491	-0.41678
43	6,77285	0.74996	-0.41511
44	3,50633	0.75206	-0.41107
45	1,01898	0.75448	-0.40645
46	1,73821	0.75747	-0.40073
47	7,97158	0.75856	-0.39866
48	0,749266	0.76061	-0.39477
49	3,26659	0.76532	-0.38587

Figura 4.23. Univariate analysis Fold change for healthy *versus* unhealthy (gastritis and atrophy) in female urine samples normalized by creatinine. Upper image. Highlighted bins mean significantly different with P<0.05 with a threshold of 1.3. **Bottom table.** Significant bins are listed in the table.

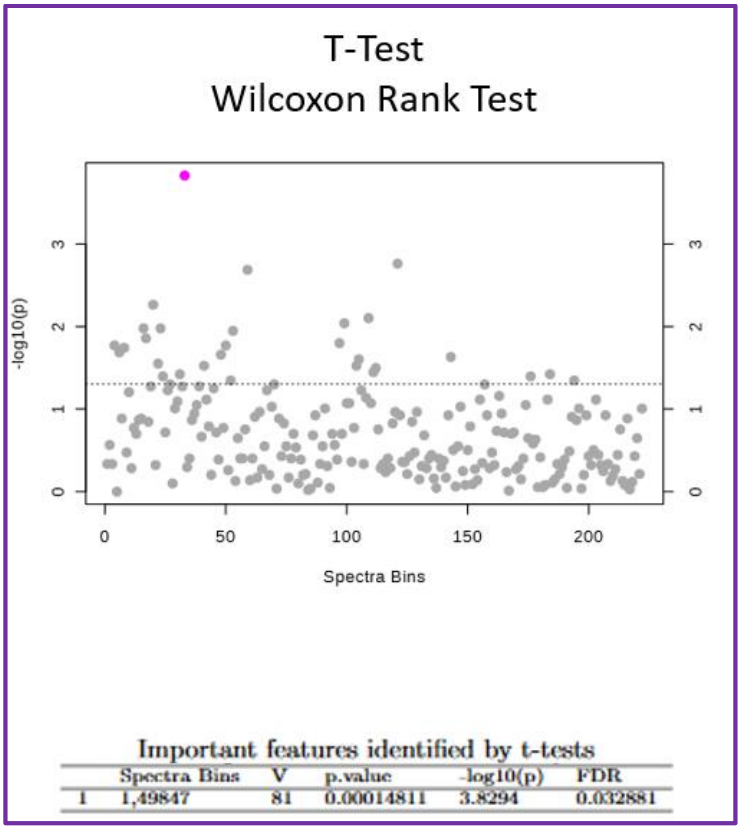

Important features identified by t-tests

	Spectra Bins	V	p.value	-log10(p)	FDR
1	1,49847	81	0.00014811	3.8294	0.032881

Figure 4.24. Univariate analysis Wilcoxon Rank Test for healthy *versus* unhealthy (gastritis and atrophy) in female urine samples normalized by urine. Upper image. Highlighted bins mean significantly different with P<0.05. **Bottom table.** Significant bins are listed in the table.

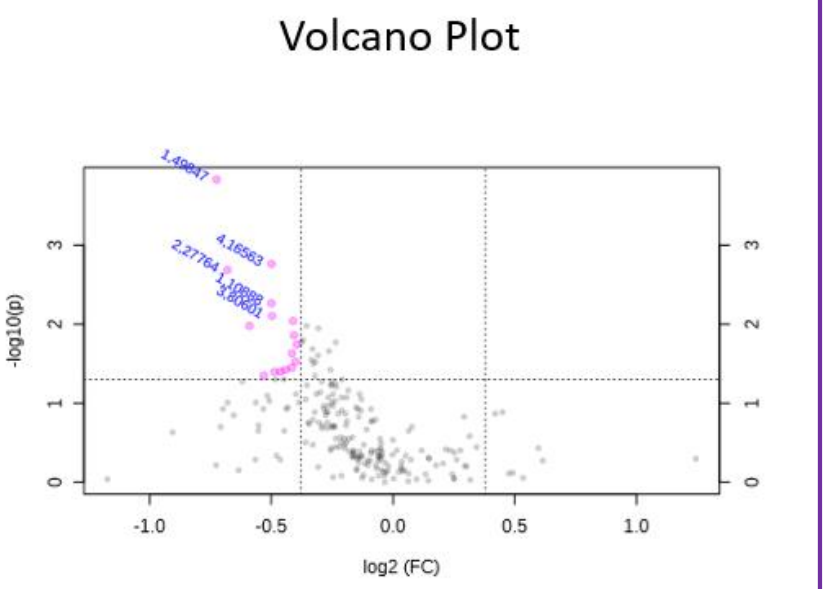

Important features identified by volcano plot

	Spectra Bins	FC	log2(FC)	raw.pval	-log10(p)
1	1,49847	0.60503	-0.72491	0.00014811	3.8294
2	4,16563	0.70743	-0.49934	0.0017317	2.7615
3	2,27764	0.62403	-0.68031	0.0020583	2.6865
4	1,10888	0.70731	-0.49959	0.0054388	2.2645
5	3,80601	0.70847	-0.49722	0.0079043	2.1021
6	3,50633	0.75206	-0.41107	0.0091349	2.0393
7	1,19879	0.66453	-0.5896	0.010529	1.9776
8	1,01898	0.75448	-0.40645	0.013876	1.8577
9	0,749266	0.76061	-0.39477	0.018101	1.7423
10	6,77285	0.74996	-0.41511	0.023377	1.6312
11	1,73821	0.75747	-0.40073	0.029899	1.5243
12	3,86595	0.7491	-0.41678	0.035736	1.4469
13	1,43853	0.73609	-0.44205	0.03788	1.4216
14	7,7618	0.71346	-0.48709	0.040131	1.3965
15	1,22876	0.72585	-0.46225	0.040131	1.3965
16	8,30123	0.69202	-0.53112	0.044963	1.3471

Figura 4.25. Univariate analysis Volcano plot for healthy *versus* unhealthy (gastritis and atrophy) in female urine samples normalized by creatinine. Upper image. Highlighted bins mean significantly different with P<0.05. **Bottom table.** Significant bins are listed in the table.

Metabolite quantification in urine samples

The analysis of 50 compounds in urine was carried out using the Bruker IVDr Quantification in URine B.I.Quant-UR b™ module. Creatinine, amines, amino acids, benzene, carboxylic acids, fatty acids, keto acids, purine, pyridine, sugars and their derivatives are automatically quantified.

Among the 50 quantified metabolites, only myo-inositol has shown significant differences in infection *H. pylori* compared to no infection in male urine samples (**Figure 4.26**).

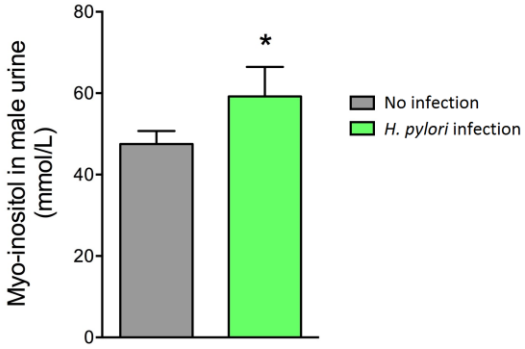

Figure 4.26. Myo-inositol concentration in male urine samples. Concentration expressed in mmol/L. The asterisk (*) indicates P<0.05 when comparing among groups.

DISCUSSION

CHAPTER 1

The main finding of this chapter are that the obestatin/GPR39 system has a functional role in the human stomach exerting a stimulatory action on the secretion of digestive enzymes: pepsinogen and lipase. Indeed, obestatin-activated pathways implicated in pepsinogen secretion have been described.

Obestatin derives from preproghrelin, the same prepropeptide that originates ghrelin. Both hormones are produced by enteroendocrine cells of the oxyntic mucosa of the stomach. Initially it was thought that obestatin was a physiological opponent to the orexigenic action of ghrelin, but this was quickly ruled out. The action of ghrelin on acidic stimulation has been reported and may be due to the release of histamine from enterochromaffin-like (ECL) cells[169]. Several functions have been reported for obestatin, but none of them related to the stomach except for the published works of our group on gastric cancer cells[124,125,126].

Our results of GPR39 positivity in chief cells of the stomach proposed a possible role in healthy stomach: the regulation of the digestive enzymes secretion. Previous studies of our group using an *in vitro* model of a cell line that endogenously expresses GPR39 and secretes pepsinogen I, demonstrated that exogenous administration of obestatin stimulates pepsinogen release. Furthermore, this effect was mediated by the GPR39 receptor[126]. An *ex vivo* human stomach explant culture was used to demonstrate not only obestatin action on pepsinogen secretion but also, its action regarding gastric lipase release. Thus, this finding provides the first functional activity for the obestatin/GPR39 system in healthy stomach.

Analyzing the obtained data, we observe how the treatment with obestatin is able to significantly increase pepsinogen and gastric lipase secretion mainly at 20 min and pepsinogen secretion also at 40 and 60 minutes. In the latter case, differences between control and obestatin treated were smaller, due to the

[169] Sakurada T, Ro S, Onouchi T, *et al.* Comparison of the actions of acylated and desacylated ghrelin on acid secretion in the rat stomach. J Gastroenterol. 2010;45(11):1111-20.

basal secretion speed. Therefore, obestatin is able to accelerate the normal secretion of pepsinogen and gastric lipase.

Taking the cellular lysate data, obestatin does not vary pepsinogen nor gastric lipase synthesis. These results agree with the work published by Hirschowitz in 1967, in which the relationship of secretion and pepsinogen synthesis is described[170]. With a stimulation, the pepsinogen granules of the chief cells are released into the lumen of the glands. By means of positive feedback the synthesis of new pepsinogen and the maturation of the granules is produced, taking between 6 and 18 hours. If the stimulus continues, pepsinogen is synthesized between 45 and 60 minutes, reaching a balance between synthesis and secretion that can be prolonged for many hours. Although there are no visible pepsinogen granules in the cells[171], there is much more pepsinogen in the mucosa than expected[172]. When the stimulus is removed, the cycle of restoration and maturation of pepsinogen granules begins, which takes several hours.

In our case, the stimulus with obestatin is maintained, so the second mechanism would be set in motion, in which there is no formation of granules and synthesis is faster. This fact is confirmed by the immunohistochemical expression of pepsinogen in the explants in culture. Treatment with obestatin enhances the emptying of pepsinogen so less immunoreactivity is observed. Although pepsinogen was continuously synthesized, formation of new granules was not observed. Obestatin would also be favouring the synthesis of pepsinogen *de novo*. Taking together the lysate and secretome data at 60 minutes in which the control would already be in equilibrium, it can be seen that the secretome stimulated with obestatin shows a greater amount of pepsinogen but the lysates maintain a similar expression, not being shown a decrease. Therefore, obestatin would not only be advancing the machinery of

[170] Hirschowitz BI. The control of pepsinogen secretion. Ann. N. Y. Acad. Sci.1967;140(2):709-723.
[171] Bowie DJ, Vineberg AM.The selective action of histamine and the effect of prolonged vagal stimulation on the cells of the gastric glands in the dog. Quart. J. Exp. Physiol. 1935;25: 247-257.
[172] Hirschowitz BI, O'Leary DK, Marks IN. Effects of atropine on synthesis and secretion of pepsinogen in the rat. Am J Physiol. 1960;198:108-12.

secretion but would be stimulating synthesis and favouring its release, to synthesize and secrete more pepsinogen and in a faster way.

Molecular mechanisms of pepsinogen secretion are not entirely clear. As mentioned above, two pathways are involved in this process. The first pathway involves the activation of adenylate cyclase (AC) by G-proteins which leads to the production of the second messenger cyclic adenosine monophoshate (cAMP). Next, protein-kinase A (PKA) is activated by binding the generated cAMP to its regulatory subunit and triggering cellular responses that lead to the secretion of pepsinogen[148].

Obestatin ability to produce cAMP has been demonstrated[107] by what could be a feasible mechanism. Our data show that obestatin significantly activates PKA so it is confirmed that this pathway is involved in obestatin-pepsinogen secretion.

In the second pathway, Go protein activates phospholipase C (PLC) which hydrolyzes phosphatidylinositol 4,5-bisphosphate (PIP2) generating diacylglycerol (DAG) and inositol trisphosphate (IP3). On the one hand, protein kinase C (PKC) is activated by DAG and the other hand, IP3 mobilizes intracellular Ca^{2+} by activating Ca^{2+}/calmoduline-dependent protein kinase II (CamKII). Both PKC and CamKII activated phosphorylate target proteins to trigger cellular responses involved in the secretion of pepsinogen[148].

Previous research showed that obestatin did not cause calcium mobilization[173] or activation of calcium-dependent PKCs in cancer gastric cells[124]. However, in this work we observed that obestatin is able to activate PKCα/β and PKC γ in healthy human stomach. Therefore, obestatin is also involved in the secretion of pepsinogen via this pathway.

Physiological stimuli acting through the calcium pathway compared to those acting via cAMP are less effective in pepsinogen synthesis. However, although both pathways are totally independent, they can act together and a

[173] Pazos Y, Alvarez CJ, Camina JP, *et al.* Role of obestatin on growth hormone secretion: An *in vitro* approach. Biochem Biophys Res Commun. 2009;390:1377-81.

synergetic efect on the pepsinogen release is produced. Obestatin activates both pathways in parallel so synergy would have to be carried out and pepsinogen would be largely secreted.

Furthermore, a third more recent pathway involves the protease-activated receptor 2 (PAR2)[174]. It has been seen that the chief cells of the gastric mucosa are strongly immunoreactive to PAR2 in both rats and guinea pigs. Kawao *et al.* showed that repeated treatment of a PAR2 agonist in pylorus-ligated rats promotes pepsinogen secretion[175].Fiorucci *et al.* corroborated this action of PAR2 in gastric-isolated chief cells from guinea pig by activating of ERK1/2 and causing Ca^{2+} mobilization, among others[176].

Proteinase-activated receptors (PARs) are members of the G protein-coupled receptor (GPCR) family that have a special proteolytic activation mechanism[177]. In addition to trypsin, other proteases of the family of metalloproteases and kallikreins have been reported as activators of this receptor. Specifically, KLK4[178], KLK5[179], KLK6[180], KLK14[179] and MMP1[181].

---

174 Kawabata A, Matsunami, M, Sekiguchi F. Gastrointestinal roles for proteinase-activated receptors in health and disease. Br. J. Pharmacol. 2008;153:S230-S240.

175 Kawao N, Sakaguchi Y, Tagome A, *et al.* Protease-activated receptor-2 (PAR-2) in the rat gastric mucosa: immunolocalization and facilitation of pepsin/pepsinogen secretion. Br J Pharmacol. 2002;135:1292-6.

176 Fiorucci S, Distrutti E, Federici B*, et al.* PAR-2 modulates pepsinogen secretion from gastric-isolated chief cells. Am J Physiol Gastrointest Liver Physiol. 2003;285(3):G611-20.

177 Gieseler F, Ungefroren H, Settmacher U, *et al.* Proteinase-activated receptors (PARs) - focus on receptor-receptor-interactions and their physiological and pathophysiological impact. Cell Commun. Signal. 2013;11:86.

178 Ramsay AJ, Dong Y, Hunt ML, *et al.* Kallikrein-related peptidase 4 (KLK4) initiates intracellular signaling via protease-activated receptors (PARs). KLK4 and PAR-2 are co-expressed during prostate cancer progression. J Biol Chem. 2008;283(18):12293-304.

179 Stefansson K, Brattsand M, Roosterman D, *et al.* Activation of proteinase-activated receptor-2 by human kallikrein-related peptidases. J Invest Dermatol. 2008;128(1):18-25.

180 Vandell AG, Larson N, Laxmikanthan G. Protease-activated receptor dependent and independent signaling by kallikreins 1 and 6 in CNS neuron and astroglial cell lines. J Neurochem. 2008;107(3): 855–870.

181 Li X, Tai HH. Thromboxane A2 receptor-mediated release of matrix metalloproteinase-1 (MMP-1) induces expression of monocyte chemoattractant protein-1 (MCP-1) by activation of protease-activated receptor 2 (PAR2) in A549 human lung adenocarcinoma cells. Mol Carcinog. 2014;53(8):659-66.

Treatment with obestatin in healthy human stomach has shown an increased secretion of all proteases studied, 29 of which significantly. Among them, MMP1 has shown an overregulated secretion induced by obestatin. In addition, KLK11 is the protease that is most reduced in cellular lysate, evidencing obestatin ability to promote its secretion. The role of this kallikrein to activate pro-KLK14 has been described[182]. Similarly, MMP3, which is capable of activating KLK4[183], is also overregulated by obestatin. These released proteases could lead to PAR2 activation, and molecular mechanisms are triggered resulting in pepsinogen secretion.

ADAM, CST, KLK and MMP families are stimulated by obestatin. It is known that in cancer there is an overregulation of these proteases by degradation of components of the extracellular matrix involved in metastatic processes.

The RTKs analysis provides contradictory data on EGFR inhibition with obestatin treatment. It is well described that the obestatin/GPR39 system causes the transactivation of this receptor[125]. These data call into question the array quality, since stains have been presented in the developing process making it difficult to quantify the spots of each antibody.

Following the signaling pathway described for obestatin, proteases are in charge of producing ligands to subsequently transactivate EGFR and other RTKs. This allows to amplify the signal induced by obestatin and act on multiple pathways involved in cell growth, proliferation and differentiation among others. Both proteases and RTKs have been shown to be overregulated in cancer. Previous studies described that obestatin increases the secretion of proteases in gastric cancer cells[130]. This, coupled with the obestatin-induced effects on proliferation, migration and invasion in these cells[126]. GPR39 expression has been found in gastric adenocarcinomas, increasing as the tumor becomes more undifferentiated[126]. Our data on a healthy stomach would support the relationship that the obestatin/GPR39

[182] Yoon H, Laxmikanthan G, Lee J, *et al.* Activation profiles and regulatory cascades of the human kallikrein-related peptidases. J Biol Chem. 2007;282(44):31852-64.
[183] Beaufort N, Plaza K, Utzschneider D, *et al.* Interdependence of kallikrein-related peptidases in proteolytic networks. Biol Chem. 2010;391(5):581-7.

system would have with this pathology. Probably the physiological context is key for the signaling cascade triggered by obestatin to produce physiological effects in the regulation of gastric enzymes or on the contrary may have effects on the gastric cancer development. Further analysis is needed to know the real role of this system in stomach tumorigenesis.

In conclusion, these findings not only demonstrate the action of the obestatin/GPR39 system to activate pepsinogen and lipase release but also unveil a function for this system in healthy human stomach. Indeed, molecular mechanisms involved in obestatin-stimulated pepsinogen secretion have been disclosed.

CHAPTER 2

AGS cell line comes from an untreated gastric adenocarcinoma[184]. It has an epithelial morphology and is adherent. KATO-III cell line was established from a ring cell carcinoma of the stomach seal, in which individual cells diffusely infiltrate the surrounding tissues[185]. It presents a spherical morphology with two phenotypes clearly differentiated in culture, one adherent and the other in suspension. They have cytological characteristics of the cells of the seal ring. NCI-N87 cell line derives from a metastasis of gastric carcinoma in the liver[186]. In culture it has an epithelial morphology and grows in an adherent monolayer formed by closely bound cells. These differential characteristics make them three cell lines ideal for the *in vitro* study of the obestatin/GPR39 system on gastric cancer.

The mitogenic effect described for obestatin was confirmed in all three cell lines. Not only that, but the $ZnCl_2$-induced apopotosis was reversed with obestatin treatment in the cells studied.

Previous studies by our research group show that exogenous obestatin treatment caused proliferation, migration and invasion on AGS cells. In addition, EMT and are regulated by obestatin in these cells[126]. Considering that this cell line comes from an adenocarcinoma, obestatin would be playing a role in the induction of an invasive phenotype tha allows dispersion to new locations to establish metastasis. However, contrary data are obtained with NCI-N87 cells. Obestatin also causes proliferation, but migration and invasion are inhibited, while MET is favoured by decreasing mesenchymal markers with obestatin treatment. It should be noted that NCI-N87 cells derive from a metastasis, thus obestatin would be favourin the settlement of metastasic cells in order to establish in a new niche. Therefore, the

[184] Barranco SC, Townsend CM Jr, Casartelli C, *et al.* Establishment and characterization of an in vitro model system for human adenocarcinoma of the stomach. Cancer Res. 1983;43(4):1703-1709.
[185] Sekiguchi M, Sakakibara K, Fujii G. Establishment of cultured cell lines derived from a human gastric carcinoma. Jpn J Exp Med. 1978;48:61-8.
[186] Park JG, Frucht H, LaRocca RV, *et al.* Characteristics of cell lines established from human gastric carcinoma. Cancer Res. 1990;50(9):2773-80.

obestatin/GPR39 system might modulate the tumourigenic and metastasic process differently depending on the cell context.

Data on the metastatic suppressor nm23-H1 further clarified the role of obestatin in these systems. Reduced expression of nm23 has been significantly associated with aggressive behaviors in melanoma and gastric, breast and colon carcinomas[187]. During the different stages of metastasis, nm23-H1 expression may be altered in a tumour, suggesting that the gene could act as a molecular switch between the floating and adherent states of cancer cells[188].

Supporting the results of other studies on liver metastases from gastric cancer[189], in which a reduction of nm23-H1 in metastases with respect to the primary tumour has been seen, obestatin treatment significantly increased nm23-H1 and inhibited the metastatic phenotype by causing the establishment of NCI-87 cells, in accordance with the data obtained on inhibition of migration of this cell line.

The study of nm23-H1 in the different populations of KATO-III cells revealed surprising data. It is known that the basal expression level of this gene in KATO-III is higher in floating than in adherent cells[190], and that these subpopulations are in equilibrium between them. In fact, when the two populations are separated, the phenotypes are modified until equilibrium is reached. However, in the experiment carried out, obestatin reduces the expression of nm23-H1 in the floating population, favouring its change to an adherent phenotype. This is important in the establishment of circulating metastatic cells in a new location causing metastasis. Conversely, in adherent

[187] Tee YT, Chen GD, Lin LY, *et al.* Nm23-H1: a metastasis-associated gene. Taiwan J Obstet Gynecol. 2006;45(2):107-13.
[188] Iizuka N, Tangoku A, Hazama S, *et al.* Nm23-H1 gene as a molecular switch between the free-floating and adherent states of gastric cancer cells. Cancer Lett. 2001;174(1):65-71.
[189] Guan-zhen Y, Ying C, Can-rong N, *et al.* Reduced protein expression of metastasis-related genes (nm23, KISS1, KAI1 and p53) in lymph node and liver metastases of gastric cancer. International Journal of Experimental Pathology. 2007;88(3):175-183.
[190] Iizukaa N, Tangokub A, Hazama S, *et al.* Nm23-H1 gene as a molecular switch between the free-floating andadherent states of gastric cancer cells. Cancer Letters. 2001; 174:65–71.

population of KATO-III, which has a lower expression of the gene, obestatin caused its increase, favouring a more invasive phenotype.

The obestatin/GPR39 system plays an important role in regulating proliferation and differentiation through parallel activated pathways, demonstrated in gastric cancer cells AGS and KATO-III[125]. The transactivation of EGFR mediated by MMPs is key to amplify the signal of obestatin and regulate its proliferative effects. Our results are controversial, as one would expect greater phosphorylation of EGFR residues when stimulated with obestatin. Analysis was performed based on the typical EGFR band of 170 kDa. However, some additional bands compatible with the several different isoforms described for EGFR have been detected. It would be convenient to analyze the remaining variants that help to clarify the role of the obestatin/GPR39 system in EGFR activation.

Obestatin is capable of favouring the overexpression of numerous proteases, including members of the families of metalloproteases and kallikreins[130], which have been described as activators of PARs signalling[191,192]. According to these data, it would be expected to observe more differences in the regulation of PARs triggered by obestatin. The analysis has been carried out 24 h after stimulation, so it will probably not be long enough to observe differences in PARs expression. New experiments should be conducted to better understand the possible contribution of PARs to obestatin effects.

Considering also the differential GPR39 expression in human gastric adenocarcinomas, these findings corroborate the functional potential of the obestatin/GPR39 system in the proliferation and malignancy of gastric cancer. The design of new therapeutic strategies could be established with the use of antagonists of this system.

---

[191] Wojtukiewicz MZ, Hempel D, Sierko E, *el al.* Protease-activated receptors (PARs)—biology and role in cancer invasion and metastasis. Cancer Metastasis Reviews. 2015;34:775-796.

[192] Abdallah RT, Keum J-S, Lee M-H, *et al.* plasma kallikrein promotes epidermal growth factor receptor transactivation and signaling in vascular smooth muscle through direct activation of protease-activated receptors. The Journal of Biological Chemistry. 2010;285(45):35206-35215.

USC
UNIVERSIDADE
DE SANTIAGO
DE COMPOSTELA

CHAPTER 3

It is well established that cellular changes are produced in the premalignant process. Atrophy is characterized by a parietal cell loss that leads to so-called oxyntic atrophy due to the fact that these cells are responsible for the acid secretion of the stomach[193]. A loss of chief cells associated with atrophy has been reported[194]. In the next stage, intestinal epithelium type cells begin to establish themselves in the gland that ends up being totally invaded, triggering intestinal metaplasia.

The immunohistochemical analysis has not revealed significant differences in the amount of enteroendocrine cells or chief cells, which express obestatin and GPR39, respectively. It is known that SPEM occurs as a step prior to intestinal metaplasia.

The chief cells of the base of the gland dedifferentiate and begin to express TFF2, emerging the antral-like cells[32]. This dedifferentiation to SPEM could be a physiological mechanism for recruiting progenitor cells in response to damage to repair gastric mucosa[194]. Therefore at this level, the cellular integrity of the gland is more compromised. As already mentioned in the results, the quality of the samples has influenced the evaluation of the positivity of the chief cells. The atrophic mucosa has a higher hardness that prevents effective biopsy and surface samples are taken. Although in all samples were found positive chief cells for GPR39 and pepsinogen, a study of cell dedifferentiation along the Correa sequence was difficult. However, the fact that SPEM originates in chief cells, which are positive for GPR39, leads us to postulate the potential role of the obestatin/GPR39 system in this cell dedifferentiation and its consequent metaplastic process.

The comparative analysis of immunohistochemical expression of dysplasia with the rest of the groups was not easy since it was selected a posteriori to study the complete sequence. Both the processing and paraffin inclusion of

[193] Goldenring JR, Nam KT. Oxyntic atrophy, metaplasia and gastric cancer. Prog Mol Biol Transl Sci. 2010;96:117-31.
[194] Mills JC, Goldenring JR. Metaplasia in the stomach arises from gastric chief cells. Cell Mol Gastroenterol Hepatol. 2017;4(1): 85–88.

the tissues have been carried out differently and immunoreactivity levels may vary.

Although the metaplastic glands did not express GPR39, an in-depth study would be interesting to study the role of the obestatin/GPR39 system in the metaplastic process. Knowing that adenocarcinomas are positive for GPR39[126], the analysis of this receptor expression in other cells different from chief cells in metaplasia and dysplasia would be useful to establish GPR39 not only as a prognostic factor, but also as a biomarker of early detection of gastric cancer.

The obestatin signaling pathway integrates factors such as MMPs and RTKs responsible for transmitting the activation of the Akt pathway and thus to mTOR[125]. In chapter 1 it has been shown a system of culture of healthy stomach explants in which the Akt activation was produced with a obestatin treatment at 5 min. Therefore, the RTKs involved have already been transactivated. In this experimental model, the obestatin treatment time was 2 h. This experimental time is excesive to detect early signalling targets. Consequently, only the analysis of the basal expression of RTKs in each of the groups has been carried out. The analysis of EGFR and IGF-IR showed surprising data. As members of the RTKs, they are overregulated in cancer. The IGF-1R pattern shows a logical tendency to increase as one progresses towards cancer. IGF-IR expression has been positively correlated with the degree of dedifferentiation of the tumor in gastric cancer[126]. In addition, the obestatin treatment over-regulates this receptor in gastric cancer cells[130]. However, the EGFR results show an opposite pattern. Probably cellular integrity loss is responsible for decreased expression. *H. pylori* is able to activate EGFR to trigger routes such as Akt. and establish its carcinogenic potential. This effect was shown in AGS cells[47], the same cell line in which our group has established the ability of obestatin to transactivate the EGFR and other RTKs through GPR39. Thus, obestatin induced over-regulation of these receptors could establish the triggering of pathways involved in tumorigenesis, analogous to what occurs with *H. pylori* infection.

The analysis of proteases revealed different patterns of expression according to different established groups. Obestatin was able to induce changes in the expression of proteases in the lysate of samples in one of the three groups analyzed. The three cathepsins analyzed were related to cancer. Thus, over-regulation of cathepsin Z has been shown to be related to tumor development[195], increased cathespin L has been seen in gastric cancer[196] and cathepsin D showed high expression in poorly differentiated gastric adenocarcinoma[130].

Secretome is necessary to interpret the results obtained in lysate and to distinguish whether the differences found, derive from variations in the synthesis or secretion of the proteases studied. However, the secretions need to be concentrated in order to be analyzed by immunoblot. In the absence of a reliable and reproducible system of concentration, their analysis has been postponed. The obtained data support the involvement of the obestatin/GPR39 system is involved in the regulation of the physiology of these proteases although further studies are necessary to completely clarify this issue.

[195] Teller A, Jechorek D, Hartig R, *et al.* Dysregulation of apoptotic signaling pathways by interaction of RPLP0 and cathepsin X/Z in gastric cancer. Pathol Res Pract. 2015;211:62-70.
[196] Russo A, Bazan V, Migliavacca M, *et al.* Prognostic significance of DNA ploidy, S-phase fraction, and tissue levels of aspartic, cysteine, and serine proteases in operable gastric carcinoma. Clin Cancer Res. 2000;6:178-84.

USC
UNIVERSIDADE
DE SANTIAGO
DE COMPOSTELA

CHAPTER 4

Gastric cancer is a high mortality pathology due to its late diagnosis. Less than 20% of patients survive at least 5 years[56]. The lack and inespecificity of the symptoms make an early diagnosis of the disease difficult. Following Correa sequence, atrophy is a stage prior to gastric cancer and is considered a risk factor in this pathology[197]. Despite the classification systems that have emerged over the years, none has achieved an effective diagnosis. The gold standard is the histology of a stomach biopsy[198]. The subjectivity of the criteria evaluated by pathologists means that atrophy is underdiagnosed[199]. Objective protocols are necessary for an effective diagnosis and the establishment of relevant guidelines for the control of the evolution to more severe stages.

Metabolomics gives us the ability to detect biomarkers for early diagnosis of diseases[92]. Through the study of metabolites in biofluids, a reliable and robust diagnostic protocol can be established. Metabolomics by NMR is widely used for its speed, reproducibility and low cost, although the sensitivity is not as good as other techniques such as mass spectroscopy[200].

Metabolomics is on the rise in recent decades, yet there are only two studies using NMR in gastric cancer[106,201]. The establishment of early diagnosis tools in gastric cancer is really necessary. In line with this idea, the use of biofluids,

---

[197] Dinis-Ribeiro M, Areia M, de Vries AC, et al. Management of precancerous conditions and lesions in the stomach (MAPS): guideline from the European Society of Gastrointestinal Endoscopy (ESGE), European *Helicobacter* Study Group (EHSG), European Society of Pathology (ESP), and the Sociedade Portuguesa de Endoscopia Digestiva (SPED). Endoscopy. 2012;44:74–94.

[198] Carpenter HA, Talley NJ. Gastroscopy is incomplete without biopsy: clinical relevance of distinguishing gastropathy from gastritis. Gastroenterology. 1995;108:917–924.

[199] Plummer M, Buiatti E, Lopez G, et al. Histological diagnosis of precancerous lesions of the stomach: a reliability study. Int J EpidemioL. 1997;**26**:716–20.

[200] Emwas AH. The strengths and weaknesses of NMR spectroscopy and mass spectrometry with particular focus on metabolomics research. Methods Mol Biol. 2015;1277:161-93.

[201] Jung J, Jung Y, Bang EJ, *et al.* Noninvasive diagnosis and evaluation of curative surgery for gastric cancer by using NMR-based metabolomic profiling. Ann Surg Oncol. 2014;21(Suppl 4):S736-S742.

as plasma and urine, could be studied in the early stages of the Correa cascade and, in that way, migh aid to the diagnosis of gastritis and atrophy accurately.

Plasma analysis reveals that our study population is stratified into groups that cannot be explained by the metadata available. The resulting groups are small and the robustness of the data obtained would be compromised. TOCSYs experiments will be carried out to deepen on the reason for these groupings and their subsequent statistical analysis will be carried out.

Normalization to creatinine was the preferred form in urine samples over the years[202]. It was assumed that creatinine clearance was constant but in the presence of metabolic deregulation levels may vary. In addition, creatinine has been shown to correlate with sex[203] and age[204]. In view of these limitations, other forms of normalization are now gaining ground. In our case, we use creatinine as a reference since we do not suspect metabolic deregulation in the patients studied. In addition, the variables sex and age are controlled since all subjects were older than 50 years and the analysis was performed separately between men and women. Normalization to creatinine and for the sum were performed in our study to verify their usefulness in this context.

Urine sample data were surprising. Univariate analysis revealed several bins significantly correlated with *H. pylori* infection and gastritis and atrophy pathologies. Despite the sex-separated study, bins common to both men and women have been obtained in both variables. In addition, common bins were found when comparing among the variables. This fact reinforces the robustness of the bins found, since both *H. pylori* infection and gastritis and atrophy are intimately linked.

---

[202] Emwas AH, Saccenti E, Gao X, *et al.* Recommended strategies for spectral processing and post-processing of 1D 1H-NMR data of biofluids with a particular focus on urine. Metabolomics. 2018;14(3):31

[203] Kochhar S, Jacobs DM, Ramadan Z, *et al.* Probing gender-specific metabolism differences in humans by nuclear magnetic resonance-based metabonomics. Analytical Biochemistry. 2006;352(2):274–281.

[204] Slupsky CM, Rankin KN, Wagner J, *et al.* Investigations of the effects of gender, diurnal variation, and age in human urinary metabolomic profiles. Analytical Chemistry. 2007;79(18):6995–7004.

The proton pump of the stomach is responsible for releasing the protons to the lumen to get the acid pH necessary for digestion. This pump is a hydrogen potassium ATPase (H^+/K^+ ATPase) and needs energy to function[205]. It is well established that the loss of parietal cells occurs in atrophy. These are the cells that contain this pump, so it is also known as oxyntic atrophy. Energy molecules derived from ATP show intensities in ppm close to the bins that were found[206]. This fact leads us to postulate if ATP or its derived molecules could be responsible for the different found intensities. The possible treatment of proton-pump inhibitors does not affect our data because all patients stopped taking these drugs at least 1 month before inclusion in the study. However, further studies are necessary to verify this hypothesis.

The TOCSY analysis will be the next to be performed to identify the metabolites responsible for these significant bins. Representing the data in two dimensions provides more information than the ^{1}H-NMR experiment carried out[207]. In addition, this analysis would provide more information on the clustering that occurs in the unsupervised PCA analysis with all samples. This experiment will allow us to know if there is any type of alteration or degradation of the samples that is responsible for this separation.

The metabolite quantification data has the importance of myo-inositol in male urine on the *H. pylori* infection group. Myositol is vitamin b8, a non-essential element since it can be synthesized, but very important for correct physiology[208,209]. This sugar alcohol is found in a lot of foods and it is absorbed in the stomach and small intestine. Being water-soluble it is eliminated by urine. The relationship of *H. pylori* with inositol was observed by Pucciarelli *et al.* In their work they show how this bacterium induces an

[205] Shin JM, Munson K, Vagin O, *et al.* The gastric HK-ATPase: structure, function, and inhibition. Pflugers Arch. 2009; 457(3): 609–22.
[206] The Human Metabolome DataBase (HMDB) (http://www.hmdb.ca)
[207] Dona AC, Kyriakides M, Scott F, *et al.* A guide to the identification of metabolites in NMR-based metabonomics/metabolomics experiments. Comput Struct Biotechnol J. 2016; 14: 135–153.
[208] Holub BJ. Metabolism and function of myo-inositol and inositol phospholipids. Annu Rev Nutr. 1986;6:563-97.
[209] Chiappelli J, Rowland LM, Wijtenburg SA, et al. Evaluation of myo-inositol as a potential biomarker for depression in schizophrenia. Neuropsychopharmacology. 2015 Aug; 40(9): 2157–2164.

increase in inositol phosphates *in vitro*[210]. The greater amounts of inositol in the urine of the pathological groups with respect to healthy control might be due to the loss of absorptive capacity.

Although the differences found in the metabolic profiling of biofluids are not very large, our data are of great clinical importance. Dyspepsia is characterized by discomfort or pain in the stomach and is a common pathology in clinical practice[211], representing up to 40% of Gastroenterology consultations. Of the 99 dyspeptic patients in the study, 38.4% had a healthy stomach. This fact underlines the importance of the development of non-invasive methodologies that correctly classify patients and allow endoscopy to be performed only in the necessary cases.

In spite of the fact that more experiments are necessary, we have confirmed the informative capacity of biofluids in these pathologies. Specifically, urine samples revealed significant bins that correlate with both *H. pylori* infection and gastritis and atrophy diseases. Therefore, the metabolomics by NMR of urine is postulated as a new system for the search for biomarkers that guarantee the correct and early diagnosis of these diseases to avoid progression to gastric cancer.

[210] Pucciarelli MG, Ruschkowski S, Trust TJ, *et al. Helicobacter pylori* induces an increase in inositol phosphates in cultured epithelial cells. FEMS Microbiol Lett. 1995;129(2-3):293-9.
[211] Mahadeva S, Goh KL. Epidemiology of functional dyspepsia: A global perspective. World J Gastroenterol. 2006; 12(17): 2661–66.

CONCLUSIONS

CHAPTER 1

The obestatin/GPR39 system is involved in the secretion of gastric enzymes such as pepsinogen and gastric lipase in human stomach. In addition, the molecular mechanisms involved were elucidated showing that obestatin activates the three pathways described for the release of pepsinogen: cAMP, PLC and PAR2.

CHAPTER 2

The obestatin/GPR39 system is involved in the development of gastric cancer by being able to intervene in EMT, proliferation, migration and invasion of gastric cancer cells. In addition, it is confirmed that these effects depend on cell status. Thus, obestatin promotes the invasive phenotype of cells derived from the primary tumor, enhancing their metastatic capacity; while in metastatic cells, obestatin promotes their settlement in a new location.

CHAPTER 3

The expression of GPR39 in the chief cells shows the possible importance of the obestatin/GPR39 system in the SPEM that originates in those cells. This process is key to the evolution to intestinal metaplasia, dysplasia and, finally, cancer. The fact that several RTKs and MMPs are expressed in a differential way in the Correa sequence and that these proteins are susceptible of being stimulated by obestatin, evidences the role of the obestatin/GPR39 system in the initiation and development of gastric cancer.

CHAPTER 4

The metabolomic study of biofluids by NMR evidences their informative capacity for the identification of biomarkers. Thus, urine metabolomic analysis reveals that there are significantly different bins among patients with *H pylori* infection *versus* uninfected patients and among gastritis and atrophy patients compared to healthy controls. These data show the possibility of establishing reliable protocols to diagnose these pathologies in a non-invasive way using biofluid metabolomics by NMR.

USC
UNIVERSIDADE
DE SANTIAGO
DE COMPOSTELA

RESUMO

USC
UNIVERSIDADE
DE SANTIAGO
DE COMPOSTELA

Anatomicamente, o estómago divídese e catro seccións: cardias, fundus, corpo e píloro. Histoloxicamente a parede presenta cinco capas que do interior ao exterior sería a mucosa, submucosa, muscular, subserosa e serosa. Dentro da mucosa atópanse as glándulas que varían segundo a localización no estómago. As glándulas oxínticas son as maioritarias e atópanse no fundus e no corpo. Presentan as células parietais que secretan ácido e as células principais que liberan zimóxenos, entre outras. En menor medida, atópanse as glándulas cardiais no cardias e as glándulas antrais no píloro.

O cancro gástrico é unha patoloxía causada polo crecemento descontrolado de células do epitelio do estómago. Caracterízase por unha baixa taxa de supervivencia, xa que a falta de síntomas leva a que a maior parte das veces a diagnose se faga en estadios tardíos da enfermidade. Aínda que estea aceptado un modelo etiolóxico multifactorial, a infección por *Helicobacter pylo*ri é o principal elemento carcinoxénico. Ademais tanto a dieta, como o alcohol e o tabaco están tamén descritos como axentes causantes do cancro gástrico. En 1975, Correa estableceu un modelo de carcinoxénese gástrica, onde se describen os pasos que se seguen dende unha mucosa sa ata o adenocarcinoma gástrico final. *H. pylo*ri infecta a mucosa orixinado unha gastrite que evolucionará sucesivamente a atrofia, metaplasia intestinal, displasia e, finalmente, cancro.

A infección crónica por *H. pylori* inicia un proceso inflamatorio e unha perda de células parietais. Esta combinación resulta imprescindible para o desenvolvemento da metaplasia cara o cancro. En humanos, atópanse tanto a metaplasia intestinal como a metaplasia que expresa o polipéptido espasmolítico (SPEM). Crese que a SPEM é a primeira en orixinarse e ante un ambiente inflamatorio e que esta evoluciona a metaplasia intestinal. Unha das explicacións do poder carcinoxénico de *H. pylori* é a súa capacidade para activar a EGFR, tanto de forma directa como coa intervención doutras moléculas. Esta transactivación conleva respostas que afectan a apoptose, migración ou proliferación celular.

O cancro gástrico é a quinta causa de morte entre todos os cancros. Os homes padecen o dobre esta doenza, e existen enormes variacións segundo a localización xeográfica. Nas últimas décadas grazas ao control de *H. pylori* e da mellora das condicións de vida, logrouse reducir a incidencia deste cancro.

A mala prognose caracterizada polo diagnóstico tardío do cancro gástrico subliña a importancia de ferramentas que permitan unha detección temperá do tumor ou das etapas precanceríxenas. A gastrite atrófica está considerada como un predito neste tipo de cancro polo que é vital a súa correcta diagnose. Non obstante, esta patoloxía atópase infradiagnosticada e a análise histolóxica dunha biopsia de estómago é a técnica de referencia. Ao longo dos anos, establecéronse biomarcadores sanguíneos, sobre todo no Xapón, para detectar aos pacientes con alto risco de desenvolver un tumor. Recentemente, xurdiron test serolóxicos que se están validando como unha metodoloxía diagnóstica menos invasiva. Neste senso, a metabolómica de biofluídos permite o establecemento de protocolos fiables e non invasivos para a diagnose de doenzas en etapas temperás. Aínda que existen datos sobre cancro gástrico, as etapas precanceríxenas do modelo de Correa non foron amplamente estudadas.

O estudo do sistema obestatina/GPR39 podería establecer novas vías para a comprensión do desenvolvemento do cancro gástrico e novas posibilidades de dianas terapéuticas.

A obestatina é unha hormona de 23 aminoácidos que deriva da escisión proteolítica da preproghrelina O seu receptor, GPR39, exprésase de forma ubicua e está vencellado tanto a funcións fisiolóxicas como a patoloxías como o cancro. A obestatina exprésase de forma maioritaria no estómago, mais obsérvanse alteracións nos seus niveis circulantes en pacientes con obesidade e anorexia, establecendo a hipótese do seu papel como unha nova hormona gastrointestinal. Non obstante, a función mellor coñecida da obestatina é a súa capacidade mitoxénica. Mediante o emprego de liñas celulares de cancro gástrico estableceuse o modelo de sinalización. A obestatina interactúa co GPR39 e actívanse dúas vías en paralelo. Por unha banda a activación consecutiva de Gi, PI3K, PKC novel (probablemente PKCε) e Src que activan a ERK1/2, implicado en proliferación. Por outra banda, a formación do complexo de sinalización de GPR39/beta-arrestina 1/Src conleva a transactivación de EGFR mediante ligandos liberados por MMPs e a consecuente activación de Akt, implicado en procesos como o crecemento celular, proliferación e diferenciación.

Os antecedentes do sistema obestatina/GPR39 en estómago demostran que a obestatina se expresa nas células enteroendócrinas e GPR39 nas células

principais da mucosa oxíntica en estómago san. En adenocarcinomas, a obestatina non é detectada mentres que o GPR39 presenta un patrón de expresión que se correlaciona positivamente co grao de dediferenciación do tumor. Isto establece ao GPR39 como un posible marcador prognóstico do cancro gástrico. Ademais, os estudos realizados nas liñas tumorais de estómago, demostran o papel da obestatina na regulación de procesos de transición epitelio mesénquima, proliferación, migración e invasión, evidenciando o papel deste sistema no desenvolvemento do cancro gástrico. Con todo isto, xurden novos camiños para a detección e tratamento do cancro gástrico, desenvolvendo antagonistas de obestatina como posibles axentes terapéuticos nesta patoloxía.

O obxectivo principal desta tese de doutoramento é o estudo do sistema obestatina/GPR39 no desenvolvemento, mantemento e malignidade do cancro gástrico.

Este obxectivo distribúese nos seguintes apartados:

1. Estudo da funcionalidade do sistema de obestatina/GPR39 no estómago san.

2. Estudo do papel do sistema de obestatina/GPR39 nas liñas celulares de cancro gástrico.

3. Estudo da expresión do sistema de obestatina/GPR39 na progresión ao cancro gástrico.

4. Estudo metabolómico de biofluídos humanos de pacientes agrupados de acordo coa secuencia precarcinoxénica gástrica de Correa.

Os nosos resultados da positividade do GPR39 nas células principais do estómago propoñen un posible papel nun estómago san: a regulación da secreción das encimas dixestivas. Os estudos anteriores do noso grupo usando un modelo *in vitro* dunha liña celular que expresa endoxenamente GPR39 e secreta pepsinóxeno I, demostraron que a administración esóxena de obestatina estimula a liberación do pepsinóxeno. Ademais, este efecto é mediado polo GPR39. Para demostrar non só a acción da obestatina na secreción do pepsinóxeno, senón tamén a súa acción con respecto á liberación da lipase gástrica, usouse un cultivo de explantes de estómagos humano. Neste sistema, a obetsatina estimulou a secreción de ambas encimas.

Polo tanto, este achado proporciona a primeira actividade funcional para o sistema de obestatina/GPR39 nun estómago san.

Malia que os mecanismos moleculares da secreción de pepsinóxeno non están completamente claros, dúas vías están implicadas neste proceso. A primeira vía implica a activación de adenilato ciclase (AC) por proteínas G, que conduce á produción do segundo mensaxeiro cAMP. Logo a proteína quinase A (PKA) actívase a través da unión da súa subunidade reguladora ao cAMP xerado e desencadea unhas respostas celulares que levan á secreción de pepsinoxéno. A capacidade da obestatina para producir cAMP demostrouse que podería ser un mecanismo viable. Os nosos datos mostran que a obestatina activa de forma significativa PKA, polo que se confirma que esta ruta está implicada na secreción de pepsinóxeno mediada por obestatina.

Na segunda ruta, a proteína Go activa a fosfolipase C (PLC), que hidroliza ao fosfatidilinositol 4,5-bifosfato (PIP2) xerando diacilglicerol (DAG) e inositol trifosfato (IP3). Por unha banda, a proteína quinase C (PKC) actívase polo DAG, e por outra banda, o IP3 mobiliza Ca^{2+} intracelular a través da activación da Ca^{2+}/Calmodulina proteína quinase II (CaMKII). Ámbolos dous, tanto PKC como CaMKII activados, fosforilan proteínas diana que conlevan a activación de respostas celulares implicados na secreción de pepsinóxeno.

Ademais, unha terceira vía máis recente implica o receptor activado por proteases 2 (PAR2). Verificouse que as células principais da mucosa gástrica son fortemente inmunorreactivas para PAR2. Estes receptores son membros da familia dos receptores acoplados a proteínas G (GPCR) que teñen un mecanismo especial de activación proteolítica. Ademais da tripsina, describiuse que outras proteases da familia das metaloproteases e kallikreínas son tamén activadoras deste receptor, específicamente, KLK4, KLK5, KLK6, KLK14 e MMP1.

O tratamento con obestatina no estómago humano san mostrou un aumento na secreción de todas as proteases estudadas, 29 das cales significativamente. Entre elas, tanto KLK11 como MMP1 mostraron unha secreción regulada pola obestatina. Ademais, KLK11 foi a protease máis reducida no lisado celular, demostrando a capacidade de obestatina para promover a súa secreción. Estas proteases liberadas poden levar á activación do PAR2 e

desencadear mecanismos moleculares que levan á secreción do pepsinóxeno e/ou da lipasa.

Estes resultados non só demostran a acción do sistema de obestatina/GPR39 para activar a liberación de pepsinóxeno e lipase, senón tamén revelan unha función para este sistema no estómago humano san.

O sistema de obestatina/GPR39 ten un papel importante na regulación da proliferación e da diferenciación a través das vías que activa en paralelo, demostradas nas células de cancro gástrico AGS e KATO-III. Os estudos previos do noso grupo de investigación mostran que a obestatina causa a proliferación, invasión e a migración nas células AGS. Ademais, tamén regula a EMT e a anxioxénese nestas células. Esta liña celular provén dun adenocarcinoma moderadamente diferenciado. A obestatina estaría desempeñando un papel na indución dun fenotipo invasivo que permite a dispersión a novos lugares para establecer a metástase. Non obstante, coas células NCI-N87 obtivéronse datos contrarios. A obestatina tamén causa proliferación pero, pola contra, inhibiu a migración e a invasión. Ademais, favoreceu a MET diminuindo marcadores mesenquimais. Tendo en conta que as células NCI-N87 derivan dunha metástase hepática dun carcinoma gástrico ben diferenciado, a obestatina estaría favorecendo o establecemento de células metastáticas para formar un novo nicho. Polo tanto, o sistema de obestatina/GPR39 modula o proceso tumoral e metastático de forma diferente dependendo do contexto celular. Estes datos son compatibles co estudo das células KATO-III. Estas células presentan dous fenotipos claramente diferenciados, un adherente e outro flotante e foron establecidas a partir dun carcinoma pobremente diferenciado. O estudo do supresor metastático nm23-H1 nas diferentes poboacións revelou datos sorprendentes. Sábese que o nivel de expresión basal deste xene en KATO-III é maior no fenotivo flotante que nas células adherentes, e que estas subpoboacións están en equilibrio entre elas. En realidade, cando as dúas poboacións están separadas, os fenotipos modifícanse ata alcanzar o equilibrio. Non obstante, no experimento realizado, a obestatina reduce a expresión de nm23-H1 na poboación flotante, favorecendo o seu cambio a un fenotipo adherente. Isto é importante no establecemento de células metastáticas circulantes nun novo lugar para orixinar a metástase. Por outra banda, na poboación adherente de KATO-III, que ten unha menor expresión

do xene, a obestatina provocou o seu incremento, favorecendo un fenotipo máis invasivo.

Tendo en conta tamén a expresión diferencial GPR39 nos adenocarcinomas gástricos humanos, estes descubrimentos corroboran o potencial funcional do sistema de obestatina/GPR39 na proliferación e malignidade do cancro gástrico. O deseño de novas estratexias terapéuticas podería establecerse mediante o uso de antagonistas deste sistema.

Segundo o modelo de carcinoxénese de Correa, está ben establecido que cambios celulares prodúcense neste proceso premaligno. A atrofia caracterízase por unha perda de células parietais, que leva á chamada atrofia oxíntica, debido ao feito de que estas células son responsables da secreción de ácido do estómago. Na seguinte etapa, unhas células similares ao epitelio intestinal comezan a establecerse na glándula, que acaba sendo invadida totalmente, desenvolvendo a metaplasia intestinal. A análise inmunohistoquímica, non revelou diferenzas significativas na cantidade de células enteroendócrinas ou células principais, nas que se expresan obestatina e GPR39, respectivamente. Sábese que a SPEM ocorre como un paso previo á metaplasia intestinal. As células principais da base da glándula dediferenciaríanse e comenzan a expresar TFF2, xurdindo células de tipo antral. Esta dediferenciación sería un mecanismo fisioloxíco de reparación ante o dano da mucosa. Polo tanto, o feito de que a SPEM se orixine nas células principais, que son positivas para GPR39, lévanos a postular o papel potencial do sistema obestatina/GPR39 na dediferenciación destas células e o seu consecuente proceso metaplásico. Aínda que as glándulas metaplásicas non expresan GPR39, sería interesante un estudo en profundidade do papel do sistema obestatina/GPR39 no proceso metaplásico. Sabendo que os adenocarcinomas gástricos son positivos para GPR39, a análise da expresión do receptor noutras células distintas das células principais que puidese xurdir en metaplasia e displasia sería útil para establecer o GPR39 non só como un factor prognóstico, senón tamén como un biomarcador da detección precoz do cancro gástrico.

A vía de sinalización de obestatina integra factores como MMPs e RTKs responsables de transmitir a activación da vía de Akt e, consecuentemente, a de mTOR. A análise de EGFR e IGF-IR en mostras de estómago san, con gastrite e con atrofia, mostrou datos sorprendentes. Como membros dos

RTKs, están sobrerregulados en cancro. O patrón IGF-IR mostra unha tendencia lóxica a aumentar a medida que avanza cara ao cancro. Estes datos apoian a estudos previos nos que este receptor se atopa sobreexpresado en cancro gástrico, observando unha correlación positiva a medida que o tumor se dediferencia. Ademáis, a obestatina é capaz de sobrerregulalo en células de cancro gástrico. Non obstante, os resultados do EGFR mostran un patrón oposto. Probablemente, a perda de integridade celular é responsable da diminución da expresión. *H. pylori* é capaz de activar EGFR para activar rutas como a da Akt e establecer o seu potencial cancerígeno. Este efecto demostrouse en células AGS, o mesmo sistema no que o noso grupo demostrou o proceso de transactivación do EGFR e outros RTKs a través do GPR39 na ruta da obestatina. Así, este péptido, induce unha sobrerregulación destes receptores que podería establecer o desencadeamento de vías implicadas na tumorixénse, de xeito análogo ao que ocorre na infección por *H. pylori*.

A análise das proteases revelou distintos patróns de expresión segundo os diferentes grupos establecidos. A obestatina foi capaz de inducir cambios na expresión de proteases no lisado de mostras nun dos tres grupos analizados. As tres catepsinas analizadas estaban relacionadas co cancro. Así, a sobrerregulación de catepsina Z está relacionada co desenvolvemento do tumor, o aumento de catepsina L foi visto en cancro gástrico e catepsina D presenta unha elevada expresión no adenocarcinoma gástrico pobremente diferenciado. Os datos obtidos apoian a implicación do sistema obestatina/GPR39 na regulación da fisioloxía destas proteases, aínda que se necesitan máis estudos para aclarar totalmente esta cuestión.

O cancro gástrico é unha patoloxía de mortalidade elevada debido ao seu diagnóstico tardío. Menos do 20 % dos pacientes sobreviven polo menos 5 anos. A falta e a inespecificidade dos síntomas dificultan o diagnóstico precoz da enfermidade. Seguindo a secuencia de Correa, a atrofia é unha etapa previa ao cancro gástrico e considérase un factor de risco nesta patoloxía. A pesar dos sistemas de clasificación que xurdiron ao longo dos anos, ningún logrou un diagnóstico efectivo conlevando a que a atrofia estea infradiagnosticada. Os protocolos obxectivos son necesarios para un diagnóstico efectivo e o establecemento de directrices relevantes para o control da evolución en etapas máis severas.

A metabolómica danos a capacidade de detectar biomarcadores para o diagnóstico precoz de enfermidades. A través do estudo dos metabolitos en biofluídos, pódese establecer un protocolo de diagnóstico fiable e robusto. A metabolómica por NMR é amplamente utilizada pola súa rapidez, reproducibilidade e baixo custo. É unha técnica en auxe nestas décadas, pero só hai dous estudos que usan NMR en cancro gástrico. O establecemento de ferramentas de diagnóstico precoz no cancro gástrico é realmente necesario. En liña con esta idea, o uso de biofluídos, como o plasma e a urina, podería ser estudado nas fases iniciais do modelo de Correa e, deste xeito, podería axudar ao diagnóstico da gastrite e atrofia con precisión.

A análise de plasma revela que a nosa poboación de estudo estratifícase en grupos que non se poden explicar polos datos dispoñibles dos doentes. Os grupos resultantes son pequenos e a robustez dos datos obtidos compromételese. Os experimentos TOCSY levaranse a cabo para determinar o motivo destes agrupamentos e realizarase a súa posterior análise estatística.

Os datos das mostras de urina foron sorprendentes. A análise univariante revelou varias zonas do espectro significativamente relacionados coa infección por *H. pylori* e patoloxías de gastrite e atrofia. Malia o estudo separado por sexo, obtivéronse zonas do espectro comúns tanto para homes como en mulleres. Ademais, atopáronse tamén zonas comúns ao comparar as variables. Este feito reforza a robustez dos datos obtidos, xa que tanto a infección por *H. pylori* como a gastrite e atrofia están intimamente ligadas.

A bomba de protóns do estómago é responsable da liberación dos protóns ao lumen para obter o pH do ácido necesario para a dixestión. Esta bomba é unha ATPase de hidróxeno e potasio (H^+/K^+ ATPase) e necesita enerxía para funcionar. Está ben establecido que a perda das células parietais ocorre na atrofia, sendo estas as células que conteñen esta bomba. As moléculas enerxéticas como o ATP e os seus derivados mostran intensidades en ppm próximas ás zonas que se atoparon. Este feito lévanos a postular se o ATP ou as súas moléculas derivadas poden ser responsables das diferencias atopadas entre variables. Non obstante, son necesarios estudos posteriores para verificar esta hipótese. A análise mediante TOCSY será o seguinte para identificar os metabolitos responsables destas sinais significativas. Ademais, esta análise proporcionaría máis información sobre o agrupamento que se produce na análise PCA non supervisada con todas as mostras. Este

experimento permitiranos saber se hai algún tipo de alteración ou degradación das mostras que se encargan desta separación.

Os datos de cuantificación dos metabolitos mostran que o mio-inositol presenta uns niveis significativamente maiores no grupo de infección de *H. pylori* fronte os sans na urina, únicamente nos homes. O mio-inositol é a vitamina B8, un elemento non esencial xa que pode ser sintetizado, pero moi importante para unha fisioloxía correcta. Este polialcol atópase en moitos alimentos e é absorbido no estómago e intestino delgado, sendo soluble en auga e eliminándose pola urina. As maiores cantidades de inositol na urina dos grupos patolóxicos con respecto ao control serían debidas á perda de capacidade de absorción do epitelio gástrico.

A pesar do feito de que son necesarios máis experimentos, confírmase a capacidade informativa dos biofluídos nestas patoloxías. En concreto, as mostras de urina revelaron zonas do espectro significativas que se relacionan coa infección por *H. pylori* e coas enfermidades de gastrite e atrofia. Polo tanto, a metabolómica por RMN de urina postúlase como un novo sistema para a procura de biomarcadores que garantan o diagnóstico correcto e precoz destas enfermidades para evitar a progresión ao cancro gástrico.

USC
UNIVERSIDADE
DE SANTIAGO
DE COMPOSTELA

ACKNOWLEDGMENTS

USC
UNIVERSIDADE
DE SANTIAGO
DE COMPOSTELA

Como punto final a esta etapa gustaríame acabar agradecendo a todas as persoas que fixeron posible este momento.

En primeiro lugar quixera agradecer aos meus tres directores de tese.

A Dra Yolanda Pazos, grazas por permitirme embarcar nesta andaina que dificilmente esquecerei. Grazas por todos os consellos, tanto profesionais como persoais, que levo ben fondo por se algún día preciso botar man deles.

Ao Dr. Juan Enrique Domínguez, grazas por demostrarme que a investigación é a mellor ferramenta para evolucionar

E finamente, ao Dr. Tomás García-Caballero, grazas por todo o asesoramento e a súa dispoñibilidade constante ao longo desta tese.

Quixera agradecer tamén ao Dr. Jesús P. Camiña, pola súa inmensa solidariedade, imprencindible para que este proxecto saíse adiante. Ao Dr. Manuel Martín, grazas por ensinarme a dar os meus primeiros pasos no universo do NMR e pola súa enorme paciencia. Grazas a Dra. Rosalía Gallego, por toda a dispoñibilidade para atenderme, pola humildade e por desvelarme o truco de maxia para unha inmuno perfecta. A Fernando Macías, grazas por toda a axuda na recollida de pacientes e polo túa calidade profesional e persoal.

Grazas ao Dr. Óscar Millet por darme a oportunidade de acollerme no seu laboratorio e xunto coa inestimable axuda da Dra. Nieves Embade, facer que sexa un pouquiño menos ignorante no apaixonante mundo da metabolómica.

Grazas ao Dr. Javier Baltar, pola colaboración na obtención das mostras tan imprescindibles para o noso traballo e ao Dr. Andrés Cervantes, por proporcionarnos de maneira altruísta a liña celular NCI-N87.

E a todos os compañeiros do IDIS, especialmente os do laboratorio 3, 4 e 12, dos cales xa fai tempo deixaron de ser simplemente compañeiros para pasar a ser amigos.

E esta andaina non sería posible sen todo o apoio recibido da mellor familia e amigos que se poden ter. Especialmente, grazas a meus pais e a miña avoa, porque sen eles todo isto non tería sentido.

BIBLIOGRAPHY

USC
UNIVERSIDADE
DE SANTIAGO
DE COMPOSTELA

1. Riihimäki M, Hemminki A, Sundquist K, *et al.* Metastatic spread in patients with gastric cancer. Oncotarget. 2016;7(32):52307-16.
2. Everett SM, Axon ATR. Early gastric cancer in Europe. Gut. 1997;41:142-150.
3. González CA, Sala N, Rokkas T. Gastric cancer: epidemiologic aspects. *Helicobacter*. 2013;18:34-8.
4. Plummer M, Franceschi S, Vignat J, *et al.* Global burden of gastric cancer attributable to *Helicobacter pylori*. Int J Cancer. 2015;136(2):487-90.
5. *Helicobacter* and Cancer Collaborative Group. Gastric cancer and *Helicobacter pylori*: a combined analysis of 12 case control studies nested within prospective cohorts. Gut. 2001;49:347–53.
6. Noto JM, Peek RM, *Helicobacter pylori*: an overview. Methods Mol. Biol. 2012;921:7–10.
7. Hooi JKY, Lai WY, Ng WK, *et al.* Global Prevalence of *Helicobacter pylori* Infection: Systematic Review and Meta-Analysis. Gastroenterology. 2017;153(2):420-429.
8. Wang F, Meng W, Wang B, *et al. Helicobacter pylori*-induced gastric inflammation and gastric cancer. Cancer Lett. 2014;345(2):196-202.
9. Chiba T, Marusawa H, Seno H, *et al.* Mechanism for gastric cancer development by *Helicobacter pylori* infection. J Gastroenterol Hepatol. 2008;23:1175–81.
10. Mladenova I, Durazzo M. Transmission of *Helicobacter pylori*. Minerva Gastroenterol Dietol. 2018;64(3):251-254.
11. Ladeiras-Lopes R, Pereira AK, Nogueira A, *et al.* Smoking and gastric cancer: systematic review and meta-analysis of cohort studies. Cancer Causes Control. 2008;19(7):689–701.
12. Jedrychowski W, Wahrendorf J, Popiela T, *et al.* A case-control study of dietary factors and stomach cancer risk in Poland. Int J Cancer. 1986;37(6):837–842.
13. La Vecchia C, Negri E, Franceschi S, *et al.* Family history and the risk of stomach and colorectal cancer. Cancer. 1992;70(1):50–55.
14. Skierucha M, Milne AN, Offerhaus GJ, *et al.* Molecular alterations in gastric cancer with special reference to the early-onset subtype. World J Gastroenterol. 2016;22(8):2460–2474.
15. Correa P, Haenszel W, Cuello C, *et al.* A model for gastric cancer epidemiology. Lancet. 1975;2:58–60.
16. Correa P. A human model of gastric carcinogenesis. Cancer Res. 1988;48:3554–60.
17. Correa P. Human gastric carcinogenesis: a multistep and multifactorial process – First American Cancer Society Award lecture on cancer epidemiology and prevention. Cancer Res. 1992;52:6735–40.
18. Kuipers EJ, Uyterlinde AM, Peña AS, *et al.* Long-term sequelae of *Helicobacter pylori* gastritis. Lancet. 1995;345:1525–8.
19. Sipponen P, Helske T, Järvinen P, *et al.* Fall in the prevalence of chronic gastritis over 15 years: analysis of outpatient series in Finland from 1977, 1985, and 1992. Gut. 1994;35:1167–71.
20. Maaroos HI, Vorobjova T, Sipponen P, *et al.* An 18-year follow-up study of chronic gastritis and *Helicobacter pylori* association of CagA positivity with development of atrophy and activity of gastritis. Scand J Gastroenterol. 1999;34:864–9.

21. Ebule IA, Djune Fokou AK, Sitedjeya Moko IL *et al.* Prevalence of *H. pylori* Infection and Atrophic Gastritis among dyspeptic subjects in Cameroon using a Panel of Serum Biomarkers (PGI, PGII, G-17, HpIgG). Sch. J. App. Med. Sci. 2017;5(4A):1230-1239.
22. Li Q, Karam SM, Gordon JI. Diphtheria toxin-mediated ablation of parietal cells in the stomach of transgenic mice. J Biol Chem. 1996;271:3671–3676.
23. Bredemeyer AJ, Geahlen JH, Weis VG, *et al.* The gastric epithelial progenitor cell niche and differentiation of the zymogenic (chief) cell lineage. Dev Biol. 2009;325:211–224.
24. El-Zimaity HMT, Ota H, Graham DY, *et al.* Patterns of gastric atrophy in intestinal type gastric carcinoma. Cancer. 2002;94:1428–1436.
25. Hattori T. Development of adenocarcinomas in the stomach. Cancer. 1986;57:1528–1534.
26. Xia HH, Kalantar JS, Talley NJ, *et al.* Antral-type mucosa in the gastric incisura, body and fundus (antralization): A link between *Helicobacter pylori* infection and intestinal metaplasia. Am. J. Gastroenterol. 2000;95:114–121.
27. Schmidt PH, Lee JR, Joshi V, *et al.* Identification of a metaplastic cell lineage associated with human gastric adenocarcinoma. Lab. Invest. 1999;79:639–646.
28. Halldorsdottir AM, Sigurdardottir M, Jonasson JG, *et al.* Spasmolytic polypeptide expressing metaplasia (SPEM) associated with gastric cancer in Iceland. Dig. Dis. Sci. 2003;48:431–441.
29. Morson BC. Intestinal metaplasia of the gastric mucosa. Br J Cancer. 1955;9:365–376.
30. Ectors N, Dixon MF. The prognostic value of sulphomucin positive intestinal metaplasia in the development of gastric cancer. Histopathology. 1986;10:1271–1277.
31. Lee HJ, Nam KT, Park HS, *et al.* Gene expression profiling of metaplastic lineages identifies CDH17 as a prognostic marker in early-stage gastric cancer. Gastroenterology. 2010;139(1):213-25.
32. Schmidt PH, Lee JR, Joshi V, *et al.* Identification of a metaplastic cell lineage associated with human gastric adenocarcinoma. Lab. Invest. 1999;79:639–646.
33. Wang TC, Goldenring JR, Dangler C, *et al.* Mice lacking secretory phospholipase A2 show altered apoptosis and differentiation with *Helicobacter* felis infection. Gastroenterology. 1998;114:675–689.
34. Fox JG, Li X, Cahill RJ, Andrutis K, *et al.* Hypertrophic gastropathy in *Helicobacter* felis-Infected wild type C57BL/6 mice and p53 hemizygous transgenic mice. Gastroenterology. 1996;110:155–166.
35. Fox JG, Wang TC, Rogers AB, *et al.* Host and microbial constituents influence *Helicobacter pylori*-induced cancer in a murine model of hypergastrinemia. Gastroenterology. 2003;124:1879–1890.
36. Nomura S, Yamaguchi H, Wang TC, *et al.* Alterations in gastric mucosal lineages induced by acute oxyntic atrophy in wild type and gastrin deficient mice. Amer. J. Physiol. 2004;288:G362–G375.
37. Goldenring JR, Ray GS, Coffey RJ, *et al.* Reversible drug-induced oxyntic atrophy in rats. Gastroenterology. 2000;118:1080–1093.
38. Fox JG, Blanco M, Murphy JC, *et al.*. Local and systemic immue responses in murine *Helicobacter* felis active chronic gastritis. Infect. Immun. 1993;61:2309–2315.
39. Yoshizawa N, Takenaka Y, Yamaguchi H, *et al.* Emergence of spasmolytic polypeptide-expressing metaplasia in Mongolian gerbils infected with *Helicobacter pylori*. Lab Invest. 2007;87:1265–1276.

40. El-Zimaity HMT, Ramchatesingh J, Saeed MA, *et al.* Gastric intestinal metaplasia: subtypes and natural history. J. Clin. Pathol. 2001;54:679–683.
41. Wallasch C, Crabtree JE, Bevec D, *et al. Helicobacter pylori*-stimulated EGF receptor transactivation requires metalloprotease cleavage of HB-EGF. Biochem. Biophys. Res. Commun. 2002;295:695–701.
42. Romano M, Ricci V, Di Popolo A, *et al. Helicobacter pylori* upregulates expression of epidermal growth factor-related peptides, but inhibits their proliferative effect in MKN 28 gastric mucosal cells. J. Clin. Invest. 1998;101:1604–1613.
43. Schiemann U, Konturek J, Assert R, *et al.* mRNA expression of EGF receptor ligands in atrophic gastritis before and after *Helicobacter pylori* eradication. Med. Sci. Monit. 2002;8:CR53–CR58.
44. Wong BC, Wang WP, So WH, *et al.* Epidermal growth factor and its receptor in chronic active gastritis and gastroduodenal ulcer before and after *Helicobacter pylori* eradication. Aliment Pharmacol. Ther. 2001;15:1459–1465.
45. Prenzel N, Zwick E, Daub H, *et al.* EGF receptor transactivation by G.-protein-coupled receptors requires metalloproteinase cleavage of proHB-EGF. Nature. 1999;402:884–888.
46. Pece S, Gutkind JS. Signaling from E-cadherins to the MAPK pathway by the recruitment and activation of epidermal growth factor receptors upon cell-cell contact formation. J. Biol. Chem. 2000;275:41227–41233.
47. Keates S, Sougioultzis S, Keates AC, *et al.* cag+ *Helicobacter pylori* induce transactivation of the epidermal growth factor receptor in AGS gastric epithelial cells. J. Biol. Chem. 2001;276:48127–48134.
48. Bauer B, Bartfeld S, Meyer TF. *H. pylori* selectively blocks EGFR endocytosis via the non-receptor kinase c-Abl and CagA. Cell. Microbiol. 2009;11:156–169.
49. Cover TL, Krishna US, Israel DA,*et al.* Induction of gastric epithelial cell apoptosis by *Helicobacter pylori* vacuolating cytotoxin. Cancer Res. 2003;63:951–957.
50. Maeda S, Yoshida H, Mitsuno Y, *et al.* Analysis of apoptotic and antiapoptotic signalling pathways induced by *Helicobacter pylori.* Gut. 2002;50:771–778.
51. Saadat I, Higashi H, Obuse C, *et al. Helicobacter pylori* CagA targets PAR1/MARK kinase to disrupt epithelial cell polarity. Nature. 2007;447:330–333.
52. Nagy TA, Frey MR, Yan F, *et al. Helicobacter pylori* regulates cellular migration and apoptosis by activation of phosphatidylinositol 3-kinase signaling. J. Infect. Dis. 2009;199:641–651.
53. Peek RM Jr, Moss SF, Tham KT, *et al. Helicobacter pylori* cagA+ strains and dissociation of gastric epithelial cell proliferation from apoptosis. J. Natl Cancer Inst. 1997;89:863–868.
54. Peek RM Jr, Wirth HP, Moss SF, *et al. Helicobacter pylori* alters gastric epithelial cell cycle events and gastrin secretion in Mongolian gerbils. Gastroenterology. 2000;118:48–59.
55. Globocan 2012.International Agency for Research on Cancer. World Health Organization. http://gco.iarc.fr/today/home.
56. Orditura M, Galizia G, Sforza V, *et al.* Treatment of gastric cancer. World J Gastroenterol. 2014;20:1635-49.
57. Kelley JR, Duggan JM. Gastric cancer epidemiology and risk factors. J Clin Epidemiol. 2003;56(1):1–9.

58. Bertuccio P, Chatenoud L, Levi F, *et al.* Recent patterns in gastric cancer: a global overview. Int J Cancer. 2009;125:666-73.
59. Goh KL, Chan WK, Shiota S, *et al.* Epidemiology of *Helicobacter pylori* infection and public health implications. *Helicobacter*. 2011;Suppl 1:1-9.
60. Parkin DM. The global health burden of infection-associated cancers in the year 2002. Int J Cancer. 2006;118:3030-44.
61. Chow WH, Blot WJ, Vaughan TL, *et al.* Body mass index and risk of adenocarcinomas of the esophagus and gastric cardia. J Natl Cancer Inst. 1998;90:150–5.
62. Lagergren J, Bergström R, Olof N. Association between body mass and adenocarcinoma of the esophagus and gastric cardia. Ann Intern Med. 1999;130:883–90.
63. Wu AH, Wan P, Bernstein L. A multiethnic population-based study of smoking, alcohol and body size and risk of adenocarcinomas of the stomach and esophagus (United States). Cancer Causes Control. 2001;12:721–32.
64. Derakhshan MH, Malekzadeh R, Watabe H, *et al.* Combination of gastric atrophy, reflux symptoms and histological subtype indicates two distinct aetiologies of gastric cardia cancer. Gut. 2008;57:298–305.
65. Robertson EV, Derakhshan MH, Wirz AA, *et al.* Central obesity in asymptomatic volunteers is associated with increased intrasphincteric acid reflux and lengthening of the cardiac mucosa. Gastroenterology. 2013;145:730–9.
66. Bertuccio P, Rosato V, Andreano A, *et al.* Dietary patterns and gastric cancer risk: a systematic review and meta-analysis. Ann Oncol. 2013;24:1450–8
67. Olefson S, Moss SF. Obesity and related risk factors in gastric cardia adenocarcinoma. Gastric Cancer. 2015;18(1):23-32.
68. Laurén P. The two histological main types of gastric carcinoma: Diffuse and so-called intestinal-type carcinoma an attempt at a histo-clinical classification. Acta Pathol Microbiol Scand. 1965;64:31-49.
69. Leocata P, Ventura L, Giunta M, *et al.* Gastric carcinoma: a histopathological study of 705 cases. Ann Ital Chir. 1998;69:331-7.
70. Edge SB, Byrd DR, Compton CC, *et al.* AJCC cancer staging manual. 7th ed. New York: Springer-Verlag. 2009.
71. Tanaka A, Kamada T, Inoue K, *et al.* Histological evaluation of patients with gastritis at high risk of developing gastric cancer using a conventional index. Pathol Res Pract. 2011; 207:354–8.
72. Toyoshima O, Yamaji Y, Yoshida S, *et al.* Endoscopic gastric atrophy is strongly associated with gastric cancer development after *Helicobacter pylori* eradication. Surg Endosc. 2017; 31(5): 2140–2148.
73. Shichijo S, Hirata Y, Niikura R, *et al.* Histologic intestinal metaplasia and endoscopic atrophy are predictors of gastric cancer development after *Helicobacter pylori* eradication. Gastrointest Endosc. 2016;84(4):618-24.
74. Dixon MF, Genta RM, Yardley JH *et al.* Classification and grading of gastritis. The updated Sydney system. International Workshop on the Histopathology of Gastritis, Houston, 1994. Am J Surg Pathol 1996;20:1161-81.
75. Aydin O, Egilmez R, Karabacak T *et al.* Interobserver variation in histopathological assessment of *Helicobacter pylori* gastritis World J Gastroenterol. 2003 Oct;9(10):2232-5.
76. Rugge M, Correa P, Di Mario F et al. OLGA staging for gastritis: A tutorial. Dig Liv Dis 2008;40(8):650-8.

77. Karnes WE Jr, Samloff IM, Siurala M, *et al.* Positive serum antibody and negative tissue staining for *Helicobacter pylori* in subjects with atrophic body gastritis. Gastroenterology. 1991;101:167–174.
78. Broutet N, Plebani M, Sakarovitch C, *et al.* Pepsinogen A, pepsinogen C, and gastrin as markers of atrophic chronic gastritis in European dyspeptics. Br J Cancer. 2003;88:1239–1247.
79. Miki K, Morita M, Sasajima M, *et al.* Usefulness of gastric cancer screening using the serum pepsinogen test method. Am J Gastroenterol. 2003;98:735–739.
80. Kitahara F, Kobayashi K, Sato T, *et al.* Accuracy of screening for gastric cancer using serum pepsinogen concentrations. Gut. 1999;44:693–697.
81. Kiyohira K, Yoshihara M, Ito M, *et al.* Serum pepsinogen concentration as a marker of *Helicobacter pylori* infection and the histologic grade of gastritis; evaluation of gastric mucosa by serum pepsinogen levels. J Gastroenterol. 2003;38:332–338.
82. Shiotani A, Iishi H, Uedo N, *et al.* Histologic and serum risk markers for noncardia early gastric cancer. Int J Cancer. 2005;115:463–469.
83. Urita Y, Hike K, Torii N, *et al.* Serum pepsinogens as a predicator of the topography of intestinal metaplasia in patients with atrophic gastritis. Dig Dis Sci. 2004;49:795–801.
84. Ohata H, Kitauchi S, Yoshimura N, *et al.* Progression of chronic atrophic gastritis associated with *Helicobacter pylori* infection increases risk of gastric cancer. Int J Cancer. 2004;109:138–43.
85. Watabe H, Mitsushima T, Yamaji Y, *et al.* Predicting the development of gastric cancer from combining *Helicobacter pylori* antibodies and serum pepsinogen status: a prospective endoscopic cohort study. Gut. 2005;54:764–68.
86. Agréus L, Kuipers EJ, Kupcinskas L, *et al.* Rationale in diagnosis and screening of atrophic gastritis with stomach-specific plasma biomarkers. Scand J Gastroenterol 2012;47(12):1525.
87. Nicholson JK, Lindon JC. Systems biology: Metabonomics. Nature. 2008;455(7216):1054–6.
88. Nicholson JK, Lindon JC, Holmes E. 'Metabonomics': understanding the metabolic responses of living systems to pathophysiological stimuli via multivariate statistical analysis of biological NMR spectroscopic data. Xenobiotica. 1999;29(11):1181–9.
89. Dunn WB, Bailey NJ, Johnson HE. Measuring the metabolome: current analytical technologies. Analyst. 2005;130(5):606–25.
90. Zhang X, Wei D, Yap Y, *et al.* Mass spectrometry-based "omics" technologies in cancer diagnostics. Mass Spectrom Rev. 2007;26(3):403–31.
91. Yin P, Zhao X, Li Q, *et al.* Metabonomics study of intestinal fistulas based on ultraperformance liquid chromatography coupled with Q-TOF mass spectrometry (UPLC/Q-TOF MS). J Proteome Res. 2006;5(9):2135–43.
92. Duarte IF, Diaz SO, Gil AM. NMR metabolomics of human blood and urine in disease research. J Pharm Biomed Anal. 2014;93:17–26. Epub 2014/05/24.
93. Bujak R, Daghir E, Rybka J, *et al.* Metabolomics inurogenital cancer. Bioanalysis. 2011; 3:913–923.
94. DeFeo EM, Wu CL, McDougal WS *et al.* A decade in prostate cancer:from NMR to metabolomics. Nat. Rev. Urol. 2011;8:301–311.
95. Ruperez FJ, Ramos-Mozo P, Teul J *et al.* Metabolomic study of plasma ofpatients with abdominal aortic aneurysm. Anal. Bioanal. Chem. 2012; 403:1651–1660.

96. Kang SM, Park JC, Shin MC, *et al.* ^{1}H nuclear magnetic resonance based metabolic urinary profiling of patientswith ischemic heart failure. Clin Biochem. 2011 Mar;44(4):293-9.
97. Bernini P, Bertini I, Luchinat C, *et al.* The cardiovascular risk of healthy individuals studied by NMR metabonomics of plasma samples, J. Proteome Res. 2011;10:4983–4992.
98. Pathmasiri W, Pratt KJ, Collier DN, *et al.* Integrating metabolomic signatures and psychosocial parameters in responsivity to an immersion treatment model for adolescent obesity. Metabolomics. 2012;8:1037–1051.
99. Munshi SU, Taneja S, Bhavesh NS, *et al.* Metabonomic analysis of hepatitis E patients shows deregulated metabolic cycles and abnormalities in amino acid metabolism. J. Viral Hepat. 2011;18:E591–E602.
100. Maher AD, Cysique LA, Brew BJ, *et al.* Statistical integration of 1H NMR and MRS data from different biofluids and tissues enhances recovery of biological information from individuals with HIV-1 infection. J. Proteome Res. 2011;10:1737–1745.
101. Sengupta A, Ghosh S, Basant A, *et al.* Global host metabolic response to Plasmodium vivax infection: a H-1 NMR based urinary metabonomic study. Malar. J. 2011;10:384.
102. Weiss RH, Kim K. Metabolomics in the study of kidney diseases. Nat. Rev. Nephrol. 2012; 8:22–33.
103. Xu XH, Huang Y, Wang G, *et al.* Metabolomics: a novel approach to identify potential diagnostic biomarkers and pathogenesis in Alzheimer's disease. Neurosci. Bull. 2012; 28:641–648.
104. Adamko DJ, Sykes BD, Rowe BH, *et al.* The metabolomics of asthma novel diagnostic potential. Chest . 2012;141:1295–1302.
105. Yu L, Aa J, Xu J, *et al.* Metabolomic phenotype of gastric cancer and precancerous stages based on gas chromatography time-of-flight mass spectrometry. J Gastroenterol Hepatol 26: 1290-1297, 2011.
106. Chan AW, Mercier P, Schiller D, *et al.* 1H-NMR urinary metabolomic profiling for diagnosis of gastric cancer. Br J Cancer. 2016;114(1):59-62.
107. Zhang JV, Ren PG, Avsian-Kretchmer O, *et al.* Obestatin, a peptide encoded by the ghrelin gene, opposes ghrelin's effects on food intake. Science. 2005;310:996-9.
108. McKee KK , Tan CP, Palyha OC, *et al.* Cloning and characterization of two human G protein-coupled receptor genes (GPR38 and GPR39) related to the growth hormone secretagogue and neurotensin receptors. Genomics. 1997;46:426-34.
109. Zhang Y, Zhao H, Peng H, *et al.* Two alternatively spliced GPR39 transcripts in seabream: molecular cloning, genomic organization, and regulation of gene expression by metabolic signals. J Endocrinol. 2008;199:457-70.
110. Camina JP, Campos JF, Caminos JE, *et al.* Obestatin-mediated proliferation of human retinal pigment epithelial cells: regulatory mechanisms. J Cell Phsiol. 2007;211:1-9.
111. Granata R, Settanni F, Gallo D, *et al.* Obestatin promotes survival of pancreatic β-cells and human islets and induces expression of genes involved in the regulation of β-cell mass and function. Diabetes. 2008;57:967-79.
112. Zhang JV, Jahr H, Luo CW, *et al.* Obestatin induction of early-response gene expression in gastrointestinal and adipose tissues and the mediatory role of G protein-coupled receptor, GPR39. Mol endocrinol. 2008;22:1464-75.

113. Gurriarán-Rodríguez U, Al-Massaddi O, Roca-Rivada A, *et al.* Obestatin as a regulator of adipocyte metabolism and adipogenesis. J Cell Mol Med. 2011;15:1927-40.
114. Gurriarán-Rodríguez U, Santos-Zas I, Al-Massadi O, *et al.* The obestatin/GPR39 system is up-regulated by muscle injury and functions as an autocrine regenerative system. J Biol Chem. 2012;287:38379-89.
115. Gurriarán-Rodríguez U, Santos-Zas I, González-Sánchez J, *et al.* Action of obestatin in skeletal muscle repair: stem cell expansion, muscle growth, and microenvironment remodeling. Mol Ther. 2015;23:1003-21.
116. Xin X, Ren AJ, Zheng X, *et al.* Disturbance of circulating ghrelin and obestatin in chronic heart failure patients especially in those with cachexia. Peptides. 2009;30:2281-5.
117. Ozbay Y, Aydin S, Dagli AF, *et al.* Obestatin is present in saliva: alterations in obestatin and ghrelin levels of saliva and serum in ischemic heart disease. BMB Rep. 2008;41:55-61.
118. Carlini VP, Schioth HB, de Barioglio SR. Obestatin improves memory performance and causes anxiolytic effects in rats. Biochem Biophys Res Commun. 2007;352:907-12.
119. Szakacs J, Csabafi K, Liptak N, *et al.* The effect of obestatin on anxietylike behaviour in mice. Behav Brain Res. 2015;293:41-5.
120. Samson WK, White MM, Price C, *et al.* Obestatin acts in brain to inhibit thirst. Am J Physiol-Regul Integr Comp Physiol. 2007;292:R637-43.
121. Nakahara T, Harada T, Yasuhara D, *et al.* Plasma obestatin concentrations are negatively correlated with body mass index, insulin resistance index, and plasma leptin concentrations in obesity and anorexia nervosa. Biol Psychiatry. 2008;64(3):252-5.
122. Harada T, Nakahara T, Yasuhara D, *et al.* Obestatin, acyl ghrelin, and des-acyl ghrelin responses to an oral glucose tolerance test in the restricting type of anorexia nervosa. Biol Psychiatry. 2008;63(2):245-7.
123. Gargantini E, Grande C, Trovato L, *et al.* The role of obestatin in glucose and lipid metabolism. Horm Metab Res. 2013;45:1002-8.
124. Pazos Y, Alvarez CJ, Camina JP, *et al.* Stimulation of extracellular signal-regulated kinases and proliferation in the human gastric cancer cells KATO-III by obestatin. Growth Factors. 2007;25:373-81.
125. Alvarez CJ, Lodeiro M, Theodoropoulou M, *et al.* Obestatin stimulates Akt signalling in gastric cancer cells through β-arrestin- mediated epidermal growth factor receptor transactivation. Endocr-Relat Cancer. 2009;16:599-611.
126. Alen BO, Leal-Lopez S, Alen MO, *et al.* The role of the obestatin/GPR39 system in human gastric adenocarcinomas. Oncotarget. 2016;7:5957-71.
127. Bhola NE, Grandis JR . Crosstalk between G-protein-coupled receptors and epidermal growth factor receptor in cancer. Front Biosci. 2008;13:1857-65
128. Normanno N, De Luca A, Bianco C, *et al.* Epidermal growth factor receptor (EGFR) signalling in cancer. Gene. 2006;366:2-16.
129. Ohtsu H, Dempsey PJ, Eguchi S. ADAMs as mediators of EGF receptor transactivation by G-protein-coupled receptors. Am J Phys Cell Physiol. 2006;291:C1-10.
130. Alén BO. Fundamental structural and biochemical features for the obestatin/GPR39 system mitogenic action. Thesis dissertation. Univesidade de Santiago de Compostela, Santiago de Compostela, Spain. 2016. http://hdl.handle.net/10347/14993
131. Rugge M, Genta RM. OLGA Group. Staging gastritis: an international proposal. Gastroenterology 2005;129:1807-8.

132. Capelle LG, de Vries AC, Haringsma J, Ter Borg F, de Vries RA, Bruno MJ *et al.* The staging of gastritis with the OLGA system by using intestinal metaplasia as an accurate alternative for atrophic gastritis. Gastrointest Endosc 2010;71(7):1150-8.
133. Raghay K, Garcia-Caballero T, Bravo S, *et al.* Ghrelin localization in the medulla of rat and human adrenal gland and in pheochromocytomas. Histol Histopathol. 2008;23:57-65.
134. Kumar D, Moore R, Nash A, *et al.* Decidual GM-CSF is a critical common intermediate necessary for thrombin and TNF induced in-vitro fetal membrane weakening. Placenta. 2014;35:1049-56.
135. Gao Z, Wang X, Wu K, *et al.* Pancreatic stellate cells increase the invasion of human pancreatic cancer cells through the stromal cell-derived factor-1/CXCR4 axis. Pancreatology 2010;10:186–193.
136. Dona AC, Jiménez B, Schäfer H, *et al.* Precision High-Throughput Proton NMR Spectroscopy of Human Urine, Serum, and Plasma for Large-Scale Metabolic Phenotyping. Anal. Chem. 2014;86(19):9887-94
137. Beckonert O, Keun HC, Ebbels TM *et al.* Metabolic profiling, metabolomic and metabonomic procedures for NMR spectroscopy of urine, plasma, serum and tissue extracts. Nature Protocols. 2007;2(11):2692-703.
138. Wishart DS. Quantitative metabolomics using NMR. TrAC Trends in Analytical Chemistry. 2008;27:228-37.
139. Giraudeau P. Quantitative 2D liquid-state NMR. Magn Reson Chem. 2014;52(6):259-72.
140. Zheng G, Torres AM, Price WS. WaterControl: self-diffusion based solvent signal suppression enhanced by selective inversion. Magn Reson Chem. 2017;55(5):447-451.
141. Louis E, Bervoets L, Reekmans G. *et al.* Phenotyping human blood plasma by 1H-NMR: a robust protocol based on metabolite spiking and its evaluation in breast cancer. Metabolomics. 2015;11:225-36.
142. Chu S, Schubert ML. Gastric secretion. Curr. Opin. Gastroenterol. 2012;28:587-593.
143. Carrière F, Grandval P, Renou C, *et al.* Quantitative study of digestive enzyme secretion and gastrointestinal lipolysis in chronic pancreatitis. Clin Gastroenterol Hepatol. 2005;3(1):28-38.
144. Goldenring JR, Nam KT, Mills JC. The origin of pre-neoplastic metaplasia in the stomach: chief cells emerge from the Mist. Exp. Cell Res. 2011;317:2759-64.
145. Cornaggia M, Capella C, Riva C, *et al.* Electron immunocytochemical localization of pepsinogen I (PgI) in chief cells, mucous-neck cells and transitional mucous-neck/chief cells of the human fundic mucosa. Histochemistry. 1986;85, 5-11.
146. Basque JR, Chénard M, Chailler P, *et al.* Gastric cancer cell lines as models to study human digestive functions. J Cell Biochem. 2001;81(2):241-51.
147. Kondo T, Yamada S. Studies on synthesis and secretion of pepsinogen in human gastric corpus mucosa by use of organ culture method. Nihon Shokakibyo Gakkai Zasshi. 1979;76:1067-1079.
148. Raufman JP. Gastric chief cells: Receptors and signal transduction mechanisms. Gastroenterology. 1992;102:699-710.
149. Steeg PS, Bevilacqua G, Pozzatti R, *et al.* Altered expression of NM23, a gene associated with low tumor metastatic potential, during Adenovirus 2 Ela inhibition of experimental metastasis. Cancer Research. 1988;48(22):6550–54.

150. Chailler P, Ménard D. Establishment of human gastric epithelial (HGE) cell lines exhibiting barrier function, progenitor, and prezymogenic characteristics. J Cell Physiol. 2005;202:263–274.
151. Wu WK, Cho CH, Lee CW, *et al.* Dysregulation of cellular signaling in gastric cancer. Cancer Lett. 2010;295:144-53.
152. Bielenberg DR, Zetter BR. The Contribution of Angiogenesis to the Process of Metastasis. Cancer J. 2015; 21(4): 267–273.
153. Oliveira MJ, Costa AM, Costa AC, *et al.* CagA associates with c-Met, E-cadherin, and p120-catenin in a multiproteic complex that suppresses *Helicobacter pylori*-induced cell-invasive phenotype. J Infect Dis. 2009;200:745-55.
154. Basque JR, Chénard M, Chailler P. Gastric cancer cell lines as models to study human digestive functions. Journal of Cellular Biochemistry. 2001, 81:241-251.
155. Saraiva-Pava K, Navabi N, Emma C Skoog EC. New NCI-N87-derived human gastric epithelial line after human telomerase catalytic subunit over-expression. World J Gastroenterol. 2015; 21(21): 6526–6542.
156. Kanat O, O'Neil B, Shahda S. Targeted therapy for advanced gastric cancer: A review of current status and future prospects. World J Gastrointest Oncol. 2015; 7(12): 401–410.
157. Martinelli E, De Palma R, Orditura M *et al.* Anti-epidermal growth factor receptor monoclonal antibodies in cancer therapy. Clin Exp Immunol. 2009; 158:1–9.
158. Normanno N, De Luca A, Bianco C *et al.* Epidermal growth factor receptor (EGFR) signaling in cancer. Gene. 2006; 366:2–16.
159. Cunningham, PS. The ghrelin receptor isoforms (GHS-R1a and GHS-R1b) and GPR39: an investigation into receptor dimerisation. Doctoral dissertation. Queensland University of Technology, Queensland, Australia. 2010.
160. Han N, Jin K, He K. Protease-activated receptors in cancer: A systematic review. Oncology Letters. 2011; 2(4):599-608.
161. O'Brien P, Molino M, Kahn M *et al.* Protease activated receptors: theme and variations. Oncogene. 2001;20(13):1570-1581.
162. Zhao P, Metcalf M, Bunnett NW. Biased signaling of protease-activated receptors. Front Endocrinol (Lausanne).2014;5:67.
163. Griffin JH, Zlokovic BV, Mosnier LO. Activated protein C: biased for translation. Blood. 2015;125(19):2898-2907.
164. Jin E, Fujiwara M, Pan X *et al.* Protease-activated receptor (PAR)-1 and PAR-2 participate in the cell growth of alveolar capillary endothelium in primary lung adenocarcinomas. Cancer. 2003;97: 703-713.
165. D'Andrea MR, Derian CK, Santulli RJ *et al.* Differential expression of protease-activated receptors-1 and -2 in stromal fibroblasts of normal, benign, and malignant human tissues. Am J Pathol. 2001;158: 2031-2041.
166. Sedda S, Marafini I, Caruso R *et al.* Proteinase activated-receptors-associated signaling in the control of gastric cancer. World J Gastroenterol. 2014;20:11977-84.
167. Craig A, Cloarec O, Holmes E, *et al.* Scaling and Normalization Effects in NMR Spectroscopic Metabonomic Data Sets. Anal. Chem. 2006;78 (7):2262–67.
168. Choi E, Roland JT, Barlow BJ, *et al.* Cell lineage distribution atlas of the human stomach reveals heterogeneous gland populations in the gastric antrum. Gut. 2014;63(11):1711-20.

169. Sakurada T, Ro S, Onouchi T, *et al.* Comparison of the actions of acylated and desacylated ghrelin on acid secretion in the rat stomach. J Gastroenterol. 2010;45(11):1111-20.
170. Hirschowitz BI. The control of pepsinogen secretion. Ann. N. Y. Acad. Sci.1967;140(2):709-723.
171. Bowie DJ, Vineberg AM.The selective action of histamine and the effect of prolonged vagal stimulation on the cells of the gastric glands in the dog. Quart. J. Exp. Physiol. 1935;25: 247-257.
172. Hirschowitz BI, O'Leary DK, Marks IN. Effects of atropine on synthesis and secretion of pepsinogen in the rat. Am J Physiol. 1960;198:108-12.
173. Pazos Y, Alvarez CJ, Camina JP, *et al.* Role of obestatin on growth hormone secretion: An in vitro approach. Biochem Biophys Res Commun. 2009;390:1377-81.
174. Kawabata A, Matsunami, M, Sekiguchi F. Gastrointestinal roles for proteinase-activated receptors in health and disease. Br. J. Pharmacol. 2008;153:S230-S240.
175. Kawao N, Sakaguchi Y, Tagome A, *et al.* Protease-activated receptor-2 (PAR-2) in the rat gastric mucosa: immunolocalization and facilitation of pepsin/pepsinogen secretion. Br J Pharmacol. 2002;135:1292-6.
176. Fiorucci S, Distrutti E, Federici B, *et al.* PAR-2 modulates pepsinogen secretion from gastric-isolated chief cells. Am J Physiol Gastrointest Liver Physiol. 2003;285(3):G611-20.
177. Gieseler F, Ungefroren H, Settmacher U, *et al.* Proteinase-activated receptors (PARs) - focus on receptor-receptor-interactions and their physiological and pathophysiological impact. Cell Commun. Signal. 2013;11:86.
178. Ramsay AJ, Dong Y, Hunt ML, *et al.* Kallikrein-related peptidase 4 (KLK4) initiates intracellular signaling via protease-activated receptors (PARs). KLK4 and PAR-2 are co-expressed during prostate cancer progression. J Biol Chem. 2008;283(18):12293-304.
179. Stefansson K, Brattsand M, Roosterman D, *et al.* Activation of proteinase-activated receptor-2 by human kallikrein-related peptidases. J Invest Dermatol. 2008;128(1):18-25.
180. Vandell AG, Larson N, Laxmikanthan G. Protease-activated receptor dependent and independent signaling by kallikreins 1 and 6 in CNS neuron and astroglial cell lines. J Neurochem. 2008;107(3): 855–870.
181. Li X, Tai HH. Thromboxane A2 receptor-mediated release of matrix metalloproteinase-1 (MMP-1) induces expression of monocyte chemoattractant protein-1 (MCP-1) by activation of protease-activated receptor 2 (PAR2) in A549 human lung adenocarcinoma cells. Mol Carcinog. 2014;53(8):659-66.
182. Yoon H, Laxmikanthan G, Lee J, *et al.* Activation profiles and regulatory cascades of the human kallikrein-related peptidases. J Biol Chem. 2007;282(44):31852-64.
183. Beaufort N, Plaza K, Utzschneider D, *et al.* Interdependence of kallikrein-related peptidases in proteolytic networks. Biol Chem. 2010;391(5):581-7.
184. Barranco SC, Townsend CM Jr., Casartelli C, *et al.* Establishment and characterization of an in vitro model system for human adenocarcinoma of the stomach. Cancer Res. 1983;43(4):1703-1709.
185. Sekiguchi M, Sakakibara K, Fujii G. Establishment of cultured cell lines derived from a human gastric carcinoma. Jpn J Exp Med. 1978;48:61-8.

186. Park JG, Frucht H, LaRocca RV, *et al.* Characteristics of cell lines established from human gastric carcinoma. Cancer Res. 1990;50(9):2773-80.
187. Tee YT, Chen GD, Lin LY, *et al.* Nm23-H1: a metastasis-associated gene. Taiwan J Obstet Gynecol. 2006;45(2):107-13.
188. Iizuka N, Tangoku A, Hazama S, *et al.* Nm23-H1 gene as a molecular switch between the free-floating and adherent states of gastric cancer cells. Cancer Lett. 2001;174(1):65-71.
189. Guan-zhen Y, Ying C, Can-rong N, *et al.* Reduced protein expression of metastasis-related genes (nm23, KISS1, KAI1 and p53) in lymph node and liver metastases of gastric cancer. International Journal of Experimental Pathology. 2007;88(3):175-183.
190. Iizukaa N, Tangokub A, Hazama S, *et al.* Nm23-H1 gene as a molecular switch between the free-floating andadherent states of gastric cancer cells. Cancer Letters. 2001; 174:65–71.
191. Wojtukiewicz MZ, Hempel D, Sierko E, *el al.* Protease-activated receptors (PARs)—biology and role in cancer invasion and metastasis. Cancer Metastasis Reviews. 2015;34:775-796.
192. Abdallah RT, Keum J-S, Lee M-H, *et al.* Plasma Kallikrein Promotes Epidermal Growth Factor Receptor Transactivation and Signaling in Vascular Smooth Muscle through Direct Activation of Protease-activated Receptors. The Journal of Biological Chemistry. 2010;285(45):35206-35215.
193. Goldenring JR, Nam KT. Oxyntic atrophy, metaplasia and gastric cancer. Prog Mol Biol Transl Sci. 2010;96:117-31.
194. Mills JC, Goldenring JR. Metaplasia in the stomach arises from gastric chief cells. Cell Mol Gastroenterol Hepatol. 2017;4(1): 85–88.
195. Teller A, Jechorek D, Hartig R, *et al.* Dysregulation of apoptotic signaling pathways by interaction of RPLP0 and cathepsin X/Z in gastric cancer. Pathol Res Pract. 2015;211:62-70.
196. Russo A, Bazan V, Migliavacca M, *et al.* Prognostic significance of DNA ploidy, S-phase fraction, and tissue levels of aspartic, cysteine, and serine proteases in operable gastric carcinoma. Clin Cancer Res. 2000;6:178-84.
197. Dinis-Ribeiro M, Areia M, de Vries AC, *et al.* Management of precancerous conditions and lesions in the stomach (MAPS): guideline from the European Society of Gastrointestinal Endoscopy (ESGE), European *Helicobacter* Study Group (EHSG), European Society of Pathology (ESP), and the Sociedade Portuguesa de Endoscopia Digestiva (SPED). Endoscopy. 2012;44:74–94.
198. Carpenter HA, Talley NJ. Gastroscopy is incomplete without biopsy: clinical relevance of distinguishing gastropathy from gastritis. Gastroenterology. 1995;108:917–924.
199. Plummer M, Buiatti E, Lopez G, *et al.* Histological diagnosis of precancerous lesions of the stomach: a reliability study. Int J EpidemioL. 1997;26:716–20.
200. Emwas AH. The strengths and weaknesses of NMR spectroscopy and mass spectrometry with particular focus on metabolomics research. Methods Mol Biol. 2015;1277:161-93.
201. Jung J, Jung Y, Bang EJ, *et al.* Noninvasive diagnosis and evaluation of curative surgery for gastric cancer by using NMR-based metabolomic profiling. Ann Surg Oncol. 2014;21(Suppl 4):S736-S742.

202. Emwas AH, Saccenti E, Gao X, *et al.* Recommended strategies for spectral processing and post-processing of 1D 1H-NMR data of biofluids with a particular focus on urine. Metabolomics. 2018;14(3):31
203. Kochhar S, Jacobs DM, Ramadan Z, *et al.* Probing gender-specific metabolism differences in humans by nuclear magnetic resonance-based metabonomics. Analytical Biochemistry. 2006;352(2):274–281.
204. Slupsky CM, Rankin KN, Wagner J, *et al.* Investigations of the effects of gender, diurnal variation, and age in human urinary metabolomic profiles. Analytical Chemistry. 2007;79(18):6995–7004.
205. Shin JM, Munson K, Vagin O, *et al.* The gastric HK-ATPase: structure, function, and inhibition. Pflugers Arch. 2009; 457(3): 609–22.
206. The Human Metabolome DataBase (HMDB) (http://www.hmdb.ca)
207. Dona AC, Kyriakides M, Scott F, *et al.* A guide to the identification of metabolites in NMR-based metabonomics/metabolomics experiments. Comput Struct Biotechnol J. 2016; 14: 135–153.
208. Holub BJ. Metabolism and function of myo-inositol and inositol phospholipids. Annu Rev Nutr. 1986;6:563-97.
209. Chiappelli J, Rowland LM, Wijtenburg SA, *et al.* Evaluation of myo-inositol as a potential biomarker for depression in schizophrenia. Neuropsychopharmacology. 2015 Aug; 40(9): 2157–2164.
210. Pucciarelli MG, Ruschkowski S, Trust TJ, *et al. Helicobacter pylori* induces an increase in inositol phosphates in cultured epithelial cells. FEMS Microbiol Lett. 1995;129(2-3):293-9.
211. Mahadeva S, Goh KL. Epidemiology of functional dyspepsia: A global perspective. World J Gastroenterol. 2006; 12(17): 2661–66.

SUPPLEMENTARY MATERIAL

USC
UNIVERSIDADE
DE SANTIAGO
DE COMPOSTELA

CHAPTER 1

Table S1. Pepsinogen I secretion from human stomach explants culture. Data refer to the secretion of pepsinogen I in arbitrary units normalized to the secretome volume (mL) and to the mucosa weight (g) of each explant. Statistics were performed by comparing each treatment to the control point at each time. Abbreviations: Pat, patient; Ob: human obestatin, S.E.M: standard error of the mean.

Time	Dose	Pat#1	Pat#2	Pat#3	Pat#4	Mean	S.E.M	P value
20 min	Control	7,44	15,80	9,40	12,05	11,17	1,81	
	Ob 50 nM	9,87	13,63	18,16	12,12	13,44	1,75	0,171
	Ob 100 nM	13,96	18,70	13,66	15,88	15,55	1,16	0,057
	Ob 200 nM	16,64	16,87	19,87	20,96	18,58	1,08	**0,014**
40 min	Control	8,10	13,79	17,32	12,91	13,03	1,90	
	Ob 50 nM	10,48	14,08	36,18	10,29	17,76	6,20	0,414
	Ob 100 nM	8,32	18,35	18,59	19,31	16,14	2,62	0,100
	Ob 200 nM	14,67	20,69	24,64	18,64	19,66	2,08	**0,029**
60 min	Control	5,77	13,62	16,31	11,80	11,87	2,24	
	Ob 50 nM	7,13	19,01	20,85	18,51	16,37	3,12	0,100
	Ob 100 nM	18,35	19,63	16,86	23,29	19,53	1,38	**0,014**
	Ob 200 nM	22,34	13,07	21,35	11,84	17,15	2,73	0,171

Table S2. Gastric lipase secretion from human stomach explants culture. Data refer to the secretion of gastric lipase in arbitrary units normalized to the secretome volume (mL) and to the mucosa weight (g) of each explant. Statistics were performed by comparing each treatment to the control point at each time. Abbreviations: Pat, patient; Ob: human obestatin, S.E.M: standard error of the mean.

Time	Dose	Pat#1	Pat#2	Pat#3	Pat#4	Mean	S.E.M	P value
20 min	Control	3,57	1,45	4,73	5,18	3,73	0,83	
	Ob 50 nM	3,89	7,55	8,74	5,85	6,51	1,06	0,057
	Ob 100 nM	9,80	9,89	9,08	6,23	8,75	0,86	**0,014**
	Ob 200 nM	4,42	5,32	7,71	8,65	6,53	0,99	0,057
40 min	Control	4,37	7,01	9,13	6,03	6,63	1,00	
	Ob 50 nM	7,34	9,21	22,32	4,50	10,84	3,95	0,171
	Ob 100 nM	5,79	5,70	9,43	9,62	7,63	1,09	0,329
	Ob 200 nM	3,11	6,03	16,37	11,42	9,23	2,94	0,329
60 min	Control	3,86	3,51	10,86	6,81	6,26	1,70	
	Ob 50 nM	4,68	5,55	14,14	10,59	8,74	2,22	0,243
	Ob 100 nM	9,42	11,99	11,06	12,92	11,35	0,75	**0,029**
	Ob 200 nM	10,44	7,08	12,47	6,27	9,07	1,45	0,171